Modelling medulloblastoma using cerebellar organoids



Max J. van Essen

The Queen's College

University of Oxford

A thesis submitted for the degree of *Doctor of Philosophy* in Clinical Neuroscience

Michaelmas, 2022

"*Problems worthy of attack prove their worth by fighting back.*"

– Piet Hein, Danish mathematician –

Acknowledgements

I would like to express my gratitude to my three supervisors Prof. Esther Becker, dr. Sally Cowley and dr. John Jacob. Throughout this DPhil, you have turned this young, fresh-out-of-university clinician almost into a (neuro)biologist. Thank you, Esther, for having me in your lab, motivating me to be precise, and for your kind support and guidance. Sally, thank you for teaching me the ins and outs regarding induced pluripotent stem cells and for showing me what experience looks like. To John, thank you for all our exciting and stimulating discussions.

I thank Cancer Research UK for their financial support which has allowed me to pursue this DPhil at the University of Oxford.

Thank you to the Becker lab for making me an even bigger coffee addict than I was before. Thank you for all the banter, crazy discussions and, most importantly, support. This DPhil would not have been the same without you.

To my parents, thank you for your unconditional love and support, and for giving me a foundation on which I can build for the rest of my life. I want to thank Arthur, Merijn, extended family and friends for bringing the joy that has allowed me to stay happy and motivated.

Most importantly, to Suus, thank you for your inspiration and for being the light of every day since we met. You are the love of my life, and I feel immensely lucky that we have been able to do this together. I cannot wait for what is next.

Abstract

Medulloblastoma (MB) is the most common malignant brain tumour in children and originates from cerebellar progenitor cells. Although extensive genomic studies have resulted in detailed molecular signatures of MB subtypes, current preclinical models often fail to capture human tumour biology accurately. Furthermore, available *in vitro* models do not harbour the most frequent mutations, limiting the translational potential of preclinical findings.

In this thesis, I describe the use of induced pluripotent stem cells (iPSC) and cerebellar organoid differentiation for MB modelling. Using CRISPR/Cas9 gene editing, I introduce a loss-of-function (LOF) mutation in the *PTCH1* gene, the most frequently mutated gene in the Sonic hedgehog (SHH) type of MB. This subtype is characterised by increased signalling of the SHH signalling pathway. I show that homozygous LOF results in changes in differentiation trajectory, while heterozygous mutants differentiate into cerebellar organoids and display features related to preneoplasia. In addition, I describe potent alternative strategies for MB modelling using the introduction of driver genes in differentiated cerebellar organoids that results in proliferative growths and tumorigenesis when transplanted in mice. Cerebellar organoid co-culture with established MB cell lines provides a third strategy and enables the study of the tumour microenvironment.

Together, these models capture various aspects of tumorigenesis and allow the study of human MB biology. The application of these strategies may overcome the current limitations of preclinical models and help bridge the gap from bench to bedside.

Publications and presentations

Publications

van Essen, M.J., Nayler, S., Becker, E.B. and Jacob, J., 2020. Deconstructing cerebellar development cell by cell. *PLoS Genetics*, *16*(4), p.e1008630.

van Essen, M.J., Riepsaame, J. and Jacob, J. (2021) 'CRISPR-Cas Gene Perturbation and Editing in Human Induced Pluripotent Stem Cells', *CRISPR Journal*. Mary Ann Liebert Inc., pp. 634–655.

van Essen, M.J., Nayler, S., Apsley, E.J., Jacob, J. and Becker, E.B., 2022. Cerebellar Modelling Using Human Induced Pluripotent Stem Cells. In *Neuromethods: Measuring Cerebellar Function* (pp. 1-21). Humana, New York, NY.

Presentations

The work in Chapter 3 and 4 was presented at the British neuro oncology society (BNOS) annual meeting 2022 (Oral presentation).

Table of contents

Modelling medulloblastoma using cerebellar organoids 1
Acknowledgements 3
Abstract 4
Publications and presentations 5
Table of contents 6
List of Figures 10
List of Tables 12
List of abbreviations 13
Chapter 1 Introduction 15
1.1 The cerebellum 17
1.1.1 Anatomy and function 17
1.1.2 Cerebellar cytoarchitecture 17
1.2 Cerebellar development 19
1.2.1 Establishment of the cerebellar territory 19
1.2.2 Cerebellar germinal zones 21
1.2.3 Granule cell development 23
1.3 SHH signalling during cerebellar development and disease 26
1.3.1 Canonical SHH signalling 26
1.3.2 The function of SHH activity in early neural tube development 29
1.3.3 SHH signalling in cerebellar development 31
1.3.4 The role of SHH signalling in cancer 32
1.4 SHH medulloblastoma 33
1.4.1 Targeted treatment 37
1.5 Classic SHH-medulloblastoma models 38
1.5.1 Cancer cell lines 38
1.5.2 Genetically engineered mouse models (GEMMs) that model genetic predisposition 39
1.5.3 Patient-derived xenografts 42
1.6 Induced pluripotent stem cells and their potential for MB modelling 43
1.7 Aims of thesis 49

Chapter 2 Methods 50
2.1 iPSC culture 50
2.2 CRISPR-gene editing of iPSC 51
2.2.1 gRNA design 51
2.2.2 Transfection 52
2.2.3 Genomic DNA extraction by DNeasy kit 53
2.2.4 Single-cell plating and clone picking 53
2.2.5 Genomic DNA extraction by ethanol precipitation 55
2.2.6 Clone selection and expansion to master stock 55
2.3 Quality control on CRISPR-edited iPSC 56
2.3.1 Sanger sequencing of region of interest 56
2.3.2 SNP analysis 56
2.3.3 Mycoplasma detection 56
2.3.4 Flow cytometry 57
2.4 Characterisation CRISPR-edited iPSC 57
2.4.1 RNA isolation 57
2.4.2 Reverse transcription and qPCR 58
2.4.3 SHH pathway activation 58
2.4.4 EdU proliferation assay of iPSC 59
2.4.1 Statistical analysis 59
2.5 Cerebellar organoid differentiation 59
2.5.1 Embryoid body formation 60
2.5.2 Cerebellar lineage induction 61
2.5.3 Cerebellar progenitor maturation up to DIV 35 61
2.5.4 Long-term maintenance of cerebellar organoids 62
2.5.5 RNA extraction and RT-qPCR from cerebellar organoids 63
2.6 Immunocytochemistry and microscopy 63
2.6.1 Procedure cryosections 63
2.6.2 Procedure whole organoid 64
2.7 Flow cytometry of organoids 65
2.8 Bulk RNA sequencing, RNA integrity measurement and transcriptome analysis 65

2.8.1 RNA isolation and quality control 65
2.8.2 Library preparation and sequencing 66
2.8.3 Transcript quantification and data analysis 66
2.9 Cyclopamine treatment of cerebellar organoids 67
2.10 Bacteria and plasmids 67
2.10.1 Plasmid retrieval from Whatman paper 68
2.10.2 Transformation, agar plating, and pDNA isolation 68
2.11 Electroporation of whole organoids 69
2.12 Co-culture of cerebellar organoids with established medulloblastoma cell lines 69
2.12.1 DAOY and ONS76 culture 69
2.12.2 MB spheroid generation 70
2.12.3 Organoid - MB-spheroid co-culture 70
2.13 Single-cell or single nuclei RNA sequencing sample preparation 71
2.13.1 Single-cell isolation and dead-cell removal 71
2.13.2 Single-cell RNA sequencing analysis 71
Chapter 3 Engineering a *PTCH1* loss-of-function mutation in human iPSC 74
3.1 Introduction 74
3.2 Results 81
3.2.1 CRISPR strategy to induce *PTCH1* loss-of-function 81
3.2.2 CRISPR gene editing and clone selection 83
3.2.3 Quality control of PTCH1 mutant iPSC 87
3.2.4 Functional characterisation of *PTCH1* mutation in undifferentiated iPSC 89
3.3 Discussion 95
3.4 Conclusion 99
Chapter 4 Characterising the effects of *PTCH1* LOF on cerebellar differentiation. 100
4.1 Introduction 100
4.2 Results 103
4.2.1 Cerebellar organoid differentiation 103
4.2.2 *PTCH1*-mutation affects cerebellar differentiation of iPSC 107
4.2.3 Altered differentiation trajectory of *PTCH1-/-* iPSC 112

4.2.4 Expansion of the rhombic lip lineage in *PTCH1* heterozygous organoids ... 121

4.2.5 *PTCH1* heterozygous organoids display features of loss-of-heterozygosity but not tumorigenesis ... 132

4.2.6 Druggable targets found upregulated in heterozygous organoids ... 134

4.3 Discussion ... 136

4.4 Conclusion ... 142

Chapter 5 Exploring alternative methods for medulloblastoma modelling in cerebellar organoids ... 143

5.1 Introduction ... 143

5.1.1 Introduction of MB driver genes into cerebellar organoids ... 143

5.1.2 MB cell line co-culture with cerebellar organoids ... 146

5.2 Results ... 149

5.2.1 MB driver gene delivery using PiggyBac transposons ... 149

5.2.2 *MYCN* overexpression in cerebellar organoids ... 151

5.2.3 Tumorigenicity of *MYCN* overexpressing cerebellar progenitors ... 158

5.2.4 MB cell line co-culture with cerebellar organoids ... 159

5.2.5 Single cell RNA sequencing of organoid co-cultures ... 161

5.2.6 Extracellular matrix upregulation in 3D conditions ... 164

5.3 Discussion ... 170

5.4 Conclusion ... 175

Chapter 6 Discussion and future directions ... 176

6.1 CRISPR gene editing is an efficient tool to introduce germline mutations in human iPSC ... 176

6.2 Cerebellar organoid differentiation models human development and aspects of early medulloblastoma tumorigenesis ... 177

6.3 Cerebellar organoids provide a versatile platform for medulloblastoma modelling ... 179

6.4 Conclusion and future perspective ... 180

Bibliography ... 181

Appendix ... 220

List of Figures

Figure 1.1: Molecular subtypes of medulloblastoma. 16
Figure 1.2: Cerebellar cytoarchitecture. 18
Figure 1.3: Cerebellar embryonic development. 21
Figure 1.4: Granule cell development. 24
Figure 1.5: SHH-signalling 29
Figure 1.6: SHH-signalling in the neural tube. 30
Figure 1.7: SHH-pathway mutations in medulloblastoma and targeted therapies.. 36
Figure 1.8: Induced pluripotent stem cells (iPSC). 44
Figure 1.9: Medulloblastoma models. 47
Figure 2.1: Filtering of low-quality cells by RNA count and mitochondrial RNA. 73
Figure 3.1: CRISPR-Cas9 gene editing and DNA repair. 77
Figure 3.2: SHH signalling induces the expression of *GLI1* and *PTCH1*. 79
Figure 3.3: CRISPR strategy to induce PTCH1 loss-of-function in human iPSC. 82
Figure 3.4: Detection of mutant genomic DNA in CRISPR gene edited iPSC pools. 84
Figure 3.5: Selection of heterozygous and homozygous *PTCH1* mutant iPSC clones. 86
Figure 3.6: *PTCH1* mutant clones maintain iPSC morphology and pluripotency marker expression. 88
Figure 3.7: Sanger sequencing does not reveal off-target activity 89
Figure 3.8: *PTCH1* mutant iPSC express increased levels of *GLI1*. 90
Figure 3.9: Aberrant splicing of mutant *PTCH1* pre-mRNA results in a loss-of-function frameshift 91
Figure 3.10: SHH-activation elicits response in wildtype but not in *PTCH1-/-* iPSC. 93
Figure 3.11: *PTCH1* mutant iPSC do not display changes in cell cycle phase proportions. 94
Figure 4.1: Overview of the cerebellar differentiation protocol. 104
Figure 4.2: Cerebellar organoid differentiation of iPSC. 105

Figure 4.3: GCP marker expression during cerebellar organoid differentiation. ... 107

Figure 4.4: *PTCH1* mutation changes organoid morphology. ... 108

Figure 4.5: Isthmic organiser marker expression in *PTCH1* mutant organoids. ... 109

Figure 4.6: Pronounced changes in cerebellar marker expression in *PTCH1* mutant organoids at DIV 35. ... 111

Figure 4.7: Genotype is the main driver behind transcriptome differences. ... 113

Figure 4.8: PTCH1 LOF prevents cerebellar differentiation and alters trajectory towards the ventral forebrain. ... 115

Figure 4.9: Evidence of SHH signalling centres in *PTCH1-/-* organoids. ... 116

Figure 4.10: Cyclopamine treatment of *PTCH1-/-* organoids induces cerebellar marker expression. ... 118

Figure 4.11: SHH-inhibition has long lasting effects on patterning in *PTCH1-/-* organoids. ... 120

Figure 4.12: Wildtype and heterozygous organoids have distinct transcriptomes. ... 121

Figure 4.13: Expression of early rhombic lip genes is elevated in heterozygous organoids. ... 123

Figure 4.14: Cell type specific gene sets reveal expansion of granule cell progenitors in heterozygous organoids. ... 124

Figure 4.15: *PTCH1+/-* cerebellar organoids express higher levels of rhombic lip genes. ... 126

Figure 4.16: Gene ontology analysis reveals upregulation of distinct patways. ... 129

Figure 4.17: Gene Ontology analysis identifies cerebellum specific changes in heterozygous organoids. ... 130

Figure 4.18: Increased expression of PAX6 and CCNB1 in *PTCH1* heterozygous organoids. ... 131

Figure 4.19: Long-term culture of *PTCH1* heterozygous organoids shows signs of wildtype *PTCH1* loss but not tumorigenesis. ... 134

Figure 4.20: Druggable targets found upregulated in heterozygous organoids. ... 135

Figure 5.1: PiggyBac transposon delivery of transgenes into cerebellar organoids. ... 145

Figure 5.2: Co-culture of MB cell lines with cerebellar organoids. ... 147

Figure 5.3: Optimised experimental conditions show effective introduction of MB drivers in cerebellar organoids. 150

Figure 5.4: *MYCN* overexpressing organoids contain proliferative rhombic lip derivatives. 154

Figure 5.5: *MYCN* overexpression conditions induce the proliferation and growth of cerebellar organoids. 157

Figure 5.6: Orthotopic injection of *MYCN* cells induces tumour growth in mice. 159

Figure 5.7: Establishment of an MB cell line – cerebellar organoid co-culture model. 161

Figure 5.8: Cerebellar organoid and medulloblastoma cells have distinct transcriptomes and can easily be identified. 164

Figure 5.9: Three-dimensional culture DAOY- and ONS-76 cells induces expression of extracellular matrix genes 166

Figure 5.10: CBO co-cultured cells upregulate distinct cell binding pathways. 168

Figure 5.11: Low cell numbers prevent comparison of CBO co-cultured ONS-76 cells with 3D counterparts. 169

Appendix figure 1: SNP array to test for chromosomal aberrations in gene edited iPSC clones. 223

List of Tables

Table 2-1: Guide RNA sequences and genotyping primers. 52

Table 5-1: Cell counts before and after quality control.. 163

Appendix Table 1: Oligonucleotides used in this thesis. 220

Appendix Table 2: Primary antibodies used in this thesis. 221

Appendix Table 3: Secondary antibodies used in this thesis. 221

Appendix Table 4: Off-target sites as predicted by CRISPOR.org 222

List of abbreviations

BMP	Bone morphogenetic protein
CBO	Cerebellar organoid
CRISPR	Clustered Regularly Interspaced Palindromic Repeats
DCN	Deep cerebellar nuclei
DIV	Days in vitro
EB	Embryoid body
ECM	Extracellular matrix
EGL	External granular layer
ESC	Embryonic stem cell
GC	Granule cell
GCP	Granule cell progenitor
GL	Granular layer
gRNA	guide RNA
GSVA	Gene set variant analysis
IGL	Inner granule layer
iPSC	Induced pluripotent stem cell
IsO	Isthmic organiser
LOF	Loss-of-function
MB	Medulloblastoma
MHB	Midbrain-hindbrain barrier
ML	Molecular layer
NBCCS	Nevoid Basal cell carcinoma syndrome
NES	Neuroepithelial stem cell
NHEJ	Non-homologous end joining
NMD	Nonsense-mediated decay
OTE	Off-target effect
PAM	Protospacer adjacent motif
PC	Purkinje cell

PCL	Purkinje cell Layer
RL	Rhombic lip
RNP	Ribonuclease protein
SAG	Smoothened agonist
scRNAseq	Single-cell RNA sequencing
SD	Splice donor site
SHH	Sonic Hedgehog
TME	Tumour microenvironment
UBC	Unipolar brush cell
URL	Upper rhombic lip
VZ	Ventricular zone
WT	Wildtype

Chapter 1 Introduction

Medulloblastoma (MB) is the most common malignant brain tumour in children (Smoll and Drummond, 2012; Ostrom *et al.*, 2018). Extensive international collaborations have characterised four main subtypes: Sonic hedgehog (SHH), WNT, group 3 and group 4) (*Figure 1.1*) (Kool *et al.*, 2008; Northcott *et al.*, 2011). Each subtype has specific biological and clinical characteristics that are relevant for understanding the disease, improving risk stratification, and providing opportunities for targeted treatment (reviewed in Juraschka & Taylor, 2019). Children with MB typically receive multimodal treatment comprised of surgical resection, radiation- and chemotherapy. Although this therapeutic strategy has improved survival, late side effects such as secondary malignancies (Garwicz *et al.*, 2000; Neglia *et al.*, 2001; Salloum *et al.*, 2019) and neurocognitive effects (Schreiber *et al.*, 2017; Albazron *et al.*, 2019) continue to impact the lives of these patients. Few preclinical models utilise the current understanding of MB biology, and development of novel human-specific models informed by this knowledge promise to be an exciting avenue to improve the outcome in MB patients.

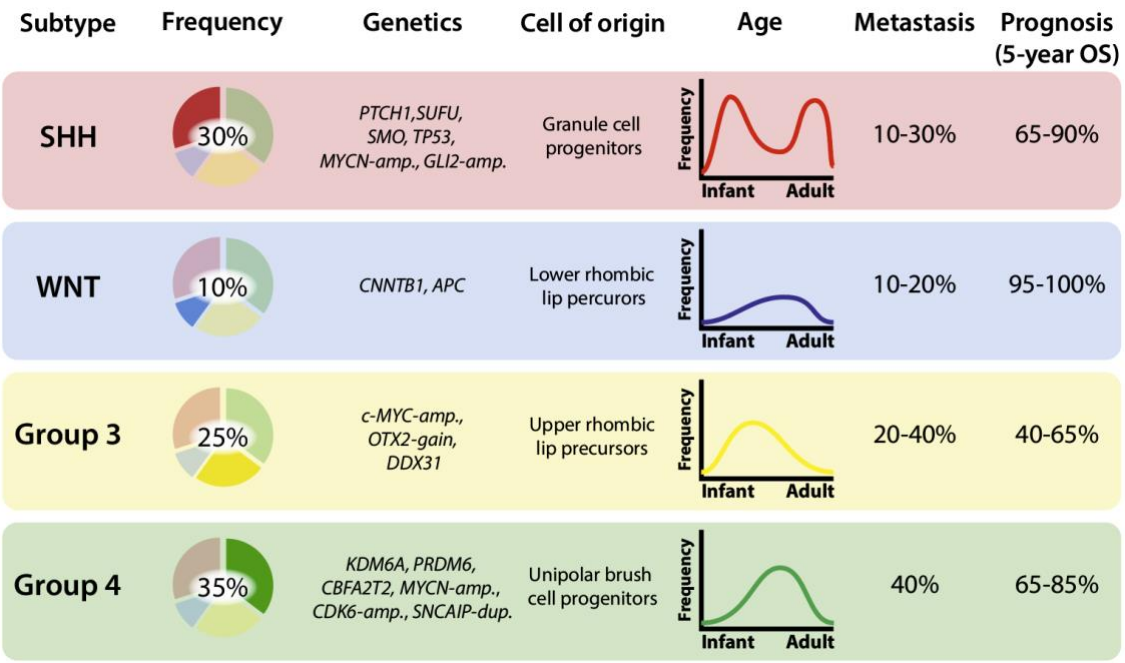


Figure 1.1: Molecular subtypes of medulloblastoma. *The four MB subtypes are SHH, WNT, group 3 and group 4. The proportion of each subtype, most frequent genetic alterations, perceived cell of origin, age distribution, frequency of metastases at diagnosis and five-year overall survival (OS) are displayed. Amp. = amplification, dup. = duplication*

Pioneering neurosurgeon Harvey Cushing and neuropathologist Percival Bailey named MB after what they believed to be the cell type of origin, the 'medulloblast' (Bailey and Cushing, 1925). Although the existence of such cells was later disproven, the assumption of malignant transformation of a cerebellar precursor was correct. Located in the cerebellum, MB arises from embryonal progenitor cells that fail to differentiate correctly into cerebellar cell types. This thesis will focus on the SHH subtype of MB that originates from a cerebellar progenitor cell type of granule cell (GC). Recognising the close relationship between MB and embryology, the following sections will describe cerebellar development, particularly that of GCs. Next, SHH signalling, its role in cerebellar development and how mutations in SHH-pathway genes can drive malignant transformation are reviewed. Lastly, existing preclinical models of SHH-MB and opportunities for innovation will be discussed.

1.1 The cerebellum

1.1.1 Anatomy and function

The cerebellum is located in the posterior fossa and has two lateral hemispheres similar to the cerebrum. In addition, it contains a third structure in the midline called the vermis. Neurons in the cerebellum receive input from the cerebral cortex and the spinal cord through multiple brain stem nuclei. This input is modulated in the cerebellar cortex before transforming into output directed towards the ventrolateral thalamus and the red nucleus. The cerebellum has a crucial role in movement guidance, planning and integrating sensory information, as well as additional roles in cognition and emotion (Sathyanesan *et al.*, 2019).

1.1.2 Cerebellar cytoarchitecture

Cerebellar neurons are either inhibitory (GABAergic) or excitatory (glutamatergic). The GABAergic lineage includes Basket cells (BC), stellate cells (SC), Purkinje cells (PCs), Golgi cells (GoC) and a subset of GABAergic deep cerebellar nuclei neurons (DCN) (*Figure 1.2*). Glutamatergic neurons include GCs, unipolar brush cells (UBCs) and glutamatergic DCN (*Figure 1.2*). In the adult cerebellum, these neuronal cell types are distributed across three layers in the cerebellar cortex (from the outside: the molecular layer (ML), Purkinje cell layer (PCL), and granular layer (GL)), and the white matter contains the deep cerebellar nuclei (DCN) (*Figure 1.2*). Neuronal activity in the cerebellum evolves around modulating the firing of PCs which provide the sole output of the cerebellar cortex. The cerebellum receives sensory input through mossy fibres (MF) and climbing fibres (CF). CF originate from the inferior olivary nucleus and connect directly to PCs and DCN neurons. MF project from the

precerebellar nuclei and convey information from various locations, including the cerebral cortex and spinal cord. In the cerebellum, MF connect to GCs in the granular layer and to DCN neurons. Axons of GCs are called parallel fibres (PF) and project up towards the molecular layer, where they branch off into a T-shape to connect with the dendritic arbours of PCs. The PC dendritic arbour projects in a single plane perpendicular to the PF. As a result, each PC connects with many PFs, and each PF connects with thousands of PCs. Two sets of interneurons further modulate the activity of PCs and GCs. Basket cells and stellate cells reside in the molecular layer and connect with PCs. GC activity is modulated by Golgi cells and UBCs. Each PC has one efferent axon that projects towards the DCN to provide real-time correction of movement and modulation of cognitive functions.

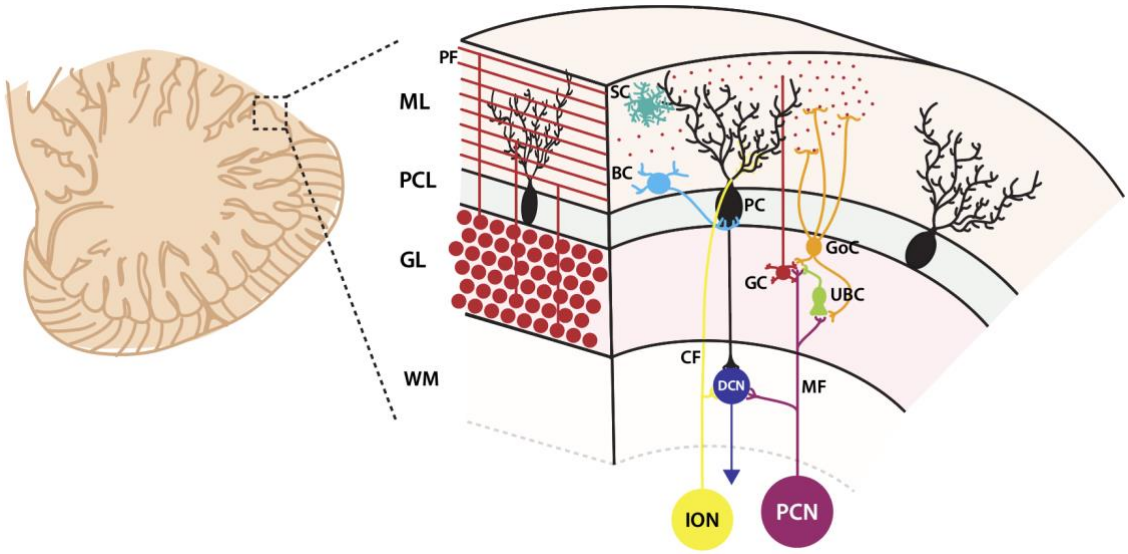


Figure 1.2: Cerebellar cytoarchitecture. *In the adult cerebellum, afferent input from the inferior olivary nucleus (ION) and precerebellar nuclei (PCN) is transmitted via climbing fibres (CF) and mossy fibres (MF), respectively. MF connect onto granule cells (GC) residing in the granular layer (GL) and project their axons up towards the molecular layer (ML), branching off into a T-shape. GC axons in the ML are called parallel fibres (PF) and travel in an orthogonal plane to Purkinje cell (PC) dendrites with which they connect. GC activity is modulated by Golgi cells (GoC) and unipolar brush cells (UBC). PC firing is modulated by stellate cells (SC) and basket cells (BC). PC output is projected to the deep cerebellar nuclei (DCN), which also receive input from CF and MF. As a result, PC provide real-time correction of cerebellar input.*

1.2 Cerebellar development

1.2.1 Establishment of the cerebellar territory

The cerebellum originates from rhombomere 1 (r1) of the dorsal hindbrain (Millet et al., 1996; Wingate and Hatten, 1999) at the midbrain-hindbrain barrier (MHB). Here, the neural tube forms a constriction, which is also referred to as the isthmus. The position of the MHB is demarcated by the cranial expression of orthodenticle homeobox 2 (*OTX2*) and caudal expression of gastrulation brain homeobox 2 (*GBX2*) which are both transcription factors (*Figure 1.3*) (Liu and Joyner, 2001; Sunmonu *et al.*, 2011). OTX2 and GBX2 act antagonistically and determine the location of a specialised group of cells called the isthmic organiser (IsO)(Li and Joyner, 2001). The IsO regulates fate-determining gene expression in adjacent structures and acts primarily through the expression of fibroblast growth factor 8 (*FGF8*) (reviewed in Sillitoe and Joyner, 2007; Leto et al., 2016). Anterior of the IsO, Wnt family member 1 (*WNT1*) expression is required for the formation of the cerebellum (McMahon and Bradley, 1990) likely through regulating *FGF8* expression (Li and Joyner, 2001)(*Figure 1.3*).

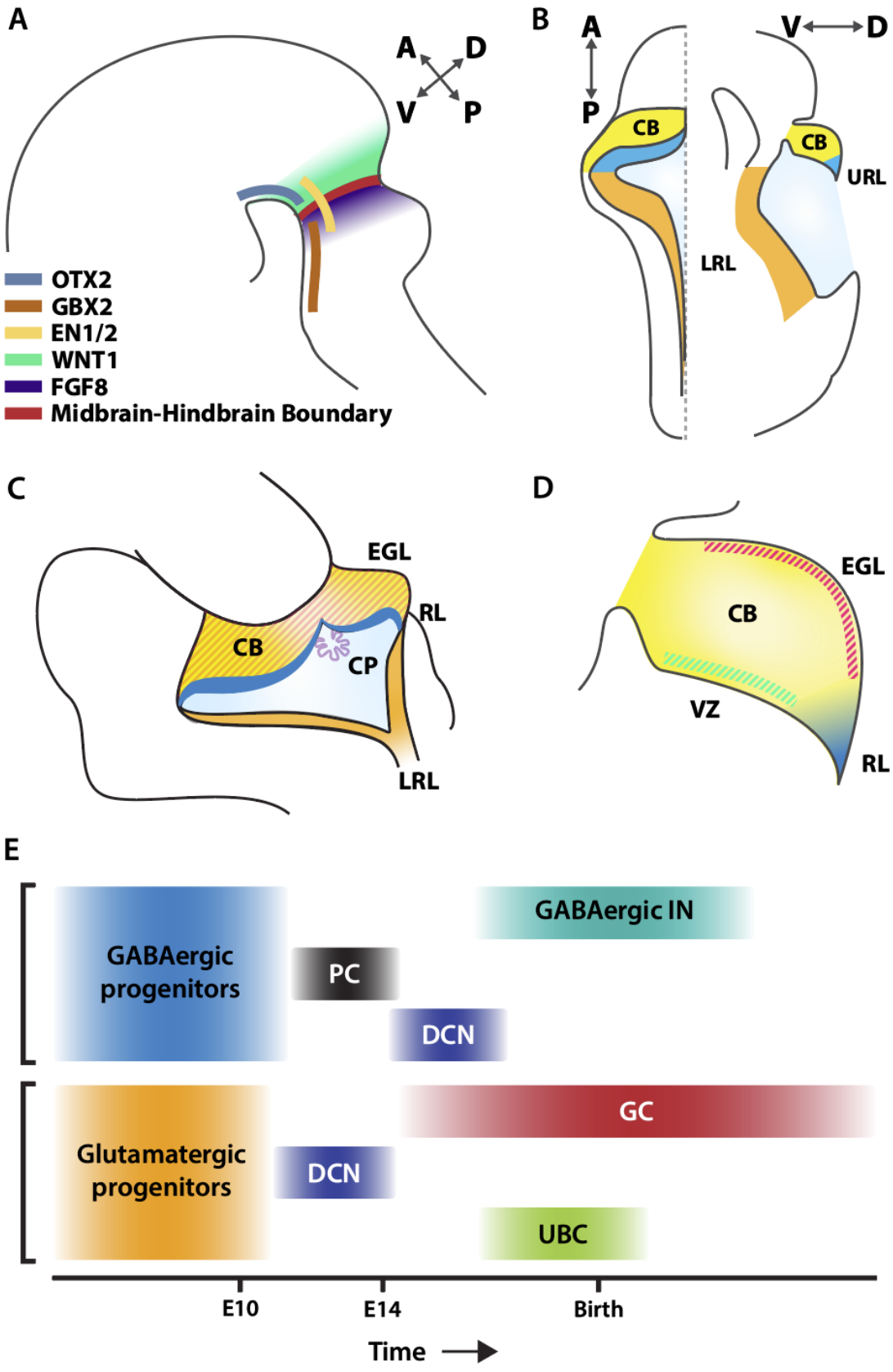

A
A
D
V
P
OTX2
GBX2
EN1/2
WNT1
FGF8
Midbrain-Hindbrain Boundary
B
A
P
CB
LRL
V
D
CB
URL
C
EGL
RL
CB
CP
LRL
D
EGL
CB
VZ
RL
E
GABAergic progenitors
PC
DCN
GABAergic IN
Glutamatergic progenitors
DCN
GC
UBC
E10
E14
Birth
Time

Figure 1.3: Cerebellar embryonic development. *A) The cerebellum develops posterior to the midbrain-hindbrain boundary (MHB) under the influence of FGF8. Cranially, the expression of WNT1 induces the formation of the midbrain and cooperates with FGF8 to form the cerebellum. Expression of GBX2 accompanied by EN1 and EN2 demarcates the cerebellar primordium, while OTX2 is expressed in the presumptive midbrain. B) The dorsal central nervous system around the rhombic lip develops in two segments, the upper rhombic lip (URL) and the lower rhombic lip (LRL). The URL provides cells to the cerebellum (CB). C) The choroid plexus (CP) secretes BMPs and WNTs that induce the formation of the external granule layer (EGL). D) Within the cerebellar primordium, the RL generates glutamatergic neurons, while the ventricular zone (VZ) provides the GABAergic neurons. E) Cerebellar cell types are born at different stages of development. Birth dates in mice are depicted along the x-axis. A: Anterior; CB: Cerebellum; CP: Choroid plexus; D: Dorsal; DCN: Deep cerebellar nuclei; E: Embryonic day; EGL: External granular layer; GC: Granule cell; IN: Interneuron; LRL: Lower rhombic lip; P: Posterior; PC: Purkinje cell; RL: Rhombic lip; UBC: Unipolar brush cell; URL: Upper rhombic lip; V: Ventral.*

1.2.2 Cerebellar germinal zones

Cerebellar cell type specification is mediated through the secretion of bone morphogenetic proteins (BMPs) and WNT by the choroid plexus (Cheng et al., 2012; Chizhikov et al., 2006; Lee & Jessell, 1999). The cooperation of the choroid plexus and the IsO defines two main germinal zones, the Ventricular Zone (VZ) and the cerebellar or upper Rhombic Lip (URL) (*Figure 1.3*). The VZ lines the dorsal side of the embryonic fourth ventricle and produces the GABAergic neurons in the cerebellum. Posterior to the VZ, the URL produces the glutamatergic neurons in the cerebellum (Hoshino *et al.*, 2005; MacHold and Fishell, 2005; Wang, Rose and Zoghbi, 2005).

1.2.2.1 The cerebellar ventricular zone

The VZ is marked by the expression of *PTF1A.* Knockout studies in mice have proven *Ptf1a* expression to be essential for the generation of the GABAergic lineage (Hoshino *et al.*, 2005; Pascual *et al.*, 2007) and its expression is regulated by the delivery of SHH through the fourth ventricle. Under the influence of Oligodendrocyte

transcription factor 2 (OLIG2), the VZ primarily generates PC progenitors (PCPs) early in development (Seto *et al.*, 2014). The earliest PCPs also express Kirre Like Nephrin Family Adhesion Molecule 2 (*KIRREL2*, also known as *NEPH3*), which is a downstream target of PTF1A (Mizuhara *et al.*, 2010). Concurrently with the generation of PCPs, GABAergic DCN arise as a result of *GSX1* expression. Later, GSX1 suppresses the expression of *OLIG2* and induces the production of Paired box gene 2 (PAX2) expressing GABAergic interneuron progenitors (Maricich and Herrup, 1999; Weisheit *et al.*, 2006; Leto *et al.*, 2009; Seto *et al.*, 2014).

1.2.2.2 Cerebellar rhombic lip

The URL (hereafter referred to as RL for simplicity) gives rise to glutamatergic progenitors which express atonal homologue 1 (*ATOH1*) (MacHold and Fishell, 2005; Wang, Rose and Zoghbi, 2005) and paired box protein pax-6 (*PAX6*) (Engelkamp *et al.*, 1999). Compared to the VZ, less is known about cell type specification within the RL. However, birth dating studies have shown that glutamatergic DCN are generated first (Fink *et al.*, 2006) before the RL produces GCs (Hanaway, 1967; Ryder and Cepko, 1994; Wingate and Hatten, 1999; Wingate, 2001; Gilthorpe et al., 2002) and then UBCs (Englund *et al.*, 2006). Recent work has suggested the human RL develops into two compartments: the RL-ventricular zone (RL^{vz}) and the RL-subventricular zone (RL^{svz}). These two zones are separated by a vascular plexus (Haldipur *et al.*, 2019) and display distinct transcriptional profiles (Aldinger *et al.*, 2021). Between these two zones, the expression of Wntless (*WLS*) distinguishes the RL^{vz} (WLS+) from the RL^{svz}.(WLS-). The RL^{vz} is thought to contain stem cells, while the RL^{svz} is composed of more differentiated, proliferative progenitors (Hendrikse *et al.*, 2022).

Although mice lack the vascular plexus, earlier work had already identified two compartments in the mouse, of which the ventricular compartment is marked by the differential expression of *Wls* (Yeung *et al.*, 2014). Nevertheless, the human RL persists longer during development than in mice and non-human primates. In humans, the RL is thought to serve as a stem cell reservoir (Haldipur *et al.*, 2019) and facilitates the remarkable increase in cerebellar neurons from late gestation into the early postnatal period (Limperopoulos *et al.*, 2005; Volpe, 2009). However, the prolonged presence of a stem cell/progenitor pool has been proposed to increase the risk of malignant transformation, and failure of differentiation within this pool has recently been linked to the development of group 3 and group 4 MB (Hendrikse *et al.*, 2022; Smith *et al.*, 2022).

1.2.3 Granule cell development

Failed differentiation of granule cell progenitors (GCPs) has long been recognised as the cause of another subtype of MB: SHH-MB. In healthy development, GCPs leave the RL and form a stream of cells along the dorsal surface of the embryonic cerebellum. This stream is called the external granular layer (EGL) and is the place where these cells proliferate. GCP proliferation is primarily driven by SHH, and persistent activation of SHH-signalling can cause MB.

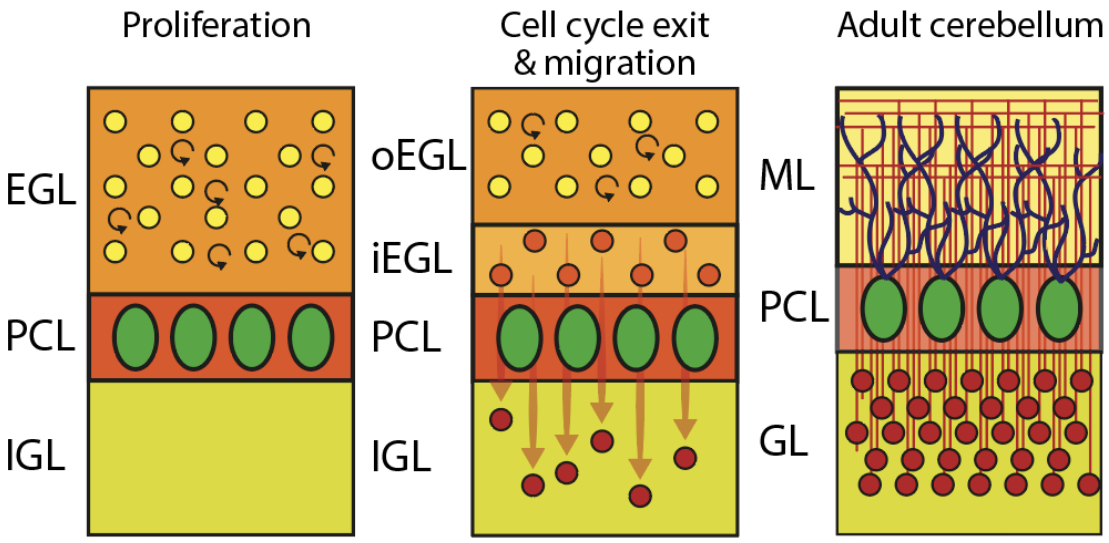


Figure 1.4: Granule cell development. *Granule cell progenitors proliferate in the EGL under the influence of SHH. Upon cell cycle exit in the outer EGL (oEGL), GCPs migrate first to the inner EGL (iEGL) before passing through the Purkinje cell layer (PCL) and settling in the inner granule layer (IGL) (in adult CB called granule layer (GL)).*

In the mouse, expression of Atoh1 has been found essential for generating GCPs (Ben-Arie *et al.*, 1997) and studies misexpressing *Atoh1* in the VZ using a *Ptf1a*^{Atoh1} mouse model show ectopic generation of GCPs (Yamada *et al.*, 2014). In addition, GCPs express zinc-finger proteins *ZIC1*, *ZIC2* and *ZIC3* throughout their development (Aruga, 2004). Although the exact mechanisms through which ZIC-family proteins act remain unclear, roles in SHH-signalling have been attributed. More specifically, similarities in DNA-binding domains (Mizugishi *et al.*, 2001) and direct interaction between ZIC proteins and GLI proteins (Koyabu *et al.*, 2001) are thought to explain how ZIC proteins can enhance SHH-signalling and GLI transcriptional activity (Brewster, Lee and Altaba, 1998). In the mouse, early post-mitotic GCs express *Neurod1*, which is required for their survival and involved in downregulating *Atoh1* (Pan *et al.*, 2009). Interestingly, recent studies have shown concurrent expression of *ATOH1* and *NEUROD1* in proliferating human ESC derived GCPs (Behesti *et al.*, 2021).

This co-expression does not occur in mice and may indicate an intermediate cellular state in the outer EGL (oEGL) that allows the GCP pool to persist for longer in humans. While *Atoh1* expression is essential for the RL- and EGL-stages of GCP development, mice lacking the expression of *Pax6* show failure of GCP migration (Engelkamp *et al.*, 1999; Swanson, Tong and Goldowitz, 2005). The expression of *Pax6* is regulated by *Meis1* (Owa *et al.*, 2018), which is thought to modulate bone morphogenic protein (BMP) signalling, an essential pathway in cerebellar development. Upregulation of BMP signalling results in Atoh1 degradation and allows GCPs to differentiate and migrate to the internal EGL (iEGL) (*Figure 1.4*). During migration, post-mitotic GCs express Contactin-2 (*CNTN2*) (also known as *Axonin-1* or *TAG-1*) which first facilitates tangential and later radial migration inwards through the ML and PCL to the internal granule layer (IGL) (*Figure 1.4*) (Baeriswyl and Stoeckli, 2008). The switch from tangential to inward migration is modulated by Semaphorin 6A (*Sema6A*) and plexin A2 (*Plxna2*) (Renaud *et al.*, 2008). Upon reaching the IGL that lies below the Purkinje layer, maturing GCs express the $GABA_A$ receptor α6 subunit (*GABRA6*), which has been shown to be a highly specific marker of this cell type (Kato, 1990; Gao and Fritschy, 1995; Bahn *et al.*, 1999). As a result of the migratory path travelled by GCs, an extensive network of PFs in the molecular layer is able to synapse onto PC dendrites, while GC cell bodies reside in the granular layer.

1.3 SHH signalling during cerebellar development and disease

The proliferation of GCPs and, more specifically, the role of SHH signalling is an extensively studied phenomenon in human biology. SHH pathway activation is responsible for the immense expansion that leads to GCs being the most abundant neuron in the human brain (Herculano-Houzel, 2009). Consequently, tight regulation of SHH signalling is required, and genetic events that disrupt this process are associated with MB.

1.3.1 Canonical SHH signalling

The SHH ligand is part of the Hedgehog (HH) family in addition to homologues Desert Hedgehog (DHH) and Indian Hedgehog (IHH). In *Drosophila,* only one Hedgehog (*Hh*) gene is present. Knockout of the *Hh*-gene leads to Drosophila embryos being covered in denticles resembling those of a hedgehog (Nüsslein-Volhard and Wieschaus, 1980), hence the name. During human development, each HH ligand has different roles, with SHH functioning primarily in the development of the central nervous – and skeletal systems (Ingham and McMahon, 2001), DHH orchestrating gonadal development (Yao et al., 2002), and IHH mediates endochondral bone formation (St-Jacques, Hammerschmidt and McMahon, 1999). HH signalling primarily occurs through the modulation of GLI protein activity which induces the transcription of target genes involved in stem cell maintenance, proliferation, and differentiation. Non-canonical HH-signalling independent of GLI has been described (reviewed in Jenkins, 2009) but is beyond the scope of this thesis.

SHH is the primary HH protein active during cerebellar development. Prior to release from SHH-producing cells, full-length SHH is cleaved and processed in the endoplasmic reticulum (Buglino & Resh, 2008), where cholesterol and palmitoyl groups are attached to the C- and N-terminus respectively (Porter, Young and Beachy, 1996; Pepinsky *et al.*, 1998). These modifications render SHH hydrophobic and anchor it to the plasma membrane. To begin signalling, Dispatched (*DISP*), a transmembrane transporter (Burke *et al.*, 1999; Yao, Whoriskey and Capel, 2002), extracts SHH from the cell membrane making it available to chaperone molecules that can then traffic it to receiving cells (Hollway *et al.*, 2006).

SHH binds to the twelve-pass transmembrane receptor patched homolog 1 (PTCH1) (Marigo *et al.*, 1996) and interacts with co-receptors growth arrest-specific 1 (GAS1), CAM-related/downregulated by oncogenes (CDO), and brother of CDO (BOC) (*Figure 1.5*) (Allen *et al.*, 2011). In the absence of SHH, PTCH1 acts as a suppressor of the SHH pathway by inhibiting Smoothened (SMO). Although the exact mechanisms through which PTCH1 prevents SMO-mediated SHH-signal transduction remain unknown, it likely prevents SMO from locating to the primary cilium by influencing the sterol concentration in cilia (Blassberg & Jacob, 2017; Corbit et al., 2005; Corcoran & Scott, 2006; Denef et al., 2000; Dwyer et al., 2007; Khaliullina et al., 2009; Nachtergaele et al., 2012; Taipale et al., 2002; Zhao et al., 2007). SHH binding to PTCH1 inhibits its function in ciliary sterol homeostasis and causes endocytosis of the receptor-ligand complex, allowing SMO to relocate to the cilia to activate the SHH pathway.

The main effector proteins of the pathway are transcription factors of the Glioma-associated oncogene (GLI) family, GLI1, GLI2 and GLI3. These proteins contain activator (GLI1/2/3) and repressor (GLI2/3) domains (*Figure 1.5*). GLI-signalling is primarily regulated through proteasomal processing. When SMO is absent at the primary cilium, the GLI proteins are ubiquitinated and undergo degradation (GLI1) or processing (GLI2 and GLI3) (Hui and Angers, 2011). The binding of SHH releases SMO from inhibition which in turn prevents proteasomal processing of GLI proteins. As a result, the activating domains present in GLI proteins are retained. The function of these activating domains supersedes the weaker repressor domain. Consequently, the full-length form of GLI2 and -3, therefore, functions primarily as a transcriptional activator. The exact mechanisms through which SMO acts are yet to be revealed but involve regulation of suppressor of fused (SUFU) (Chen *et al.*, 2009; Wilson, Chen and Chuang, 2009). In the absence of SHH ligand (and inhibited state of SMO), SUFU prevents the nuclear transport of GLI proteins (Barnfield *et al.*, 2005) and facilitates the degradation of GLI proteins (Kise *et al.*, 2009). Due to the differences in activating and repressor domains, GLI-proteins have both overlapping and distinct roles in SHH-signalling (von Mering and Basler, 1999; Aza-Blanc *et al.*, 2000; Park *et al.*, 2000). *Gli1* knockout in mice alone does not lead to a phenotype in the mouse. In contrast, homozygous *Gli2* knockouts displayed a severe phenotype with ventral neural tube defects, and lung abnormalities (Park et al., 2000) and Gli2 was found to be the principal transcriptional activator in the pathway (Ding *et al.*, 1998; Bai *et al.*, 2002). In contrast, GLI3 acts primarily as a repressor (Persson *et al.*, 2002) and is

induced by PAX6 (Lek *et al.*, 2010). The processed activator form of GLI3 cooperates with GLI2 to induce *GLI1* expression (Bai, Stephen and Joyner, 2004).

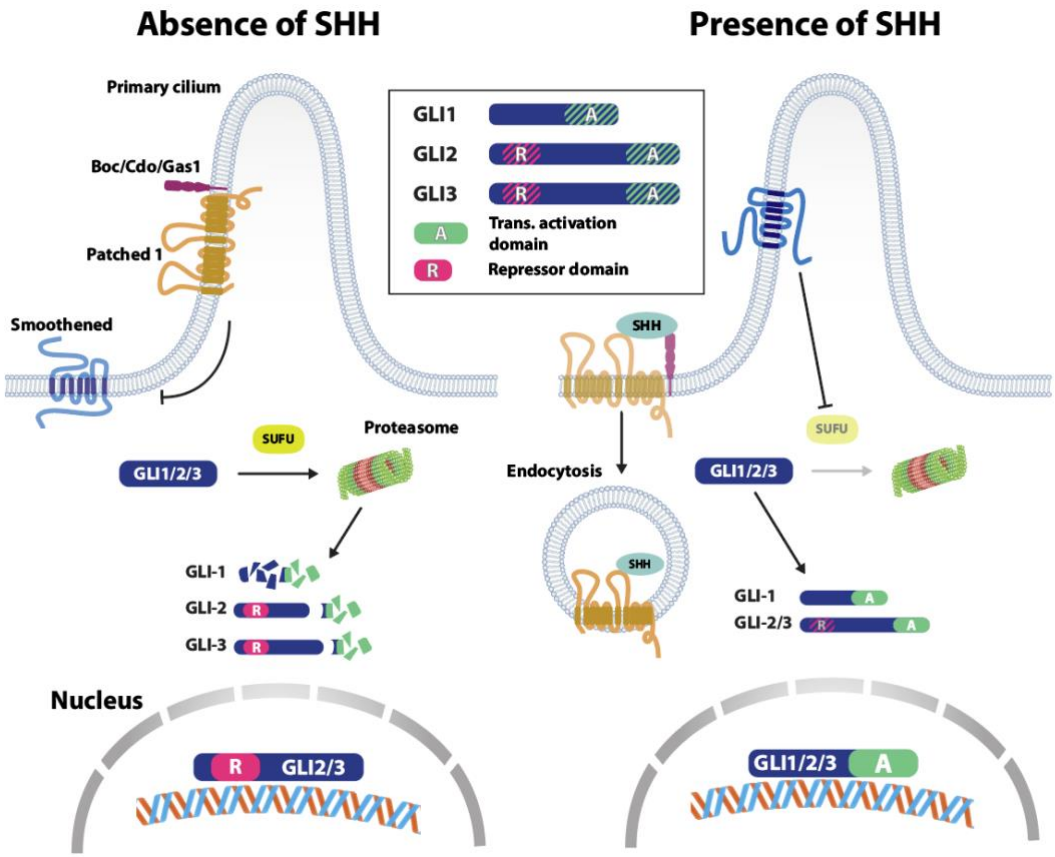


Figure 1.5: SHH-signalling. *In the absence of SHH, Smoothened (SMO) is prevented from locating to the primary cilium by Patched 1 (PTCH1). In a process mediated by SUFU, GLI-proteins (GLI1/2/3) are (partially) degraded by the proteasome, and transcription activation domains are removed from GLI2 and -3. These processed GLI-proteins have a repressor function on the transcription of GLI-target genes. When SHH binds PTCH1 and co-receptors BOC, CDO and GAS1, inhibition of SMO is relieved, and PTCH1 undergoes endocytosis. SMO prevents the degradation of GLI proteins, likely through inhibiting SUFU, leaving the activation domains intact. As a result, the transcription of GLI-target proteins is activated.*

1.3.2 The function of SHH activity in early neural tube development

In the context of cerebellar development, SHH signalling is best known for driving the proliferation of GCPs in the EGL. However, earlier in development, SHH functions

as a patterning molecule, or morphogen, and has extensively been studied for its ventralising role in the neural tube. During the early stages of foetal development, the expression of SHH is largely restricted to the ventral neural tube and SHH is produced by the notochord and floor plate (reviewed in Patten & Placzek, 2000). An SHH-signalling gradient is established from ventral to dorsal and controls the expression of transcription factors, and influences neuronal differentiation. High SHH-signalling is associated with the transcription of NK2 homeobox 2 (*NKX2-2*) and NK6 homeobox 1 (*NKX6-1*), while suppressing the expression of *PAX6* and developing brain homeobox 2 (*DBX2*) (*Figure 1.6*) (Ericson, Rashbass, Schedl, Brenner-Morton, Kawakami, V. van Heyningen, *et al.*, 1997a, 1997b; Briscoe *et al.*, 2000; Sander *et al.*, 2000). Interactions of SHH signalling with BMP signalling going from dorsal to ventral (reviewed in Liu & Niswander, 2005) result in highly orchestrated patterning of neuronal fate.

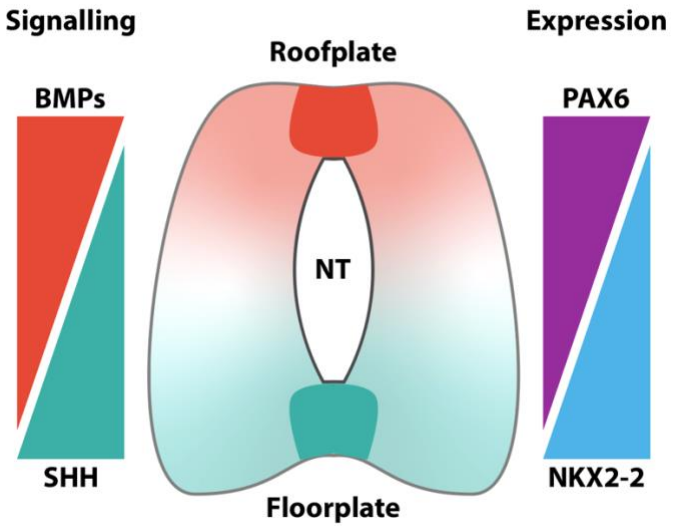


Figure 1.6: SHH-signalling in the neural tube. *In the neural tube, SHH- and BMP signals are secreted on opposite sides. The floorplate produces SHH and induces the expression of NKX2-2. In the dorsal neural tube, BMPs are produced by the Roof plate, inducing the expression of PAX6.*

1.3.3 SHH signalling in cerebellar development

In addition to the morphogenic role in neural tube patterning, SHH is an essential molecule in cerebellar development (Guizzetti and Costa, 2008; Aguilar *et al.*, 2012). In the cerebellum, SHH regulates the expansion of GCPs (Dahmane and Ruiz I Altaba, 1999; Wechsler-Reya and Scott, 1999) and proliferation of GABAergic interneurons and astrocytes (Huang *et al.*, 2010). Although it remains unclear which factors induce the mitogenic rather than the morphogenic role of SHH in GCPs, some factors have been suggested to enhance SHH-induced proliferation. However, these effects were only seen at specific stages of GC development (Klein *et al.*, 2001; Rubin, Choi and Segal, 2002), and the exact mechanisms that induce the mitogenic role of SHH remain elusive. Mouse studies have found PCs as the source of SHH secretion in the embryonic cerebellum (Wallace, 1999) and ablation of the PC layer in early postnatal mice results in thinning of the EGL (Smeyne *et al.*, 1995). It has, however, been suggested that in humans, the first SHH production might occur elsewhere. Compared to mice, human PCs may not have reached the same level of maturity when SHH-induced proliferation first occurs (Zecevic & Rakic, 1976), and one study suggested that the first SHH secretion may come from within the EGL (Haldipur *et al.*, 2012) Further studies are required to elucidate the exact source of SHH in this initial phase.

In GCPs, SHH-signalling causes phosphorylation and stabilisation of Atoh1 and is essential for GCP neurogenesis (Ben-Arie *et al.*, 1997; Forget *et al.*, 2014). Atoh1 regulates differentiation through modulation of the Notch signalling pathway (Gazit, Krizhanovsky and Ben-Arie, 2004). The proliferation of GCPs is maintained by

Notch2 signalling, likely through the upregulation of jagged 1 (*JAG1*) (Solecki *et al.*, 2001) and antagonising effects of specific BMPs (Zhao *et al.*, 2008). BMPs are essential for cell type specification of GCPs (Alder *et al.*, 1999; Mizuseki *et al.*, 2003) and induce GCP differentiation. As a result, the downregulation of BMPs is required for appropriate GCP expansion. In addition, expression of several cell cycle genes, including Cyclin D1 (*CCND1*) and v-Myc myelocytomatosis viral-related oncogene (*MYCN*) (Kenney et al., 2003; Kenney & Rowitch, 2000) is induced under the influence of SHH-activation. CCND1 is required for progression through the G1 phase (Baldin et al., 1993) and regulates Cyclin-dependent kinase 4 (CDK4) (Matsushime et al., 1992). Loss of CCND1 reduces GCP proliferation and markedly lowers tumour frequency in SHH-MB mouse models (Pogoriler et al., 2006). Similarly, *Mycn*-null mice also display reduced cerebellar mass (Knoepfler, Cheng and Eisenman, 2002). This reduction coincided with a high expression of Cdk inhibitors (Cdkn1b, Cdkn2c) and Mycn may normally repress these proliferation inhibitors.

1.3.4 The role of SHH signalling in cancer

Overactive SHH-pathway activity has been implicated in various types of cancer, including Basal Cell Carcinoma (BCC) and MB (reviewed in Ruiz i Altaba, Sánchez and Dahmane, 2002; Rubin and de Sauvage, 2006). Apart from the clear role in driving cell proliferation, SHH supports several hallmarks of malignancy, such as stem cell maintenance (Machold *et al.*, 2003; Ahn and Joyner, 2005; Liu *et al.*, 2006) epithelial to mesenchymal transition (Katoh and Katoh, 2008) and cancer-supporting mechanisms such as angiogenesis (Pola *et al.*, 2001).

In the last century, pathologist Robert Gorlin described a syndrome that predisposes to BCC (Gorlin and Goltz, 1960; Gorlin, 1995). Although the syndrome was initially named after him (i.e., Gorlin's syndrome), it is nowadays known as Nevoid Basal Cell Carcinoma Syndrome (NBCCS). NBCCS was quickly linked to germline *PTCH1* mutations (Hahn *et al.*, 1996; Johnson *et al.*, 1996), connecting the SHH pathway to these types of cancer. This was reinforced by studies that identified loss-of-function mutations in *PTCH1* in 90% of sporadic BCC (Gailani *et al.*, 1996; Aszterbaum *et al.*, 1998). Remaining patients frequently harbour activating mutations in *SMO* (Reifenberger *et al.*, 1998; Xie *et al.*, 1998) The relationship between cancer and SHH-signalling is further illustrated by the name-giving of GLI proteins (glioma-associated oncogene) after it was initially discovered in human glioma (Kinzler *et al.*, 1987). Additional members of the GLI protein family (*GLI1,2,3*) were identified through their homology with *GLI1* (Ruppert *et al.*, 1988) and have distinct roles in cancer (Niewiadomski *et al.*, 2019). Overactive SHH signalling is found in many types of cancer (reviewed in Toftgård, 2000) but might be best known for its role in the aetiopathogenesis of the second most prevalent subtype of MB.

1.4 SHH medulloblastoma

SHH-MB arise from GCPs that acquire mutations in SHH-pathway regulators, leading to uncontrolled proliferation and failure to differentiate. The role of SHH signalling was recognised early on through the increased incidence of MB in patients with germline *PTCH1* loss-of-function (LOF) mutations (Lacombe *et al.*, 1990) and later confirmed using molecular profiling (Kool *et al.*, 2008). In fact, *PTCH1* is the most frequently altered gene in SHH-MB (44%) (Skowron *et al.*, 2021), followed by

activating mutations in *SMO* (9-12%), LOF mutations in *SUFU* (10%) and *TP53* (8-11%), and amplifications of *GLI2* (9%) and *MYCN* (6-7%) (Kool *et al.*, 2014; Northcott *et al.*, 2017; Skowron *et al.*, 2021). The prevalence of germline mutations that predispose to MB is high in SHH-MB, especially compared to the other subtypes. Over 40% of all SHH-MB cases harbour inherited mutations (Waszak *et al.*, 2018, 2020) and 4.5% have heterozygous germline *PTCH1* mutations.

Most of aberrant SHH-signalling in MB biology involves impaired degradation of GLI activating domains. As reviewed in section 1.3.1, PTCH1 normally prevents SMO from locating to the primary cilium and allows proteasomal processing of GLI proteins to remove the activating domains in the proteasome. In the case of PTCH1-LOF, impairment of this regulation allows SMO to locate freely to the primary cilium and facilitate signal transduction that prevents proteasomal processing (*Figure 1.7*). Activating mutations in SMO cause a strong localisation of SMO to the primary cilium, independent of SHH presence (Chen *et al.*, 2002) resulting in a similar effect. Downstream of SMO, SUFU is well known as a tumour suppressor in MB (Taylor et al., 2002), and germline SUFU-LOF is associated with an increased risk of MB (7.4%) due to its role in GLI2/3 processing. In addition to SUFU, there are various intracellular pathways involved in GLI-protein modification, and dysregulation of these pathways are associated with SHH-MB. Protein kinase A (PKA) phosphorylates GLI2 and 3 and induces degradation (Pan, Wang and Wang, 2009; Niewiadomski *et al.*, 2014). Cyclic adenosine monophosphate (cAMP) is increased by G_s protein α subunit ($G\alpha s$) – mediated adenylyl cyclase activation and regulates PKA activity (Dorsam and Gutkind, 2007; Tuson, He and Anderson, 2011; Nozawa, Lin and

Chuang, 2013). Mutations in *GNAS*, the gene encoding for Gαs, are found in 4.4% of SHH-MB (Skowron *et al.*, 2021) and cause MB in *Gnas*-/- mice (He *et al.*, 2014). Furthermore, reduced PKA activation in *Gnas* mutant MB results in increased GLI2 activation and accumulation at the primary cilium of GCPs, leading to overactive SHH signalling. The importance of GLI2 in SHH-signalling (see section 1.3.1) is further emphasised by the frequency of MB caused by *GLI2*-overexpression or amplifications. *GLI2* alterations are rarely accompanied by mutations in other SHH-signalling components (Skowron *et al.*, 2021) since additional mutations do not confer additional survival or proliferation advantage. Other pathways that have been linked to GLI-protein processing include the PI3K/AKT/mTOR pathway, exemplified by the incidence of *PIK3CA* mutations (8%) in SHH-MB. While *Pik3ca* mutations alone are not sufficient to cause MB in mouse models, they accelerate MB growth in combination with activating *Smo* mutations or *Ptch1* LOF (Niesen *et al.*, 2020). Collectively, mutations in these key pathway regulators are seen in 86% of all SHH-MB, clearly defining the role of SHH-signalling in this MB subtype (*Figure 1.7*).

In 45% of SHH-MB cases, alterations in genes controlling the cell cycle and DNA damage repair are found (Skowron et al., 2021). A significant portion of SHH-MB is caused by mutations affecting the expression (6-7%) (*Figure 1.7*) or stability of MYCN (10.2% in SHH-MB). MYCN is part of the MYC-protein family and is well known for its role in cerebellar neurogenesis (see section 1.2.3) (Hatton et al., 2006; Knoepfler et al., 2002). Through its role as a transcription factor, MYCN induces the expression of genes involved in cell proliferation (Kenney *et al.,* 2004) and regulates stem cell maintenance and differentiation (Yoshida, 2018). Mutations in *MYCN* have

been associated with poorer prognosis in infants (Park *et al.,* 2012), and direct targeting is difficult due to its essential role in normal development and stem cell maintenance.

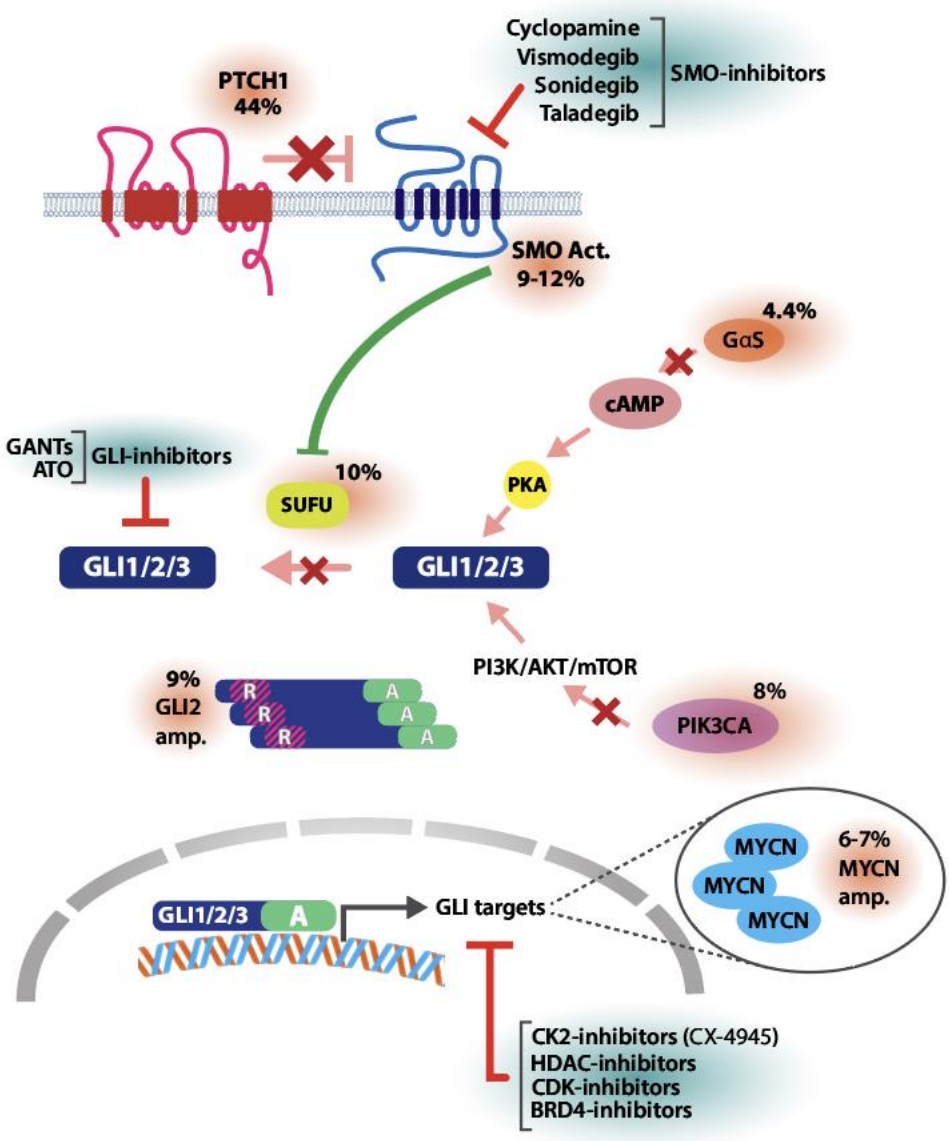


Figure 1.7: SHH-pathway mutations in medulloblastoma and targeted therapies. Mutation frequencies are depicted in percentages. *Loss-of-function (LOF) mutations in PTCH1 occur in 44% of SHH-MB and impair the inhibition of SMO. Mutations in SMO that render it resistant to PTCH1 inhibition (SMO activating mutations) and cause MB in 9-12%. Processing GLI-proteins to their repressor form is impaired by SUFU-(10%), GαS-(4.4%) and PIK3CA mutations (8%). Amplifications of GLI2 and downstream target MYCN are seen in 9% and 6-7%, respectively.*

1.4.1 Targeted treatment

The identification of the SHH pathway as the driving element in this subtype of MB provides opportunities for targeted treatment. One of the first SHH-signalling inhibitors was a naturally occurring steroid alkaloid that was discovered after it caused cyclopia in sheep (Chen, 2016). Cyclopia is a form of holoprosencephaly characterised by the failed division of the orbital cavity, resulting in a single eye in the centre of the face. Furthermore, it is a hallmark phenotype of SHH deficiency, and the molecule was named Cyclopamine. Cyclopamine functions as an SMO antagonist (*Figure 1.7*) (Cooper *et al.*, 1998; Taipale *et al.*, 2002) but showed unacceptable adverse effects and cytotoxicity for clinical application. In 2009, Vismodegib, showed antitumour efficacy in mouse allograft models of SHH-MB (*Figure 1.7*) (Robarge *et al.*, 2009). Vismodegib was the first SHH-pathway inhibitor that gained FDA approval and has now been used in several clinical trials for relapsed or refractory SHH-MB (NCT00939484, NCT01601184, NCT01239316 and NCT00822458). However, tumours rapidly acquired resistance to this treatment, leaving questions as to which patients are best served with this treatment (Lou, Nelson and Kool, 2019). Another SMO inhibitor, Sonidegib, has shown promising effects in mice (Pan *et al.*, 2010) and phase I studies (Kieran *et al.*, 2017). However, like Vismodegib, some tumours develop resistance through additional mutations that reactivate SHH signalling (Buonamici *et al.*, 2010). Although these drugs are currently the most advanced treatments specifically targeting the SHH pathway, they rely on SMO being a factor in the overactive SHH signal. Tumours with genetic alterations downstream of SMO are barely affected by the treatment, explaining varying treatment responses (Kool

et al., 2014). Therefore, efforts have been made to directly target the effects of GLI-protein-induced transcription activation. Direct GLI antagonists (GANTs) (Lin *et al.*, 2016)and arsenic trioxide (ATO) (Beauchamp *et al.*, 2011) have shown antitumour effects in preclinical models (*Figure 1.7*). Furthermore, inhibition of GLI-targets such as BRD4 (Tang *et al.*, 2014), CK2 (Purzner *et al.*, 2018), CDK (Liu *et al.*, 2019) and HDACs (Dhanyamraju *et al.*, 2015; Coni *et al.*, 2017) have shown antitumour effect in mouse models but have yet to reach clinical trials (*Figure 1.7*). Although many promising therapies are being developed, few reach clinical trials. This is, in part, due to limitations in currently available preclinical models. Thus, new models that better recapitulate human SHH-MB biology are urgently needed to overcome this gap between bench and bedside.

1.5 Classic SHH-medulloblastoma models

1.5.1 Cancer cell lines

The establishment of cell lines from various types of malignancies has enabled the study of cancer biology *in vitro*. Over the past four decades, more than 40 MB cell lines have been continuously cultured and used by researchers (reviewed by Ivanov et al., 2016). Immortalised cell lines are easy to maintain and provide a cost-effective and unlimited model to study MB. The SHH-MB cell line DAOY was established over 30 years ago (Jacobsen, Jenkyn and Papadimitriou, 1985) and has been studied extensively (Srivastava and Nalbantoglu, 2008; Martelli *et al.*, 2016). Despite the widespread use, few discoveries translate to clinical progress due to limitations inherently associated with cell line cultures.

Conventional cell line culture as two-dimensional (2D) monolayers lack an extracellular matrix and a pathophysiological tumour microenvironment (*Figure 1.9*). In recent years, both have been recognised for their significant roles in cancer progression and treatment evasion (Jin and Jin, 2020; Winkler *et al.*, 2020), emphasising the need to include these factors in preclinical models. Moreover, long-term maintenance of cell lines has homogenised these cultures, while tumour heterogeneity is suggested as a main source of treatment resistance (Dagogo-Jack and Shaw, 2018). Drug-resistant populations within tumours are positively selected, causing treatment failure and tumour recurrence. Another difficulty with MB cell lines, and cancer cell lines in general, is the strong selection bias towards aggressive phenotypes. Exemplary of this is the high percentage of *TP53*-mutant SHH-MB cell lines (50%) compared to only 8-11% of *TP53* mutations found in SHH-MB patients. Furthermore, DAOY and UW228 cells are used in over 50% of all publications on MB, while neither harbour one of the main tumour-driving mutations (e.g., *PTCH1, SMO, SUFU*), thus restricting the translational potential of *in vitro* findings. Finally, tumour cell lines have also been reported to undergo genetic drift and acquire additional mutations that are specific to *in vitro* conditions (Ben-David *et al.*, 2018). Collectively, these limitations have stimulated the search for improved MB models that better recapitulate true pathophysiology.

1.5.2 Genetically engineered mouse models (GEMMs) that model genetic predisposition

Genetically engineered mouse models (GEMMs) overcome several of the issues associated with monolayer cell line culture. Various SHH-MB models are currently in

use for preclinical research and therapy testing (reviewed in Roussel & Stripay, 2020). The *Ptch1*+/- mouse model by Goodrich et al. (1997) has been extensively studied and was generated by homologous recombination targeting exons 1 and 2, flipping the orientation of the protein in the cell membrane and causing LOF. While mouse embryos lacking functional Ptch1 died between embryonic day (E) 9.0 and 10.5 due to abnormal heart development of the heart. Furthermore, a subset of heterozygous mice developed a similar phenotype to human NBCCS patients. This included the development of tumours resembling MB in a small number of cases. However, this model showed a low penetrance and long latency of tumour formation, similar to the human syndrome, and is therefore less suited for high-throughput research applications.

Several additional mutations were found to promote tumorigenicity in mice. *Tp53* mutations in *Ptch1+/-* mice remarkably increased tumour incidence to over 95% and accelerated tumour progression (Wetmore, Eberhart and Curran, 2001). Further studies corroborated these findings and found several other genes involved in DNA repair and cell cycle regulation to increase MB incidence in *Ptch1+/* mice (Lee *et al.*, 2003; Uziel *et al.*, 2005; Briggs *et al.*, 2008a; Ayrault *et al.*, 2009; Tamayo-Orrego *et al.*, 2016a). However, strong evidence for the co-occurrence of these mutations in humans is lacking. Moreover, recent studies found *PTCH1* and *TP53* mutations to be mutually exclusive (Skowron *et al.*, 2021), questioning the relevance of these models. Conditional knockout of *Ptch1* has proven a successful alternative for medulloblastoma modelling and helped uncover GCPs as the cell-of-origin of SHH-MB (Yang *et al.*, 2008). Moreover, restriction of this genomic event to cells expressing

Gfap, Nestin or *Atoh1* greatly reduced tumour latency and increased tumour penetrance to 100% (Schüller *et al.*, 2008; Yang *et al.*, 2008; Li *et al.*, 2013). In addition to the variety of *Ptch1+/-* models, expression of constitutively active Smo variant SmoA1 in *Neurod2*-expressing cells (ND2:SmoA1) resulted in a tumour incidence of 48% in heterozygous (Hallahan *et al.*, 2004) and 94% in homozygous mice (Hatton *et al.*, 2008). While cerebellar development of ND2:SmoA1 mice was not significantly altered, a second Smo variant, SmoA2, caused severe cerebellar dysplasia concurrently with tumorigenesis at similar rates (Dey *et al.*, 2012). Mice with heterozygous *Sufu*-LOF mutations require an additional driver event for MB growth and show lower rates of MB-formation compared to *Ptch1+/-; Tp53-/-* mice (58% vs 93%) (Lee *et al.*, 2007).

Although *Ptch1+/-* and other models capture relevant aspects of MB biology, several limitations arise from interspecies differences (*Figure 1.9*). Genetic events are known to have vastly different effects in mice compared to humans. Specifically, mice harbouring *Tp53* mutations mainly develop sarcomas, while in humans, this predisposition is associated with the development of carcinomas (Jacks *et al.*, 1994; Bouaoun *et al.*, 2016). Furthermore, mutations in the tumour suppressor gene *Rb* cause pituitary adenomas in mice, compared to retinoblastoma in humans (Jacks *et al.*, 1992). Specific to MB, there is a significant mismatch between human and mouse models, with most models displaying classic histology and few exhibiting metastatic phenotypes (Ivanov *et al.*, 2016) As a result, few treatments reach clinical testing due to the failure of mouse-to-human translation and the limited variety of models.

1.5.3 Patient-derived xenografts

Orthotopic introduction of patient-derived xenografts (PDX) provides an alternative way to study human-specific tumour biology while benefiting from the presence of a microenvironment. In PDX models, tumours are xenografted into immunocompromised mice and can be serially transplanted and expanded. Compared to monolayer culture, this technique better preserves intra-tumour heterogeneity (Byrne *et al.*, 2017), and PDX tumours remain molecularly similar to the primary tumour (Zhao *et al.*, 2012). In MB, tumour cells are found at various stages of differentiation, making cell type-specific treatment strategies challenging and emphasising the need for models that capture this intratumor heterogeneity. However, PDX are costly, time-consuming and, similar to cancer cell lines, suffer from selection bias towards aggressive genotypes (*Figure 1.9*). The lack of a functional immune system also takes away an important element that has been gaining attention since the development of immunotherapies. Although this may be overcome by humanised PDX models with human immune systems, no such model yet exists for MB. In addition to the absent immune system, PDX have been shown to undergo mouse-specific tumour evolution in other cancers (Ben-David *et al.*, 2017), questioning their translatability and arguing for complete human models.

1.6 Induced pluripotent stem cells and their potential for MB modelling

While the classic models for MB have provided invaluable insights into MB tumour biology and aided drug testing and discovery, their limitations remain a significant reason for the existing gap between bench and bedside. Innovative models that capture human-specific tumour biology and progression within a relevant microenvironment are urgently needed to further our understanding and improve the treatment of MB patients. In addition, the gained knowledge of molecular subtypes within MB has not been used to its full potential and is limited by the lack of models that faithfully capture human biology.

1.6.1.1 Induced pluripotent stem cells (iPSC)

The emergence of human induced pluripotent stem cell (iPSC) technology has resulted in new possibilities for tissue- and disease modelling (*Figure 1.8*). IPSC can be derived from post-mitotic, differentiated somatic cells through reprogramming cells back into a pluripotent stem cell state. These cells can then be differentiated into almost every cell type in the human body, allowing the study of development and specific cell types such as neurons. Although human embryonic stem cells (ESC) already enabled the generation of specific cell types and organ-like structures (hereafter referred to as organoids), their use is limited through ethical constraints related to the embryonic origin (reviewed in de Wert & Mummery, 2003 and Robertson, 2001) The generation of iPSC from consenting adults overcomes some of these constraints and may be the revolution that unleashes the full potential of stem

cell research. Furthermore, the derivation of iPSC from carriers of genetic conditions brings new opportunities to study patient- and disease-specific cell biology.

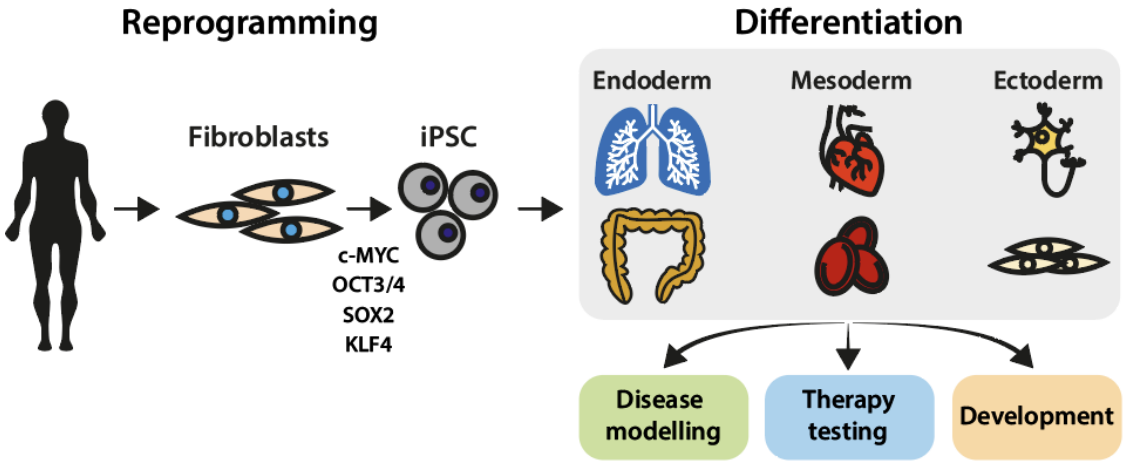


Figure 1.8: Induced pluripotent stem cells (iPSC). *Somatic cells, such as skin cells from healthy donors and patients, can be reprogrammed by Yamanaka factors c-MYC, OCT3/4, SOX2 and KLF4 to pluripotent stem cells, the iPSC. These cells can be differentiated into cell types from all three germ layers, including alveolar epithelial cells, cardiomyocytes and neurons. Generated cells can be used for disease modelling, therapy testing and the study of human development.*

Induced pluripotent stem cells can be generated from somatic cells through reprogramming. This process was first developed by Shinya Yamanaka, who discovered that the induced expression of four key genes (*c-MYC, OCT3/4, SOX2* and *KLF4*), now known as the Yamanaka factors, could convert cells back into a pluripotent stem cell state (Takahashi and Yamanaka, 2006). Initial work was performed in mice, and the technique rapidly translated to human research (Takahashi *et al.*, 2007). While the earliest methods of introducing the Yamanaka factors into cells used retroviral delivery systems (Takahashi and Yamanaka, 2006) and then lentiviruses (Sommer *et al.*, 2009), non-integrating systems such as episomal plasmids (Junying *et al.*, 2009; Okita *et al.*, 2011), synthetic mRNAs

(Warren *et al.*, 2010) and Sendai viruses (Fusaki et al., 2009; Nishimura et al., 2011) are now most commonly used to improve safety and potential for clinical application.

Before the emergence of pluripotent stem cell (PSC) differentiation protocols, the study of the human central nervous system (CNS) *in vitro* was difficult to realise due to the delicate nature of the brain that limits the harvest of primary cells. Even more challenging was the study of the developing human brain as mouse models do not completely recapitulate human neurogenesis, and the use of human embryos faces ethical dilemmas. Differentiating PSC (ESC and iPSC) into various types of CNS cells offers unprecedented opportunities to study the earliest aspects of neurogenesis as well as CNS cellular biology.

Despite its tremendous promise, some challenges affect PSC research. Variability between PSC lines due to donor differences as well as their sensitivity to small variations in experimental conditions are well known to hinder reproducibility of results (Volpato and Webber, 2020). In addition, PSC are prone to acquire karyotypic abnormalities, necessitating frequent genome integrity testing (Taapken *et al.*, 2011). Specific to iPSC, the retention of the epigenetic signature of the donor tissue can influence gene expression in low passage iPSC (Kim *et al.*, 2010, 2011), while this 'epigenetic memory' is increasingly erased in higher passage cells (Nishino *et al.*, 2011). When interpreting results from PSC differentiations, these limitations should be taken into consideration.

1.6.1.2 Orthotopic injection of MB-iPSC and derived cell types

Several studies have illustrated the use of iPSC for MB modelling combining neuroepithelial stem cell (NES) differentiation with the introduction of SHH-MB driver events (*Figure 1.9*) (Čančer et al., 2019; Huang et al., 2019; Susanto et al., 2020). Transformed NES were orthotopically injected into mice and effectively formed tumours resembling the human disease. NBCCS-patient-derived iPSC (*PTCH1+/-*) produced tumours with varying latencies between donors (100-360 days) (Huang *et al.*, 2019; Susanto *et al.*, 2020). Further investigation of this variation found additional genetic events to affect the tumorigenicity of the different clones. While these studies highlight the potential of iPSC-derived MB models, the requirement of orthotopic injection restricts widespread adoption similar to PDX models. Furthermore, mouse-specific effects on tumour biology may affect findings and limit translation.

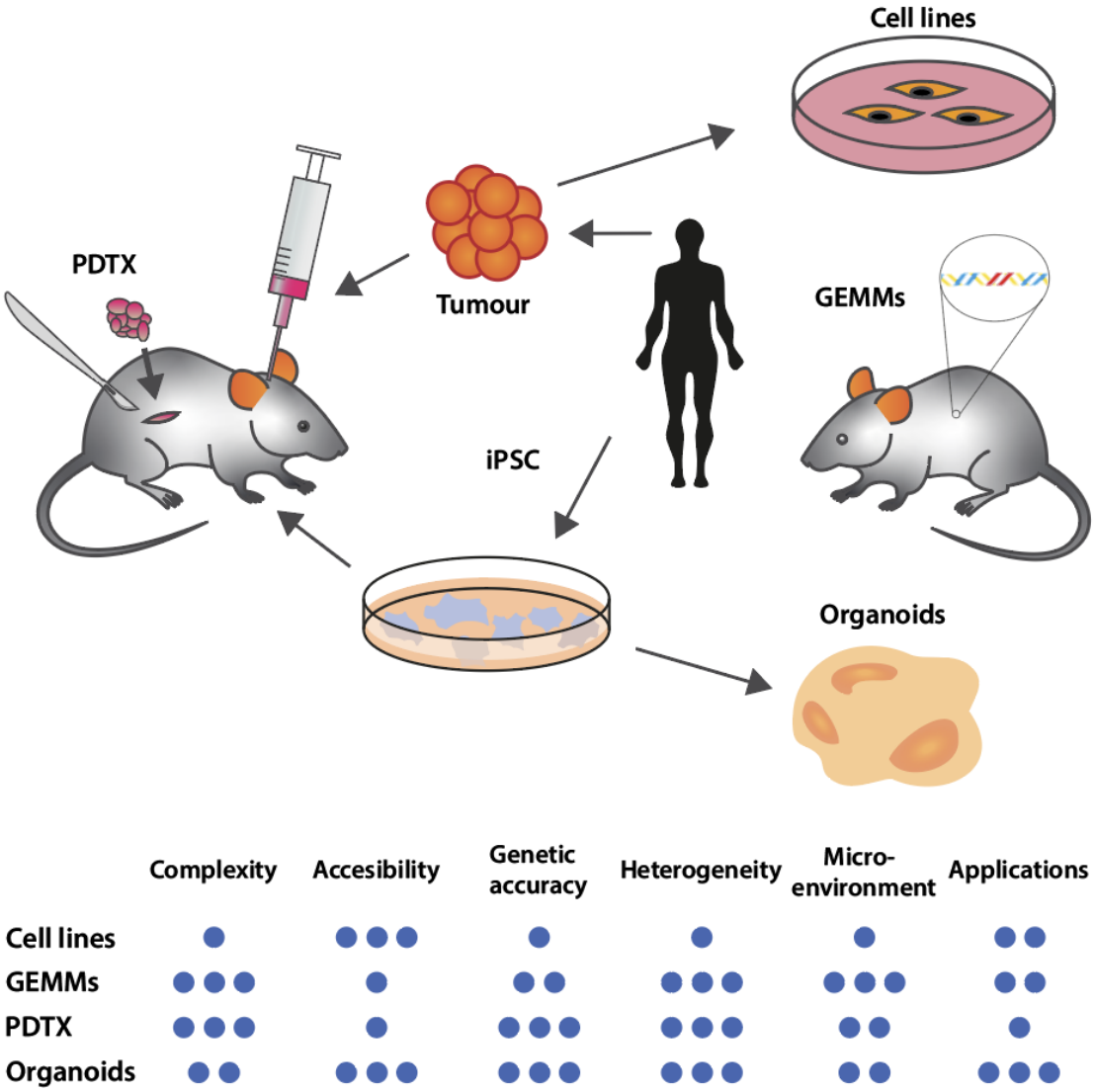


Figure 1.9: Medulloblastoma models. *Cell lines derived from tumours and maintained for prolonged periods of time provide accessible models for preclinical research at the expense of complexity, heterogeneity and a microenvironment. Genetically engineered mouse models (GEMMs) harbour known MB-driver mutations. GEMMs provide in vivo complexity and a microenvironment but lack accuracy in recapitulating human-specific effects of genetic events. Patient-derived mouse models (PDX) are generated through the transplantation of tumour tissue into mice, either orthotopic or subcutaneous. Limitations are an incomplete microenvironment due to the use of immunocompromised mice and the restricted access to live tumour tissue. Organoids derived from induced pluripotent stem cells (iPSC) capture important aspects of the microenvironment and are genetically accurate and accessible to researchers. Complexity is largely preserved, and heterogeneity develops as found in human tumours. Organoids can be used in a wide variety of applications, such as gene editing, therapy testing and genomics*

.

1.6.1.3 Organoids and their potential for in vitro iPSC-MB modelling

In vitro modelling of the cerebellum using PSC-derived organoids provides an alternative to mouse models and offers exciting opportunities for disease modelling. Organoids contain various different cell types and model essential aspects of human development. Cerebellar organoids have been shown to contain all major cerebellar developmental cell types, including GCPs (Nayler *et al.*, 2021). Several groups have now used iPSC to study cerebellar diseases *in vitro,* such as spinocerebellar ataxia (Ishida *et al.*, 2016), autism spectrum disorder (Sundberg *et al.*, 2018) and more recently, MB (Ballabio *et al.*, 2020, 2021). Using electroporation transfection, group 3-MB drivers were introduced into five-week-old cerebellar organoids (Ballabio *et al.*, 2020). The combination of either *OTX2*- or *GFI1*-overexpression with *c-MYC* overexpression resulted in growths resembling the human disease and could be used for *in vitro* therapy testing. Using conditional overexpression, specific cerebellar neural stem cell lineages susceptible to malignant transformation could be identified (Ballabio *et al.*, 2021). These reports illustrate how *in vitro* cerebellar organoids may be used for verification of findings in recent genomic studies on the cell-of-origin of group 3 MB.

1.7 Aims of thesis

The high frequency of *PTCH1* mutations in SHH-MB and the failure of targeted therapies in clinical trials present a clear need for advanced, human-specific models that overcome the limitations of currently available models. This thesis proposes a novel way to model germline SHH-MB predisposition, combining cerebellar organoid differentiation with the gene editing technique Clustered Regularly Interspaced Short Palindromic Repeats (CRISPR). In addition, alternative methods for medulloblastoma modelling using cerebellar organoids will be explored.

This thesis describes the following aims:

1. Generate genetically engineered human induced pluripotent stem cells to harbour the MB-driver mutation *PTCH1*.
2. Characterise the effects of PTCH1 LOF on cerebellar differentiation.
3. Explore alternative methods for medulloblastoma modelling in cerebellar organoids.

Chapter 2 Methods

2.1 iPSC culture

The human induced pluripotent stem cell (iPSC) line AH017-3, used in this research, was derived from the fibroblast of a healthy a 67-year-old female donor recruited through the Oxford Parkinson's Disease Centre (Handel *et al.*, 2016). This donor has given signed informed consent for the use of this line for research. The Ethics Committees that specifically approved this part of the study National Health Service, Health Research Authority, NRES Committee South Central, Berkshire, UK, REC 10/H0505/71). All experiments were performed in accordance with UK guidelines and regulations and as set out in the REC. The donor's fibroblasts were reprogrammed using Sendai virus vectors expressing the Yamanaka factors: Oct3/4, Sox2, Klf4, and c-Myc.

Induced pluripotent stem cells were cultured on tissue culture plates coated with hESC-qualified Matrigel matrix (Corning®, Cat# 354277) in mTeSR 1 medium (Stemcell Technologies, Cat# 85850) or OXE8 medium (2 mM GlutaMax, 0.1 μg/mL Heparin, 0.22 mM Ascorbic Acid, 15 mM HEPES pH 7.4, 100 ng/mL FGF2, 2ng/mL TGFβ in Advanced DMEM/F12) (Vaughan-Jackson *et al.*, 2021). iPSC require a basement membrane extract (BME) to grow *in vitro* and a culture medium containing Fibroblast growth factor 2 (FGF2) and Transforming growth factor beta (TGF-β). Matrigel was aliquoted following the manufacturer's instructions and diluted in F-12 (Gibco™, Cat# 31765027). iPSC-containing cryovials were defrosted in a 37°C water bath, pelleted at 300 x *g* for 5 minutes and resuspended in a culture

medium containing 10 μM Rho kinase inhibitor (Ri) Y-27632 (Abcam, Cat# ab120129). iPSC were typically plated in 6-well or 12-well plates. The culture medium was changed daily, and iPSC were passaged at 70-80% confluency. Areas of differentiation are microscopically identifiable as cells losing the typical iPSC morphology: round cells with large nuclei and little cytoplasm packed in colonies with distinct borders and defined edges. Macroscopically, differentiation is visible as white specks. Prior to any passage, areas of differentiation were mechanically removed using a pipette tip and aspirated. To detach iPSC, cells were incubated with 0.5 mM EDTA in PBS for 5 minutes. Subsequently, the EDTA solution was taken off, and cells were resuspended in a culture medium and split in a ratio of 1:4-1:8, depending on the intended use. To minimise the chance of karyotypic changes, cells were kept in culture for a limited number of passages and no longer than five weeks. For each new experiment, a vial was used from the original master stock. This stock had passed quality control including single nucleotide polymorphism (SNP) genotyping and mycoplasma testing (see section 2.3).

2.2 CRISPR-gene editing of iPSC

2.2.1 gRNA design

Using the online tool CCtop (Stemmer *et al.*, 2015), a pair of gRNAs were designed to excise a 200 bp sequence, including the SD of exon 3 of the *PTCH1* gene (Table **2-1**). The two gRNAs were selected based on their specificity score, predicted efficiency and the number of off-target sites. Only gRNAs of which the top off-target sites contained more than four or more mismatches were considered. Ultimately, the

exonic gRNA GT GTT GTA GGA GCG CTT CTG and intronic gRNA GA TTT ATC GTT TCT CGA GTT were picked. Off-target sites are listed in Appendix Table **4**.

Table 2-1: Guide RNA sequences and genotyping primers.

Oligonucleotide	Sequence	Direction	Tm
Exonic gRNA	GTGTTGTAGGAGCGCTTCTG	3' - 5'	-
Intronic gRNA	GATTTATCGTTTCTCGAGTT	3' - 5'	-
Genotyping primer Forward	TACTGCTCACACATCAGCCAG	5' - 3'	56°C
Genotyping primer Reverse	AGTTCAGCAAGGGCAATTCAA	3' - 5'	56°C

2.2.2 Transfection

Per transfection reaction, one 24-well-plate-well was first coated with Geltrex (Life Technologies, Cat#A141133-02) and filled with mTeSR® + 10 μM Ri. In addition, one 6-well-plate-well of iPSC at 80% confluency was selected and pre-treated with 10 μM Ri (Abcam, Cat#ab120129) for 1 hour before transfection. During this incubation, the gRNAs were mixed with tracrRNAs into crRNA/tracrRNA hybrids in a 1:1 ratio at a final concentration of 44 μM sgRNAs in Buffer R (Life Technologies, NeonTM Transfection System Cat#MPK10096) and heated to 95°C. After cooling, both crRNA/tracrRNA hybrids (exonic and intronic) were added together in a 1:1 ratio and half of that mixture was complexed with 36 μM Alt- R® S.p. HiFi Cas9 Nuclease V3 (IDT, Cat#1081060) in Buffer R for 20 minutes at room temperature to form ribonuclease proteins (RNPs). After incubation with Ri, iPSC were detached using 0.5 mM EDTA in PBS and resuspended into a single cell suspension and centrifuged at 200 x *g* for 4 minutes. After pelleting, the supernatant was aspirated, and cells were resuspended in Buffer R at a final concentration of 2.2 x 10^7 cells / mL. To make the electroporation mix, 9 μL cell suspension (200,000 cells total) was combined with 1 μL RNPs was mixed with and 2 μL transfection enhancer (IDT,

cat#1075915). This mixture was electroporated using a Neon pipette (Life Technologies, NeonTM Transfection System Cat#MPK10096; HiTrans 1400V 20ms width, one pulse) using the 10 μL Neon pipette tips. Immediately after electroporation, cells were transferred into the prepared 24-well plate-well containing pre-warmed mTeSR® + Ri, and the plate was returned to the incubator. The medium was changed daily in the following days. Once the cells reached confluence, the cells were detached using 0.5 mM EDTA in PBS. Half of the cells were pelleted for genomic DNA extraction to assess the efficiency of the CRISPR reaction, and the other half was frozen down in a freezing medium containing 10% dimethyl sulfoxide (DMSO) (Sigma, Cat#D2650) and 30% embryonic stem cell grade FCS (Life Technologies, Cat#16141-079).

2.2.3 Genomic DNA extraction by DNeasy kit

DNA was extracted using the DNeasy kit (Qiagen, Cat#69504), and DNA was resuspended in 50 μL TE buffer. The target region was amplified using polymerase chain reaction (PCR) over 40 cycles at 56°C with primers targeting 100bp upstream of the exonic gRNA and 100bp downstream of the intronic gRNA. The PCR product was visualised using a 1% Agarose in TAE gel. The mutant product was expected to be 200-bp shorter compared to the wildtype sequence. The ratio of the intensity of both bands was used as an indication of CRISPR efficiency.

2.2.4 Single-cell plating and clone picking

From the pool of successfully transfected cells, individual clones were selected. This procedure aims to select clones derived from a single cell. To improve survival, iPSC

are thawed on a mouse embryonic feeder layer. Therefore, one day prior to the thawing of the pool, irradiated mouse embryonic feeder (MEF) cells plated on a 0.1% gelatin (Sigma, Cat#G1393-100ML) coated 6-well plate in a density of 200 cells / cm^2 and cultured in MEF medium (10% FCS, 1X GlutaMAX and 1/1000 β -Mercaptoethanol in Advanced DMEM). The day after, the transfected pool was thawed as described above and plated onto the MEFs, and cultured in Knock out DMEM (Gibco™, Cat#10829) containing 20% knock out Serum replacement (Gibco™, Cat#10828), 1% Non-essential Amino acids (Gibco™, Cat#11140), 1% GlutaMAX (Gibco™, Cat#35050), 0.1% 2-Mercaptoethanol (Gibco™, Cat#31350), 1% 10.000 U/L Penicillin/Streptomycin (Gibco™, Cat#15140-122) and 5 ng/mL FGF2 (R&D, Cat#234-FSE/CF). Cells were seeded at 1,000, 2,000, and 4,000 cells per well. Half-volume medium changes were performed daily until colonies could be identified. This was usually after seven days of culture.

Prior to harvesting clones, a flat-bottom 96-well plate was coated with Geltrex for 1 hour. The medium of the iPSC clones was changed with mTeSR + 10 μM Ri one hour prior to clone picking. Clones were visualised using a dissecting microscope placed in a tissue culture hood. A clone was picked using a wide bore p200 pipette tip (made by cutting off the end) and transferred into a well of the prepared 96-well plate. Clones were cultured and, after reaching confluency, expanded to 3 x 96-well plates in total. One of these plates was used for DNA extraction; the other two plates were frozen in freezing medium as described above.

2.2.5 Genomic DNA extraction by ethanol precipitation

DNA extraction was performed in the 96-well plate. Cells were rinsed with PBS and lysed in lysis buffer (10mM tris pH 7.5, 10mM EDTA, 10mM NaCl, 0.25% triton X-100, 1mg/ml proteinase K (Sigma, P6556-100mg)) overnight at 55°C. The next day, an ice-cold precipitation solution (5M NaCl in 100% Ethanol) was added and left for 2 hours to precipitate the DNA. After expelling the solution, the plate was washed with 70% ethanol and left to air dry. DNA was resuspended in diH_2O by incubation at 4°C overnight, and concentration was quantified using NanoDrop. Identification of mutant clones was done using PCR with the primers as described above. Five homozygous clones, identified by a single band of 200bp shorter size than the wildtype sequence, and seven heterozygous clones, identified as containing both the wildtype and mutant PCR product, were selected.

2.2.6 Clone selection and expansion to master stock

These clones were taken from the previously frozen plate by first thawing the plate in the incubator before transferring all of the wells into a V-bottom 96-well plate. This plate was centrifuged at 400 x *g* for 3 minutes. Most of the medium was removed without disturbing the cell pellet, and cells of the selected clones were resuspended in mTeSR and plated into a Geltrex-coated 24-well plate containing warm mTeSR. Cells were expanded to create a master stock. All downstream experiments were performed using these master stocks.

2.3 Quality control on CRISPR-edited iPSC

2.3.1 Sanger sequencing of region of interest

Genomic DNA was isolated using the DNeasy kit, as described above (see section 2.2.3). Wildtype and mutant bands were excised and processed using the NEB gel extraction kit following the manufacturer's instructions. The products were submitted for Sanger sequencing using the Genotyping primer Forward primer to confirm the deletion of the 200 bp region.

2.3.2 SNP analysis

Genomic DNA from the master stocks of each clone was also submitted to a genotyping array to test for gross chromosomal aberrations. The Infinium Global Screening Array-24 v3.0 (Illumina) measures over 650,000 SNPs in the human genome, allowing the comparison with the originating iPSC line. Results were analysed using Genome Studio software.

2.3.3 Mycoplasma detection

After the generation of the master stocks, each clone was also tested for mycoplasma using the MycoAlert PLUS Mycoplasma detection kit (Lonza cat# LT07-703). This kit utilises the conversion of ADP to ATP by enzymes produced by mycoplasma and is reported to detect close to 200 different mycoplasma species. For the assay, the supernatant of iPSC cultured for 24 hours was centrifuged at 400 x *g* for 5 minutes. The assay was then performed following the manufacturer's instructions with the addition of multiple reads after the application of the substrate to gain certainty in

the result. Samples that showed a read-B/read-A ratio below one were considered negative. None of the tested iPSC clones showed any presence of mycoplasma.

2.3.4 Flow cytometry

Expression of pluripotency markers Tra-1-60 and NANOG was measured using flow cytometry. iPSC were detached using TrypLE and fixed in 2% PFA for 10 minutes before permeabilisation with 100% methanol. Permeabilized cells were washed with FACS buffer (1% FBS, 10ug/mL IgG from human serum, 0.01% Sodium azide in PBS) and incubated with antibodies against Tra-1-60 (Biolegend Cat#330614, 1:100), NANOG (Cell Signalling cat#5448S, 1:100) of isotype control antibodies (IgM 488 Biolegend cat#401617 or IgG 647 Cat# 2985S both 1:100) for 1 hour. Unbound antibody was washed off with FACS buffer, and cells were submitted for flow cytometry analysis.

2.4 Characterisation CRISPR-edited iPSC

2.4.1 RNA isolation

RNA was isolated using the RNeasy Plus mini kit (Qiagen, cat# 74034) following the manufacturer's protocol. RNA concentration was measured using a Nanodrop device. Human iPSC were lysed in RLT buffer directly in the plate and either stored at - 20°C until RNA isolation or processed immediately following the manufacturer's protocol. Three replicates extracted from different passages were collected per clone. RNA was eluted in 30 μL RNAse-free water.

2.4.2 Reverse transcription and qPCR

Subsequently, 1 μg RNA per sample was reverse transcripted into cDNA using the SuperScript™ III First-Strand Synthesis System (Invitrogen™, cat# 18080051). Standard curves to determine primer efficiency and optimal cDNA input were run prior to the experiment. RT-qPCR was performed using Fast SYBR Green Master Mix (Applied Biosystems, Cat#4385612) on the Applied Biosystems StepOne Plus qPCR machine with primers designed using Primer3Plus. The primers used are listed in (**Appendix Table 1**). Expression of genes of interest (GOI) was normalised to the expression of ACTB and GAPDH (REF) to generate delta-CT values ($\Delta CT = CT^{GOI} - CT^{REF}$). The average of these delta-CT values was used for statistical analysis and visualisation. In comparisons with a control group, ΔΔCT values were calculated ($\Delta\Delta CT = \Delta CT^{Test} - \Delta CT^{Control\ Average}$). The expression of reference genes in each experiment was subjected to statistical testing for changes associated with the different conditions. Expression of ACTB and GAPDH did not change significantly between conditions and were therefore considered suitable as reference genes.

2.4.3 SHH pathway activation

To determine SHH-pathway gene expression, iPSC were treated with 500 nM smoothened agonist (SAG) diluted in DMSO for 48 hours. Control conditions were treated with DMSO. Cells were lysed in the plate in RLT buffer for subsequent RNA extraction and processing as described above.

2.4.4 EdU proliferation assay of iPSC

The proliferation of PTCH1+/- and PTCH1-/- iPSC clones was determined using the Click-iT® Plus EdU Alexa Fluor® 647 Flow Cytometry Assay Kit (Invitrogen™, cat# C10634) following the manufacturer's protocol. In brief, cells were incubated with 10 μM of 5-Ethynyl-2′-deoxyuridine (EdU) for 2 hours, then detached using TrypLE. Cells were washed with washing buffer (1% BSA in PBS) and fixed using the Click-IT fixative for 15 minutes. After fixation, cells were washed in washing buffer and permeabilised using the Click-iT saponin-based permeabilisation buffer. Subsequently, the Click-it reaction cocktail (prepared as per the manufacturer's instructions) was added and incubated for 30 minutes. After washing, cells were analysed using flow cytometry.

2.4.1 Statistical analysis

Statistical analysis was performed in *R* programming software. Statistical difference between more than two groups was determined using ANOVA with Dunnett's post hoc test or Tukey's post hoc test. Statistical differences between two groups were performed by students t-test. P-values were corrected for multiple testing using Benjamini-Hochberg Procedure. An adjusted p-value below 0.05 was considered significant. Error bars represent standard deviation (SD) unless otherwise indicated.

2.5 Cerebellar organoid differentiation

This section describes the differentiation protocol are described resulting in the generation of cerebellar neuron progenitors (described in van Essen et al., 2022).

Different methods for long-term culture maintenance past DIV 35 are chosen based on the downstream application.

2.5.1 Embryoid body formation

One well of iPSC contains enough cells for at least two 96 well plates of embryoid bodies (EBs). This method section describes the procedure starting with one well. Scaling up was done as required.

One well of iPSC at 60-70% confluence was selected, and cells were detached using TrypLE™ Express Enzyme (1X) (Gibco™, Cat# 12604013). Cells were resuspended in PBS and centrifuged for five minutes at 400 x *g* at room temperature. Subsequently, the cell pellet was resuspended in Induction Medium (50% Iscove's Modified Dulbecco's Medium (Gibco™, Cat# 31980022), 50% Ham's F-12 Nutrient Mix (Gibco™, Cat# 31765027), 7 μg/mL insulin (10 mg/mL stock in acidic water (pH 2.0), stored in aliquots at -20°C)(Sigma, Cat# I1882), 5 mg/mL BSA (250 mg/mL stock in distilled water, stored in aliquots at -20°C)(Sigma, Cat# A3156-5G), 1% Chemically Defined Lipid Concentrate (100X stock, stored in aliquots at -20°C) (Gibco™, Cat# 11905031), 450 μM 1-thioglycerol (stored at 4°C)(Sigma, Cat# M-6145), 15 μg/mL apo-transferrin (10 mg/mL stock in distilled water, aliquots stored at -20°C)(Sigma, Cat# T1147), 1 % Penicillin/Streptomycin (10.000 U/mL stock, aliquots stored at -20°C) (Gibco™, Cat# 15140122)) containing 50 µM Rho-kinase inhibitor (Ri)(Abcam, Cat# ab120129) and 10µM SB431542 (SB)(Tocris, Cat# 1614/10) to a concentration of 1.0 - 1.2 x 10^5 cells / mL. Using a multi-channel pipette, 100 μL of cell suspension was added to each well of a low-attachment V-bottom 96-well plate (S-Bio, Cat# MS-

9096VZ or Greiner Bio-one, Cat# 651970) to allow re-aggregation and EB formation (1.0 - 1.2 x 10^4 cells per well). Plates are gently placed in an incubator at 37°C with 5% CO_2.

2.5.2 Cerebellar lineage induction

Differentiation into the cerebellar lineage was induced using FGF2 (200 ng/μL stock in PBS with 0.1% BSA, stored in aliquots at -20°C) (R&D Systems, Cat# 4114-TC-01M) added two days after the start of EB formation. First, one-fifth of the culture medium was removed and replaced with the same volume containing 250 ng/mL. This results in a final concentration of 50 ng/mL FGF2 in each well. Subsequent medium changes were performed weekly. On day in vitro (DIV) 7, one-third of the medium was changed, and on other days the medium was changed in full. After two weeks of total culture, organoids were transferred from the 96-well plate into low-attachment 48-well plates (Greiner Bio-one, Cat# 677970). Prior to the transfer, 48 well plates were filled with 200 μL of Induction Medium and plates were placed in the 37°C incubator for at least 15 minutes. Organoids were transferred using a wide bore p200 pipette tip (this can be made by cutting off the end of a regular p200 tip) with the pipette set to 100 μL. From this point onwards, organoids were cultured in 300 μL unless stated otherwise.

2.5.3 Cerebellar progenitor maturation up to DIV 35

On DIV 21, the culture medium was changed to Differentiation medium (Neurobasal® medium (Gibco™, Cat# 21103049), 1% GlutaMAXTM (stored at 4°C) (Gibco™, Cat# 35050061), 1% N2 supplement (100X stock, aliquots stored at -20°C)

(Gibco™, Cat# 17502048), 1% Penicillin/Streptomycin (10.000 U/mL stock, aliquots stored at -20°C) (Gibco™, Cat# 15140122)). Care was taken to remove as much old medium as possible without disturbing the organoid. 2/3 of the medium was refreshed on DIV 28 and DIV 35 of the differentiation.

2.5.4 Long-term maintenance of cerebellar organoids

Cerebellar organoids can be maintained in suspension or cultured on an air-liquid interface (ALI) on transwell membranes. While the former method preserves the 3D morphology better, the latter culture method offers advantages in improved oxygen availability (Giandomenico *et al.*, 2019). This does, however, require an additional transfer, and the organoids are less amenable to downstream applications.

2.5.4.1 Organoid culture in suspension

When kept in suspension, cerebellar organoids can be maintained for more than 90 days. After DIV 35, the medium was changed twice per week with 2/3 medium replaced. In some experiments, organoids were kept in low attachment 24-well plates to facilitate larger volumes of the medium.

2.5.4.2 Organoid culture at the air-liquid interface (ALI)

For ALI culture of cerebellar organoids, 1 mL of Differentiation Medium was added per well of a six-well plate and transwell inserts (PTFE 0.4 μm pore size) (Millicel, Cat# PICM0RG50) were gently placed on top of the medium. The plate with transwells was then returned to the incubator to equilibrate to 37°C. Using a wide bore p200 tip, individual organoids were transferred onto the membrane, taking

care not to transfer too much medium. Any residual medium was taken off with a regular p200 tip. The medium was changed fully three times per week.

2.5.5 RNA extraction and RT-qPCR from cerebellar organoids

DIV 21 gene expression levels were determined from a pool of 20-30 organoids, while gene expression at DIV 35 was determined from a pool of 10-20 organoids. RNA was extracted as described above using either the Qiagen RNeasy Micro or mini kits. Single organoids at 50, 70 and 90 days of differentiation were processed using the Qiagen Rneasy micro kit (Qiagen, Cat#74004). Per sample, 0.5 – 1 μg mRNA was reverse transcribed and CT values were generated and processed as described above (see section 2.4.2). Statistical analysis was performed as described above (see section 2.4.1).

2.6 Immunocytochemistry and microscopy

2.6.1 Procedure cryosections

Organoid samples for immunocytochemistry were fixed for 20 minutes in 4% paraformaldehyde (PFA) at room temperature, washed three times in PBS and embedded in Optimal Cutting Temperature (OCT) compound and frozen on dry ice. Samples were cryosectioned into 6-12 μm sections, placed onto microscope slides and stored at -80°C. All following steps were performed at room temperature unless otherwise specified. Prior to staining, samples were brought to room temperature and rehydrated in PBS. Samples were permeabilised in 0.3% Triton-X100 (Sigma, Cat#X100-100ML) in PBS (PBST) for 30 minutes, followed by blocking with 2% skim milk (Thermofisher, Cat#LP0031B) in PBST for 1 hour. Afterwards, overnight

incubation with primary antibodies (**Appendix Table 2**) was performed at 4°C. After washing with 0.05% Tween20 (Bio-rad, Cat#1662404) in PBS, secondary antibodies (**Appendix Table 3**) were applied and incubated for 2 hours. Subsequently, samples were washed with 0.05% Tween20 in PBS, incubated with Hoechst (Thermofisher, Cat#62249) for 10 minutes, and mounted in anti-fading mounting solution (Vectashield, Cat#H-1000-10). Immunostained cryosections were imaged using the Zeiss Axioplan 2 widefield microscope.

2.6.2 Procedure whole organoid

Whole organoids were prepared for immunofluorescence staining and imaging following an adapted protocol from Dekkers et al., 2019. Samples were fixed as described above (see section 2.6.1). Organoids were then permeabilised using 0.3% Triton- X100 in PBS (PBST) for 60 minutes and blocked in 2% skim milk in PBST for 1 hour. Primary and secondary antibodies were diluted in PBS with 0.1% Triton-X100 and 0.2% BSA and organoids were incubated at 4°C overnight. After incubation, samples were washed three times for 2 hours in washing buffer. Secondary antibody incubation was performed at 4°C overnight, followed by another three washes and subsequently incubated with Hoechst for 30 minutes. Tissues were cleared by incubating in a clearing solution (60% glycerol and 2.5 M fructose in dH_2O) for 20 minutes. After clearing, organoids were mounted on coverslips in clearing solution and imaged using the Olympus FV1000 laser scanning confocal microscope.

2.7 Flow cytometry of organoids

Cells were washed once in PBS at room temperature and enzymatically digested using Neuron Isolation Enzyme (ThermoFisher, Cat #88285). The incubation times were adjusted depending on the 'age' of the organoids. For DIV 35 organoids, digestion time was between 10 - 15 minutes. Single-cell isolation was performed as described above. To measure viability, cells were stained using the Zombie Violet™ Fixable Viability Kit (Biolegend, cat#423113), following the manufacturer's protocol. Cells were washed in FACS buffer (1% BSA in PBS). Cells were then fixed in 4% PFA for 10 minutes. For intracellular staining, cells were permeabilised using permeabilisation buffer (FACS buffer + 0.1% saponin) for 30 minutes. Cells were then washed with FACS buffer before incubation with antibodies for 30 minutes. Cells were washed once more in FACS buffer and either analysed using FC or stained with a nuclear stain such as Hoechst of Propidium Iodide (PI). Flow cytometry was performed on the FACS Canto BD. Mean fluorescent intensity of 50,000 cells was measured and statistical analysis was performed as described above (see section 2.4.1).

2.8 Bulk RNA sequencing, RNA integrity measurement and transcriptome analysis

2.8.1 RNA isolation and quality control

RNA was isolated using the RNeasy Plus Micro kit (Qiagen Cat# 74034). RNA integrity was measured using the RNA 6000 Pico kit (Agilent Cat# 5067-1513) on the 2100 Bioanalyzer instrument (Agilent). Samples that passed this quality measurement (RIN > 9) were submitted for RNA sequencing. RNA concentration was

determined using Qubit™ 4 Fluorometer following the manufacturer's protocol. A total of 400ng per sample was submitted for library preparation.

2.8.2 Library preparation and sequencing

Library preparation and sequencing were performed by Novogene Co Ltd. Messenger RNA was purified from total RNA using poly-T oligo-attached magnetic beads. After fragmentation, the first strand cDNA was synthesised using random hexamer primers, followed by the second strand cDNA synthesis. The library was ready after end-repair, A-tailing, adapter ligation, size selection, amplification, and purification. The library was checked with Qubit and real-time PCR for quantification and bioanalyser for size distribution detection. Quantified libraries were pooled and sequenced on Illumina NovaSeq 6000 platform according to effective library concentration and data amount. Each library was submitted to 25 million paired-end reads (50M total).

2.8.3 Transcript quantification and data analysis

Gene transcripts were quantified using Salmon 15.2 with GC content bias and sequencing length bias correction. No custom code was used for the analyses. Please refer to https://github.com/mxvssn to request access the code. Transcript quantifications were imported in '*R* programming software' using 'tximeta' (version 1.14.1) (Ensembl Homo sapiens release 97). Differential gene expression was performed using 'DESeq2' (version 1.36.0) (Love, Huber and Anders, 2014) and the *lfcshrink* function that uses Bayesian shrinkage estimators for effect sizes (Zhu,

Ibrahim and Love, 2019). Differentially expressed genes were identified as having a Benjamini-Hochberg adjusted p-value below 0.05.

Gene expression was normalised using Variance-stabilising transformation (VST) ('vsn' package version 3.64.0). Principal component analysis (PCA) was performed using prcomp ('stats' package version 4.2.1) using the top 1000 most variable genes and visualised using 'ggplot2' (version 3.3.6). Gene expression was visualised using 'pheatmap' (version 1.0.12). Gene set variation analysis (GSVA) was performed using the GSVA package (version 1.44.2). Gene ontology analysis was performed using the Clusterprofiler package (version 4.4.4).

2.9 Cyclopamine treatment of cerebellar organoids

Embryoid bodies (EBs) of AH017-3 (WT) and H3 (*PTCH1-/-*) iPSC were made using the protocol described above (see section 2.5). After two days, treatment was started and either DMSO, 1 μM Cyclopamine, 5 μM Cyclopamine, or 500 nM SAG was added to the medium when the medium was changed. After 35 days, RNA was extracted as described above and analysed for gene expression using RT-qPCR. Organoids that were collected for immunofluorescence microscopy were fixed in 4% PFA, cryoprotected in 20% sucrose in PBS and embedded in OCT.

2.10 Bacteria and plasmids

The PiggyBac plasmids were kindly provided by our collaborators J. Bunt and M. Kool (Princes Maxima Centrum, Utrecht).

2.10.1 Plasmid retrieval from Whatman paper

Plasmid DNA was received as spotted on Whatman paper. The marked area containing the dried plasmid DNA (pDNA) was cut out using scissors and placed in an Eppendorf tube using forceps. 100 μL TE buffer (10 mM Tris·Cl, pH 8.0, 1 mM EDTA) was added onto the paper and distributed by flicking the tube. This was incubated for 10 minutes at room temperature before centrifugation in a microtube centrifuge to collect the TE buffer containing pDNA. The retrieved pDNA was either used immediately for bacterial transformation or stored at -20°C. Any unused filter paper containing pDNA was stored at room temperature.

2.10.2 Transformation, agar plating, and pDNA isolation

NEB® Stable Competent E. coli (NEB Cat# C3040H) strain was used for plasmid generation. E. coli were transformed following the manufacturer's protocol. Per transformation reaction, 1 μg plasmid DNA was used. After transformation, bacteria were plated on LB agar plates with Ampicillin (100mg/mL) and cultured at 30 ∘C for 16 hours. Colonies were picked using a pipette tip and cultured in 5mL LB broth with Ampicillin (100mg/mL). From here on, pDNA was either isolated using the Qiagen Miniprep kit (Qiagen Cat# 27104), or bacteria were further expanded in 100-500 mL LB broth with Ampicillin (100mg/mL) for Maxiprep (Qiagen Cat# 12162). For applications involving iPSC or organoids, pDNA was isolated using the EndoFree maxiprep kit (Qiagen Cat# 12362). Plasmid DNA was always diluted in MiliQ water, and the concentration was determined using Nanodrop.

2.11 Electroporation of whole organoids

Only high concentration pDNA (>3ug/uL) in MiliQ was used to prepare electroporation mixes as transfection efficiency is reduced by the amount of added components. Each electroporation mix was made up with the specified pmol per plasmid in 200 μL Nucleofector™ Solution V with Supplement 1 (Lonza Cat# VCA-1003). Up to four organoids per condition were placed in the electroporation mix using a wide bore pipette and incubated for 1 minute at room temperature. The electroporation mix with organoids was transferred into the electroporation cuvette and electroporated. Several programmes were tested, and programme A-020 proved to be the most efficient. After electroporation, organoids were washed out using 0.5 mL Differentiation medium into a 6-well plate. Electroporated organoids were subsequently placed back into low-attachment 48-well plates in Differentiation Medium and returned to the incubator. The medium was refreshed weekly up until DIV 35 and every two times a week from DIV 35 onwards. Electroporation efficiency was observed as fluorescence using the EVOS live cell imaging system. Changes in fluorescence and organoid growth were subjected to statistical analysis as described above (see section 2.4.1).

2.12 Co-culture of cerebellar organoids with established medulloblastoma cell lines

2.12.1 DAOY and ONS76 culture

DAOY (provided to us as a gift from Prof. V. D'Angiolella, University of Oxford) and ONS76 cells (provided to us as a gift from Prof. L. Chesler, Institute of Cancer Research London) were cultured in T75 flasks or 6-well plates. DAOY cells were

cultured in Minimal Essential Medium (MEM) (Gibco, Cat# 11095080) supplemented with 1% FBS, 1% GlutaMAX and 1% Penicillin/Streptomycin. ONS76 cells were cultured in Roswell Park Memorial Institute (RPMI) 1640 Medium (Gibco, Cat# 21875091) supplemented with 1% FBS, 1% GlutaMAX and 1% Penicillin/Streptomycin. Both cell lines were passaged upon reaching 90% confluency. For passaging, cells were washed once with PBS and detached by incubation Trypsin-EDTA for 5 minutes at 37°C. Trypsin was inactivated by the addition of culture medium and cells were typically split in a 1:14 ratio.

2.12.2 MB spheroid generation

DAOY and ONS76 cells were detached from the cell culture plate by incubation with TrypLE for 5 minutes at 37°C. Afterwards, TrypLE was diluted with PBS and cells were pelleted by centrifugation for 5 minutes at 400 x *g*. Cells were then resuspended in Differentiation Medium. Cells were then diluted to the required concentration and plated in low-attachment V-bottom 96 well plates and returned to the incubator.

For a co-culture experiment, spheroids were generated five days prior to the start of the co-culture. For spheroid monocultures, half of the medium was changed twice a week.

2.12.3 Organoid - MB-spheroid co-culture

DIV 35 organoids were placed in a low-attachment 24-well plate (Corning®, Cat# 3473 or similar). Upon the start of co-culture, tumour spheres were added to the organoids, and the plate was placed back into the incubator at a 45° angle to facilitate

the binding of the tumour sphere to the organoid. After two days, the plate was placed in the normal orientation and co-cultures were checked for the fusion of the spheroid to the organoid. In subsequent culture, the medium was changed every 3-4 days until application.

2.13 Single-cell or single nuclei RNA sequencing sample preparation

2.13.1 Single-cell isolation and dead-cell removal

Organoids were dissociated using Neuron isolation enzyme (ThermoFisher, Cat #88285). Large organoids (>2 mm) were cut into four pieces prior to enzymatic digestion to facilitate access of the enzyme to all parts of the organoids. After dissociation, cells were pelleted and processed using the MACS Dead cell removal kit (Miltenyi Biotech Cat#130-090-101) to obtain a single-cell suspension of viable cells. Cells were counted using the Countess II automated cell counter with Trypan Blue (Gibco™ Cat #15250061) exclusion dye to detect dead cells. Cells were centrifuged once more at 400 x g for five minutes, resuspended at 1000 cells / μL in HBSS (Invitrogen, Cat# 14180046) + 0.04% BSA (Sigma-Aldrich, Cat# A9576-50m) in DNA LoBind Eppendorf tubes and submitted to the Oxford Genomics Centre (OGC) for single-cell barcoding in the 10X Chromium system and sequencing

2.13.2 Single-cell RNA sequencing analysis

Transcript quantification was performed by the OGC using the CellRanger platform. The count matrices produced by CellRanger were imported into '*R* programming software' using the Seurat package (version 4.1.1). No custom code was used for the

analyses. Please refer to https://github.com/mxvssn to request access the code. Single-cell transcriptomes were analysed using the standard workflow available in the Seurat documentation. Using this package, the datasets were merged. Low-quality cells were identified by a low RNA feature count (<200), relating to the number of different genes detected, and a high proportion of mitochondrial RNA (>18%), as dying cells express high levels of mitochondrial RNA (*Figure 2.1*). Count matrices were normalised, and variance stabilised using the 'SCTransform' function and mitochondrial RNA content, and cell cycle phase were regressed out. Single-cell transcriptomes were visualised using the Uniform Manifold Approximation and Projection (UMAP) dimensionality reduction technique. DAOY and ONS-76 cells were identified by their location in UMAP space. The clustering of DAOY and ONS-76 cells was performed by a shared nearest neighbour (SNN) modularity optimisation built in the Seurat package. A resolution of 0.4 based on optimally distinguishing biologically relevant cell clusters was chosen to identify meaningful clusters and perform subsequent analyses. Differentially expressed genes were identified with the FindAllMarkers function in the Seurat package. Gene ontology analysis was performed using Clusterprofiler package (version 4.4.4). Comparison of the expression of neuron-specific cell cycle genes was performed using a previously published gene list by O'Connor et al., 2021).

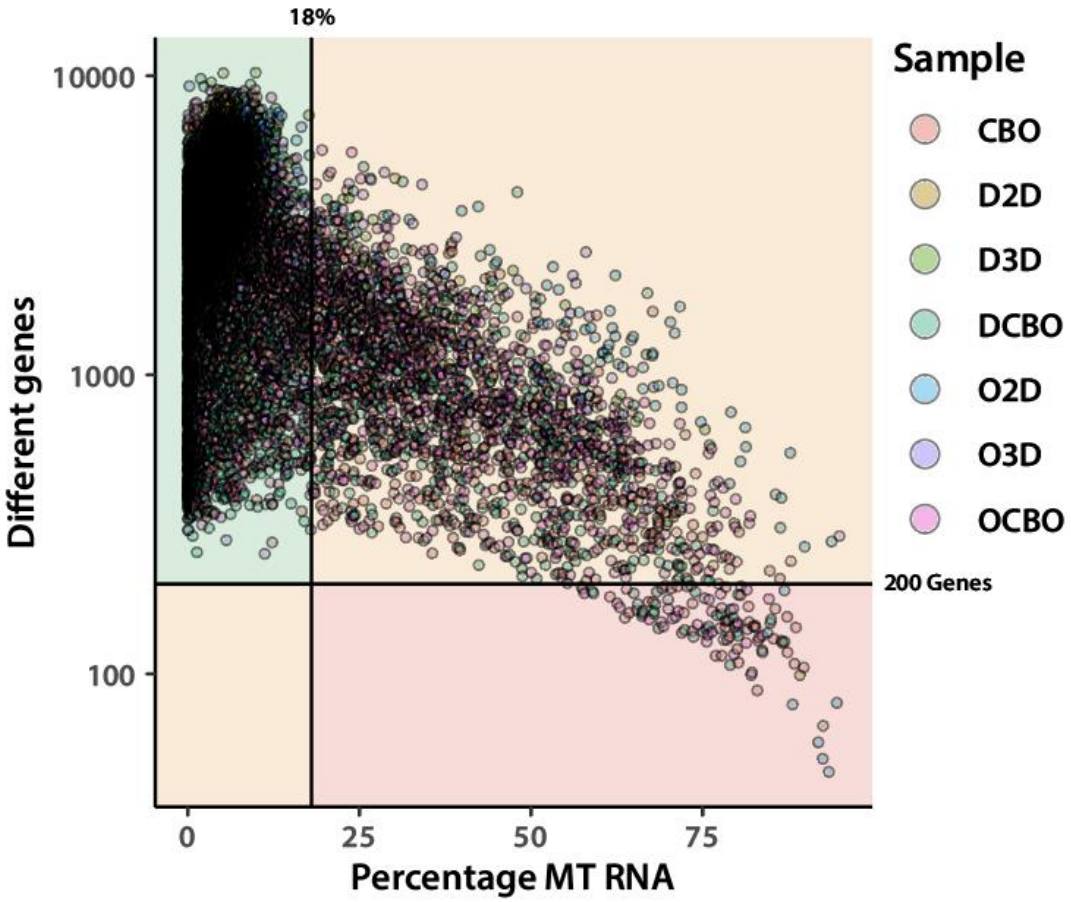


Figure 2.1: Filtering of low-quality cells by RNA count and mitochondrial RNA. *The different samples are marked by different coloured dots. There is no clear difference in the number of cells falling outside the optimal thresholds between the different samples.*

Chapter 3 Engineering a *PTCH1* loss-of-function mutation in human iPSC

3.1 Introduction

Around 44% of all SHH-MB harbour LOF mutations in PTCH1 (reviewed in Garcia-Lopez et al., 2021; Northcott et al., 2019). The *PTCH1* gene encodes a transmembrane receptor for proteins from the Hedgehog family (HH) of which SHH is the most prominent member. Together with SUFU, PTCH1 is the primary intracellular negative regulator of SHH-signalling, explaining the large contribution to SHH-MB. Despite the significant role of *PTCH1*-mutations in SHH-MB tumorigenesis, relatively few preclinical models have been developed. The *Ptch1*+/- mouse model by Goodrich et al (1997) has been the most elaborately studied and the base for multiple mouse models with compound mutations (Wetmore, Eberhart and Curran, 2001; Schüller *et al.*, 2008; Yang *et al.*, 2008; Li *et al.*, 2013). However, limitations of murine models and their translation to human disease have driven the search for human models.

iPSC have transformed the way human development and disease is studied. The ability to generate human specific cell types and tissues allows the study of the earliest aspects of human development *in vitro*. Induced pluripotent stem cells can be generated from somatic cells through reprogramming (see section 1.6.1.1) and offer unique opportunities in the study of cell and developmental biology. Using specific growth factors and small molecules, iPSC can be differentiated into virtually every cell type in the human body, including cerebellar progenitors (Watson *et al.*, 2018; Nayler *et al.*, 2021). Pluripotent stem cell differentiation occurs through many

of the same steps as during *in vivo* embryogenesis, allowing the functional study of specific genes during development. The embryonic origin of MB as well as the high frequency of germline mutations in MB (6%) (Waszak *et al.*, 2018) makes iPSC differentiated into cerebellar progenitors an ideal to model and study early tumorigenesis.

Several studies have derived human iPSC from Gorlin syndrome patients with *PTCH1+/-* germline mutations (Gorlin-iPSC) (Hasegawa *et al.*, 2017; Ikemoto *et al.*, 2017, 2020; Huang *et al.*, 2019; Ikehara *et al.*, 2019; Susanto *et al.*, 2020; Nagao *et al.*, 2022). However, limitations arise from the use of patient-derived iPSC due to unrecognised, additional mutations or variants that interfere with results. This is highlighted by findings in Huang et al. (2019) that discover one of their two Gorlin-iPSC lines to also harbour a mutation in *PTCH2*. In this study, the additional *PTCH2* mutation caused a more aggressive phenotype and reduced tumour latencies (102-206 days compared to 254-360 days). These mutations may be acquired later in life, either at random or as a result of PTCH1 LOF and introduce heterogeneity that cannot be controlled for. In addition, studies have found specific gene variants to increase or decrease the risk of basal cell carcinomas in Gorlin syndrome patients (Yasar *et al.*, 2015), emphasizing a role of the genetic background in disease phenotype. A more controlled model is required to study PTCH1 LOF on cerebellar development and MB formation without interference of unrecognised genomic events. Gene editing techniques such as CRISPR in healthy donor iPSC can generate mutant lines that can be compared to the parental isogenic control, overcoming some of the limitations associated with patient iPSC lines.

CRISPR (Clustered Regularly Interspaced Short Palindromic Repeats) is an acquired immune system found in prokaryotes (Jinek *et al.*, 2012) and its applications for gene editing have revolutionised genetic research. The much improved accessibility, ease of use and versatile applicability of CRISPR gene editing over older techniques has made it the preferred method of genome engineering by researchers. Coupling of iPSC differentiation and CRISPR-gene editing allows the study of specific genes in the earliest stages of life and disease, with unprecedented precision and control (reviewed in van Essen et al., 2021).

The CRISPR machinery consists of CRISPR-associated protein (Cas), a DNA nuclease, which is guided to specific sites in the genome by a guide RNA (gRNA). This gRNA is traditionally composed of a 20-bp CRISPR RNA (crRNA) and a trans-activating RNA (tracrRNA) (Jinek *et al.*, 2012). The crRNA contains the guiding sequence and binds the tracrRNA to form the active complex that binds the Cas nuclease. Unmodified versions of Cas9, the most widely used Cas protein, originates from *Streptococcus pyogenes* and uses a NGG protospacer adjacent motif (PAM) on the non-target strand to recognise a potential target site (*Figure 3.1*) (Cong *et al.*, 2013; Mali *et al.*, 2013). Upon successful pairing of the crRNA with the target DNA strand (Hsu *et al.*, 2013; Stemmer *et al.*, 2015), a double strand break (DSB) is induced three nucleotides upstream of the PAM (Jinek *et al.*, 2012). Following DSB, several different DNA repair pathways can restore genome integrity, each with differing results. Non-homologous end joining (NHEJ) is the most frequently used method of repair and requires the resection of DNA ends to expose complementary DNA strands (Wyman and Kanaar, 2006). However, this pathway is highly error-prone and frequently results in the

insertion or deletion of base pairs (Tutt *et al.*, 2001; Iliakis *et al.*, 2004; Ghezraoui *et al.*, 2014). More precise DNA repair pathways such as homology directed repair (HDR) require a homologous DNA sequence that serves as a template for the repair but are less efficient (Liang *et al.*, 1998; Heyer, Ehmsen and Liu, 2010). While NHEJ can be used to disrupt genes for knockout studies, HDR can be used to specifically introduce mutations and variants (Lackner *et al.*, 2015).

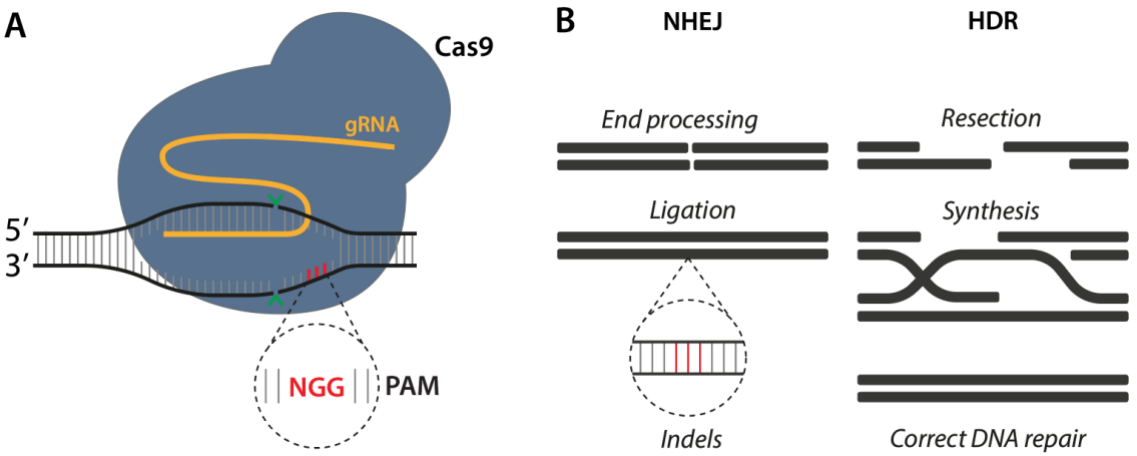


Figure 3.1: CRISPR-Cas9 gene editing and DNA repair. *A) The Cas9 nuclease identifies potential binding sites by the presence of the protospacer adjacent motif (PAM). For Cas9 derived from S. pyogenes this PAM sequence is NGG. Binding occurs at genomic loci complementary to the guide RNA that is captured in its scaffold. Upon binding, a double strand break (DSB) is induced 3 nucleotides downstream from the PAM. B) Following DSB, DNA repair generally occurs in one of two ways: Non-homologous end joining (NHEJ) or Homology directed repair (HDR). NHEJ requires resection and end processing of the loose DNA ends before ligation, frequently resulting in insertions or deletions (indels). HDR uses a DNA template such as an unaffected allele to correctly repair the DNA without aberrations.*

Despite the remarkable efficiency of CRISPR to target specific sites in the human genome, off-target effects (OTEs) need to be considered as gRNA binding still allows a low level of mismatches (reviewed in Kimberland et al., 2018). Strategies to reduce OTEs include limiting the time the CRISPR machinery is present, modified versions of Cas9 that reduce off-target activity and optimisation of gRNAs selection that reduces overlap with off-target genomic loci. Initial studies used plasmid Cas9

delivery systems but were soon replaced due to increased likelihood of OTEs (Kim *et al.*, 2014) and cellular toxicity that is associated with the presence of exogenous double stranded DNA (Hornung and Latz, 2010). Compared to plasmids, the use of ribonuclease proteins (RNPs), consisting of a gRNA in complex with Cas9 protein provide better temporal control and reduces OTEs (Hendel *et al.*, 2015). RNPs are immediately active upon introduction yet rapidly decayed, reducing the time for OTEs. Engineering of Cas9 nucleases has provided a second method to mitigate OTEs. A single point mutation in the *Cas9* gene (R691A) has shown to reduce off-target activity while increasing on-target efficiency (Vakulskas *et al.*, 2018). Finally, efficiency and OTEs are strongly influenced by gRNA sequence (Pattanayak *et al.*, 2013) and optimised algorithms that predict off-target binding have been used to reduce OTEs (Stemmer *et al.*, 2015). Nevertheless, careful quality control of CRISPR-edited cell lines is still required to identify OTEs and prevent unreliable experimental results.

Loss-of-function of PTCH1 renders cells vulnerable to uncontrolled SHH pathway activation. Although SHH signalling has roles in stem cell maintenance in cancers (see section 1.3.4), its role in pluripotent stem cell maintenance is limited (Wu *et al.*, 2010). Nevertheless, ESC (Kiprilov *et al.*, 2008; Wu *et al.*, 2010) and iPSC (Nathwani *et al.*, 2014; Kilander *et al.*, 2018; Schmidt *et al.*, 2022) express all functional SHH-pathway components including primary cilia, and have endogenous activation of the SHH-pathway. In the absence of PTCH1, SMO can locate to the primary cilium and prevent degradation of the GLI-proteins (*Figure 3.2*) (see section 1.3.1). The expression of *GLI1* and *PTCH1* is upregulated upon SHH-pathway activation

(Goodrich *et al.*, 1996; Lee *et al.*, 1997) and is therefore frequently used as functional readouts of SHH signalling. The effect of the introduced mutation in the iPSC clones generated in this chapter will be assessed using these readouts, to assess the functional effect of the *PTCH1* mutation.

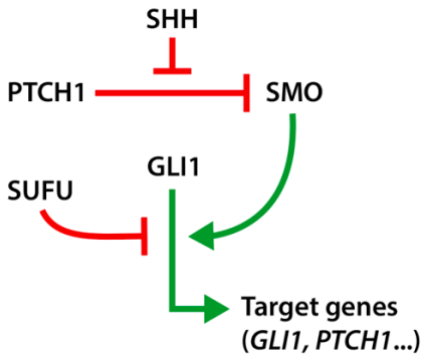


Figure 3.2: SHH signalling induces the expression of GLI1 and PTCH1. *In the absence of SHH, PTCH1 inhibits SMO. As a result, GLI1 is degraded under the influence of SUFU, and no transcription of target genes occurs. Upon binding of SHH to PTCH1, or in the case of loss-of-function of PTCH1, SMO inhibition is relieved. SMO prevents degradation of GLI1 which can induce expression of target genes such as GLI1 and PTCH1.*

The comparison of mutant cell lines with an isogenic control forms a cornerstone for the study of gene function. Although isogenic control iPSC lines could be generated by correcting the mutant allele in Gorlin syndrome patient lines, several advantages arise from of introducing a new mutation in healthy donors. Firstly, gene knockout can be achieved through NHEJ while correction requires HDR using a corrected donor DNA template. NHEJ occurs more frequently than HDR, increasing the efficiency of generating isogenic mutant and control lines. Secondly, patients frequently harbour point mutations and corrections can be challenging to screen. In contrast, gene knockout can be achieved through the removal of larger genomic sequences which are easily detected using conventional polymerase chain reaction (PCR) and gel electrophoresis. Lastly, generating heterozygous and homozygous

mutants is a one-step procedure when using healthy donor cells. Some iPSC will be edited on one allele and others on both. Conversely, derivation of an isogenic control from patient iPSC requires a CRISPR reaction with a correction DNA template while the introduction of a mutation in the healthy control allele requires a different DNA template. Taken together, the use of healthy donor iPSC provides an attractive strategy to generate *PTCH1* heterozygous and homozygous mutant iPSC lines with isogenic controls. This chapter describes the generation, quality control and functional characterisation of *PTCH1* mutant iPSC clones that can be used to study the effects of *PTCH1* mutations in cerebellar development and MB tumorigenesis.

3.2 Results

3.2.1 CRISPR strategy to induce *PTCH1* loss-of-function

A CRISPR strategy was designed to target an essential region of *PTCH1* that is expected to cause LOF. As there are no disease-related mutational hotspots found in the *PTCH1* gene (Reinders *et al.*, 2018), an early, highly conserved exon, present in all known isoforms was chosen to maximise the chance of LOF. Regions conserved in multiple isoforms are likely to have importance for protein function, especially as *PTCH1* has large regions of homology throughout the animal kingdom. Although different starting codons have been identified (Kogerman *et al.*, 2002; Shimokawa, Rahnama and Zaphiropoulos, 2004; Shimokawa *et al.*, 2007), exon 3 is preserved across all known isoforms. Furthermore, mutations in exon 3 have been found in Gorlin syndrome patients (Okamoto *et al.*, 2014), demonstrating its importance in PTCH1 function. Disruption of the gene was attempted through deletion of the splice donor site (SD) of exon 3. Removal of the SD site of exon 3 is expected to alter splicing and result in retention of the intronic sequence between exon 3 and exon 4 during pre-mRNA to mRNA processing (*Figure 3.3*). This intronic sequence contains multiple stop codons in all three possible reading frames affecting mRNA processing and translation.

During pre-mRNA splicing, premature translation-termination codons (PTCs) can trigger a quality control machinery called nonsense mediated decay (NMD)(reviewed in Kurosaki et al., 2019). Multiple mechanisms may be responsible for NMD including the presence of a downstream exon-junction complex which interferes with the translation termination complex (TTC) or unusually long 3’

untranslated regions (UTRs) that prevent efficient recruitment of the TTC to the last exon-junction complex. Alternatively, the presence of an early stop codon results in a significantly truncated protein containing just the first transmembrane region of PTCH1 (*Figure 3.3*).

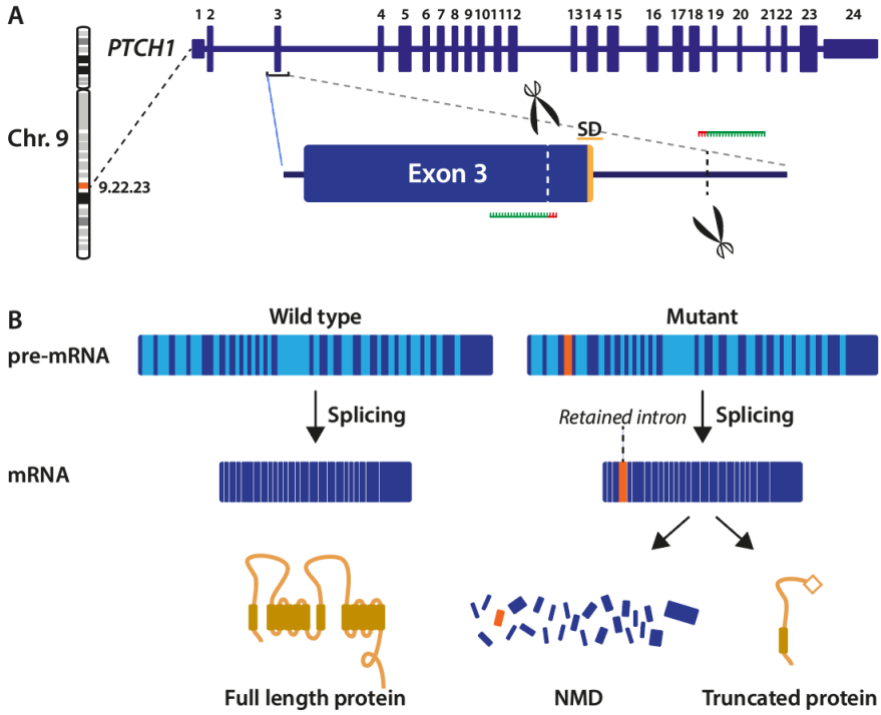


Figure 3.3: CRISPR strategy to induce PTCH1 loss-of-function in human iPSC. *A) PTCH1 is located on Chromosome 9 (9.22.23). The gene knows 24 exons and exon 3 is the first conserved exon among isoforms. The gRNAs are designed to excise a 243bp region spanning the splice donor site (SD) of exon 3. B) Compared to wildtype, mutant pre-mRNA will contain the intron between exon 3 and 4. This is recognised by the splicing machinery and expected to trigger nonsense mediated decay (NMD) due to the presence of premature translation-termination codons (PTC). Alternatively, if NMD is not triggered, the PTC will cause truncation of the protein.*

A pair of gRNAs was designed to excise a 243-bp sequence including the SD of exon 3 of the *PTCH1* gene using the online tool CCTop (Stemmer *et al.*, 2015). The two gRNAs were selected based on their specificity score, predicted efficiency and the number of off-target sites. Only gRNAs of which the top off-target sites contained

four or more mismatches were considered. Ultimately, the exonic gRNA GA TTT ATC GTT TCT CGA GTT TGG and intronic gRNA GT GTT GTA GGA GCG CTT CTG TGG were selected.

3.2.2 CRISPR gene editing and clone selection

PTCH1 mutant iPSC clones were generated from the human iPSC line AH017-3. This line was originally derived from a healthy a 67-year-old female donor recruited through the Oxford Parkinson's Disease Centre (Handel *et al.*, 2016). This line was chosen as previous work by the lab has shown it differentiates well into cerebellar organoids (Watson *et al.*, 2018). Single gRNAs were formed by multiplexing of the designed crRNA and tracrRNA before complexation with HiFi Cas9 Nuclease V3 to form RNPs. This engineered Cas9 has shown improved specificity over wildtype Cas9 while maintaining on-target editing activity (Vakulskas *et al.*, 2018). In two rounds (A and B), RNPs were transfected into iPSC using electroporation to generate two screening pools. To control for transfection related effects, iPSC were transfected with Cas9 nuclease without sgRNA (mock). PCR and gel electrophoresis was used to confirm editing in both screening pools. Successful gene editing was identified by the presence of the shorter PCR product derived from mutant genomic DNA (*Figure 3.4*).

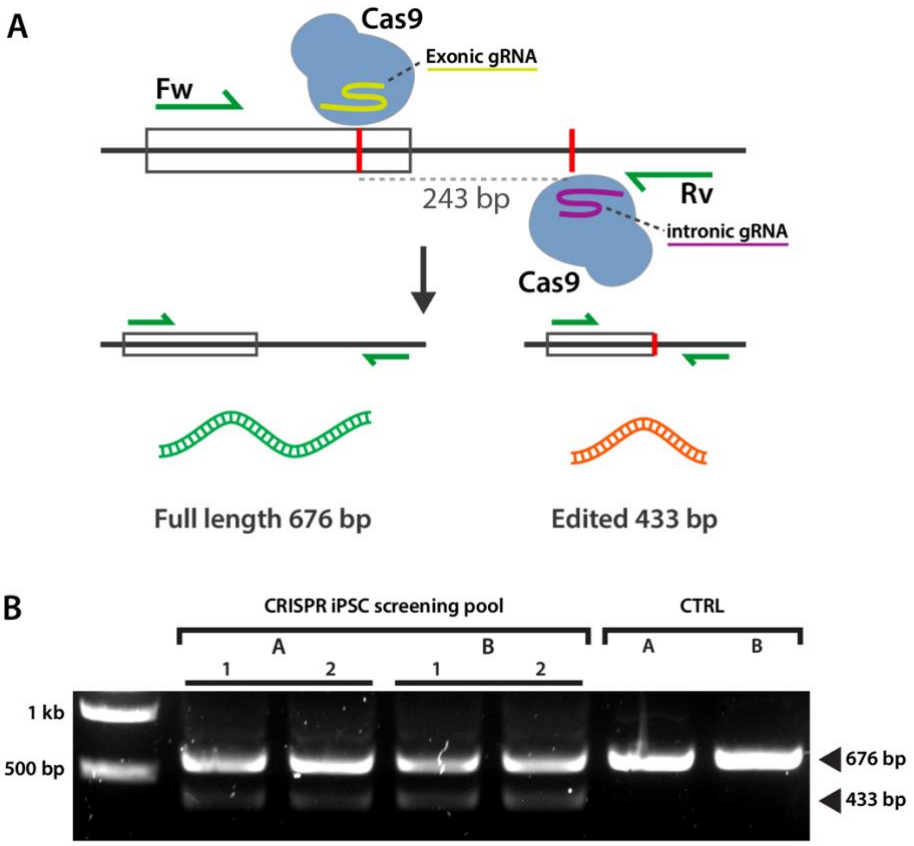


Figure 3.4: Detection of mutant genomic DNA in CRISPR gene edited iPSC pools. *A) Cas9 nucleases loaded with exonic (light green) and intronic (purple) guide RNAs induce double strand breaks and resect a 243bp sequence. PCR primers (green) amplify the genomic region spanning the target site. Wildtype, unedited genomic DNA produces the full-length product of 676bp. Conversely, successful editing is detected as a shorter amplicon of 433bp. B) PCR amplification of the two transfected iPSC pools in duplicate. Pool A and pool B show presence of the shorter, mutant product that is absent in mock transfected iPSC pools.*

To generate monoclonal *PTCH1* mutant iPSC lines, CRISPR-pool A was plated as single cells on a Mouse Embryonic Feeder (MEF) layer. Single cell plating on MEFs has shown to improve survival compared to regular plating (Yang *et al.*, 2013). Clonal colonies derived from a single cell were handpicked and genotyped using PCR with the same primers as used for checking the pool. Out of 92 clones tested, PCR revealed 37 to have a heterozygous and 8 to have a homozygous genotype, translating to an editing efficiency of 28.3% (53 out of 184 alleles). Six heterozygous and three homozygous *PTCH1* mutant clones were selected (*Figure 3.5*). Sanger

sequencing confirmed deletion of the 243-bp region between the two target sites in all mutant alleles (*Figure 3.5*). Cutting was uniform at the intronic target site compared to more heterogeneous effects at the exonic target site. In addition, a single point mutation (G>A) was found at the intronic target site in three out of the four selected heterozygous clones (A3, B2 and C6). Although functional effects of the intronic point mutation are unlikely, introns do contain regulatory elements that affect gene expression and alternative splicing (reviewed in le Hir et al., 2003; Shaul, 2017) and result in altered protein function. Functional characterisation will elucidate the exact effects of the introduced mutations on PTCH1 function. In conclusion, these results show successful introduction of heterozygous and homozygous *PTCH1* mutations in iPSC clones.

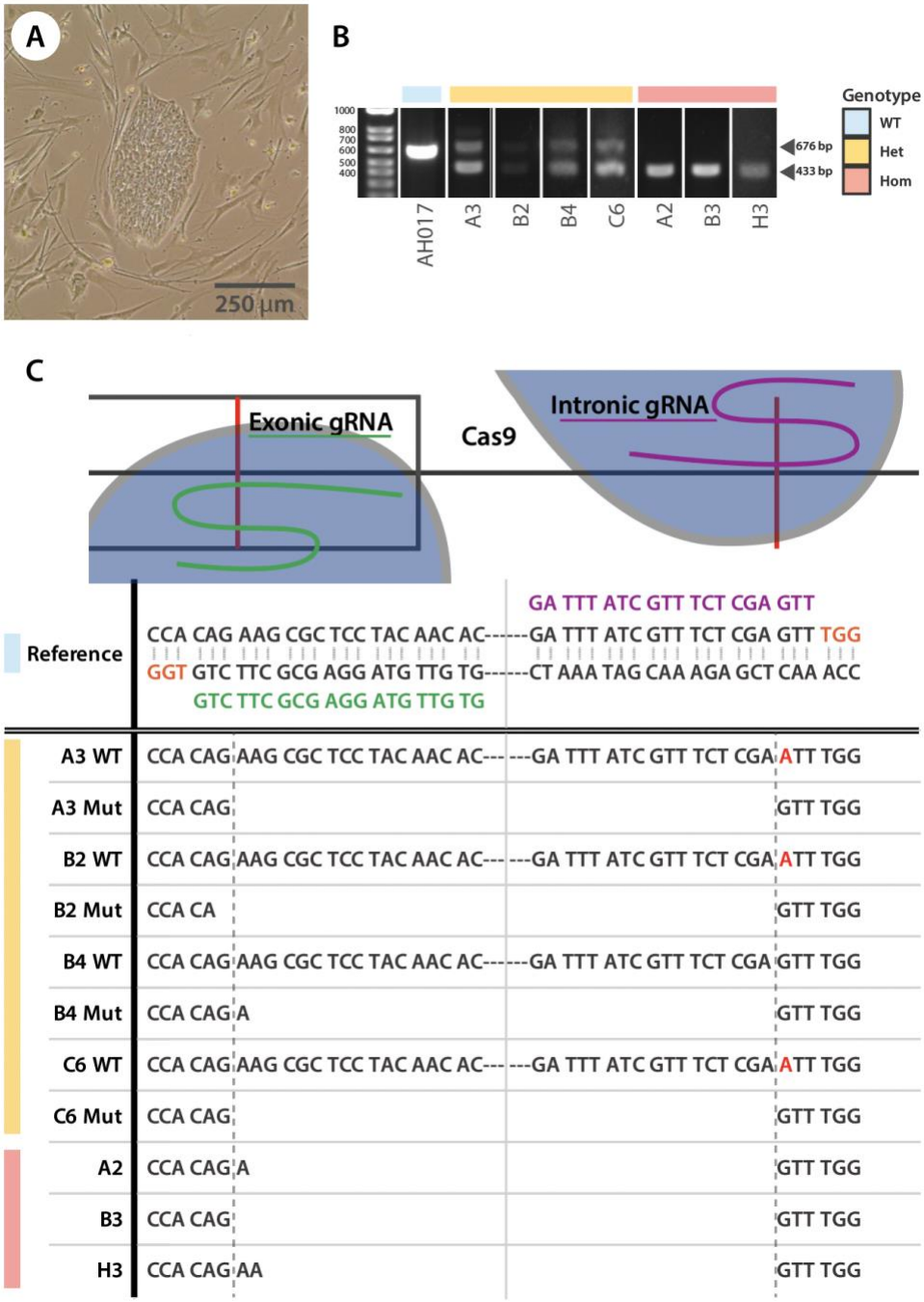


Figure 3.5: Selection of heterozygous and homozygous PTCH1 mutant iPSC clones. *A) Representative brightfield image of an iPSC colony after single cell plating on mouse embryonic fibroblasts. B) Genotyping using primers as in Figure* ***3.4*** *to detect heterozygous clones producing both wildtype (676bp) and mutant (433bp) PCR amplicons as well as homozygous clones producing only the mutant amplicon (433bp). C) Sanger sequencing reveals uniform cutting at the intronic target site compared to more heterogeneous cutting at the exonic target site. The genomic DNA region between the target sites is absent in the mutant amplicons (mut). Point mutations at the intronic target site are detected in heterozygous clones (A3, B2 and C6) (G>A) (marked in red).*

3.2.3 Quality control of PTCH1 mutant iPSC

All selected clones were subjected to quality control to assess possible effects of the mutation on pluripotency and off-target genomic events. All clones displayed normal iPSC morphology growing in compact colonies of small round cells with a high nucleus-to-cytoplasm ratio (*Figure 3.6*A).All clones expressed pluripotency markers NANOG and Tra-1-60 to similar levels, as measured by flow cytometry (*Figure 3.6*B). To assess off-target effects of the CRISPR strategy, the top five off-target sites of each of the gRNAs in the genome of homozygous clone H3 were amplified using PCR and submitted for Sanger sequencing (*Figure 3.7*). This revealed no off-target activity on any of the tested sites. A wider screen for chromosomal aberrations using a SNP-array testing over 600.000 sites in the human genome did not reveal any new amplifications, deletions, or re-arrangements (***Appendix figure 1***). All clones were tested for mycoplasma and found negative. Taken together, these results confirm the successful generation of isogenic *PTCH1*-mutant iPSC clones.

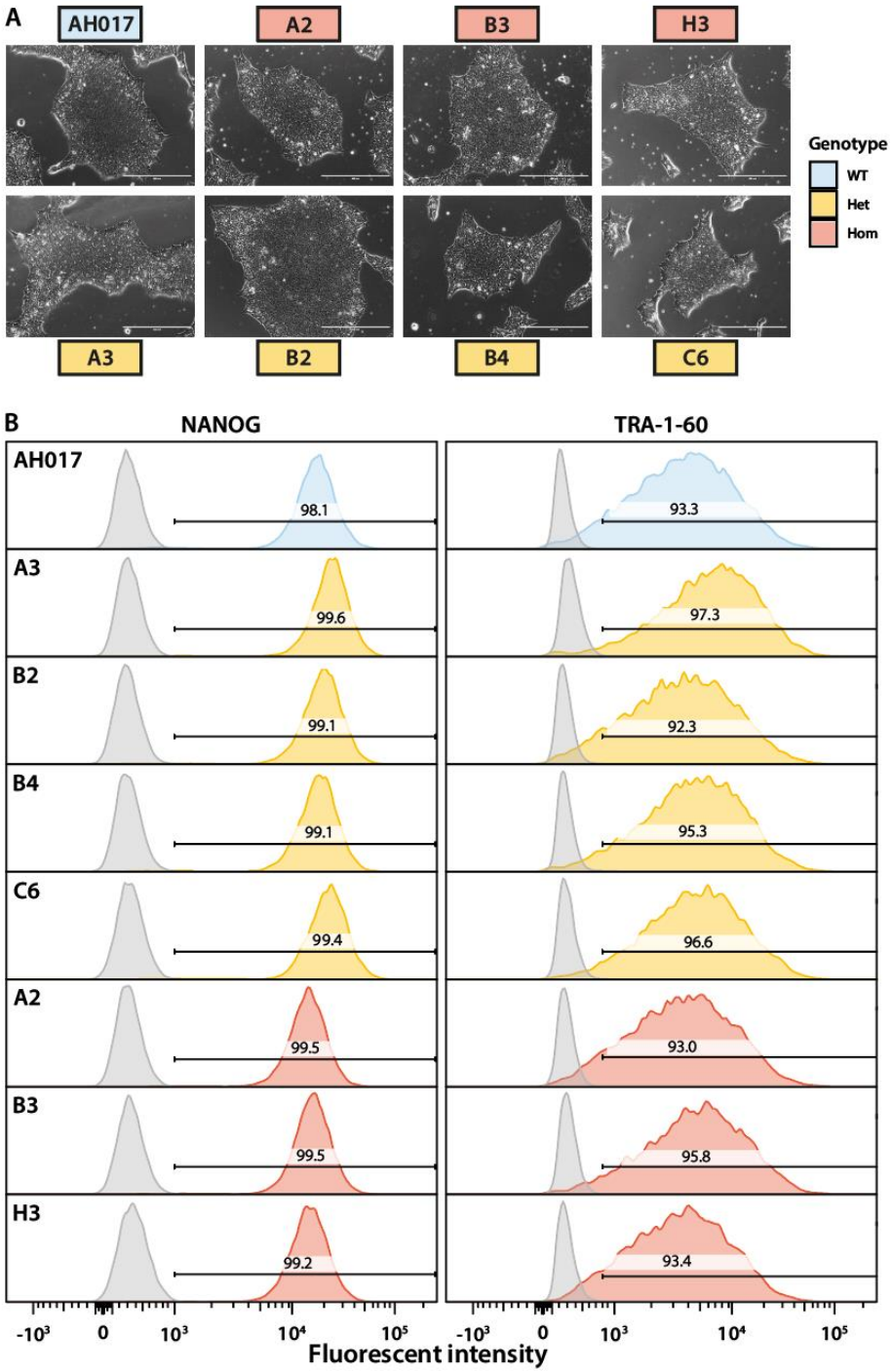


Figure 3.6: PTCH1 mutant clones maintain iPSC morphology and pluripotency marker expression. *A) Brightfield images of iPSC clones. bars are 1000 µm. All clones display normal iPSC morphology with large nucleus to cytoplasm ratio and growth in densely packed colonies. B) A total of 50.000 cells were measured by flow cytometry. A density plot shows the distribution of fluorescent intensity along the x-axis. Coloured histograms represent cells stained with antibodies targeting NANOG (left) or TRA-1-60 (right). Grey histograms represent cells stained with isotype control antibodies to assess unspecific binding and autofluorescence. The percentage of cells with fluorescent intensities above the isotype control condition are depicted.*

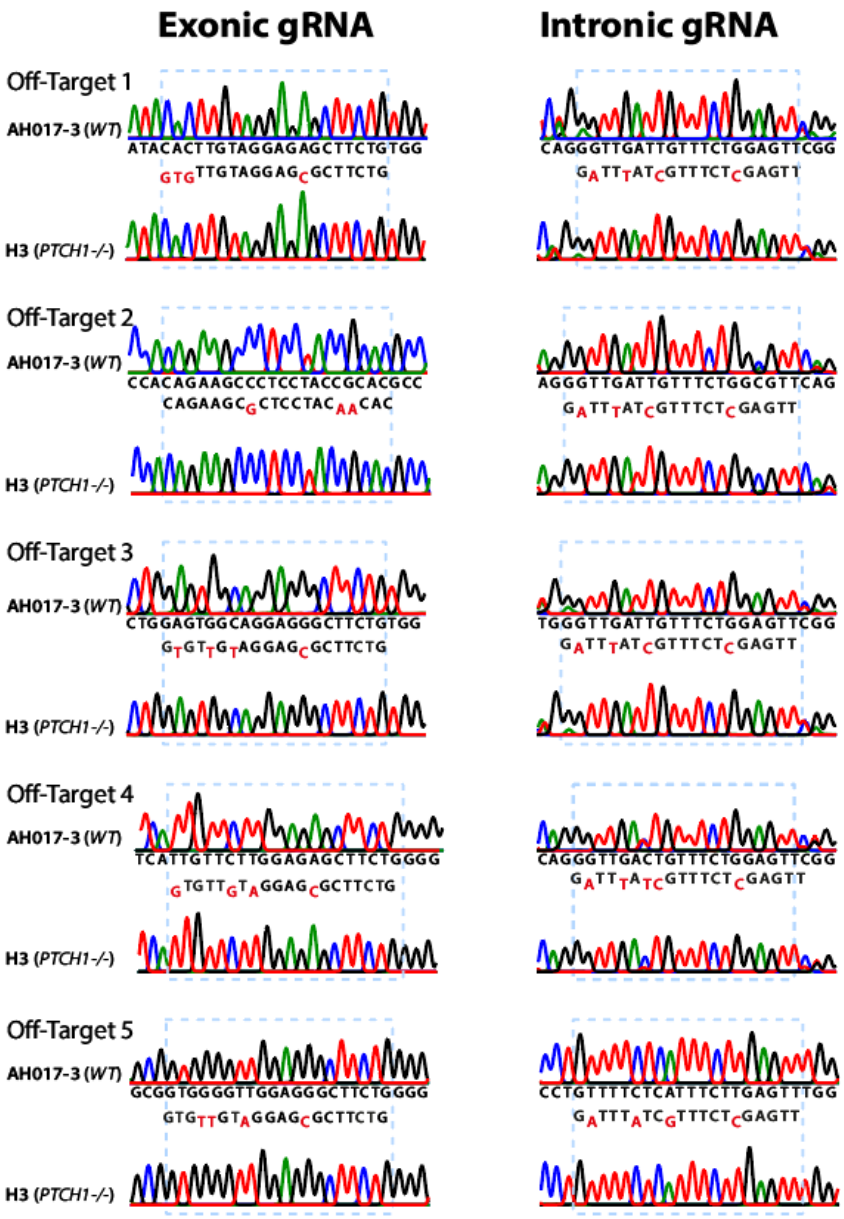


Figure 3.7: Sanger sequencing does not reveal off-target activity. *Sanger sequencing of the top five off-target sites of each guide RNA. The alignment with each respective gRNA is shown below the wildtype strand with mismatches shown in red. Sequence trace of both the wildtype and tested homozygous mutant (H3) proved to be identical, consistent with no off-target CRISPR-events.*

3.2.4 Functional characterisation of *PTCH1* mutation in undifferentiated iPSC

The introduced mutation is expected to cause loss-of-function of PTCH1, potentially leading to increased levels of SHH-signalling and cell proliferation (see section 1.3.1).

SHH-pathway activation induces the expression of *GLI1* and *PTCH1* which can be used as readouts for the level of signalling. Using reverse transcriptase quantitative PCR (RT-qPCR), mRNA levels of *GLI1* and *PTCH1* were measured in wildtype (AH017 parent line), heterozygous (A3, B2, B4, and C6) and homozygous (A2, B3, and H3) iPSC (*Figure 3.8*). At genotype level, increased levels of *GLI1* mRNA were measured in heterozygous and homozygous iPSC (p=0.027 and p<0.001 respectively) (*Figure 3.8*). Furthermore, expression of *PTCH1* was significantly higher in homozygous but not heterozygous iPSC (p=0.01) (*Figure 3.8*). Together, the modestly increased expression of *GLI1* and *PTCH1* mRNA are in line with reduced function of PTCH1 protein. Interestingly, these results also suggest *PTCH1* mRNA is not degraded through triggering of NMD by the introduced PTC.

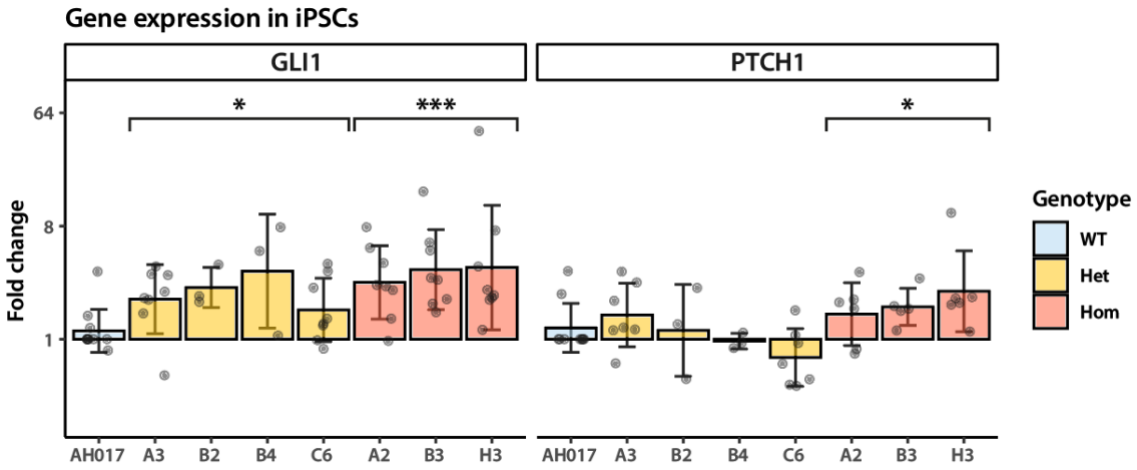


Figure 3.8: PTCH1 mutant iPSC express increased levels of GLI1. *Messenger RNA expression of GLI1 and PTCH1 as measured by RT-qPCR. Expression is relative to the wildtype parent line (AH017) and normalized using ACTB and GAPDH. Statistically significant differences on the genotype level are calculated on the ΔΔCt values by one way ANOVA with Dunnett's post hoc test. Significance is indicated by asterisks, * = P<0.05, *** = p<0.001. Error bars represent standard deviation. Data points are generated from independent passages. N>3 for all clones.*

In the absence of NMD, it is unclear how mutant *PTCH1* mRNA differs from wildtype and how this results in the reduced functionality as evidenced by increased SHH-signalling. Therefore, post-transcriptional effects of the mutation on *PTCH1* mRNA were investigated by Sanger sequencing of *PTCH1* mRNA. This revealed the mutation causing alternative splicing of the mutant mRNA resulting in exclusion of exon 3 (*Figure 3.9*). As exon 3 is an asymmetric exon (not a multiple of three base pairs), this results in a -1 frameshift with multiple stop-codons in the new reading frame. Due to the mutation, the resulting protein is truncated at the first extracellular loop. Although the exact mechanism through which PTCH1 inhibits SMO is unknown, the increased levels of *GLI1* mRNA suggest this truncation event is sufficient to impair PTCH1 protein function.

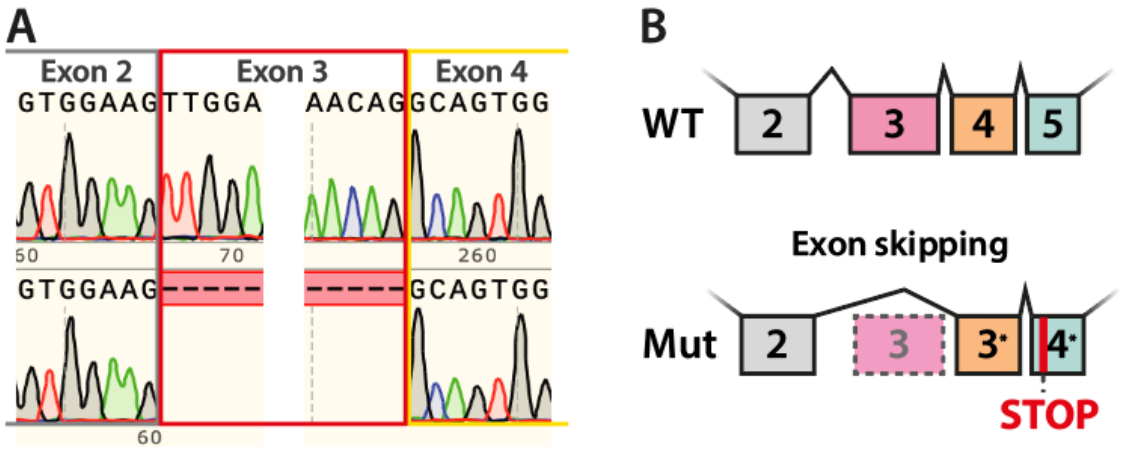


Figure 3.9: Aberrant splicing of mutant PTCH1 pre-mRNA results in a loss-of-function frameshift. *A) Sanger sequencing of PTCH1 mRNA reveals the exclusion of exon 3 in the mutant mRNA. B) Schematic depiction of the effect of exon 3 exclusion on the new mRNA. Exon 3 is asymmetric (meaning not a multiple of 3) and would receive a nucleotide from exon 2 and donate 2 nucleotides to exon 4. Excision results in a frame shifts which introduces premature translation termination codons in neo-exon 4. This is expected to truncate the protein in the first extracellular loop.*

Efforts to analyse PTCH1 protein truncation using Western blot using multiple different antibodies (NB200-118, MAB41041, ab53715) and lysis conditions proved unsuccessful. As a large transmembrane protein, PTCH1 is difficult to capture, and groups studying the protein structure either use tagged versions to allow immunoprecipitation or apply elaborate purification steps to allow measurement of PTCH1 (Gong *et al.*, 2018; Qi *et al.*, 2018, 2019). These techniques are not compatible with the low levels of expression of PTCH1 in undifferentiated iPSC, making the verification of the knockout at the protein level impractical.

Potential functional effects of the mutation in iPSC were further investigated by measuring SHH-signalling upon stimulation of cells with an agonist of the pathway. iPSC were exposed to 500 nM Smoothened agonist (SAG) for 48 hours after which *GLI1*, *PTCH1* and *PTCH2* mRNA were measured using RT-qPCR (*Figure 3.10*). *Ptch2* has been shown to mediate Shh response in *Ptch1-/-* mouse ESC derived neutralized embryoid bodies (Alfaro *et al.*, 2014) and is upregulated upon SHH-signalling. Expression of *PTCH2* was measured to assess whether upregulation could be observed in *PTCH1-/-* iPSC. SAG induced a statistical increase in expression of *PTCH1 and PTCH2* in wildtype but not in heterozygous or homozygous clones. A trend could be observed where SAG induces the biggest change in wildtype iPSC and the smallest change in homozygous iPSC. Although variability prevents final conclusions, these results may indicate that homozygous *PTCH1* mutant iPSC cannot be stimulated further.

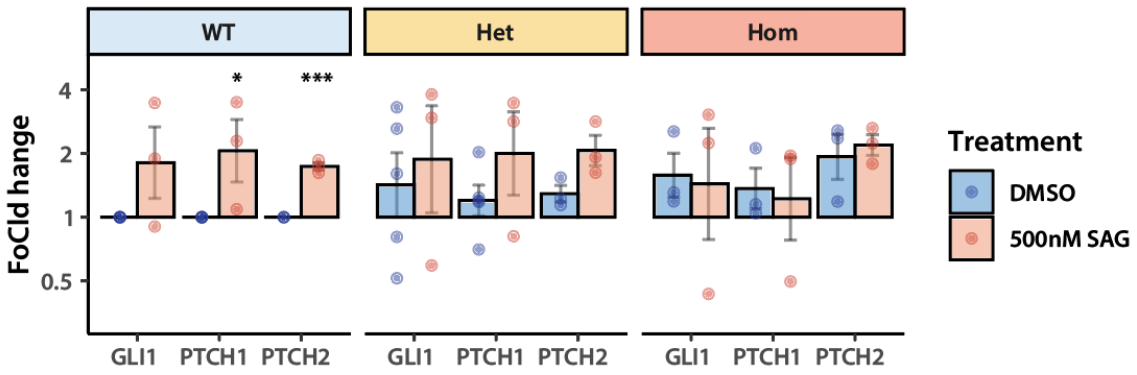


Figure 3.10: SHH-activation elicits response in wildtype but not in PTCH1-/- iPSC. *Messenger RNA expression of GLI1, PTCH1 and PTCH2 as measured by RT-qPCR. Expression is relative to the DMSO condition of wildtype parent iPSC line (AH017) and normalized using ACTB and GAPDH. Statistically significant differences on the genotype level are calculated on the ΔΔCt values by two-way t-test. Significance is indicated by asterisks, * = P<0.05, *** = p<0.001. Error bars represent standard error. Data points are generated from independent passages. N>3 for all clones and conditions.*

The SHH-pathway is known to induce proliferation in various cell types. To test the effects of increased endogenous SHH-signalling on proliferation of *PTCH1* mutant iPSC, cells were exposed to pulse labelling with 5-ethynyl-2'-deoxyuridine (EdU) which allows analysis of cell cycle phases. Cells were cultured to 60% confluency before incubation with EdU. EdU incorporates in the DNA during DNA-replication and therefore labels cells that are in S-phase. In combination with a DNA dye such as Hoechst 33342, the proportions of cells in different stages of the cell cycle can be determined. Between four independent passages, no significant differences were seen in cell cycle phase between the different genotypes and different clones. Slight differences could be seen in the proportions of cells in S-phase, albeit not statistically significant. In the original WT clone (AH017-3), 63.7% of cells were in S-phase (EdU positive), compared to 64.3% (range 63.7 - 65.5) and 63.0% (range 62.5 - 63.4) of heterozygous and homozygous clones, respectively (*Figure 3.11*). This suggests that the increased SHH-activity present in the *PTCH1* mutant iPSC does not lead to a

measurable increase in proliferation. Taken together with the assays of SHH responsiveness, these data indicate that the phenotype of WT and *PTCH1* mutant iPSC are not strongly regulated by SHH signalling.

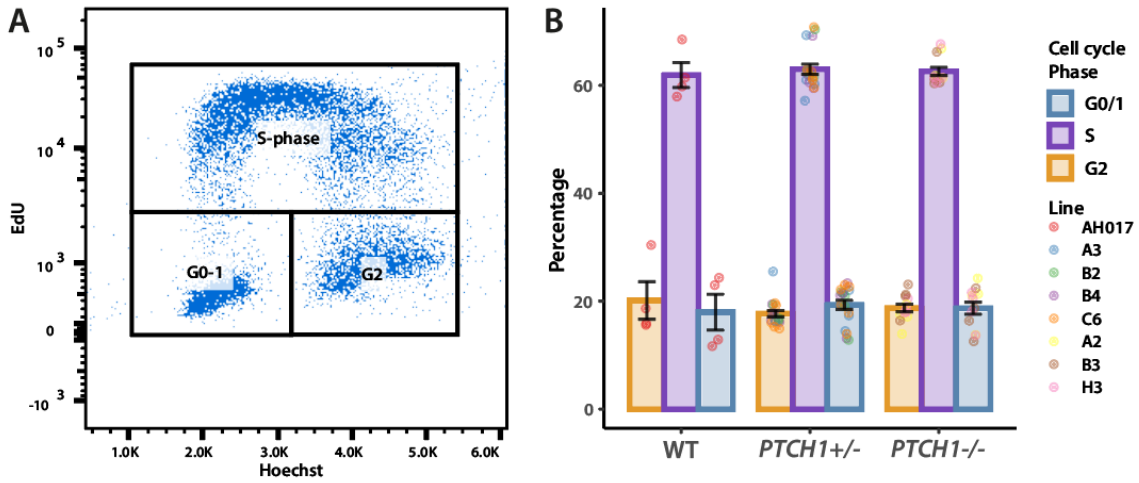


Figure 3.11: PTCH1 mutant iPSC do not display changes in cell cycle phase proportions. *Cells at 60% confluency were incubated with 10 uM ethynyl deoxyuridine (EdU) for one hour and subsequently processed for analysis using flow cytometry. A) Flow cytometry scatterplot illustrating the gating strategy on AH017-3 (PTCH1 wildtype) iPSC. B) Proportions of cells in G0/1 phase (red), S phase (blue) and G2 phase (green) as percentage of whole. Data points are generated from independent passages. N=3 for all clones.*

3.3 Discussion

In this chapter the strategy to generate *PTCH1* mutant human iPSC and their subsequent quality control and functional characterisation are described. These results show that CRISPR/Cas9 efficiently and specifically targets *PTCH1* in human iPSC. Heterozygous and homozygous clones maintained pluripotency marker expression and iPSC morphology. Furthermore, endogenous SHH-signalling was modestly increased but did not significantly affect proliferation in the clones tested.

The dual gRNA CRISPR strategy used to induce the mutation in *PTCH1* proved to be effective in deleting the 243-bp target sequence. The use of two gRNAs has been shown to improve efficiency of inducing LOF mutations over single gRNA strategies, which rely on indels inducing a frame shift (Mandal *et al.*, 2014; Zheng *et al.*, 2014; Zhou *et al.*, 2014; Kang *et al.*, 2015; Liu *et al.*, 2016). After the excision of the target region, the DNA is repaired through ligation of the blunt ends, making this method highly predictable and precise. This is reflected by the similarity in mutations found in the different iPSC clones.

The initial strategy was based on the inclusion of the intronic sequence between exon 3 and 4 that contains multiple stop codons. Surprisingly, mutant *PTCH1* mRNA did not include any intronic sequence nor did it contain exon 3. The resulting -1 frameshift causes early truncation of the protein in the first extracellular domain. Correct splicing of human pre-mRNA is regulated by elements called exon splicing enhancers (ESEs) and exon splicing suppressors (ESSs) (Cartegni, Chew and Krainer, 2002). The alternative splicing effect seen in the *PTCH1* mutant mRNA is likely due

to the disruption of one or more exon splicing enhancers (ESEs) resulting in aberrant splicing. In fact, point mutations affecting ESEs and ESSs causing alternative splicing are implicated in large number of genetic disorders (Krawczak, Reiss and Cooper, 1992; Lord *et al.*, 2019). When an asymmetric exon (meaning the length of the exon is not a multiple of three) is spliced out, a frame shift occurs. Depending on the presence of stop-codons in the other reading frames, this may lead to truncation of the protein, which is the proposed mechanism of LOF in the *PTCH1* mutant iPSC generated in this chapter. Utilising this as a specific strategy has been described previously and it may provide more control over the exact effect of CRISPR-induced mutations (Tuladhar *et al.*, 2019). The *PTCH1* mutant iPSC clones generated in this chapter all have the same mutant mRNA, lacking exon 3, thereby improving the consistency between clones and enhancing the comparisons between heterozygous and homozygous clones.

The most commonly used readout of SHH-pathway activity is *GLI1* mRNA expression. Expression levels of *GLI1* mRNA in *PTCH1* mutant iPSC are indicative of a modest increase in SHH-signalling. This finding is consistent with studies of Gorlin syndrome patient-derived iPSC that have shown constitutive high expression of *GLI1* (Hasegawa *et al.*, 2017; Nagao *et al.*, 2022). Other studies have found no difference but presented a low number of replicates (n=2) and large variability in measurements (Ikehara *et al.*, 2019). The only study to date that characterised *PTCH1-/-* human iPSC targeted the wildtype allele of Gorlin-iPSC clones using CRISPR (Nagao *et al.*, 2022). Similar to the findings in this chapter, these Gorlin derived *PTCH1-/-* iPSC showed increased expression of *PTCH1* and *GLI1* over both

their heterozygous parent line and a CRISPR-corrected isogenic *PTCH1+/+* line. SHH-stimulation experiments suggest that *PTCH1*-mutant iPSC might have a reduced ability for further activation. Similarly, in Hasegawa et al. (2017) Gorlin iPSC (*PTCH1+/-*) responded less to further SHH-activation than control iPSC. Taken together, these results are supportive of the introduced mutation in *PTCH1* causing loss-of-function.

In addition to being an essential morphogen, SHH is known to increase proliferation in a number of different cell types including GCPs and spinal cord progenitors, (Duman-Scheel *et al.*, 2002; Ruiz i Altaba, Palma and Dahmane, 2002; Wetmore, 2003). However, increased SHH-activity in *PTCH1*-mutant iPSC did not result in measurable increases in proliferation. Multiple factors influence the possibility of changes in proliferation, most importantly the baseline proliferation. As evidenced by the high percentage of EdU positive cells and the almost equal proportions of cells in G0/1 and G2, iPSC are highly proliferative. The doubling time of iPSC is typically between 18-20 hours, which could be the reason no significant differences were seen (Chatterjee *et al.*, 2016). Previous studies have used *PTCH1* mutant iPSC such as those derived from Gorlin syndrome patients and measured proliferation. Ikemoto et al. (2020) characterised proliferation in three Gorlin-patient derived iPSC lines (*PTCH1+/-)* and found no differences compared to a control line. Nagao et al (2022) made *PTCH1-/-* iPSC by disrupting the wildtype allele in Gorlin syndrome patient derived iPSC and found slight increases in proliferation in some but not all generated *PTCH1-/-* iPSC lines. Furthermore, two studies describe proliferation of *PTCH1*-mutant iPSC-derived NES of which one was able to identify a difference in growth

rate while the other did not show such a phenotype (Huang *et al.*, 2019; Susanto *et al.*, 2020). Taken together, it remains unclear whether iPSC proliferate more under SHH-activity, and differences are likely to be small compared to wildtype iPSC.

Comparison with an isogenic parent control line to truly study the effects of *PTCH1* LOF on cerebellar development and medulloblastoma tumorigenesis is essential and now possible with the iPSC-clones generated in this chapter. The use of *PTCH1* mutant iPSC for MB modelling is exemplified by tumour formation assays of Gorlin-iPSC injection in mice. Ikemoto and colleagues were the first to report a *PTCH1+/-* iPSC line. Although their first study focussed on the somatic mosaicism found in two of the generated iPSC clones, their second study reported tumorigenicity after subcutaneous implantation of iPSC into immunodeficient mice. In addition, one of these tumours showed loss of heterozygosity, similar to the human disease (Ikehara *et al.*, 2019). Gorlin derived CRISPR edited *PTCH1-/-* showed a higher frequency of tumours in a teratoma formation experiment that expressed TUBB3, Synaptophysin and MKI67. Although the authors conclude these tissues are medulloblastoma-like, comprehensive analysis of these tumours is required as none of these markers is specific to MB. Furthermore, the fact that unidentified additional genomic events in Gorlin iPSC may play a role limits the extent to which findings can be extrapolated to all *PTCH1* mutant medulloblastoma. To date, only one study has reported the generation of *PTCH1* mutant iPSC using wildtype human iPSC (Zu *et al.*, 2021), but did not perform any functional characterisation. This chapter is therefore the first to describe the generation and functional characterisation of *PTCH1+/-* and *PTCH1-/-* iPSC from a wildtype background.

3.4 Conclusion

While maintaining the expression of pluripotency markers, the iPSC clones generated in this chapter exhibit modestly increased SHH-pathway activity consistent with LOF of PTCH1. Extensive quality control did not reveal any unwanted effects on the top predicted off-target sites and large-scale mapping of SNPs showed maintained genome integrity of the generated mutant clones. Compared to iPSC derived from Gorlin-syndrome patients, the *PTCH1* mutant iPSC generated in this chapter provide the advantage of having an isogenic control line along with the possibility to study both heterozygous and homozygous LOF on the same genetic background. In Chapter 4, the effect of PTCH1 LOF on cerebellar development and potential MB tumorigenesis will be evaluated using a cerebellar organoid model.

Chapter 4 Characterising the effects of *PTCH1* LOF on cerebellar differentiation.

4.1 Introduction

Pluripotent stem cells can be used to generate various cell types and tissues, including cerebellar neurons. Early work used mouse and ESC and induced cerebellar differentiation through the addition of patterning molecules expressed in the IsO (Su *et al.*, 2006; Salero and Hatten, 2007). The IsO is the primary regulator of cell type specification at the midbrain-hindbrain barrier (see section 1.2). *OTX2* is expressed cranially from the IsO and marks the presumptive midbrain. Caudally, *GBX2* expression marks the hindbrain and the prospective cerebellar territory. IsO signalling occurs through FGF8, which regulates the expression of *OTX2* and *GBX2* and interacts with WNT1. BMP- and WNT-signalling from the choroid plexus further pattern the cerebellar anlage to produce two germinal zones: the VZ that generates GABAergic neurons and the RL, which originates glutamatergic neurons. Although the initial protocols from Su and Salero et al. efficiently generated cells displaying GCs characteristics, the production of PCs was far less efficient.

To overcome this problem, Muguruma et al. (2010) differentiated ESC as embryoid body (EB)-like aggregates. This approach was based on the seminal work of Watanabe et al. that was the first to show how differentiation in floating EBs could be directed to specific dorsal and ventral neural fate (Watanabe *et al.*, 2005). In these 3D cultures, the addition of only insulin and FGF2 was sufficient to induce the

formation of an IsO-like signalling centre and start cerebellar patterning. This protocol was more efficient in generating PCs, and this was successfully applied to human ESC (Muguruma *et al.*, 2015) and later induced pluripotent stem cells (iPSC) (Ishida *et al.*, 2016; Muguruma, 2018). The generated 3D structures are commonly referred to as cerebellar organoids. Their differentiation uses the self-inducive capacities of EBs to recapitulate MHB organisation and cerebellar lineage formation. Single-cell RNA sequencing (scRNAseq) of cerebellar organoids maintained for 90 DIV revealed the presence of all cerebellar developmental cell types (Nayler *et al.*, 2021). Among other cell types, clusters containing rhombic lip (RL), GC-progenitors (GCPs), proliferating GCs and post mitotic GCs were identified. Comparisons with published single-nuclei RNA sequencing (snRNAseq) data (Aldinger *et al.*, 2021) and the Brainspan Data (Miller *et al.*, 2014) revealed that the organoids matched human developmental stages post conceptual weeks (PCW) 14-21. Thus, cerebellar organoids allow the study of human specific development and provide opportunities to generate novel disease models.

The generation of PSC-derived disease models has gained momentum (Shi *et al.*, 2017), and groups have begun to model cerebellum-specific neurodegenerative disorders such as spinocerebellar ataxias (SCAs) with iPSC (reviewed in Wong et al., 2017). More recently, reports of medulloblastoma (MB)-modelling have been published, focussing on group 3 subtype (Ballabio *et al.*, 2020, 2021). In this work, cerebellar organoids were generated, followed by the introduction of MB driver genes using electroporation. Twenty-five days post-electroporation, excessive cell proliferation was observed in organoids electroporated with a combination of either

GFI1 + *c-MYC* or *OTX2* + *c-MYC*. In a methylation array, cells electroporated with either combination clustered towards group 3 MB, suggesting a resemblance to the human disease. In their second report, conditional expression of *GFI1* and *c-MYC* restricted to specific progenitor populations was used in an attempt to elucidate the cell of origin in group 3 MB (Ballabio *et al.*, 2021). However, despite the efficacy in generating growths in cerebellar organoids, forced expression of onco-driver genes might form a biased model not representing the full complexity of genetic events underlying MB tumorigenesis.

Modelling genetic predisposition may therefore provide a more truthful recapitulation of *in vivo* pathogenesis. Several predisposition syndromes are associated with MB, including carriers of *PTCH1* mutations (Waszak *et al.*, 2018). PTCH1 is the primary negative regulator of the SHH-pathway activity, and inherited LOF mutations cause an increased risk of the SHH-MB. Two groups have modelled SHH-MB using NES differentiated from iPSC from patients carrying *PTCH1* mutations (Huang *et al.*, 2019; Susanto *et al.*, 2020). Following orthotopic injection, injected mice developed MB-like tumours, sharing characteristics with the human disease. However, relevant drawbacks to this strategy include the high cost of mouse research and species specific copy number alteration acquisition or 'mouse-specific tumour evolution' (Ben-David *et al.*, 2017). To date, no studies have reported complete *in vitro* MB tumorigenesis modelling from a genetic predisposition background. This chapter describes the generation of cerebellar organoids from *PTCH1* mutant iPSC, investigates the effects of *PTCH1* LOF on *in vivo* neural development and highlights human-specific aspects of cerebellar neurogenesis.

4.2 Results

4.2.1 Cerebellar organoid differentiation

Induced pluripotent stem cells can be differentiated into cerebellar organoids that mimic cerebellar development. Using a differentiation protocol established in the Becker group (Watson *et al.*, 2018) that is based on the original Muguruma protocol (Muguruma *et al.*, 2015) cerebellar differentiation of embryoid bodies is initiated through the addition of FGF2 and insulin (*Figure 4.1*). Insulin acts as a moderate caudalising factor (Wataya *et al.*, 2008) and induces neural fate through its involvement in BMP- (Pera *et al.*, 2001) and Wnt signalling (Richard-Parpaillon *et al.*, 2002; Haramoto *et al.*, 2015). FGF2 (also known as basic FGF or bFGF) is well known as a patterning molecule in neuronal differentiation of PSC (reviewed in Guillemot & Zimmer, 2011) and has been shown to control anterior-posterior identity of iPSC-derived neuron progenitors in a dose-dependent manner (Zhou *et al.*, 2016). At the same time, mesenchymal and endodermal differentiation are suppressed using the TGF-β inhibitor SB431542 (Chambers *et al.*, 2009). Finally, cell dissociation can induce apoptosis in PSCs which is countered by treatment with Rho-associated kinase (ROCK) inhibitor Y-27632 (Watanabe *et al.*, 2007). Over several weeks, hallmarks of cerebellar development at several different stages can be seen, and long-term maintenance of organoids allows the maturation of cerebellar cell types.

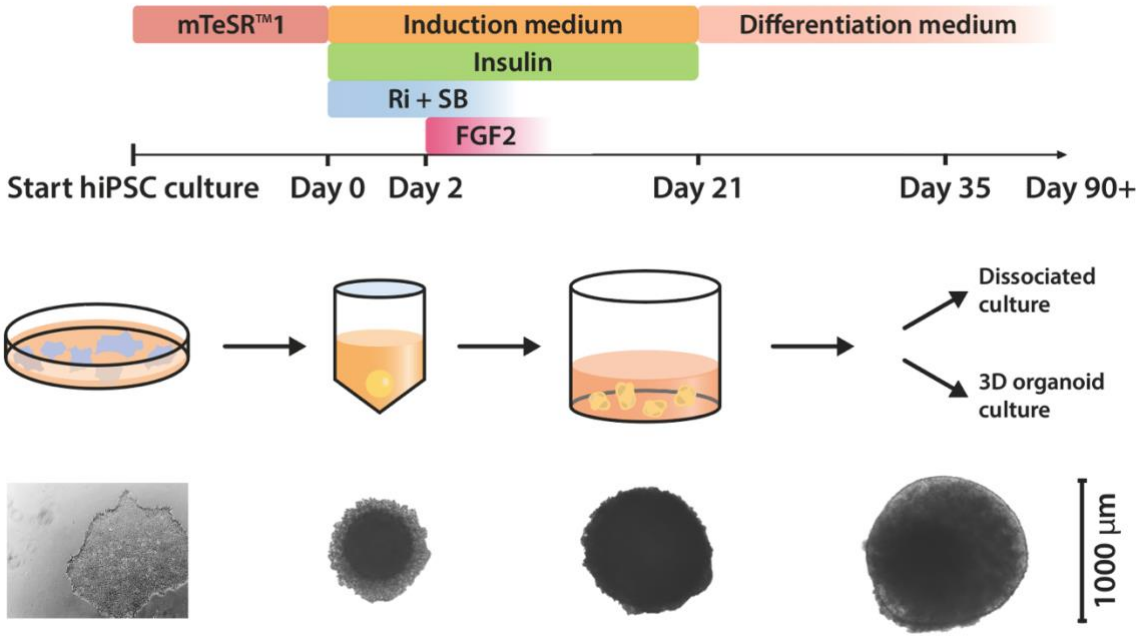


Figure 4.1: Overview of the cerebellar differentiation protocol. *Induced pluripotent stem cells (iPSC) are maintained in mTeSR1 medium before seeding into ultra-low-attachment V-bottom 96-well plates. The Induction Medium contains Rho kinase inhibitor Y-27632 (Ri) and TGF-b signalling inhibitor SB431542 (SB) to prevent apoptosis and mesendodermal differentiation, respectively. Fibroblast growth factor 2 (FGF2) is added on DIV 2 to induce cerebellar lineage formation. Neural aggregates are transferred into low-attachment 48-well plates on DIV 14. On DIV 21, the medium is changed to differentiation medium consisting of Neurobasal, N2 supplement and GlutaMAX. After 35 days, organoids can be maintained floating in suspension or cultured at the air-liquid interface. Representative brightfield images show, from left to right, an iPSC colony, embryoid body (EB)(DIV 1), neural aggregate (DIV 21), and organoid (DIV 35).*

After 21 DIV, engrailed 1 (*EN1*) and gastrulation brain homeobox 2 (*GBX2*) are expressed while orthodenticle homeobox 2 (*OTX2*) that is expressed caudally to the IsO is not expressed (*Figure 4.2*). After 35 DIV, markers associated with the two main germinal zones in the cerebellum are expressed: Atonal bHLH transcription factor 1 (*ATOH1*), marking the rhombic lip (RL) lineage that produces all the glutamatergic neurons in the cerebellum as well as kirre-like nephrin family adhesion molecule 2 (*KIRREL2*), a membrane protein that marks the ventricular zone (VZ), producing GABAergic neurons. Long-term differentiation sees the expression of calbindin

(*CALB1*), a marker for PCs. These neuronal tissues also express βIII-tubulin (*TUBB3*), a pan-neuronal marker, and RL-derivative marker paired box 6 (*PAX6*).

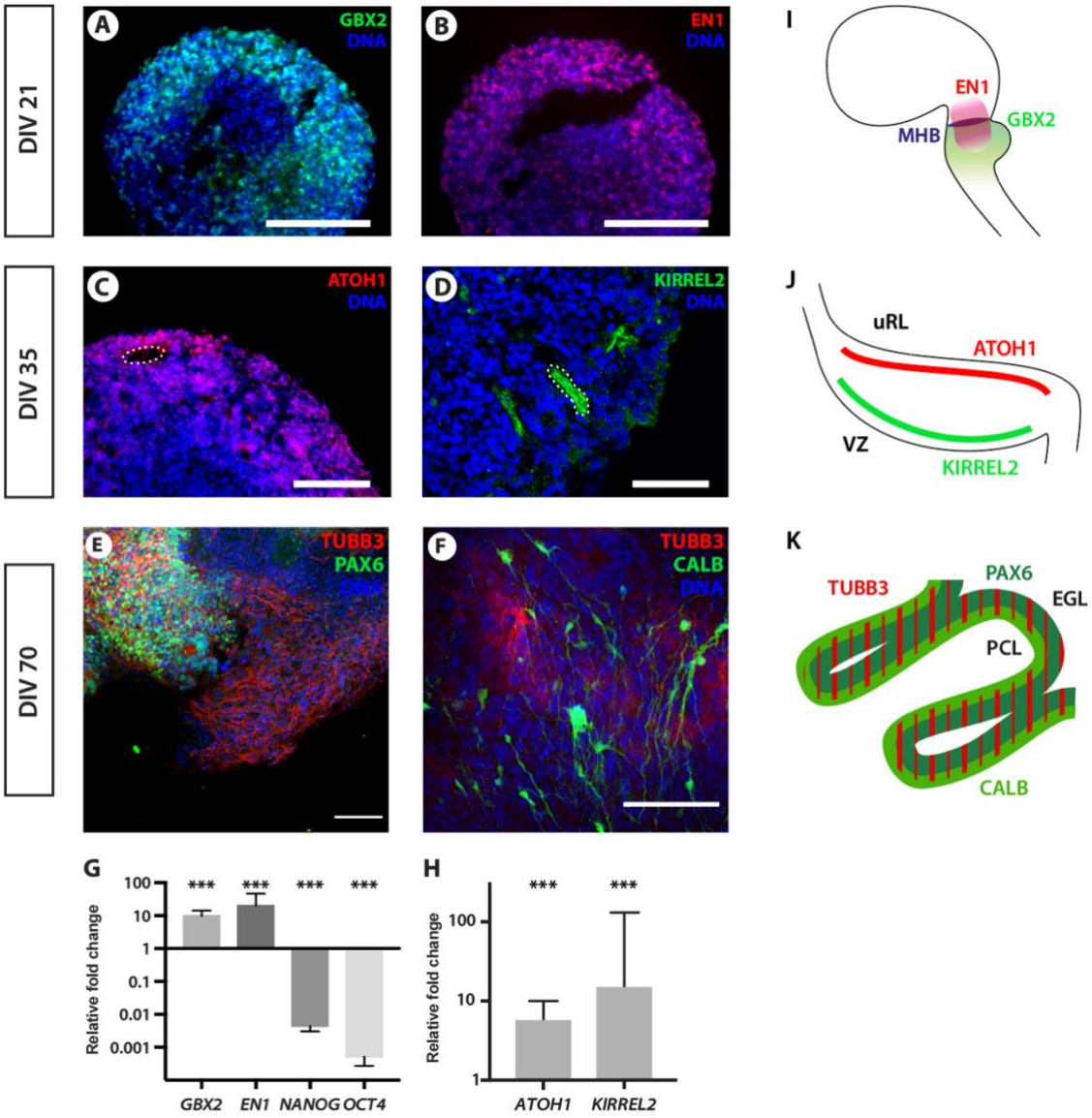


Figure 4.2: Cerebellar organoid differentiation of iPSC. *A, B) Expression of hindbrain markers GBX2 (green) and EN1 (red) in DIV 21 cerebellar organoids, visualised using immunofluorescent antibody staining. Nuclei are visualised in blue by Hoechst staining. Scale bars 150 µm. (C, D) Expression of rhombic lip precursor marker ATOH1 (red; C) and ventricular zone precursor marker KIRREL2 (green; D) visualised using immunofluorescent antibody staining. Nuclei are visualised in blue by Hoechst staining. The dashed line indicates an example of a neuroepithelial lumen (rosette). Scale bars 150 µm. (E, F) Expression of pan-neuronal marker TUBB3, granule cell progenitor marker (PAX6) and Purkinje cell marker (CALB) visualised using immunofluorescence antibody staining. Scale bars 100 µm. (G) Relative mRNA*

expression of GBX2, EN1, NANOG and OCT4 in DIV 21 cerebellar organoids compared to iPSC. Expression is normalised to the reference gene GAPDH and composed of three biological replicates. Error bars represent SD. All results were significant with P-values <0.0001 (***), computed with unpaired t-tests. (H) Mean fold change in mRNA expression of markers in DIV 35 organoids relative to iPSC and normalised to the reference gene GAPDH. Data are composed of three biological replicates. Error bars represent SD. All results were significant with P-values <0.0001, computed with unpaired t-tests. (I) Schematic representation of GBX2 (green) and EN1 (red) expression at the midbrain-hindbrain boundary (MHB) in the early developing human brain. (J) Schematic representation of ATOH1 (red) and KIRREL2 (green) expression in the developing human cerebellum, associated with the upper rhombic lip (URL) and ventricular zone (VZ), respectively. (K) Schematic representation of PAX6 (dark green) expressing cells in the external granule layer (EGL) and CALB (light green) expressing cells in the Purkinje cell layer (PCL) in developing human cerebellar folia. TUBB3 (red) expression as pan-neuronal marker is depicted across both layers.

Although the expression of markers associated with Purkinje cells has been extensively characterised (Muguruma *et al.*, 2015; Watson *et al.*, 2018; Nayler *et al.*, 2021), less attention has been paid to RL-derivatives and granule cell progenitors (GCPs). Single-cell RNA sequencing data from Nayler et al. (2021) revealed the presence of GCP-like cells after 90 days of culture. Yet, the expression of GCP markers earlier in the differentiation trajectory has not been investigated. Therefore, the characterisation of cerebellar organoids between 17 and 40 days post-seeding was carried out to establish the expression of genes associated with GCP development. Temporal expression of *ATOH1-, PAX6-, ZIC1-, ZIC3-, PDE1C-, CNTN2-* and *MYCN*-mRNA was measured using RT-qPCR (*Figure 4.3*). *ATOH1* and *PAX6* showed a linear trend with the highest expression towards the end of the time period. Although the expression of *ZIC1*, *PDE1C* and *CNTN2* significantly increased from iPSC levels, it remained more stable during the differentiation. *MYCN* and *ZIC3* were not significantly upregulated in their expression compared to iPSC. This is likely due to the already high expression of these transcription factors in iPSC, which are both involved in regulating pluripotency genes (Lim *et al.*, 2007; Cotterman and

Knoepfler, 2009). The expression of these markers suggests the presence of RL-derivatives and GCPs in the differentiated cerebellar organoids and further support their use for MB modelling.

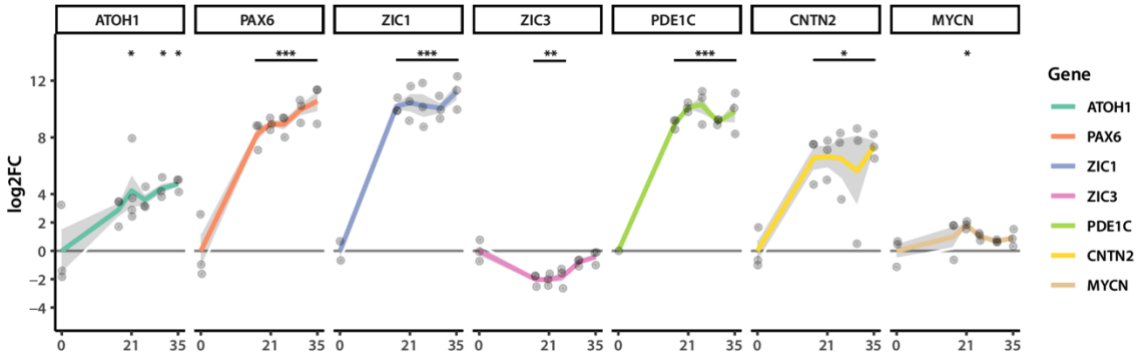


Figure 4.3: GCP marker expression during cerebellar organoid differentiation. *Log2 fold change in gene expression as measured by RT-qPCR, relative to iPSC levels and normalised using ACTB and GAPDH. Data are composed of three biological replicates. Ribbons represent SD. P-values are depicted as p<0.05 = *, p<0.01=**, p<0.001= *** by ANOVA with Dunnett's post-hoc test.*

4.2.2 *PTCH1*-mutation affects cerebellar differentiation of iPSC

4.2.2.1 Growth and morphology

Having established that cerebellar organoids contain the cell-of-origin of SHH-MB, the GCP, this model provides opportunities to test the effect of *PTCH1* mutations on cerebellar- and GCP development. Thus, heterozygous and homozygous *PTCH1* iPSC generated in Chapter 3 were differentiated into cerebellar organoids. *PTCH1* heterozygous and homozygous mutants showed an increased growth rate during 35 days of differentiation, with homozygous organoids being larger than heterozygous organoids (*Figure 4.4*). Heterozygous organoids exhibited a similar shape to control organoids. In contrast, homozygous organoids showed changed morphology with more irregular growth and more polarisation of the tissue, marked by the more

translucent edges on brightfield imaging. The increased growth rate and changed phenotype indicate a substantial impact on the differentiation of *PTCH1* mutant iPSC.

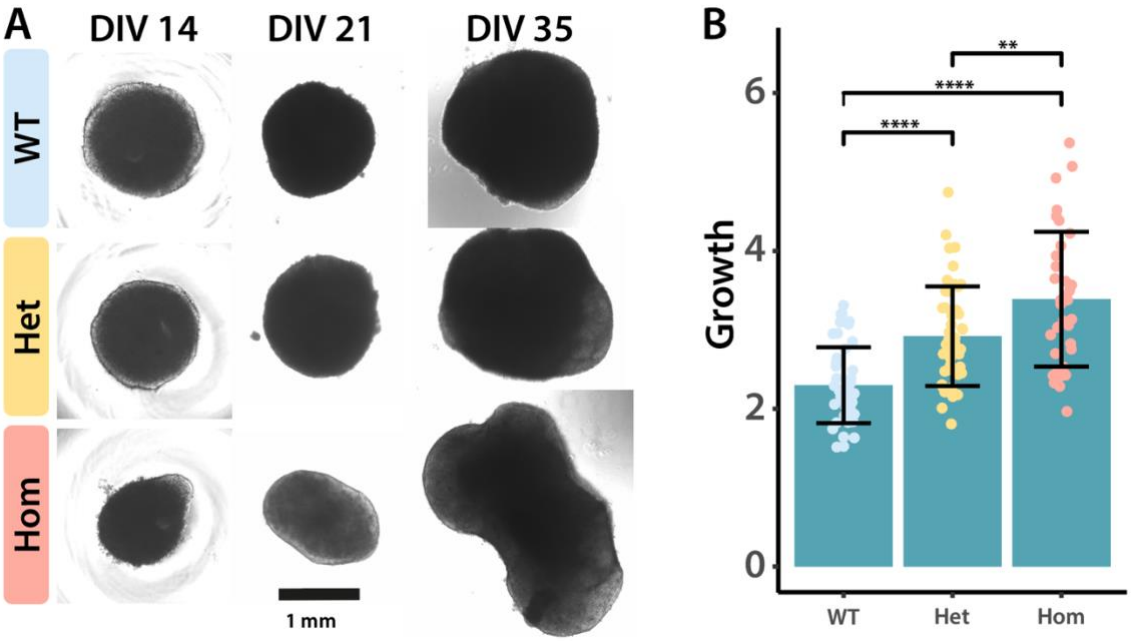


Figure 4.4: PTCH1 mutation changes organoid morphology. *A) Representative images of organoids during differentiation. B) Relative size of organoids at DIV 35 compared to DIV 7. Data are composed of 46 (WT), 48 (Het) and 35 (Hom) individual organoids across three differentiations. Statistical significance is indicated as p<0.05=*, p<0.01=**, p<0.001=*** computed by ANOVA with Tukey post-hoc test.*

4.2.2.2 Differentiation into midbrain-hindbrain boundary (MHB) progenitors

At the MHB, the presumptive hindbrain expresses *EN1* and *GBX2*, while *OTX2* is expressed cranially in the midbrain. Expression of *EN1*, *GBX2* and, as a control, *OTX2* was measured after 21 days of differentiation to evaluate the effects of PTCH1 LOF on hindbrain specification (*Figure 4.5*). Heterozygous and homozygous organoids expressed significantly higher levels of *EN1* compared to control (both p=0.01), while *GBX2* expression remained similar. Expression of *OTX2* was not significantly different between WT and heterozygous (p=0.85) but showed non-statistically significant elevation in homozygous organoids (p=0.146). Gene expression changes

were reflected in immunofluorescence staining with higher EN1 signal apparent in heterozygous and homozygous organoids and no changes in GBX2 staining (*Figure 4.5*). Taken together, changes in patterning genes in *PTCH1*-/- organoids suggest phenotypic changes in cellular/progenitor identities.

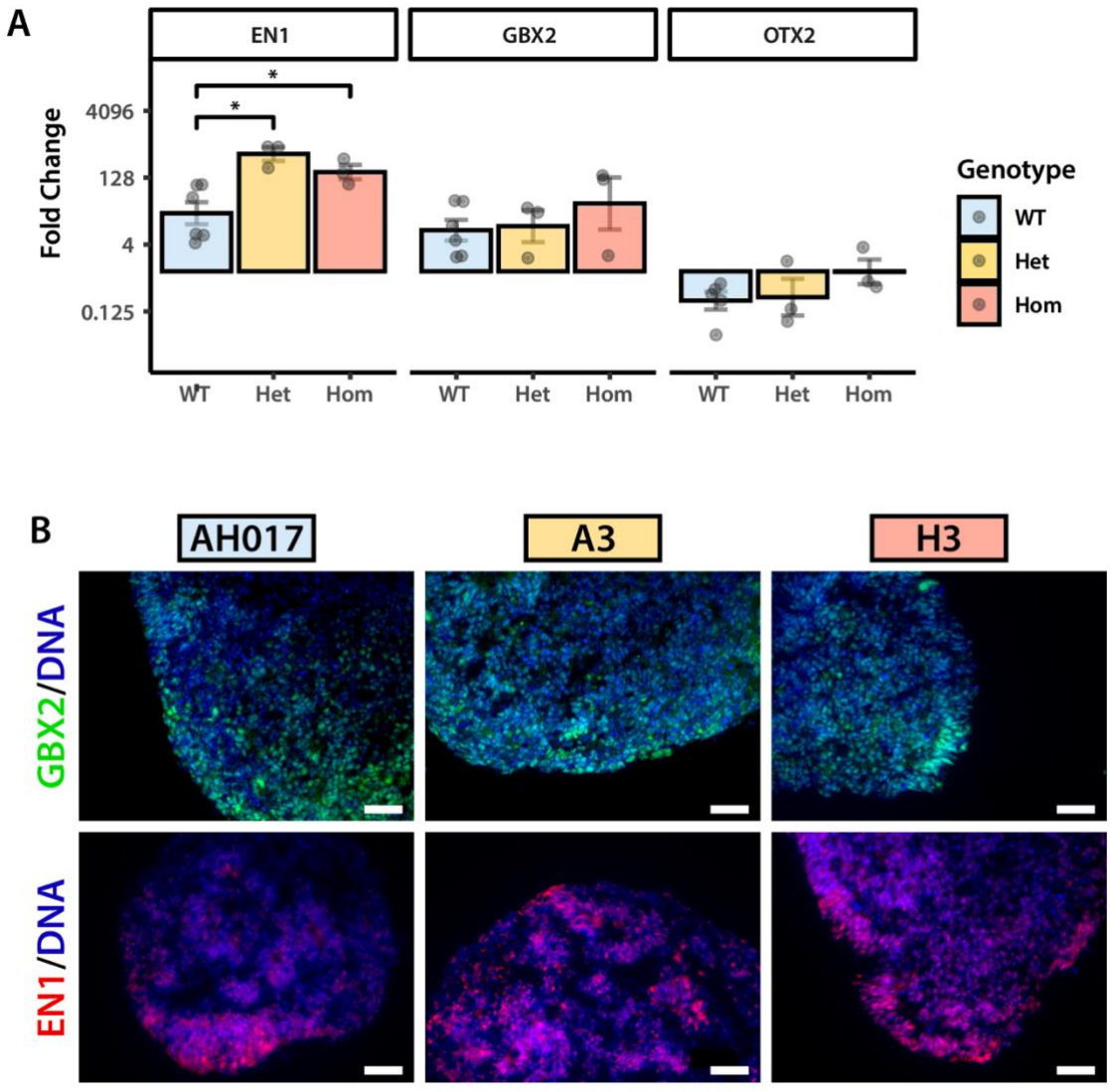


Figure 4.5: Isthmic organiser marker expression in PTCH1-mutant organoids. *A) Expression of EN1, GBX2 and OTX2 at DIV 21 relative to iPSC in heterozygous (A3) and homozygous (H3) organoids as measured by RT-qPCR normalised to GAPDH and ACTB. Data are composed of three or more biological replicates from separate differentiations. Statistical significance indicated as p<0.05=*, computed by ANOVA with Dunnett's post-hoc test. B) Immunofluorescence staining of DIV 21 neural aggregates with antibodies specific to the hindbrain markers GBX2 (green) and EN1 (red). Nuclei are visualised in blue by Hoechst staining. Scale bars 150 µm.*

4.2.2.3 Differentiation into cerebellar lineages

In control (WT) organoids, expression of cerebellar lineage markers is measurable after 35 days of differentiation. To investigate how different *PTCH1* genotypes affect the development of glutamatergic and GABAergic cerebellar neurons, gene expression of *ATOH1*, *PAX6* (glutamatergic) and *KIRREL2* (GABAergic) were measured using RT-qPCR (*Figure 4.6*). Expression of both glutamatergic and GABAergic markers was significantly lower in homozygous organoids compared to WT. In contrast, *ATOH1* and *KIRREL2* expression in heterozygous organoids were not significantly different. In fact, the expression of *PAX6* was substantially higher in heterozygous organoids compared to WT ($p<0.001$), which was opposite to the effect seen in homozygous organoids. These changes were accompanied by increased SHH-pathway activity as measured by the expression of the transcription factor GLI1 as a readout for canonical SHH-signalling (see section 1.3.1). Changes appeared in a 'dose-dependent' manner, where heterozygous organoids expressed lower levels of *GLI1* than homozygous organoids. Strikingly, the expression of *SHH* encoding the activating ligand of the pathway was also increased, possibly indicating the presence of self-inductive feedback. Changes in PAX6 and KIRREL2 expression as markers for the RL and VZ were confirmed using immunocytochemistry (*Figure 4.6*). Homozygous organoids did not express these cerebellar markers, while PAX6 expression was moderately increased in heterozygous organoids compared to wildtype. Together with the lower expression of cerebellar lineage markers, this indicates significant changes in cellular phenotype in *PTCH1-/-* organoids. The maintained expression of cerebellar markers in heterozygous organoids suggests

that sufficient levels of functional PTCH1 are present in these organoids to facilitate the initial stages of cerebellar development.

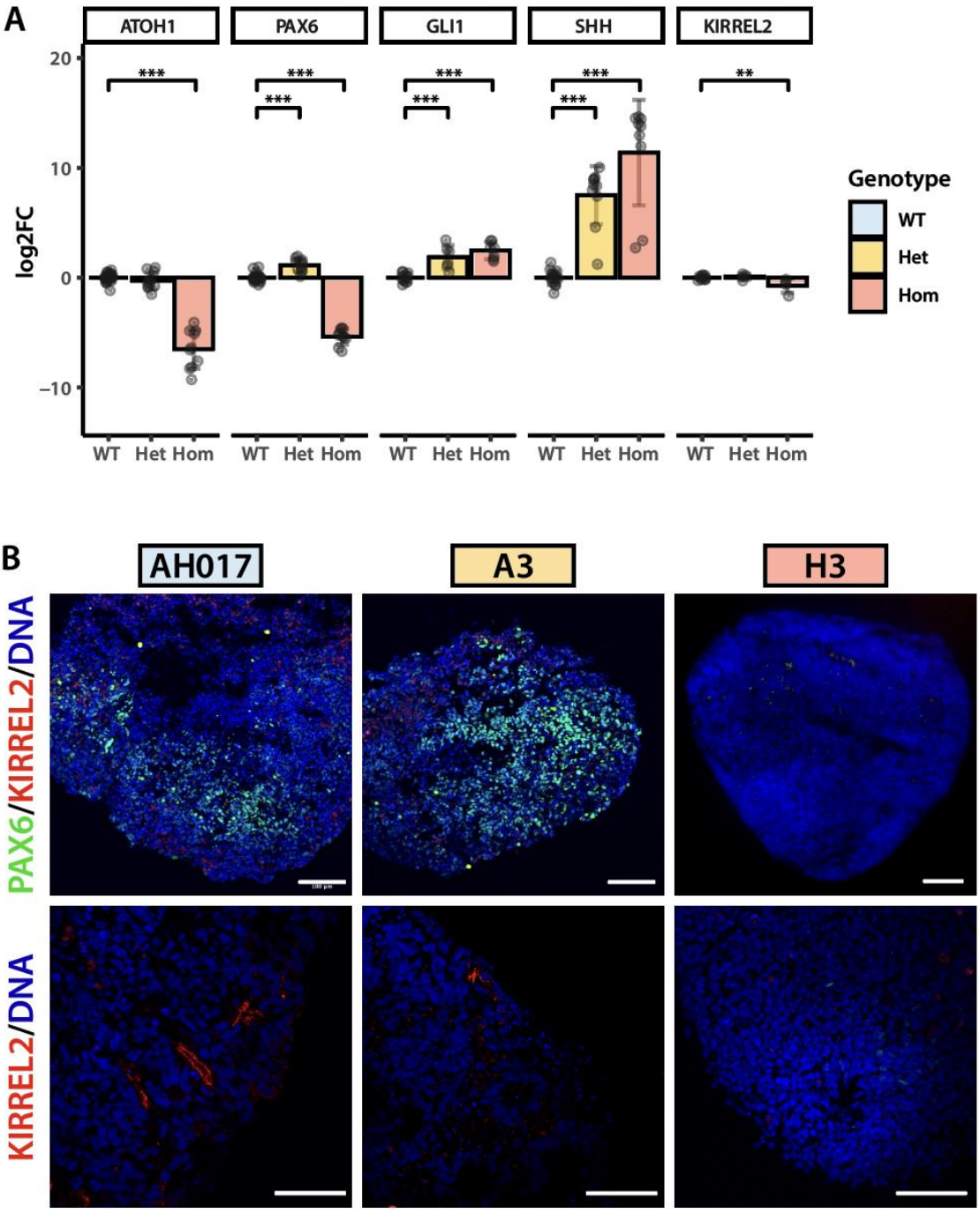


Figure 4.6: Pronounced changes in cerebellar marker expression in PTCH1 mutant organoids at DIV 35. *A) Expression of cerebellar and SHH-pathway genes, measured by RT-qPCR. Each data point represents an experimental replicate. At least three replicates per genotype. Statistical tests were computed with ANOVA, followed by Dunnett's post-hoc test.*

Data are composed of at least three biological replicates from separate differentiations. P<0.05=, p<0.01=**, p<0.001=***. B) Immunofluorescence staining of DIV 35 organoids with antibodies specific to the rhombic lip lineage marker PAX6 (green) and ventricular zone marker KIRREL2 (red). Nuclei are visualised in blue by Hoechst staining. Scale bars 100 µm.*

4.2.3 Altered differentiation trajectory of *PTCH1-/-* iPSC

Transcriptomic changes underlying these results were further investigated by bulk RNA sequencing of DIV 35 organoids. Despite extensive quality control and evaluation of potential off-target CRISPR activity, there is still a chance of unidentified events in different clones. Therefore, three clones of heterozygous and homozygous iPSC were differentiated into DIV 35 organoids and submitted for sequencing to control for clone-specific effects. High-quality RNA (RNA integrity number >9) was isolated from a pool of 15 organoids per clone and sequenced to 25 million reads per sample. Gene expression was quantified using Salmon 15.2. Interrogation of the transcriptomes was then performed using DESeq2 (version 1.36.0).

Initial analysis of sample similarity was performed by principal component analysis (PCA) and calculation of Euclidean distances. Due to the dropout of one sample, the initial analysis was performed on a dataset containing just two heterozygous samples. For subsequent analyses, a second round of sequencing was performed with another three wildtype and four heterozygous samples to enhance power. Differential gene expression analysis of wildtype compared to heterozygous and homozygous samples was performed separately to mitigate batch effects. Gene expression was normalised using Variance-stabilising transformation (VST), which allows for better normalisation of the lower-count genes compared to traditional log

transformation. PCA with the 1000 most variable genes showed apparent clustering of the samples by genotype, clustering heterozygous samples closer to wildtype than to homozygous organoids (*Figure 4.7*). This was also seen in Euclidean distances measured between the samples when including all genes (*Figure 4.7*). These results are consistent with genotype contributing most to the variation between samples.

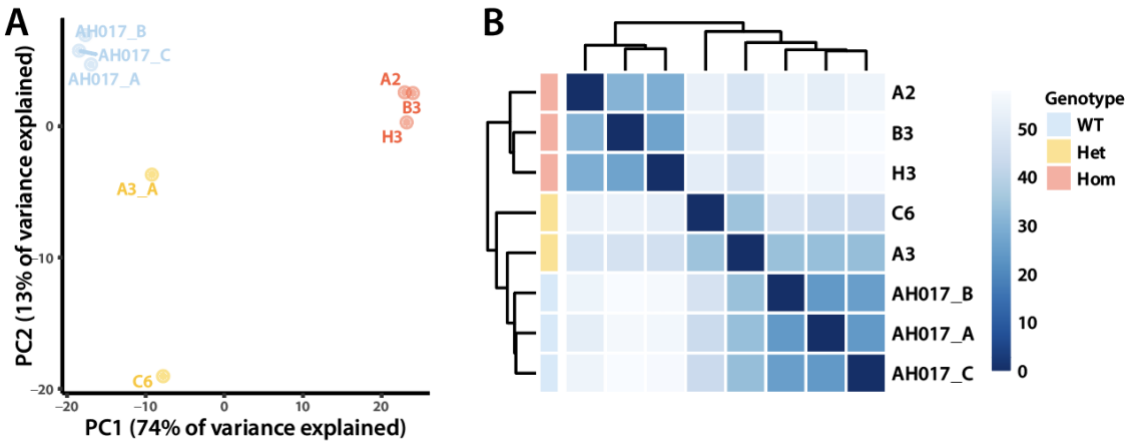


Figure 4.7: Genotype is the main driver behind transcriptome differences. *A) Principal component analysis using the 1000 most variable genes showing the separation of samples in principal component (PC) 1 and PC2. B) Hierarchical clustering of dissimilarities between samples measured using Euclidean distances.*

4.2.3.1 Differential gene expression analysis of homozygous organoids

Transcriptome changes in homozygous organoids were further investigated by differential gene expression analysis performed using *DESeq2* (version 1.34.0) (Love, Huber and Anders, 2014) with a false discovery rate (FDR) cut-off of <0.05 to determine differential expression. Effect sizes were moderated through shrinkage of logarithmic fold change (LFCs) using Approximate Posterior Estimation for generalised linear model, *apeglm* (Zhu, Ibrahim and Love, 2019). In total, 4054 genes met the adjusted p-value cut-off and had a mean expression of at least 50 counts. Examination of the most differentially expressed genes (DEGs) revealed increased

expression of genes associated with the ventral neural tube (*SHH* and *FOXA2*) in homozygous organoids. In contrast, genes marking the dorsal neural tube (*WNT3A* and *TLX3*) were less expressed than in wildtype organoids (*Figure 4.8*). These results are consistent with mouse data showing the absence of the dorsal neural tube in *Ptch1-/-* animals, together with an expansion of the floorplate (Goodrich *et al.*, 1997). Upon further exploration, gene expression associated with the developing forebrain, such as *NKX2.1, FOXG1* and *SIX3,* was higher in homozygous organoids along with lower expression of hindbrain markers such as *GBX2, ATOH1,* and *LMX1A* (*Figure 4.8*). These findings indicate that the complete absence of PTCH1 function results in changes affecting both the ventral-dorsal axis and the rostral-caudal axis. Interestingly, while the expression of *GLI1* as a readout for SHH-signalling was increased compared to control, this difference was not statistically significant. This could, however, be due to the sample size not being sufficient, especially as the difference was significant when tested with RT-qPCR (*Figure 4.6*A). Moreover, the related genes *GLI2* and *GLI3* were downregulated in the homozygous organoids. In contrast, downstream targets *MYCN* and *SFRP1* were upregulated. Although SHH-signalling primarily functions through the proteasomal processing of GLI proteins, reduced levels of *GLI2* and *GLI3* might suggest roles for non-canonical, GLI-independent SHH-signalling and tissue-specific SHH-signal transduction.

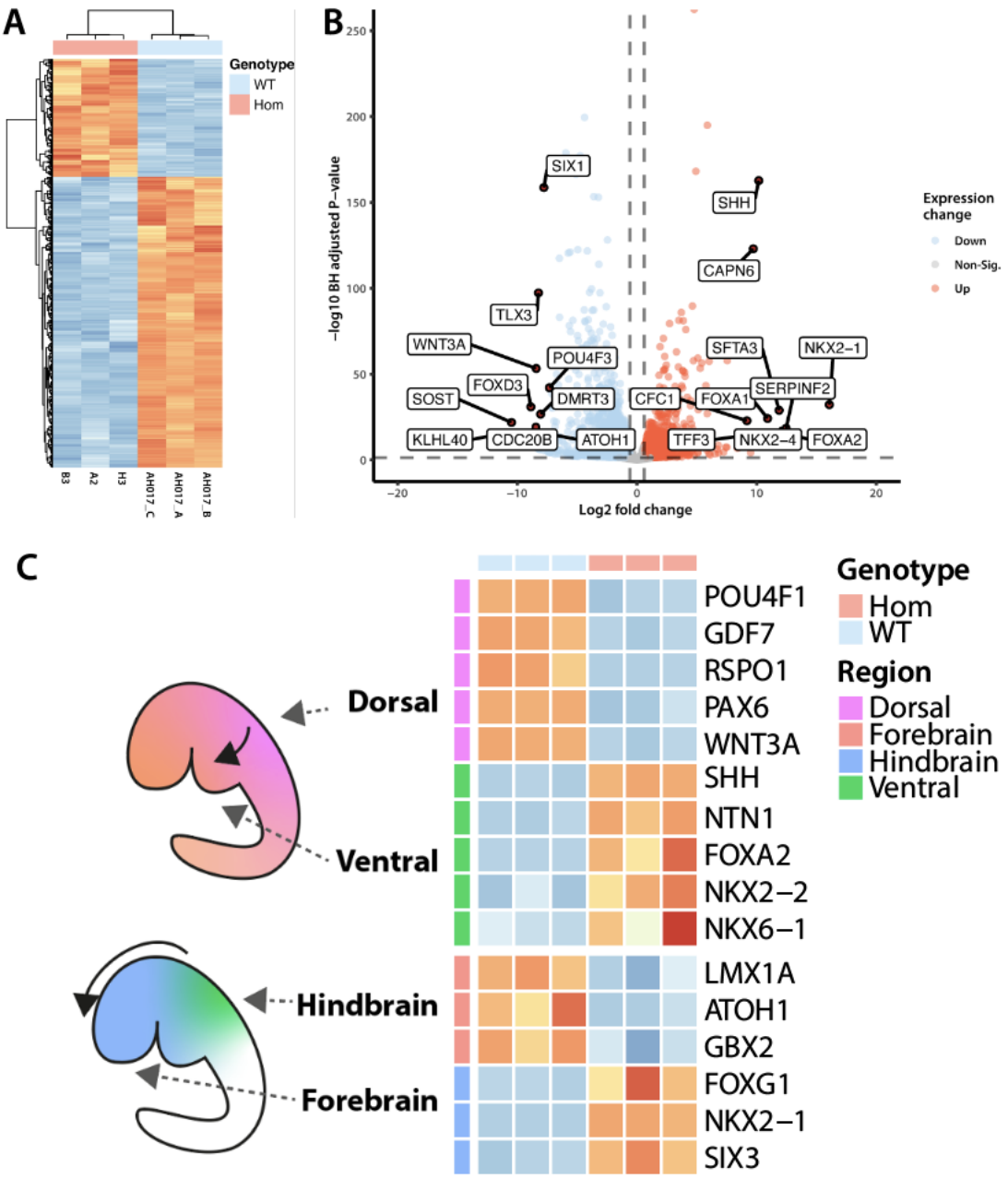


Figure 4.8: PTCH1-LOF prevents cerebellar differentiation and alters trajectory towards the ventral forebrain. *A) Heatmap showing expression of the top 500 differentially expressed genes between wildtype and homozygous organoids. B) Volcano plot of the ten genes with the most significant change in either direction. C) Expression of genes associated with the dorsal neural tube (Dorsal), ventral neural tube (Ventral), hindbrain and forebrain.*

In homozygous organoids, ablation of PTCH1 function results in increased SHH signalling from an early stage of neural differentiation. This likely leads to self-

induction of SHH production and the formation of ventral neural tube phenotype within the organoid. The presence of ventral neural tube structures was confirmed by immunostaining of homozygous organoids for the ventral neural tube marker NKX2.2. Multiple regions within homozygous organoids expressed high levels of NKX2.2, suggesting the presence of signalling centres within the organoid that cause ventralisation (*Figure 4.9*).

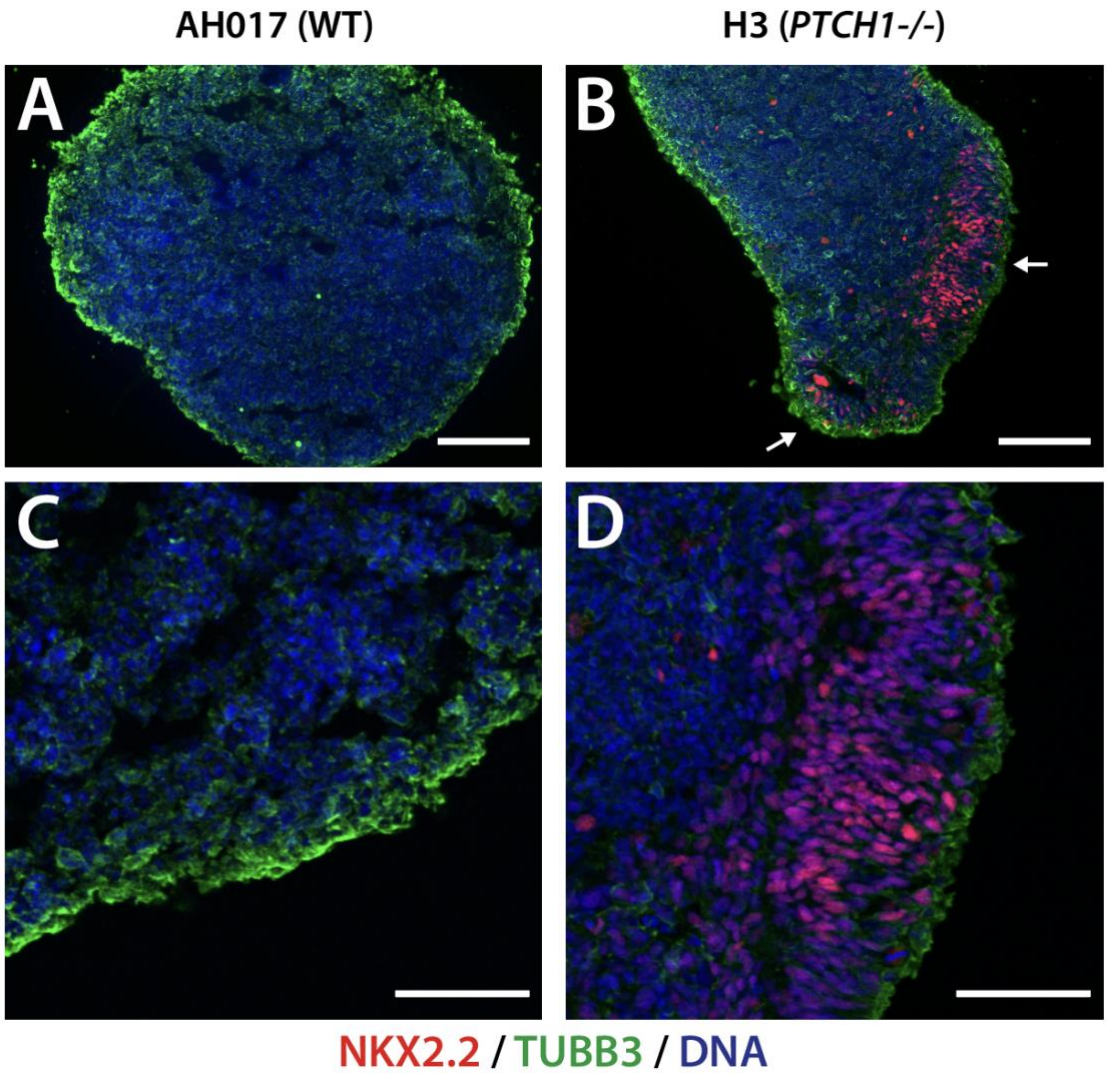


Figure 4.9: Evidence of SHH signalling centres in PTCH1-/- organoids. *Immunofluorescence staining of DIV 35 organoids with antibodies specific to pan-neuronal marker TUBB3 (green) and floorplate marker NKX2.2 (red). Nuclei are visualised in blue by Hoechst staining. Scale bars in A and B are 250 µm, and in C and D are 100 µm.*

The role of SHH signalling during the altered differentiation trajectory of *PTCH1*-/- organoids was further investigated using SMO-inhibitor Cyclopamine. During the 35 days of differentiation, organoids were exposed to either 1 µM or 5 µM Cyclopamine that was added to every medium change (once per week) and compared to the DMSO control (*Figure 4.10*). In addition, wildtype organoids were treated with 500 nM SAG to simulate enhanced SHH stimulation. Treatment with SAG significantly increased the expression of *SHH* while decreasing the expression of *ATOH1* and *PAX6* in wildtype organoids. Conversely, Cyclopamine treatment had minor effects on gene expression in wildtype organoids. In homozygous organoids, Cyclopamine rescued the expression of both *ATOH1* and *PAX6* in a dose-dependent manner, while marginally reducing *SHH* expression. Protein expression of PAX6 and NKX2.2 as respective readouts of the dorsal and ventral neural tube phenotype was determined using immunofluorescence staining. This showed a marked increase in expression of PAX6 in homozygous organoids, surpassing PAX6 expression in wildtype organoids. In addition, upon Cyclopamine treatment KIRREL2 staining returned along with the elimination of NKX2.2 expression, while TUBB3 expression remained unchanged. These results confirm the change of differentiation trajectory in *PTCH1*-/- organoids to be SHH-dependent and demonstrate how cerebellar marker expression can be rescued in homozygous organoids by drug treatment.

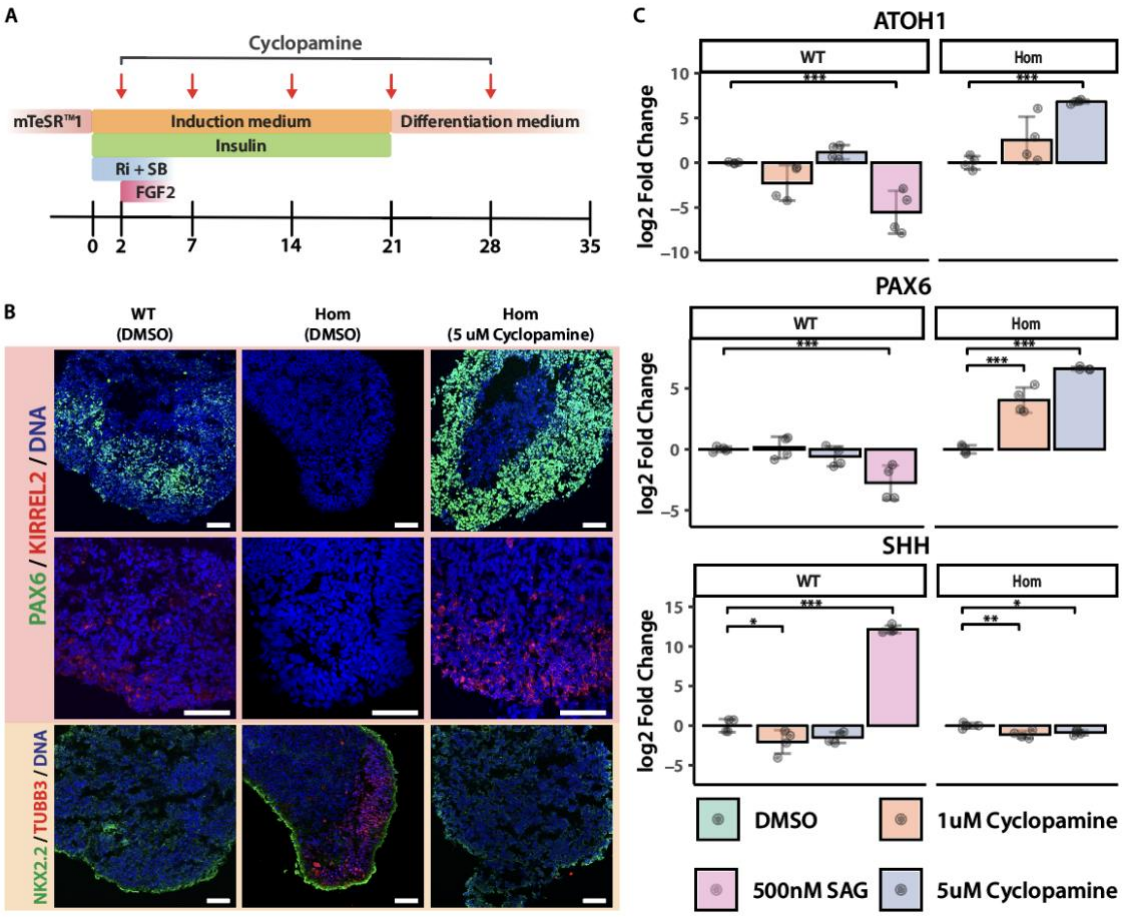


Figure 4.10: Cyclopamine treatment of PTCH1-/- organoids induces cerebellar marker expression. *A) Schematic of experimental design to test the effect of SHH pathway inhibition on PTCH1-/- cerebellar organoid differentiation. B) Immunofluorescence staining of DIV 35 organoids with antibodies specific to PAX6 (green) and KIRREL2 (red) or TUBB3 (green) and NKX2.2 (red). Nuclei are visualised in blue by Hoechst staining. Scale bars 100 µm. C) Gene expression of DIV35 organoids in different treatment conditions as measured by RT-qPCR (n=4 per condition from two differentiations). Statistical significance was determined using ANOVA followed by Dunnett's post-hoc test. P<0.05=*, p<0.01=**, p<0.001=***.*

Early, high-level SHH signalling is proposed to result in a cell fate switch to the ventral forebrain marked by the expression of *NKX2.2* and *NKX2.1*, which was shown to be reversed by treatment with Cyclopamine. This raises the interesting question whether Cyclopamine treatment of homozygous organoids could permanently rescue dorsal-hindbrain differentiation. The effects of SHH inhibition relief were investigated by the continued culture of Cyclopamine-treated DIV 35 organoids for

another 15 days without any ongoing treatment with Cyclopamine (*Figure 4.11*). Gene expression of *ATOH1, BARHL1, PAX6, SHH, NKX2.1* and *NKX2.2* was measured using RT-qPCR. Only *NKX2.*2 remained significantly lower in homozygous organoids that received 5 μM Cyclopamine for the full 50 days compared to organoids that did not receive treatment after 35 days, suggesting that most gene expression changes were long-lasting. A more comprehensive examination of gene expression profiles was performed by PCA of the ΔCT values generated by RT-qPCR. Wildtype organoids exposed to SAG treatment clustered towards homozygous DMSO-treated organoids, suggesting similarity in gene expression. Cyclopamine treatment caused homozygous organoids to cluster away from DMSO-treated homozygous organoids in PC1, depending on the dose of Cyclopamine. This indicates that SHH signalling is the main driving factor in the gene expression profile. This is corroborated by *SHH* being the main contributing gene in PC1, while cerebellar GCP genes *ATOH1*, *PAX6*, and *BARHL1* all act in opposing direction. Taken together, these results show that high-level and early SHH signalling induces the ventral-forebrain differentiation trajectory in *PTCH1* homozygous organoids. Using SHH inhibition, this change is prevented resulting in lasting rescue of the dorsal-hindbrain phenotype.

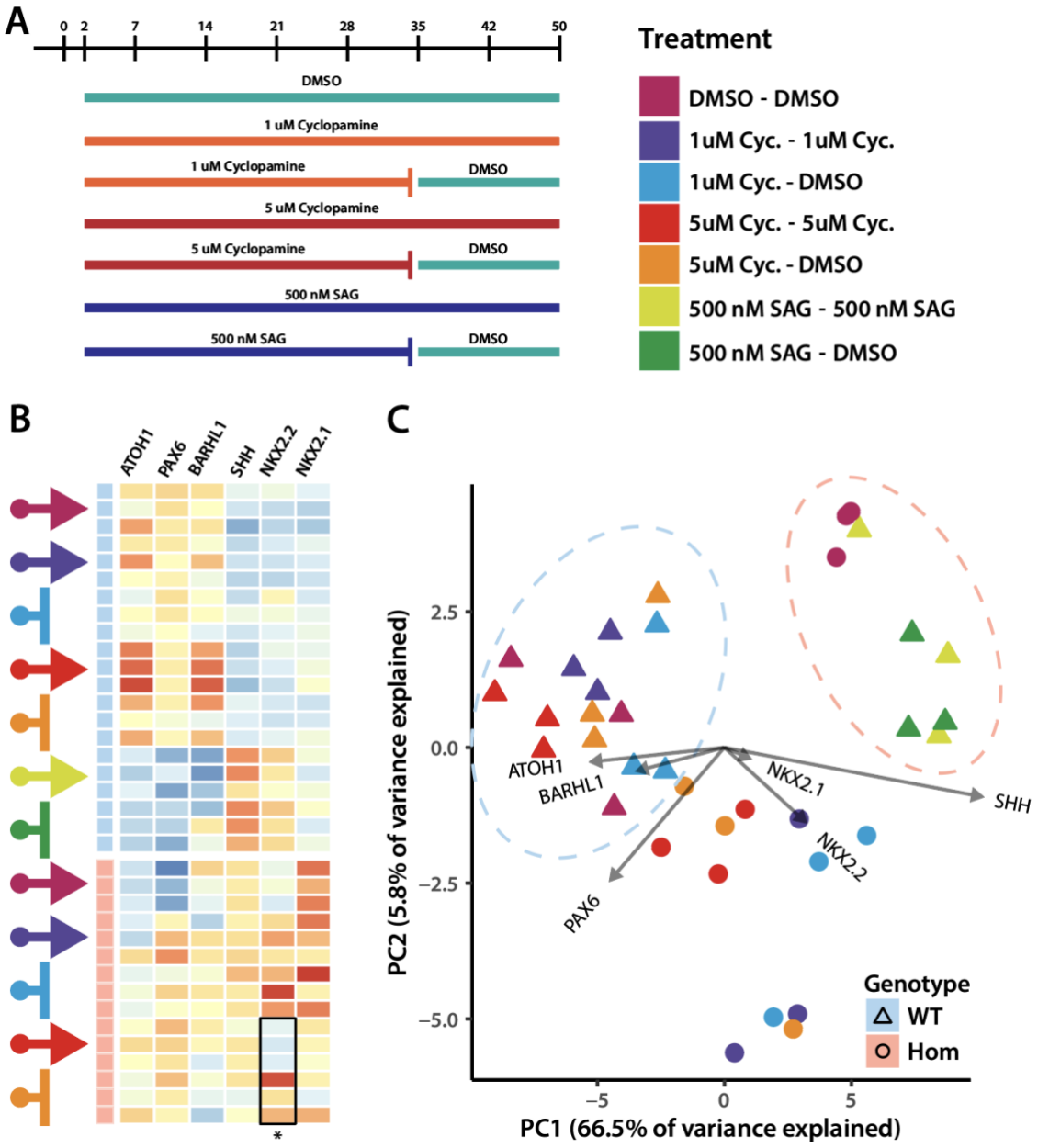


Figure 4.11: SHH-inhibition has long lasting effects on patterning in PTCH1-/- organoids. *A) Experimental design to test the effect of Cyclopamine treatment cessation on cerebellar marker expression. B) Heatmap showing the ΔCt values normalised to ACTB and GAPDH in each condition. The asterisk indicates significance computed by a two-tailed t-test (n=3) in comparing treatment cessation with continued treatment, * = p<0.05. C) Principal component analysis showing different treatment and genotype conditions. The contribution of each gene to the principal components (PCs) shown is indicated by the arrow; the length of the arrow relates to the size of the contribution.*

4.2.4 Expansion of the rhombic lip lineage in *PTCH1* heterozygous organoids

Transcriptomic differences between heterozygous and wildtype organoids were further investigated after the sequencing of additional clones. Initial processing and sample similarity analysis were performed as described above, with the addition of the removal of batch effects by fitting a linear model followed by the removal of the component due to the batch effects. As before, PC1 (explaining 45% of transcriptome variance) separated samples by genotype (*Figure 4.12*), which was confirmed by hierarchical clustering of dissimilarities.

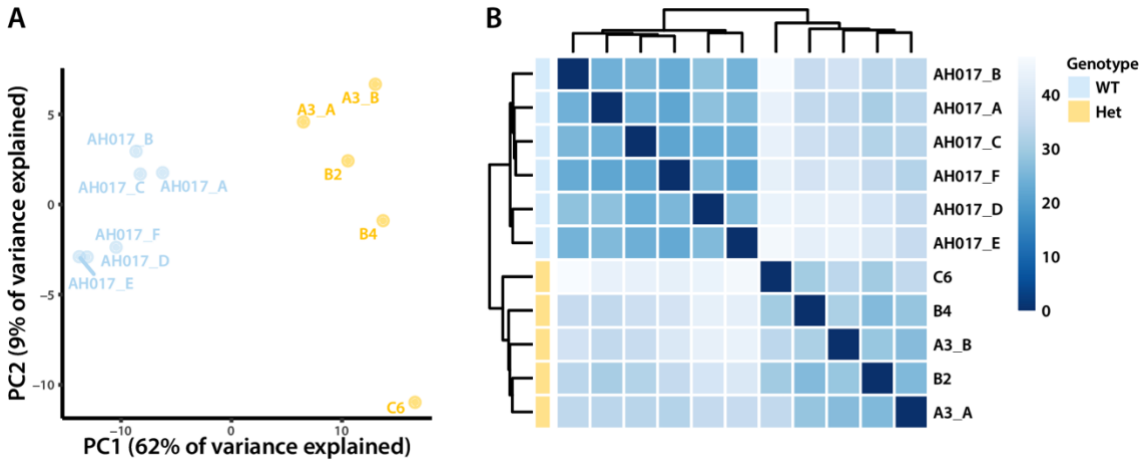


Figure 4.12: Wildtype and heterozygous organoids have distinct transcriptomes. *A) Principal component analysis using the 1000 most variable genes showing the separation of samples in principal component (PC) 1 and PC2. B) Euclidean distances between samples with hierarchical clustering.*

Transcriptome differences between wildtype and heterozygous organoids were analysed as described above. A total of 3452 genes reached the FDR p-value cut-off (<0.05) and had a mean expression of more than 50 counts. SHH pathway genes *GLI1, GLI2, GLI3* and *PTCH1* were significantly upregulated in heterozygous organoids (*Figure 4.13*). In contrast to the homozygous organoids, this was not accompanied by

a shift in brain region identity and forebrain markers were not differentially expressed. Furthermore, hindbrain markers were expressed to similar or higher levels as compared to wildtype. These results suggest *PTCH1+/-* organoids maintain cerebellar differentiation while experiencing increased levels of SHH-signalling.

GCP markers *PAX6, ZIC1*, and *ZIC2* were also among the DEGs in heterozygous organoids (*Figure 4.13*). This was accompanied by the increased expression of genes associated with cell cycle and proliferation (*PCNA, MKI67, TOP2A*, *DLGAP5* and *CCND1*). Concurrently, early post-mitotic (*NEUROD1, NEUROD2*) and migrating GC markers (*CNTN2, CNTN1, UNC5C*) were decreased (Stoykova and Gruss, 1994; Ackerman *et al.*, 1997; Miyata, Maeda and Lee, 1999). The increased expression of GCP markers was accompanied by the elevation of *EOMES* and *TBR1* (Fink *et al.*, 2006; Mugnaini, Sekerková and Martina, 2011), marking the two other main cell types derived from the RL, UBCs and glutamatergic DCN, respectively. There was no evidence for differential expression of genes associated with more differentiated UBCs (*CALB2, GRM1*) (Mugnaini, Sekerková and Martina, 2011). However, *DCX,* which marks migrating glutamatergic DCN (Rahimi-Balaei et al., 2018), was significantly decreased. These results may indicate an increased proportion of GCPs in heterozygous organoids and a broader effect of SHH-induced proliferation on RL derivatives.

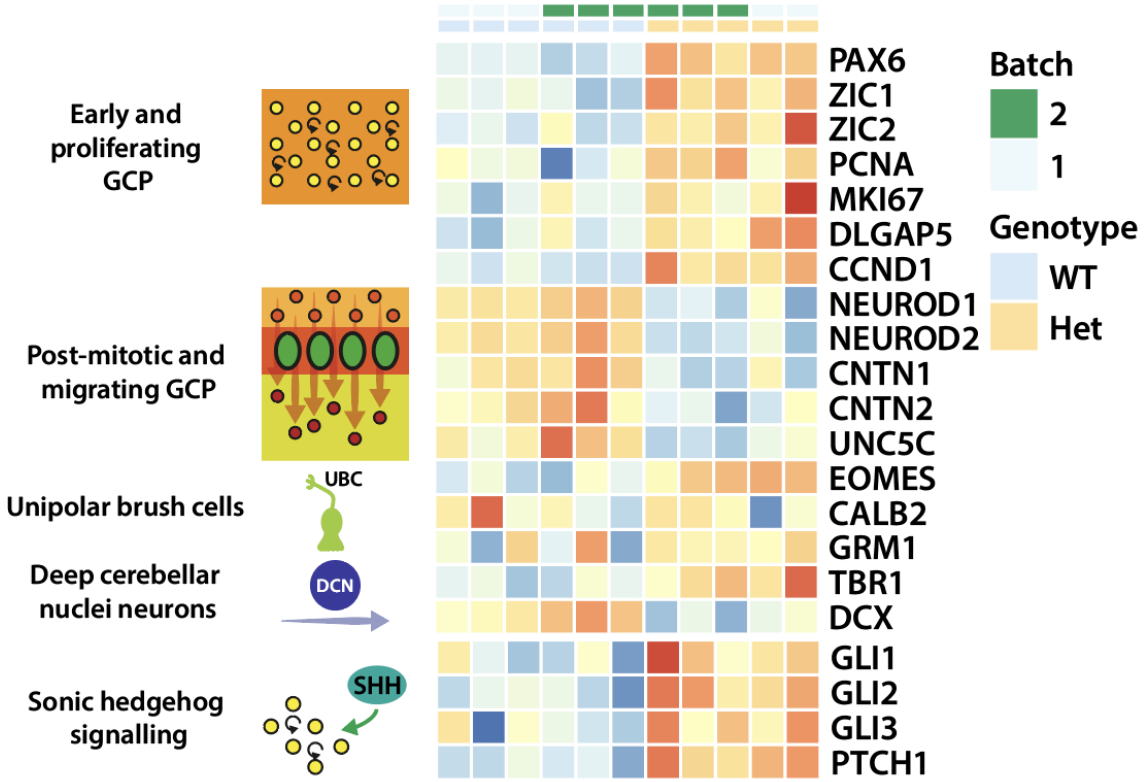


Figure 4.13: Expression of early rhombic lip genes is elevated in heterozygous organoids. *Expression of genes associated with different stages of rhombic lip (RL) development and RL derivatives. Only differentially expressed genes are displayed.*

A more comprehensive and objective comparison of genes associated with specific cell types in the cerebellum was performed using gene set variation analysis (GSVA) (Hänzelmann, Castelo and Guinney, 2013) on gene sets marking all developmental cerebellar cell types. These gene sets were obtained from a single-nuclei RNA sequencing (snRNAseq) dataset generated from human cerebellar tissue spanning the developmental trajectory of 7 PCW into adulthood (Sepp *et al.*, 2021). This analysis showed that the gene set marking GCPs ('GCP') was significantly upregulated in heterozygous organoids, while 'GC_diff_2', marking post-mitotic differentiating GCs, was significantly downregulated (*Figure 4.14*). Exploration of

these two gene sets and comparison with DEGs in heterozygous organoids revealed primarily genes associated with proliferation (*HMMR, IQGAP3*), DNA-replication (*TOP2A, ECT2*), and the centromere (*CENPE, CENPF, OIP5, NUF2*) to be significantly upregulated. In contrast, genes such as *SEMA7A* (neuronal axon guidance and migration), *RBFOX3* (pre-mRNA alternative splicing regulator and GC marker), and *CDH7* (mature GC marker, regulating mossy fibre growth) were downregulated. This unbiased comparison with a publicly available dataset further supports the finding that the GCP population is expanded in heterozygous organoids.

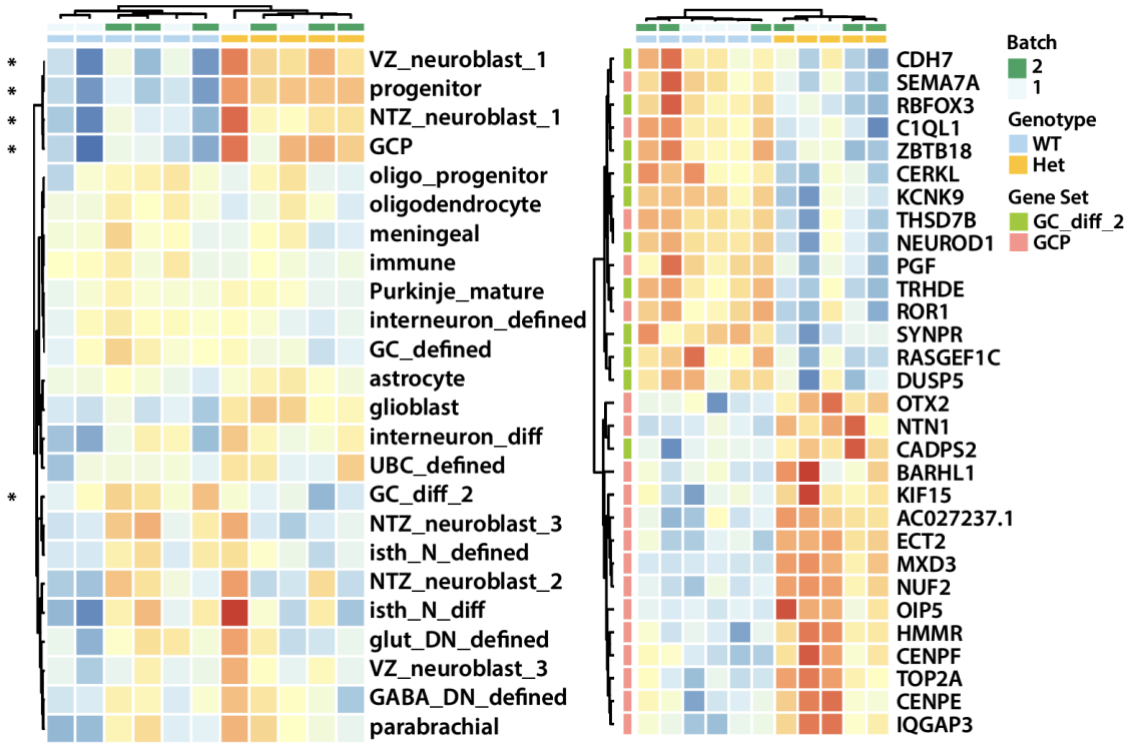


Figure 4.14: Cell type specific gene sets reveal expansion of granule cell progenitors in heterozygous organoids. *A) Heatmap showing the relative expression of gene sets defined using single-nuclei RNA sequencing datasets published in (Sepp et al., 2021). Asterisks mark gene sets that are differentially expressed between wildtype and heterozygous organoids. B) Heatmap showing the expression of differentially expressed genes present in the GCP (red in annotation left hand side) and GC_diff_2 (green in annotation left hand side) gene sets.*

Interrogation of another established dataset generated from laser capture microdissected (LCM) samples of the developing human cerebellum (pcw 9 to 19) (Aldinger *et al.*, 2021) was performed to validate these results. Differentially upregulated genes marking the RL, EGL and PCL, described in the original publication, were compared to genes upregulated in heterozygous organoids. Most of heterozygous DEGs overlapped with RL and EGL genes (*Figure 4.15*). Similarity with the different regional samples was then assessed by measuring Euclidean distances between LCM samples and organoid samples using the subset of spatial region defining genes. Organoids showed the most similarity with bulk samples at ages 15-17 PCW (*Figure 4.15*). Between the LCM samples, organoids were most similar to RL samples at 15 PCW and EGL samples at 17 PCW. Analysing distances of organoid samples to each respective region showed that heterozygous samples were closer to RL samples compared to wildtype. These results are consistent with the hypothesis that heterozygous organoids display expansion of the RL population.

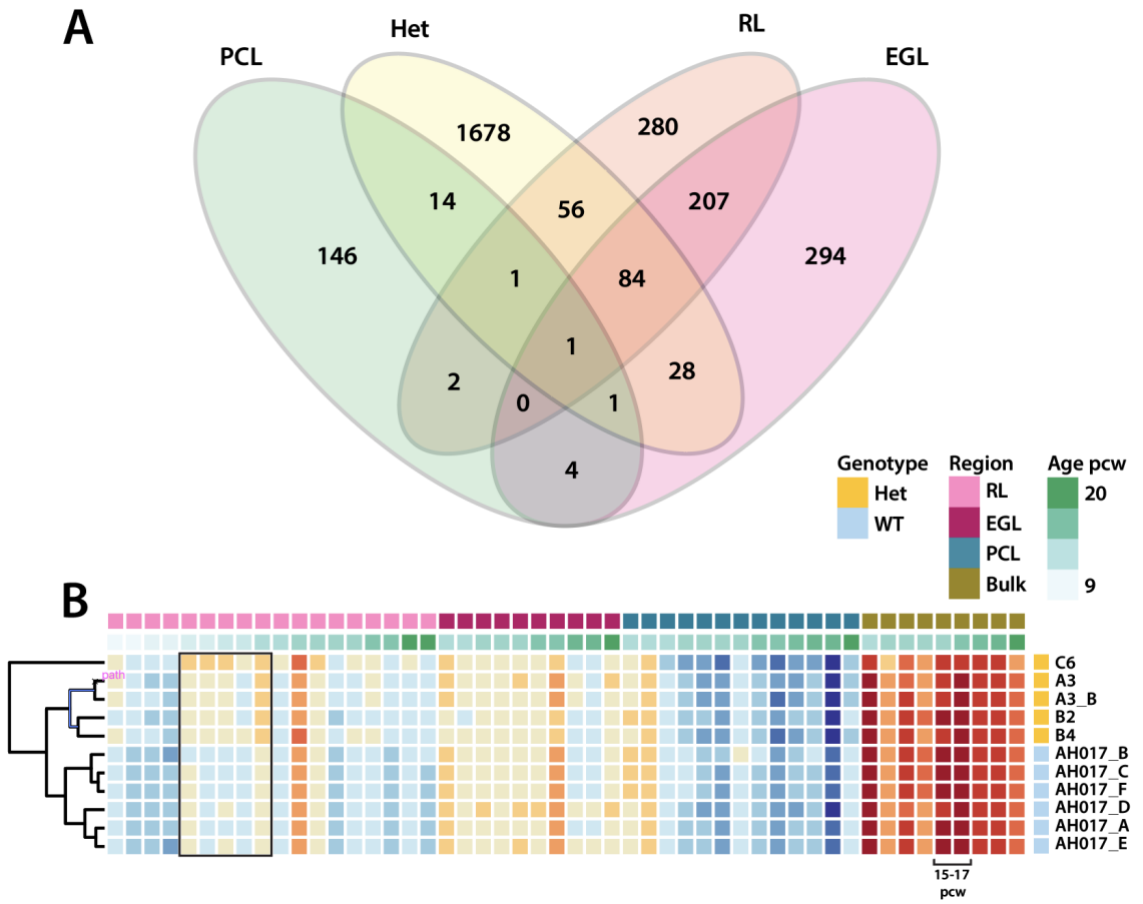


Figure 4.15: PTCH1+/- cerebellar organoids express higher levels of rhombic lip genes. *A) Venn diagram displaying the overlap in differentially upregulated genes. B) Euclidean distance measurements of organoid samples with laser capture microdissected (LCM) regional samples. Samples are organised by region and age. Measurements are scaled in rows. A black outline indicates the difference in similarity to RL samples seen between heterozygous and wildtype organoids. In bulk samples, the time points with the highest similarity are marked.*

Using Gene Set Variation Analysis (GSVA), biological pathways (BPs) from the Broad Institute Molecular Signatures Database (MSigDB) were identified that were associated with DEGs in heterozygous organoids (*Figure 4.16*). Among the most upregulated BPs were pathways associated with cell proliferation, chromosome separation and neuronal patterning. In addition, interrogation of the KEGG and REACTOME databases revealed a significant enrichment of pathways associated with cholesterol synthesis, mismatch repair and hedgehog signalling in

heterozygous organoids. The association of SHH pathway activity with cholesterol synthesis is well known, and the trafficking of sterols to and from the primary cilium is thought to be one of the main regulatory elements of SHH signalling (Corcoran and Scott, 2006; Khaliullina *et al.*, 2009; Blassberg and Jacob, 2017; Qi and Li, 2020). Indeed, genes encoding enzymes involved in the conversion of Acetyl-CoA to cholesterol (*HMGCR, MVD, FDFT1, SQLE*) were upregulated in the heterozygous organoids. It remains unclear whether this upregulation is a direct effect of SHH signalling or induced by the increased cholesterol demands. This effect does, however, not seem to be cell type-specific as homozygous organoids also displayed elevated levels of cholesterol synthesis genes.

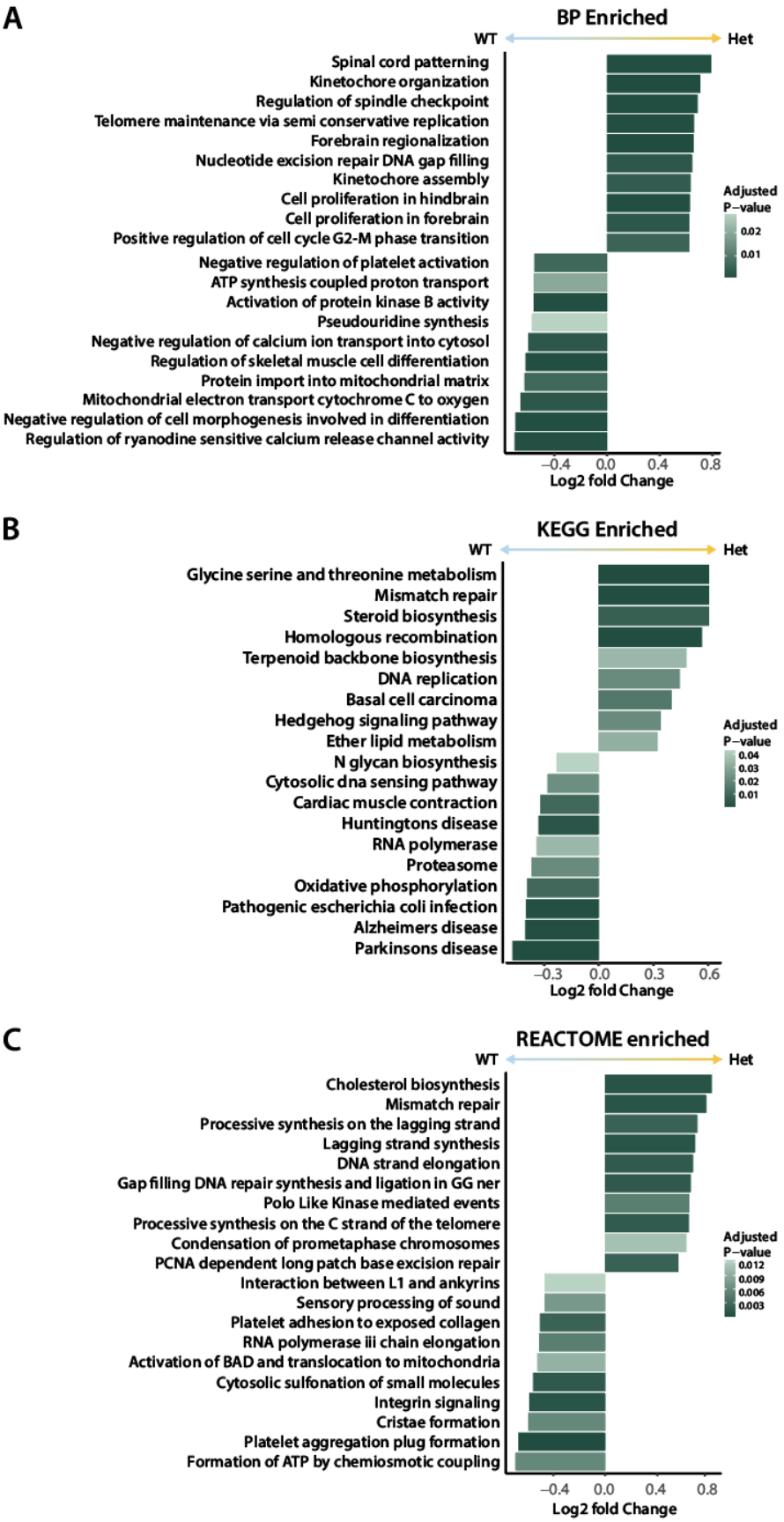

A
BP Enriched
WT
Het
Spinal cord patterning
Kinetochore organization
Regulation of spindle checkpoint
Telomere maintenance via semi conservative replication
Forebrain regionalization
Nucleotide excision repair DNA gap filling
Kinetochore assembly
Cell proliferation in hindbrain
Cell proliferation in forebrain
Positive regulation of cell cycle G2-M phase transition
Negative regulation of platelet activation
ATP synthesis coupled proton transport
Activation of protein kinase B activity
Pseudouridine synthesis
Negative regulation of calcium ion transport into cytosol
Regulation of skeletal muscle cell differentiation
Protein import into mitochondrial matrix
Mitochondrial electron transport cytochrome C to oxygen
Negative regulation of cell morphogenesis involved in differentiation
Regulation of ryanodine sensitive calcium release channel activity
Adjusted P−value
0.02
0.01
−0.4
0.0
0.4
0.8
Log2 fold Change
B
KEGG Enriched
WT
Het
Glycine serine and threonine metabolism
Mismatch repair
Steroid biosynthesis
Homologous recombination
Terpenoid backbone biosynthesis
DNA replication
Basal cell carcinoma
Hedgehog signaling pathway
Ether lipid metabolism
N glycan biosynthesis
Cytosolic dna sensing pathway
Cardiac muscle contraction
Huntingtons disease
RNA polymerase
Proteasome
Oxidative phosphorylation
Pathogenic escherichia coli infection
Alzheimers disease
Parkinsons disease
Adjusted P−value
0.04
0.03
0.02
0.01
−0.3
0.0
0.3
0.6
Log2 fold Change
C
REACTOME enriched
WT
Het
Cholesterol biosynthesis
Mismatch repair
Processive synthesis on the lagging strand
Lagging strand synthesis
DNA strand elongation
Gap filling DNA repair synthesis and ligation in GG ner
Polo Like Kinase mediated events
Processive synthesis on the C strand of the telomere
Condensation of prometaphase chromosomes
PCNA dependent long patch base excision repair
Interaction between L1 and ankyrins
Sensory processing of sound
Platelet adhesion to exposed collagen
RNA polymerase iii chain elongation
Activation of BAD and translocation to mitochondria
Cytosolic sulfonation of small molecules
Integrin signaling
Cristae formation
Platelet aggregation plug formation
Formation of ATP by chemiosmotic coupling
Adjusted P−value
0.012
0.009
0.006
0.003
−0.4
0.0
0.4
0.8
Log2 fold Change

Figure 4.16: Gene ontology analysis reveals upregulation of distinct pathways. *A) Gene Set Variation Analysis (GSVA) of the Broad institute biological pathways (BP) molecular signatures database (MsigDB), differentially expressed in heterozygous organoids. Statistical tests were computed by fitting a linear model followed by empirical Bayes moderation to establish differentially expressed gene sets (Benjamini-Hochberg adjusted p-value<0.05). B) GSVA of the Kyoto Encyclopedia of Genes and Genomes (KEGG) collection of gene sets relating to biological processes. C) GSVA of the REACTOME gene set database.*

In total, 1577 differentially expressed genes (DEGs) were unique to heterozygous organoids and not significantly altered or changed in opposing direction in homozygous organoids. Out of these, 870 were upregulated and 707 were downregulated. Gene ontology analysis was performed and revealed the enrichment of 154 pathways, including those marking neural precursor formation, anterior-posterior specification, cilium assembly, axon guidance and axonogenesis, and WNT signalling (*Figure 4.17*). Seven pathways were depleted, including those involved in ribonucleoprotein complex biogenesis, mitochondrial translation and localisation, and protein kinase signalling. Fragmentation of mitochondria has been described in GCPs stimulated with SHH, possibly explaining the decreased expression of mitochondria associated pathways (Malhotra *et al.*, 2016). Among upregulated pathways were those involved with assembly and organisation of the primary cilium, which could relate to the pivotal role of the primary cilium in the rhombic lip and granule cell development (Haldipur *et al.*, 2019). Furthermore, pathways involved in WNT signalling were enriched in heterozygous organoids. This was unexpected as typically WNT plays an antagonistic role over SHH-signalling (Ulloa and Martí, 2010). These results highlight cell type- and tissue-specific effects of increased SHH signalling in heterozygous organoids.

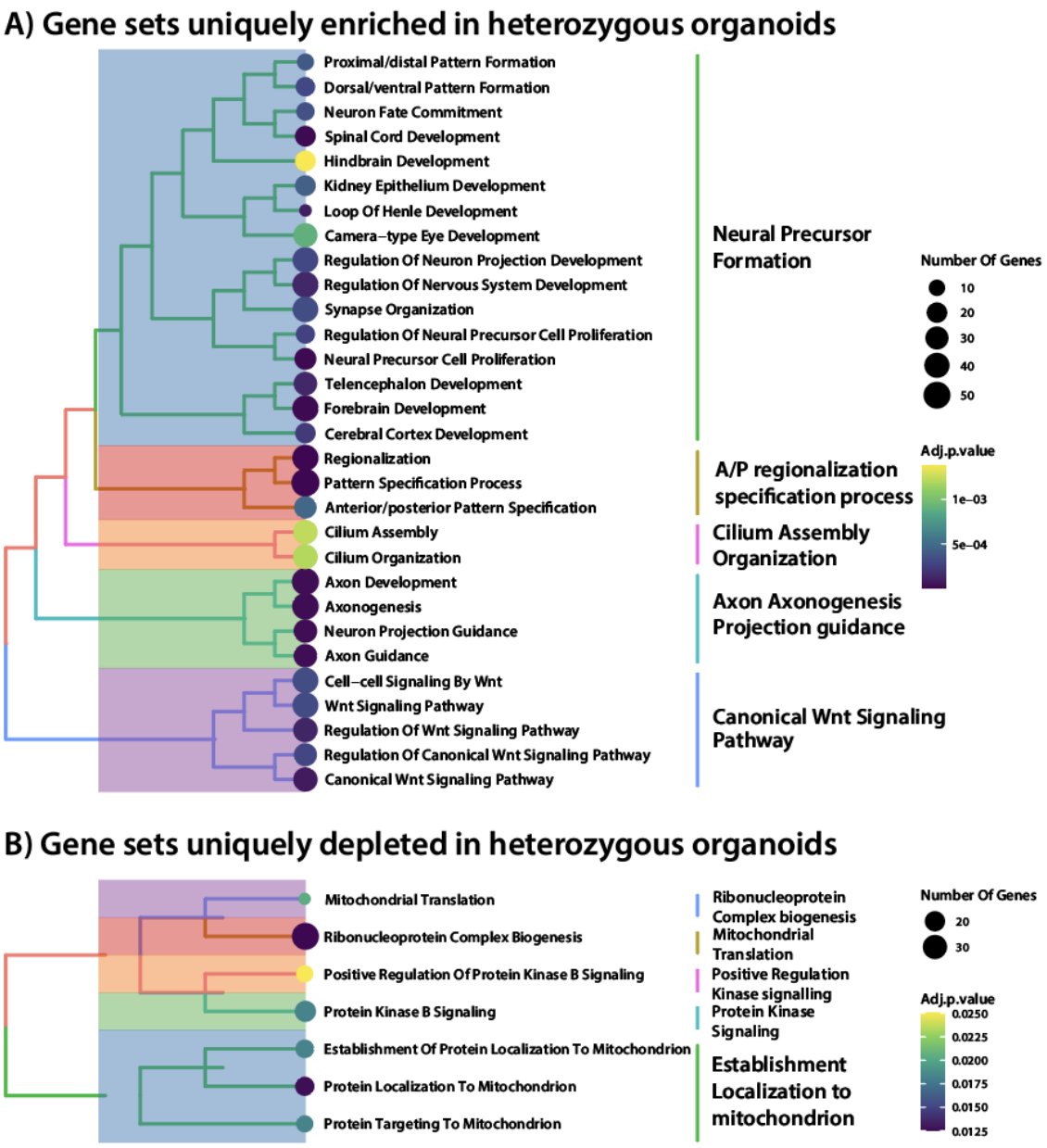


Figure 4.17: Gene Ontology analysis identifies cerebellum specific changes in heterozygous organoids. *A) Gene sets uniquely enriched in heterozygous organoids. The Colour of the dots corresponds to the Benjamini-Hochberg adjusted p-value, and the size of the dots corresponds to the number of genes allocated to each gene set. B) Gene sets uniquely depleted in heterozygous organoids.*

The transcriptomic changes in heterozygous organoids are consistent with the increased proliferation of GCPs in the EGL that is found in *Ptch1* heterozygous mice (Oliver *et al.*, 2005). To evaluate these changes on a protein level, DIV 50 organoids

were dissociated, stained with anti-PAX6 antibodies, and analysed using flow cytometry. The mean fluorescence intensity (MFI) of PAX6 was significantly higher (p=0.0015) in heterozygous organoids compared to wildtype (*Figure 4.18*). In addition, the expression of Cyclin B1 (CCNB1), marking cells transitioning from G2 to M phase, was analysed across organoids from three differentiations. Expression of CCNB1 was normalized to DAPI to correct for the number of nuclei in each organoid. Heterozygous organoids expressed significantly more CCNB1 compared to WT (p=0.005). These results further indicate increased proliferation in heterozygous organoids along with the expansion of the PAX6-positive cell population.

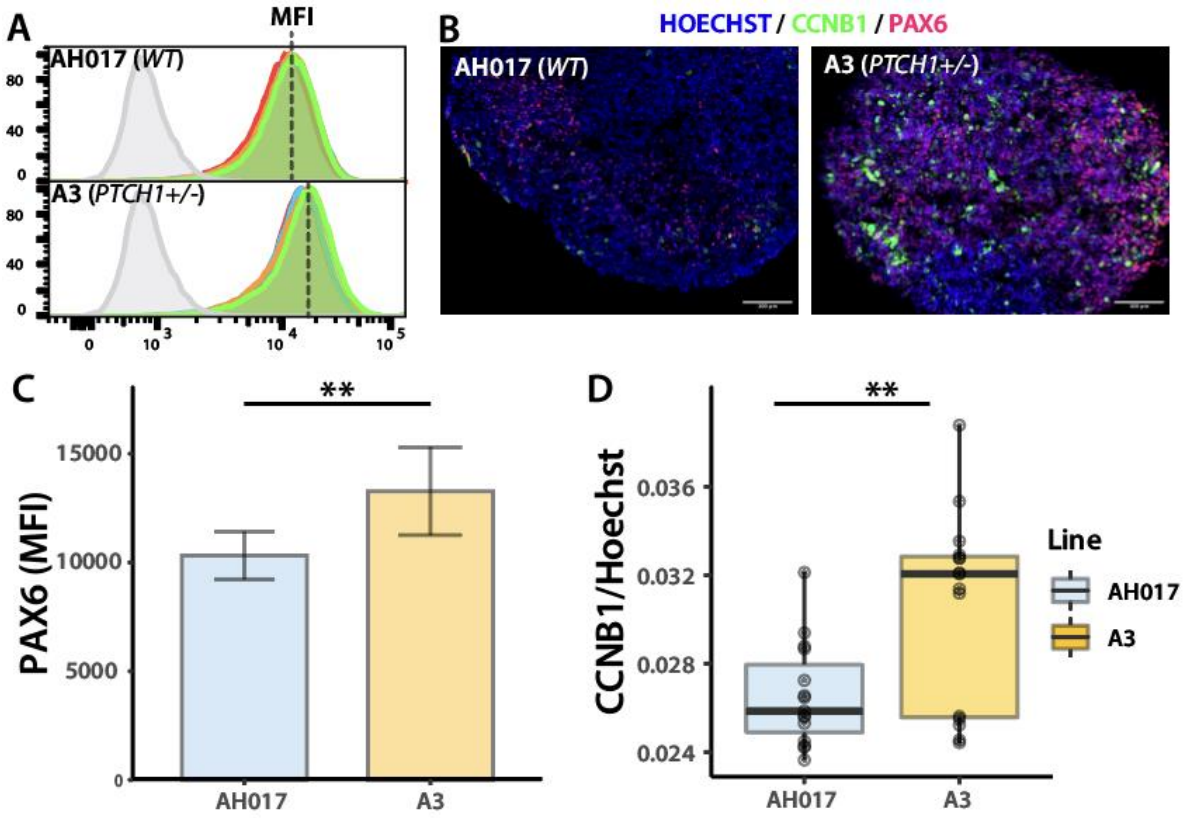


Figure 4.18: Increased expression of PAX6 and CCNB1 in PTCH1 heterozygous organoids. *A) Flow cytometry plots of PAX6 fluorescence intensity of wildtype and heterozygous organoids. Coloured curves represent four different pools of five dissociated organoids per*

*genotype, and grey curves represent the negative control. The mean fluorescence intensity (MFI) is marked with the dashed line. B) Immunofluorescence staining of DIV 35 organoids with antibodies specific to PAX6 (red) and proliferation marker CCNB1 (green). Nuclei are visualised with Hoechst. Scale bars represent 100 um. C) Bar graph of MFI values of the replicates depicted in (A). Asterisks indicate statistical significance computed by student's t-test. ** = p<0.01. D) The relative expression of CCNB1 normalised to Hoechst expression to correct for the number of nuclei in each organoid. Data points represent five different organoids from three differentiations. Asterisks indicate statistical significance computed by student's t-test. ** = p<0.01.*

4.2.5 *PTCH1* heterozygous organoids display features of loss-of-heterozygosity but not tumorigenesis

In addition to signs of increased proliferation, *Ptch1* heterozygous mice display pre-neoplastic lesions with loss-of-heterozygosity (LOH) that frequently precedes malignant transformation (Oliver *et al.*, 2005). To examine the possible loss of wildtype *PTCH1* expression in heterozygous organoids, the relative expression of *PTCH1* was measured at five time points (DIV 0, -35, -50, -70, -90) by RT-qPCR. Mutant *PTCH1* mRNA found in heterozygous organoids does not contain exon 3. By comparing the amplification of a region present in both the wildtype and mutant mRNA with the amplification of exon 3, a ratio can be calculated relating to the prevalence of wildtype mRNA. It is expected that this ratio will be smaller in the case of LOH. PCR amplification from primers spanning exon-exon junction 2-3 and 5 only occurs from wildtype *PTCH1* mRNA (*Figure 4.19*). Ct values generated from these primers were normalised to Ct values produced using primers that amplify exons 13 to 14 which are present in both wildtype and mutant *PTCH1* mRNA. Linear regression showed a statistically significant age-dependent decrease of wildtype *PTCH1* mRNA in heterozygous organoids ($p=0.003$) but not wildtype, which could correspond to LOH. Long-term maintenance (DIV 70) of wildtype and heterozygous organoids did not reveal signs of malignant transformation when proliferating cells

were visualised using KI67 (*Figure 4.19*). Identification of malignant cells could, however, be hampered by the high baseline level of proliferating cells in the organoids due to their early embryonal stage. Furthermore, the limited culture time might not allow for additional genetic damage required for malignant transformation.

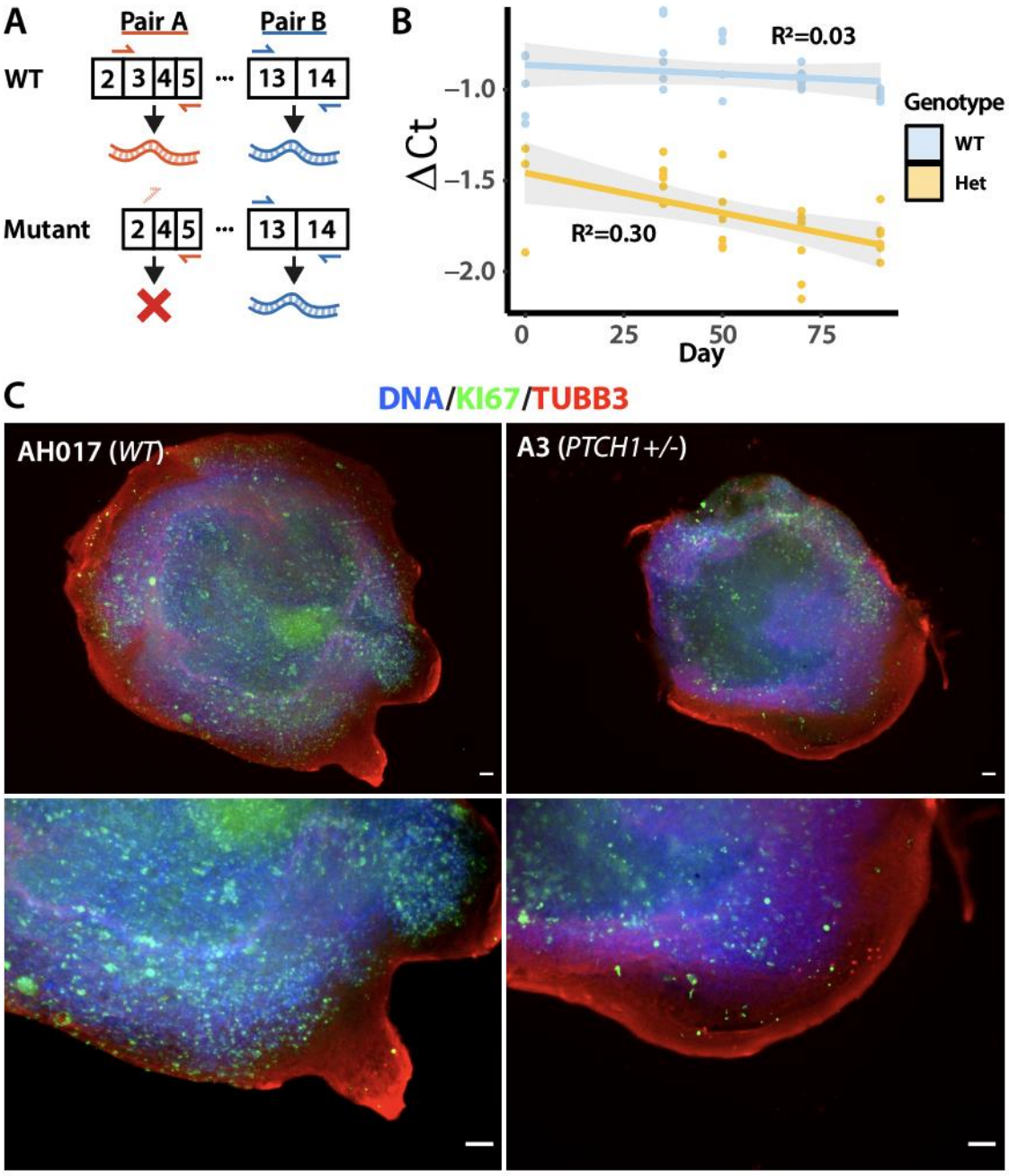


Figure 4.19: Long-term culture of PTCH1 heterozygous organoids shows signs of wildtype PTCH1 loss but not tumorigenesis*. A) Schematic of priming sites of primer pair A and B. Wildtype PTCH1-mRNA will allow amplification from both primer pairs, while mutant only allows the amplification from pair B. B) Dot plot of DCT values generated by normalising the expression of pair A to pair B. Linear regression line shows the relation of the DCt with time. Lower values represent the lower relative expression of pair A, correlating with the respective expression of wildtype PTCH1-mRNA. Data are composed of more than three biological replicates across separate differentiations. R^2 are displayed indicating the fit of the linear regression model. C) Immunofluorescence staining of wildtype and heterozygous organoids at DIV 70 with antibodies targeting proliferation maker KI67 and pan-neuronal marker TUBB3. Scale bars indicate 150 um.*

4.2.6 Druggable targets found upregulated in heterozygous organoids

As heterozygous organoids display features associated with GCP proliferation and pre-neoplastic stages of medulloblastoma, examination of DEGs for druggable targets may provide valuable insights on pre-symptomatic medulloblastoma tumours and targeting of tumour stem cells. Features present in early stages of the disease are more likely to be common between all cells within a medulloblastoma tumour, as heterogeneity lies within genetic alterations acquired during tumour progression. This is evidenced by the fact that various genes encoding known cancer targets were differentially expressed in heterozygous organoids (*Figure 4.20*). MB-specific targets such as TOP2A (inhibited by etoposide)(Ruggiero *et al.*, 2010; Su *et al.*, 2022), as well as targets known in other types of cancer such as PLK1 (volasertib), Aurora kinase B (AURKB)(Barasertib)(Bavetsias and Linardopoulos, 2015), receptor tyrosine kinases (Pertuzumab, afatinib)(Hynes and MacDonald, 2009), histone deacetylases (vorinostat)(Perla *et al.*, 2020), vascular endothelial-derived growth factor A (VEGFA) (Apte, Chen and Ferrara, 2019), fibroblast growth factor receptors (Krook *et al.*, 2021) and YAP-signalling components (Brodowska et al., 2014; Hamanaka et al., 2019), were upregulated in heterozygous organoids (*Figure*

4.20). Together, these changes show that heterozygous organoids may be used for target discovery that guide future studies and drug screening.

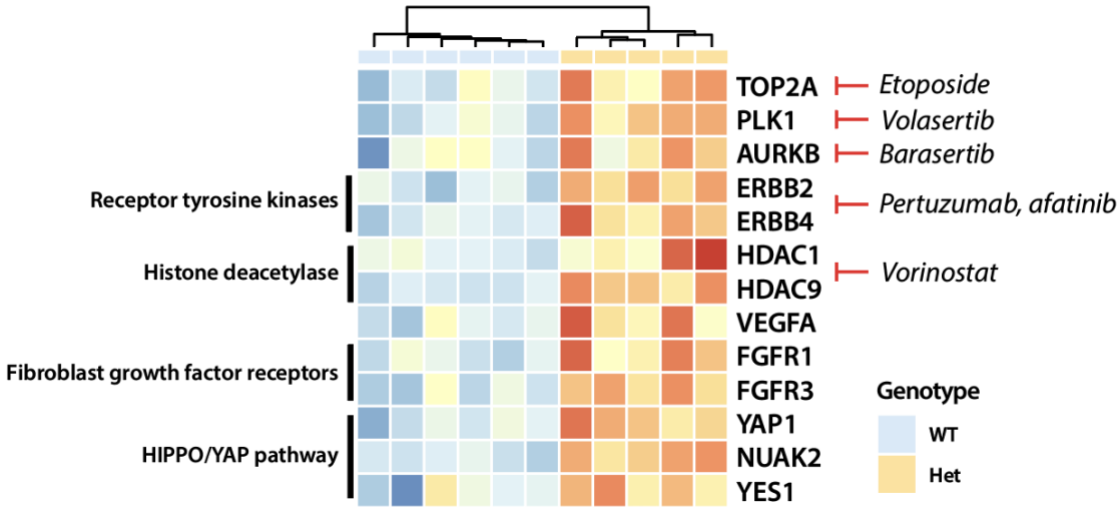


Figure 4.20: Druggable targets found upregulated in heterozygous organoids. *Example genes associated with druggable targets that were found to be upregulated in heterozygous organoids.*

4.3 Discussion

In this chapter, the cerebellar differentiation of *PTCH1* mutant iPSC is described. Complete loss-of-function of PTCH1 prevents the differentiation into cerebellar organoids due to early-onset, high-level SHH signalling. Heterozygous *PTCH1* mutant iPSC retain the ability to form cerebellar structures and show increased proportions of RL derivatives. Together, these results demonstrate the use of CRISPR/Cas9-genome editing and iPSC differentiation to model specific effects of genetic alterations on human brain development.

The pronounced effect of PTCH1 LOF on cerebellar differentiation is in line with previous findings of *Ptch1-/-* mouse studies. Mouse embryos that lack any functional Ptch1 die between E9.0 and 10.5, mostly due to abnormal development of the heart (Goodrich *et al.*, 1997). In addition, significant changes to neural tube development are seen with failed neural tube closure and enlargement of the ventral neural tube as the major phenotype. In the neural tube, SHH signalling is responsible for organising neuronal identity along the dorsoventral axis (Briscoe and Ericson, 1999; Martí and Bovolenta, 2002; Ribes and Briscoe, 2009). SHH is first produced in the notochord and induces the formation of the floor plate, a structure located in the ventral midline of the neural tube (Echelard *et al.*, 1993; Roelink *et al.*, 1994). The floor plate will then start producing SHH to facilitate dorsoventral patterning and differentiation (Marti et al., 1995). A gradient of SHH is established, resulting in specific domains of progenitor pools with distinct identities. Each of these pools, as well as the floor plate and the roof plate, can be distinguished by the expression of defining markers (reviewed in Ribes & Briscoe, 2009). The floor plate expresses high

levels of SHH, FOXA1 and FOXA2, while the adjacent domain expresses NKX2.2. In domains further away from the SHH signalling centre, increasing levels of PAX6 are seen. In both the developing spinal cord and the forebrain, expression of NKX2.2 and PAX6 is mutually exclusive and dependent on the concentration of SHH (Ericson et al., 1997; Briscoe and Ericson, 1999). In line with this, *PTCH1-/-* organoids, which displayed high levels of SHH expression, were marked by NKX2.2 expressing signalling centres and the absence of PAX6. Only a part of the organoid was expressing NKX2.2, suggesting that some level of spatial patterning may take place. The absence of PAX6 results from increased SHH signalling levels in *PTCH1-/-* cells. Although *GLI1* upregulation might have occurred earlier during differentiation, the absence of *GLI1* upregulation at DIV 35 may indicate a role for non-canonical SHH signalling. SMO has been shown to exert an effect on cytoskeletal reorganisation and cell migration independently of GLI proteins (Yam *et al.*, 2009; Polizio *et al.*, 2011), which may contribute to the cell fate shift observed.

The expression of cerebellar markers was rescued in *PTCH1-/-* organoids treated with SMO inhibitor Cyclopamine. In addition, ceasing treatment after 35 days did not result in a reversal of the phenotype within the experimental time frame. Cyclopamine has been shown to suppress SHH-signalling through direct inhibition of SMO (Cooper *et al.*, 1998; Incardona *et al.*, 1998; Chen *et al.*, 2002), and it has proven effective in inhibiting SHH pathway activity in *Ptch1-/-* cells (Talpale *et al.*, 2000). Furthermore, Cyclopamine is frequently used to induce dorsal patterning, while SAG induces ventral neural fate (Gaspard *et al.*, 2009; Cao *et al.*, 2017; Ogura *et al.*, 2018; Zheng *et al.*, 2019). *PTCH1-/-* organoids illustrate how gene function in

region-specific neural differentiation can be modelled and manipulated in cerebellar organoids and offer opportunities to study developmental SHH-signalling *in vitro*.

SHH-induced changes in organoid differentiation and neuronal identity have been modelled previously in human pluripotent stem cell-derived organoids. Cederquist et al. (2019) used inducible expression of SHH in forebrain organoids to show the establishment of posterior and ventral identity under the influence of SHH secretion (Cederquist *et al.*, 2019). Along with the suppression of PAX6, expression of NKX2.1, DKK1, SIX3 and TCF7L2 was seen close to the SHH-signalling centre. In these forebrain organoids, *DKK1* expression, a WNT signalling inhibitor, was SHH-dose dependent. Moreover, *Dkk1* is an essential inducer of anterior specification as mouse embryos lacking *Dkk1* do not develop head structures rostral to the midbrain (Mukhopadhyay *et al.*, 2001). The findings in this thesis are consistent with this, as *PTCH1-/-* organoids did express higher levels of *DKK1*, while *PTCH1+/-* organoids did not. This further strengthens the idea that, while complete LOF results in a neuronal fate change, retention of some PTCH1 function is sufficient to keep differentiation along the cerebellar developmental trajectory in the organoid model.

While high SHH-signalling widely supresses PAX6 in most vertebrate tissues (Ericson, Rashbass, Schedl, Brenner-Morton, Kawakami, van Heyningen, et al., 1997), the cerebellar external granule layer (EGL) forms an exception. In the EGL, PAX6 is involved in the early migration of GCPs from the oEGL to the iEGL (Engelkamp *et al.*, 1999) and is expressed close to GCPs that undergo SHH induced proliferation. The co-occurring increase of *PAX6, GLI1* and *GLI2* expression in *PTCH1* heterozygous organoids suggests these organoids display this tissue-specific

circumstance. Furthermore, the higher levels of *TBR1* and *EOMES* in heterozygous organoids may suggest a broader effect of SHH signalling on RL derivatives in the developing cerebellum. In the mouse, Shh is secreted by PCs and drives the proliferation of GCPs in the EGL (Dahmane and Ruiz I Altaba, 1999). In humans, however, SHH signalling appears before PCs start to produce SHH (Haldipur et al., 2012). Moreover, human RL development displays additional differences to mice that were until recently underappreciated (Haldipur *et al.*, 2019): The human RL consists of a subventricular and ventricular zone and is seen to persist longer through cerebellar development. RL-related disorders such as cerebellar vermis hypoplasia (CVH) have been linked to failed RL development. A significant part of all CVH is caused by mutations in genes related to the primary cilium. Ciliopathies are characterised by impaired SHH-dependent proliferation in human GCPs. Although the dependency of SHH signalling on the primary cilium has been well described, effects specifically on RL development were not recognised before in mouse models (Aguilar *et al.*, 2012). Previous literature has implicated impaired WNT signalling, rather than SHH signalling, as a causative factor (Lancaster *et al.*, 2011). Interestingly, *PTCH1+/-* organoids displayed increased expression of WNT pathway genes, compared to homozygous organoids which showed decreased expression of WNT signalling genes. Although the exact mechanism through which this effect occurs remains unclear, this suggests a tissue-specific effect of SHH activation on WNT signalling mediated by cell specific. The complex interplay between these pathways has long been described (Ulloa and Martí, 2010), yet stark discrepancies between murine and human cerebellar development may obscure the true nature of

the interaction. The co-occurring increase in gene expression related to RL-lineage, SHH pathway, WNT pathway and cilia support roles of SHH signalling earlier in cerebellar development.

PTCH1 heterozygous organoids displayed features of increased GCP proliferation and loss of wildtype *PTCH1* expression yet failed to develop tumour-like structures. Decreasing levels of wildtype *PTCH1* mRNA align with findings in *Ptch1+/-* mice, which exhibit a persisting hyperplastic EGL and pre-neoplastic lesions that have lost the wildtype allele (Oliver *et al.*, 2005). The fact that LOH is a common occurrence in these lesions might stem from SHH activation-induced DNA replication stress (Tamayo-Orrego *et al.*, 2020). Replication stress is known to cause copy number variation (CNV) and LOH (Arlt *et al.*, 2009; Zheng *et al.*, 2016), promoting malignant transformation (di Micco *et al.*, 2006; Tomasetti, Li and Vogelstein, 2017). LOH likely occurs through erroneous recombination events (Lasko, Cavenee and Nordenskjöld, 1991; Hastings *et al.*, 2009; Malkova and Haber, 2012) and is frequently seen in both mouse models (Pazzaglia *et al.,* 2006; Ishida *et al.,* 2010), and human *PTCH1*-mutant MB (Northcott *et al.*, 2017; Tamayo-Orrego *et al.*, 2020). Shh ligand binds to the SHH-pathway co-receptor BOC (Tenzen *et al.*, 2006; Allen *et al.*, 2011; Izzi *et al.*, 2011) through which it promotes DNA damage mediated by Cyclin D1 (Mille *et al.*, 2014). Furthermore, Shh DNA replication dynamics lead to replication stress and elevated homologous recombination (Tamayo-Orrego *et al.*, 2020). Despite this clear association between SHH-signalling and LOH, only a small number *of Ptch1* heterozygous mice continue to develop MB (Goodrich *et al.*, 1997; Oliver *et al.*, 2005). The current consensus is that additional genetic events are necessary for the

malignant transformation of pre-neoplastic cells (Oliver *et al.*, 2005; Tamayo-Orrego *et al.*, 2016a), and mouse models have shown dramatic increases in tumour penetrance upon the addition of a second mutation (Wetmore, Eberhart and Curran, 2001; Uziel *et al.*, 2005; Lee *et al.*, 2006; Briggs *et al.*, 2008a; Ayrault *et al.*, 2009). The fact that no tumours were seen in the organoids could be the combination of a low penetrance and the limited maintenance period (<90 DIV) that does not allow enough time for additional genomic insults. In fact, tumours in *Ptch1+/-* mice typically arise over 90 days postnatally and require additional mutations to accelerate this process (Goodrich *et al.*, 1997; Briggs *et al.*, 2008b; Mille *et al.*, 2014; Tamayo-Orrego *et al.*, 2016b; Kutscher *et al.*, 2020). Nevertheless, features of DNA repair, mismatch repair and homologous recombination were already seen in DIV 35 organoids which, along with signs of loss of wildtype *PTCH1*, suggest these models may be useful in gaining further insights into these events. Moreover, increased expression of known cancer targets shows that heterozygous organoids demonstrate relevant phenotypes in human MB. These findings could be used to guide future drug discovery and improve the clinical translation.

4.4 Conclusion

The findings in this chapter highlight crucial developmental mechanisms in spatial organisation and regionalisation and distinct effects of increased SHH signalling on the foetal cerebellum. Differentiation of *PTCH1* mutant iPSC shows close resemblance with *in vivo* cerebellar development in mutant mice. Homozygous mutant organoids show how early SHH activation prevents the formation of the cerebellar anlage and exemplify how these tissues can be manipulated *in vitro* to unravel complex developmental processes. Similarities with preneoplasia and tissue-specific effects of SHH signalling found in heterozygous organoids support the use of these organoids in future studies to identify human-specific factors underlying early stages of MB and malignant transformation. Drug screening guided by differential phenotypes found in these organoids and the application of more advanced screening methods such as CRISPR screens are poised to elucidate which mechanisms lie at the core of MB tumorigenesis.

Chapter 5 Exploring alternative methods for medulloblastoma modelling in cerebellar organoids

5.1 Introduction

Previous chapters described the generation of *PTCH1* mutant iPSC lines and subsequent cerebellar differentiation, thereby modelling genetic predisposition to MB. This chapter explores alternative strategies for MB modelling using cerebellar organoids, either by the introduction of MB driver genes or through co-culture with established MB cell lines. Several specific advantages arise from leveraging each of these two strategies. Introduction of onco-driver genes allows temporal control over the potential malignant transformation and can be coupled to the expression of a fluorescent protein for real-time tracing of targeted cells. Co-culture of established MB cell lines enables the study of these cells in different microenvironments.

5.1.1 Introduction of MB driver genes into cerebellar organoids

Organoids form an innovative, human specific model in which known tumour drivers can be introduced through lentiviral delivery (Ogawa *et al.*, 2018) or using non-viral integrating vectors such as transposon systems (Ballabio *et al.*, 2020). Transposons or transposable elements (TEs) are DNA sequences that can be moved from one genomic location to another (Wells and Feschotte, 2020) and are found in most eukaryotic genomes. The relocation of transposons is mediated by transposases, a class of enzymes that cleave the transposase out of the genome and facilitate ligation

into the target site. Transposons can be used to introduce DNA sequences, such as genes with similar efficiency to lentiviral delivery (Muñoz-López and García-Pérez, 2010). While lentiviruses can infect cells autonomously, transposons cannot cross the cell membrane autonomously, making them safer for studies that require the insertion of oncogenes. Furthermore, screens on the Sleeping Beauty transposon system have shown a higher frequency of integrations in intergenic regions compared to typical lentivirus integrations, reducing the chances of unwanted gene disruption (Yant *et al.*, 2005). Recently, group 3 MB genes were introduced into cerebellar organoids using the PiggyBac (PB) transposon (Ballabio *et al.*, 2020). The PB transposon system is composed of a transgene vector and a vector encoding the PB transposase. The PB transposase recognises inverted terminal repeats (ITRs) in the transgene plasmid and facilitates transgene insertion. Using electroporation transfection, these vectors can be introduced into organoid cells. Once in the cell, the transgene is removed from the transgene vector by the PB transposon and inserted at TTAA sequences in the genome (Ding et al. 2005) (*Figure **5.1***). Expression of transgenes can be coupled to that of a fluorescent protein, allowing real-time tracking of targeted cells. Transposon-mediated transgene insertion particularly lends itself to modelling gene amplification and overexpression as multiple copies are inserted in targeted cells. Furthermore, introducing MB-driver genes using PB transposon electroporation provides temporal control over the start of malignant transformation. As a result, this technology may better facilitate high-throughput applications that require scalability and time efficiency.

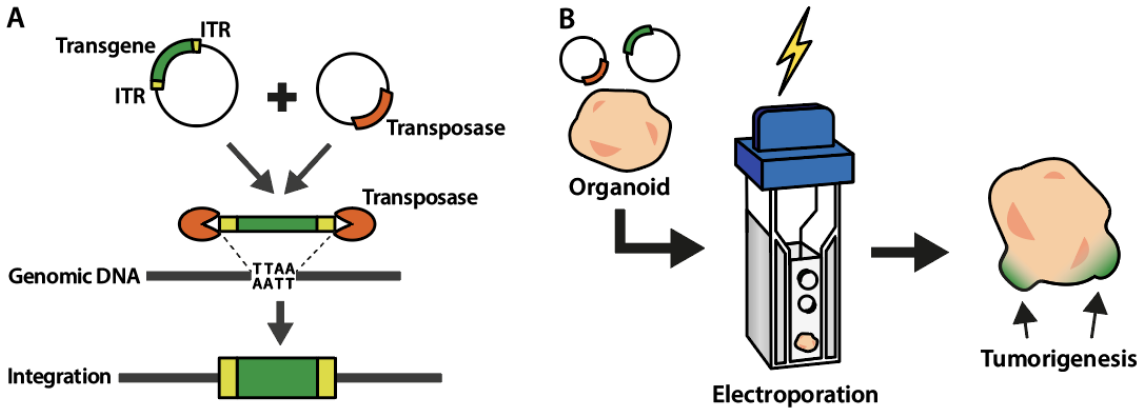


Figure 5.1: PiggyBac transposon delivery of transgenes into cerebellar organoids. *A) The PiggyBac transposon system requires a transgene and a transposase plasmid. The transposase recognises flanking inverted terminal repeat (ITR) sequences to cut and paste the transgene from the expression vector into TTAA sites in the genome. B) Organoids are electroporated with the PiggyBac system in cuvettes and observed for tumour growth.*

Gene amplification or overexpression has been recognised as a major tumour-driving event in human MB, frequently causing aggressive phenotypes. Several amplifications have been characterised in SHH-MB, including *MYCN*, *GLI2, YAP1* and *PPM1D* (Northcott *et al.*, 2012). These genetic events are associated with a poor prognosis (Cavalli et al., 2017; Schwalbe et al., 2017), emphasising the need for novel preclinical models for tumour biology study and therapy testing. *MYCN* is essential for neurogenesis (Knoepfler, Cheng and Eisenman, 2002) and belongs to the MYC family of transcription factors which induce the expression of proliferation genes and regulate cell growth, stem cell maintenance and differentiation. Consequently, deregulated expression of *MYC* genes has been associated with various cancers (Dang, 2012). *MYCN* is one of the primary targets of SHH-signalling and drives the proliferative expansion of granule cell progenitors (GCPs) (Kenney, Cole and Rowitch, 2003). Amplifications are found in 7% of SHH-MB (Northcott *et al.*, 2019) and frequently coincide with *TP53* mutations and *GLI2* amplification (Rausch *et al.*,

2012; Northcott *et al.*, 2017). Patients with this combination are stratified as very high risk and require aggressive treatment (Ramaswamy *et al.*, 2016). This chapter explores the potential of PB transposon-mediated oncogene delivery into cerebellar organoids for MB modelling using these high risk-associated driver genes.

5.1.2 MB cell line co-culture with cerebellar organoids

Co-culture of established MB cell lines presents a second strategy to model MB tumour biology in cerebellar organoids. Cell lines are typically homogeneous which allows comparison of different microenvironments with limited interexperimental variability. Furthermore, cancer cell lines can easily be labelled with fluorescent proteins prior to co-culture, simplifying their identification. Derived from SHH-medulloblastoma tumours, DAOY and ONS-76 are among the oldest MB cell lines currently available and were both established over 30 years ago (Jacobsen, Jenkyn and Papadimitriou, 1985; Yamada *et al.*, 1989). The DAOY line, especially, has a prominent role in MB research as the most frequently cited MB cell line (Ivanov *et al.*, 2016) and has been extensively characterised (Srivastava and Nalbantoglu, 2008; Martelli *et al.*, 2016). Spheroid culture of these MB cell lines has shown a closer resemblance to *in vivo* tumours that infiltrate the surrounding extracellular matrix (ECM) compared to monolayer cultures, and show decreased responsiveness to standard-of-care chemotherapy (Neve *et al.*, 2017; Santhana Kumar *et al.*, 2018; Schönholzer *et al.*, 2020; Roper *et al.*, 2021). Many therapies that show *in vitro* successes fail to translate to *in vivo*. The lower response to chemotherapy in spheroids suggests the lack of a 3D microenvironment in monolayer cultures may be

a contributing factor in this mismatch. Furthermore, using an SHH-MB cell line (UW228-3), spheroid co-culture with neural stem cells showed their value in therapy testing that optimises cytotoxicity in cancer cells while limiting unwanted effects in healthy neural stem cells (Ivanov *et al.*, 2015). Nevertheless, the complex cerebellar cytoarchitecture is not fully represented in these models. Therefore, cerebellar organoids that mimic the developing cerebellum may provide an improved co-culture model, more closely resembling an MB-relevant microenvironment (*Figure **5.2***).

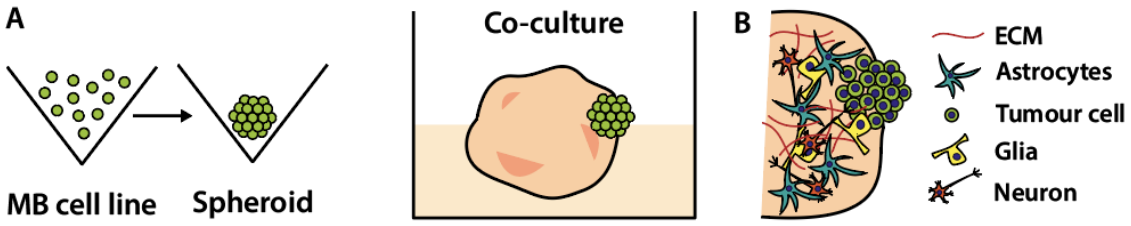


Figure 5.2: Co-culture of MB cell lines with cerebellar organoids. *A) Schematic of co-culture strategy. MB cell lines are plated in conical low-attachment plates to form spheroids. After addition to cerebellar organoids, MB spheroids fuse and interact with organoid cells. D) The created microenvironment contains ECM, astrocytes, glial cells and neurons, which all interact with tumour cells.*

The tumour microenvironment (TME) is increasingly recognised for its role in cancer biology and has been shown to regulate progression and therapeutic responsiveness (Quail and Joyce, 2017). Specific to MB, differences in vascularisation and blood-brain-barrier (BBB) may explain the significant difference in response to chemotherapy seen between WNT (disrupted BBB) compared to other subtypes (intact BBB) (Phoenix *et al.*, 2016). Furthermore, ECM modelling of subtype-specific MB-cell lines revealed that group 3 and group 4 MB but not SHH-MB cells produce vitronectin, promoting invasion and migration, correlating to the clinical phenotype

(Linke *et al.*, 2021). Finally, astrocytes have been shown to promote SHH-MB progression through the secretion of SHH (Liu *et al.*, 2017). In PTCH1 deficient cells, SHH is not required for canonical SHH-pathway signalling. However, Liu et al. show that SHH drives the expression of *Nestin* in a non-canonical, GLI1-independent manner. In these cells, Nestin promotes SHH-MB tumorigenesis by blocking GLI3 mediated SHH-pathway suppression (Li *et al.*, 2016). The lack of astrocytes and astrocyte-derived ECM has been proposed to explain the downregulation of SHH-signalling when SHH-MB cells are cultured *in vitro,* impairing preclinical translation (Sasai *et al.*, 2006; Cheng *et al.*, 2020). Together, these studies highlight the importance of an appropriate TME for *in vitro* MB modelling and support the use of cerebellar organoids which contain relevant cell types, such as astrocytes (Nayler *et al.*, 2021), for the co-culture of established MB cell lines. In this chapter, the development of MB cell line – CBO co-cultures is described. Subsequently, single-cell RNA sequencing is used to perform exploratory analyses of MB – CBO co-cultures and compare these with 2D and 3D culture techniques to investigate relevant TME interactions.

5.2 Results

5.2.1 MB driver gene delivery using PiggyBac transposons

The introduction of MB tumour driver genes yields great potential for MB modelling. Overexpression and amplification of distinct genes can be achieved by introducing transgenes with transposon systems. The PB transposon machinery can be transfected into cells using electroporation. However, the electroporation of intact organoids poses specific challenges. Therefore, initial experiments aimed to establish electroporation conditions that optimise transfection efficiency and organoid survival. Cerebellar organoids were differentiated as described in Chapter 4. At DIV 28, organoids were electroporated using different programs (A-007, A-020 and A-021) using the Amaxa Nucleofector® II device together with the Cell Line Nucleofector™ kit V (Lonza) and cultured for seven days post electroporation. Previous literature described plasmid dosages of 15-35 μg per transfection (corresponding to 4-6 pmol) but did not specify the number of organoids and electroporation volume (Ballabio *et al.*, 2020). As a starting concentration, the PB vector pPB-CAG-Venus, encoding the bright yellow fluorescent protein Venus (Nagai *et al.*, 2002), was transfected into the organoids at 4 pmol per 100 μL transfection reaction. Successful targeting of cells was observed using live cell fluorescence imaging (Figure *5.3*). Program A-020 yielded the highest efficiency combined with the best organoid survival (Figure *5.3*) and was therefore selected for subsequent experiments.

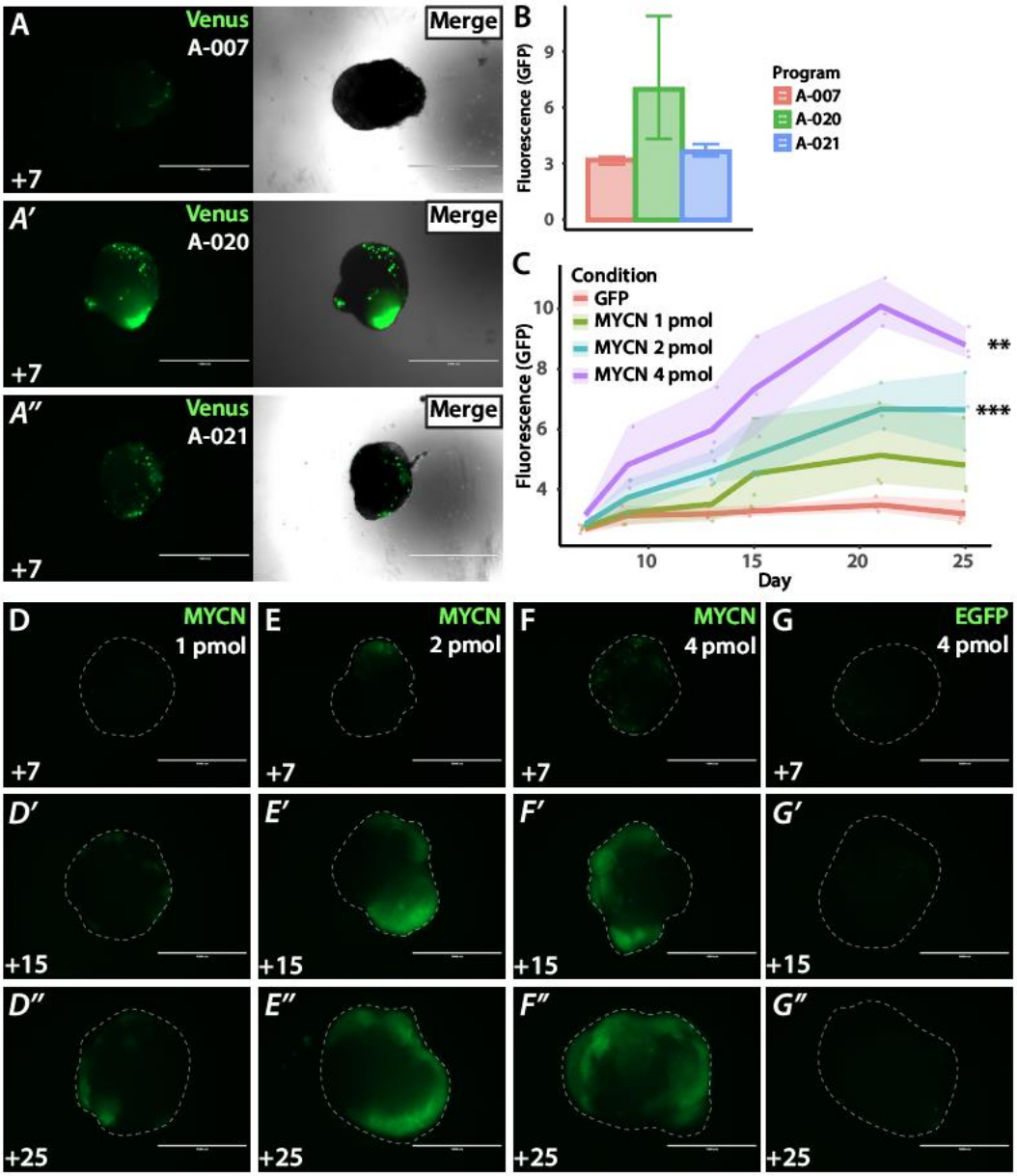


Figure 5.3: Optimised experimental conditions show effective introduction of MB drivers in cerebellar organoids. *A) Different Nucleofector II™ programs resulted in varying efficiency and organoid survival. Program A-020 (A') outperformed programs A-007 (A) and A-021 (A''). B) Mean fluorescence signal in GFP channel at seven days post electroporation. Error bars indicate the range. N=3 for each condition. C) Mean fluorescence signal in GFP signal at the time course ranging from 7 to 25 days post electroporation. The ribbon indicates range. N=3 for each condition. ** indicates p-value <0.01, *** indicates p-value <0.001 computed by ANOVA with Dunnett's post hoc test. D-G) GFP channel images at 7 (D-G), 15 (D-G'), and 25 (D-G'') days post electroporation of a representative organoid in each condition. White lines mark the outline of the respective organoids.*

Subsequent experiments aimed to determine if *MYCN* expression could be visualised using the PiggyBac vector pPB-CAG-MYCN-IRES-EGFP and to optimise plasmid concentrations. In addition, organoids were monitored for potential growths of EGFP-positive cell clusters that could indicate *MYCN*-induced proliferation. DIV 35 organoids were transfected with the pPB-CAG-MYCN-IRES-EGFP vector at three different concentrations (1-, 2-, and 4 pmol/100 μL) and observed over 25 days for fluorescent cells (Figure *5.3*). Clear growth of EGFP-positive cells was visible after 15 days at 2 pmol and 4 pmol concentrations and after 25 days at 1 pmol concentration, but not in EGFP control organoids. The change in fluorescence was significant in organoids electroporated with 2 and 4 pmol compared to GFP over the time course (measured as the area under the curve; 2 pmol $p=0.006$, 4 pmol $p < 0.001$) (Figure *5.3*C). Together, these experiments show optimised experimental conditions for the insertion of transgenes in cerebellar organoids using the PiggyBac system. The next experiments in this thesis will therefore use 2 pmol/100 μL per plasmid as it produces similar results to 4 pmol at a lower input plasmid DNA requirement. In addition, these results give strong indications of increased proliferation of targeted CBO-cells under *MYCN*-overexpression.

5.2.2 *MYCN* overexpression in cerebellar organoids

MYCN-vector electroporated organoids were analysed for cell identity and expression proliferation markers. All EGFP positive cells showed expression of the pan-neuronal marker TUBB3/TUJ1 (*Figure 5.4*), and many transfected cells expressed PAX6, possibly pointing towards an RL-lineage origin. Although it cannot

be excluded that MYCN induces the expression of PAX6, this would be unlikely as PAX6 stimulates cell cycle exit and GCP migration (see section 1.2.3), while MYCN promotes cell cycle entry in model systems (Singh *et al.*, 2022). Cell cycle marker MKI67 was abundantly expressed in EGFP-positive cells, confirming the proliferative phenotype of these cells. In addition to immunofluorescence antibody labelling, a small-scale bulk RNA sequencing experiment was used to compare the transcriptome of *MYCN*-electroporated organoids to that of control organoids. A combined total of six samples were submitted for RNA sequencing as described in Chapter 4: one EGFP control and two *MYCN* organoids electroporated at either 28 or 35 DIV and subsequently cultured for 25 days (*Figure 5.4*). To support the comparison of wildtype and *MYCN*-electroporated organoids, three wildtype un-electroporated DIV 35 organoids (batch 1 from chapter 4) were added to the analysis. Although the unbalanced group sizes prevented differential gene expression testing that was controlled for the age of the organoid, it did allow transcriptome exploration and GSVA. Gene expression differences were visualised using PCA. In PC1, samples separated by the expression of *MYCN* suggesting a pronounced effect of the experimental condition on the organoid transcriptome (*Figure 5.4*). Expression of *MYCN* was markedly increased in *MYCN*-electroporated organoids, verifying successful overexpression of the gene (*Figure 5.4*). GSVA was performed on the Oncogenic Signature gene sets from the Broad institute molecular signature database (MSigDB). This revealed increased expression of genes upregulated with *MYC* gene family-induced transcription (*Figure 5.4*). In addition, expression of a gene set marking upregulated genes in SHH-stimulated GCPs was

notably higher in *MYCN*-electroporated organoids. This set consists of genes upregulated in *ex vivo* cultured mouse GCPs that were stimulated with SHH for 24 hours (Zhao *et al.*, 2002). Collectively, these results show successful *MYCN* overexpression that induces proliferation in cerebellar organoid neurons, which are likely RL derivatives and/or GCPs.

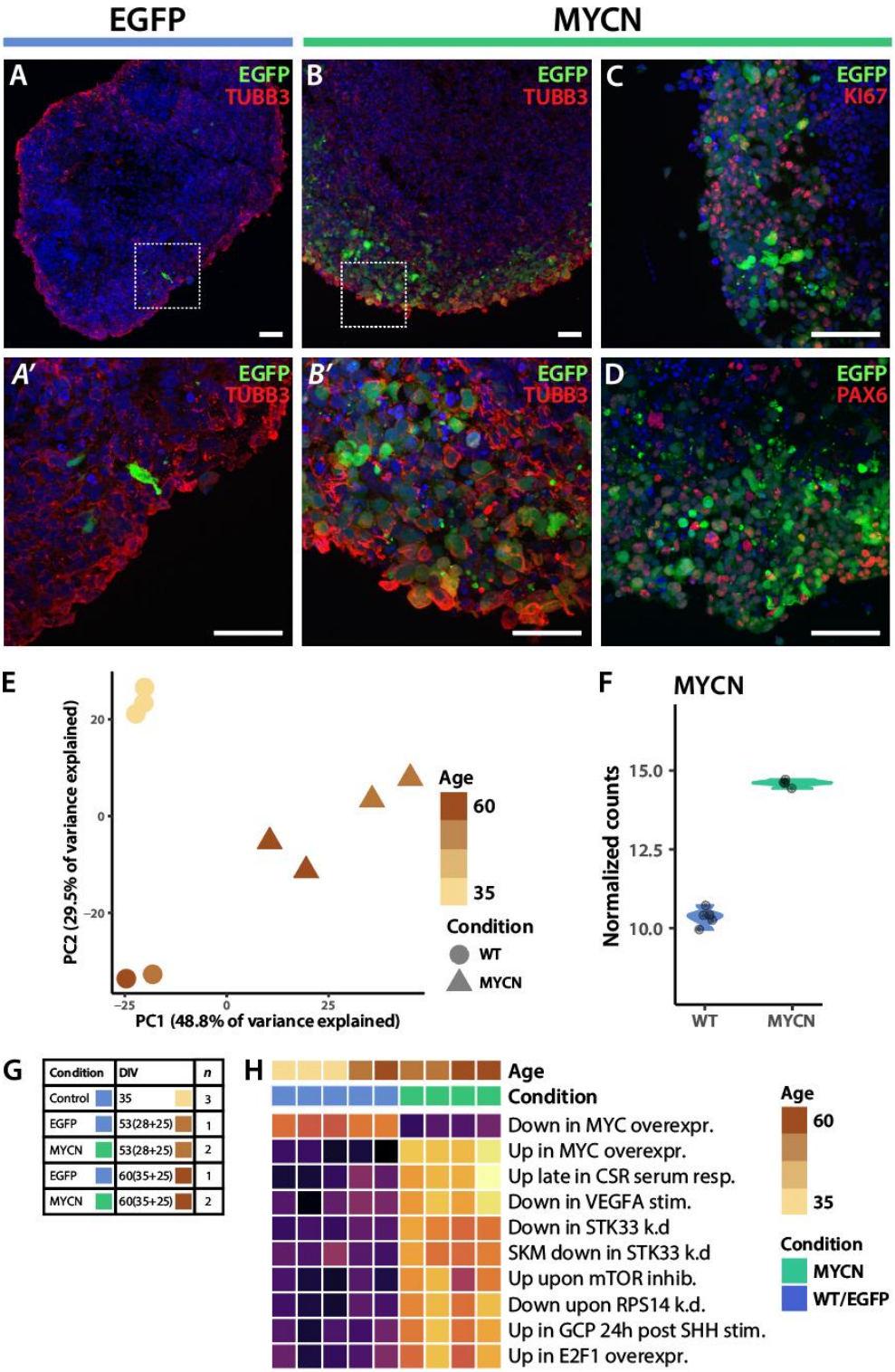


Figure 5.4: MYCN overexpressing organoids contain proliferative rhombic lip derivatives. *A-C) Immunofluorescent antibody labelling revealing GFP-positive MYCN expressing cells are TUBB3, PAX6 and KI67 positive. Organoids electroporated with EGFP control express TUBB3 but contain few GFP-positive cells. B) Principal component analysis of included samples. Colour corresponds to the age of the organoid and shape to the respective*

condition (WT includes both control and EGFP electroporated organoids). F) Variance stabilising transformation (VST) normalised expression of MYCN in different samples grouped by condition. G) Sample types included in RNA sequencing analysis. H) Gene set variation analysis (GSVA) on oncogenic signature gene sets from the Broad institute molecular signature database (MSigDB).. Yellow colour corresponds to high expression of gene sets; black colour corresponds to low gene set expression.

Although *MYCN* overexpression is a potent driver of SHH-MB it is often accompanied by other co-occurring or compound genetic events. *TP53* LOF and *GLI2* overexpression coincide frequently with *MYCN* overexpression and are found in highly aggressive tumours (Ramaswamy *et al.*, 2016). The use of cerebellar organoids to model these compound genetic events was investigated. This experiment also provides sample materials for single-nuclei RNA sequencing (snRNAseq) to be performed by collaborators. Cerebellar organoids were electroporated at DIV35 with *MYCN*-vector (pPB-CAG-MYCN-IRES-mCherry) alone or in combination with vectors encoding a dominant negative *TP53* variant (*DNp53*) (pPB-CAG-DNp53-IRES-Luciferase) and *GLI2*-overexpression (pPB-CAG-GLI2-IRES-EGFP) (*Figure 5.5*). All conditions without *GLI2* were supplemented with the pPB-CAG-GFP to normalise the plasmid DNA input as transfection efficiency is strongly affected by the total amount of plasmid DNA present in the electroporation mix. For each vector, 2 pmol per 100 μL was used. Fluorescence was compared to an empty vector control condition (pPB-CAG-mCherry + pPB-CAG-GFP, referred to as CTRL). Organoids in the different conditions were monitored for 45 days post-electroporation, and samples for snRNAseq were harvested every 15 days. Growth of fluorescent cells was observed in all MYCN conditions, seen in 95% of organoids overexpressing *MYCN* (38/40), 91% of organoids overexpressing *MYCN* and

expressing *DNp53* (40/44), and 93% of organoids overexpressing *MYCN* and *GLI2* and expressing *DNp53* (43/46) but not in the empty vector control (*Figure 5.5*). The fluorescence of mCherry increased significantly more in all *MYCN* transfections (all $p<0.001$) compared to the control condition. In addition, at every time point, fluorescence was significantly higher in *MYCN* transfected conditions compared to the control (all $p<0.001$). Organoids in the *MYCN* transfected conditions tended to be larger than control organoids (all time points $p<0.001$ by ANOVA), however, due to the inherent variability of organoid growth, only the *MYCN* + *DNp53* + *GLI2* condition was significant in individual comparison to control ($p<0.001$ by Dunnett's post hoc test). Although snRNAseq of these organoids is yet to be performed, these experiments readily illustrate how efficiently *MYCN* and compound genetic alterations induce proliferation in cerebellar organoids and strongly support further exploration of this approach for MB modelling.

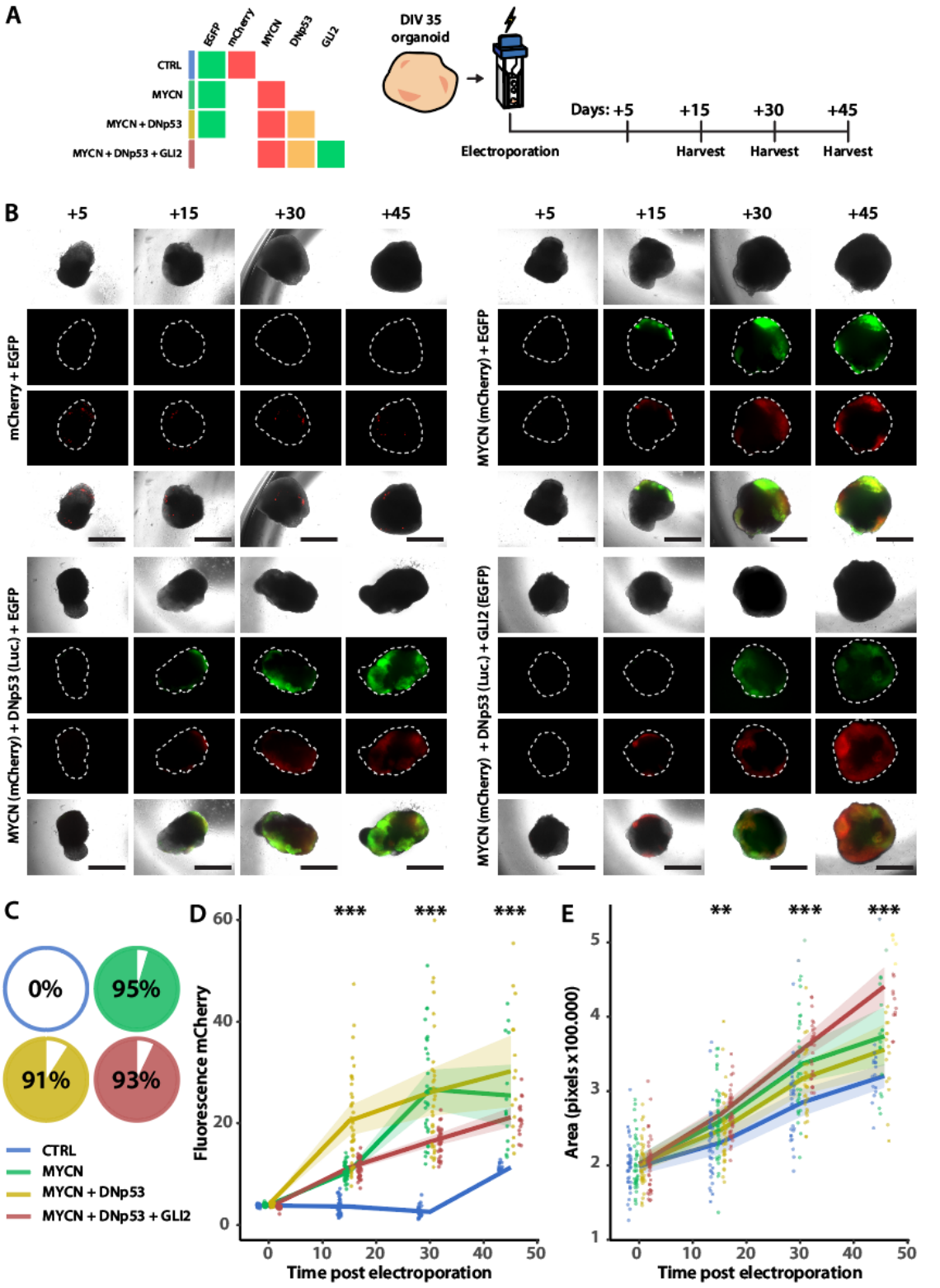


Figure 5.5: MYCN overexpression conditions induce the proliferation and growth of cerebellar organoids. *A) Schematic of experimental design to test the effect of different MYCN overexpression conditions on proliferation and growth of cerebellar organoids. B)*

*Representative images of different electroporation conditions after +5, +15, +30 and +45 days post electroporation: CTRL (pPB-CAG-mCherry + pPB-CAG-EGFP), MYCN (pPB-CAG-MYCN-IRES-mCherry + pPB-CAG-EGFP), MYCN + DNp53 (pPB-CAG-MYCN-IRES-mCherry + pPB-CAG-DNp53-IRES-Luciferase + pPB-CAG-EGFP) and MYCN + DNp53 + GLI2 (pPB-CAG-MYCN-IRES-mCherry + pPB-CAG-DNp53-IRES-Luciferase + pPB-CAG-GLI2-IRES-EGFP). Dashed lines in fluorescence images mark organoid outlines. The scale bar represents 1 μm. C) Proportions of organoids with fluorescent growths. D) mCherry fluorescence signal for 45 days post electroporation. Time is represented in days. Asterisks mark significance computed by ANOVA: ***=p<0.001. E) Growth of organoids represented as the area of the organoids in pixels over time. Time is represented in days. Asterisks mark significance computed by ANOVA: **=p<0.01, ***=p<0.001.*

5.2.3 Tumorigenicity of *MYCN* overexpressing cerebellar progenitors

The significant growth of fluorescent cells in *MYCN* transfected conditions suggests an increased proliferation under the influence of these transgenes that could mimic tumorigenesis. A classic tumorigenicity assay is the orthotopic injection of targeted cells into immunocompromised mice. The tumorigenicity of cells transfected with the plasmid combinations as described above was analysed using orthotopic injection into NSGmice in collaboration with the group of Marcel Kool at the Hopp-Kindertumorzentrum Heidelberg. Ten organoids from each condition were mechanically dissociated into a single-cell suspension. One million cells were injected into the left cerebellar hemisphere of NSG mice (n=3 per condition). Within three weeks post-injection, the first mice injected with the *MYCN* only and *MYCN* + *DNp53* + *GLI2* conditions succumbed to tumour growth (*Figure 5.6*). By seven weeks, all mice injected with cells from the *MYCN* overexpression conditions had to be culled while all mice injected with the empty vector transfected cells were still alive after 75 days of follow up (log-rank test p=0.0088). Haematoxylin and eosin staining of *MYCN*-transfected cerebellar organoid cells revealed nuclei rich tumours with

signs of vascularisation (*Figure 5.6*). This experiment demonstrates the tumorigenicity of cerebellar organoid cells in the MYCN conditions and encourages further analysis of both *in vivo* and *in vitro* cultured MYCN-transfected CBO cells.

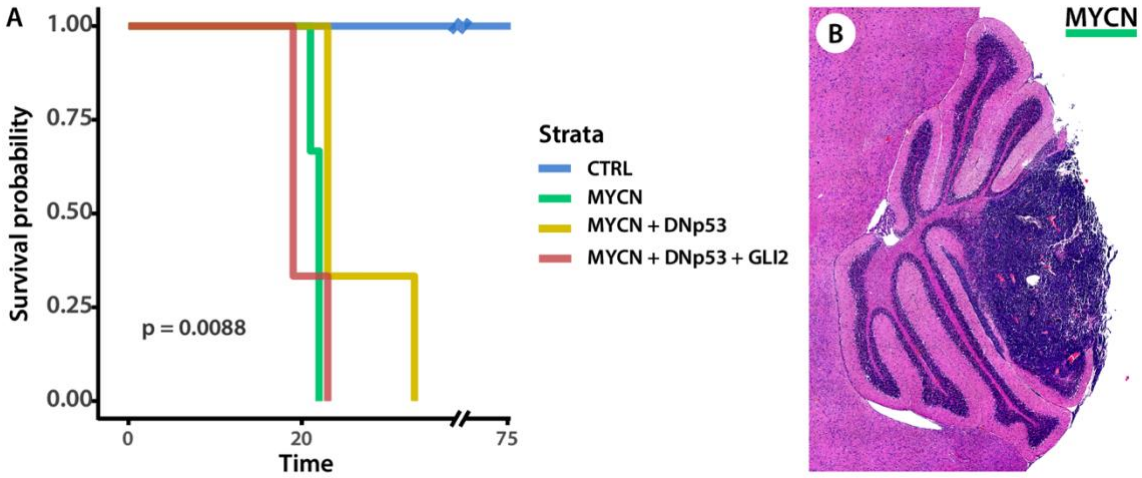


Figure 5.6: Orthotopic injection of MYCN cells induces tumour growth in mice. *A) Three NSG mice per condition were injected with 1x10⁶ DIV35 + 45 cerebellar organoid cells. Survival was observed for a total of 75 days. This experiment was performed by the group of Marcel Kool at the Hopp's Kindertumorenzentrum in Heidelberg. Statistical analysis was performed using the Log-rank test (p=0.0088).B) Haematoxylin and eosin staining showing a tumour in the cerebellum of a mouse injected with MYCN transfected organoid cells. The sectioning, staining and imaging was performed by C. Meulenbroeks at the Princes Maxima Centrum in Utrecht.*

5.2.4 MB cell line co-culture with cerebellar organoids

Co-culture of established MB cell lines offers possibilities to study different aspects of MB tumour biology such as the TME. To test this, a co-culture model of MB cell lines DAOY and ONS-76 was developed. The DAOY line used for these experiments also expressed GFP which was introduced using a pMigr lentiviral vector by collaborators. Therefore, this cell line was used to test the possibilities for MB cell detection in the co-culture system using the intrinsic fluorescence. Both cell lines are typically maintained in two-dimensional (2D) monolayer culture in their respective

classic medium: Earles Minimal Essential Medium (MEM) for DAOY and Roswell Park Memorial Institute (RPMI) 1640 Medium for ONS-76. To facilitate three-dimensional (3D) culture, an approach similar to the generation of embryoid bodies was used. In each well of a low-attachment V-bottom 96-well plate, 20,000 cells were seeded in organoid differentiation medium. Two days after seeding, MB cells had formed spheroid that could be maintained individually or used for co-culture with cerebellar organoids (*Figure **5.7***). Co-culture was initiated by the application of 5-day-old MB-spheroids to DIV 35 cerebellar organoids. Plates were cultured at a 45° angle for two days to facilitate fusion. Within 24 hours, successful fusion could be seen in most co-cultures, and during the subsequent 25 day culture, spheroids of both DAOY and ONS76 cells were slowly incorporated into the organoid. As the DAOY cell line expressed GFP, these cells could be identified in the organoid using immunofluorescence staining and were used for proof-of-principle, and their relative proportion in the co-culture could be assessed using flow cytometry. This analysis showed clear integration of the MB-spheroid into the organoid without showing signs of the infiltration of the organoid by individual MB cells. In addition, flow cytometry for GFP-positive cells revealed DAOY cells to make up 5.84% of cells. Together, these results show that successful co-culture of MB cell lines with cerebellar organoids was accomplished and how fluorescent DAOY cells could be identified.

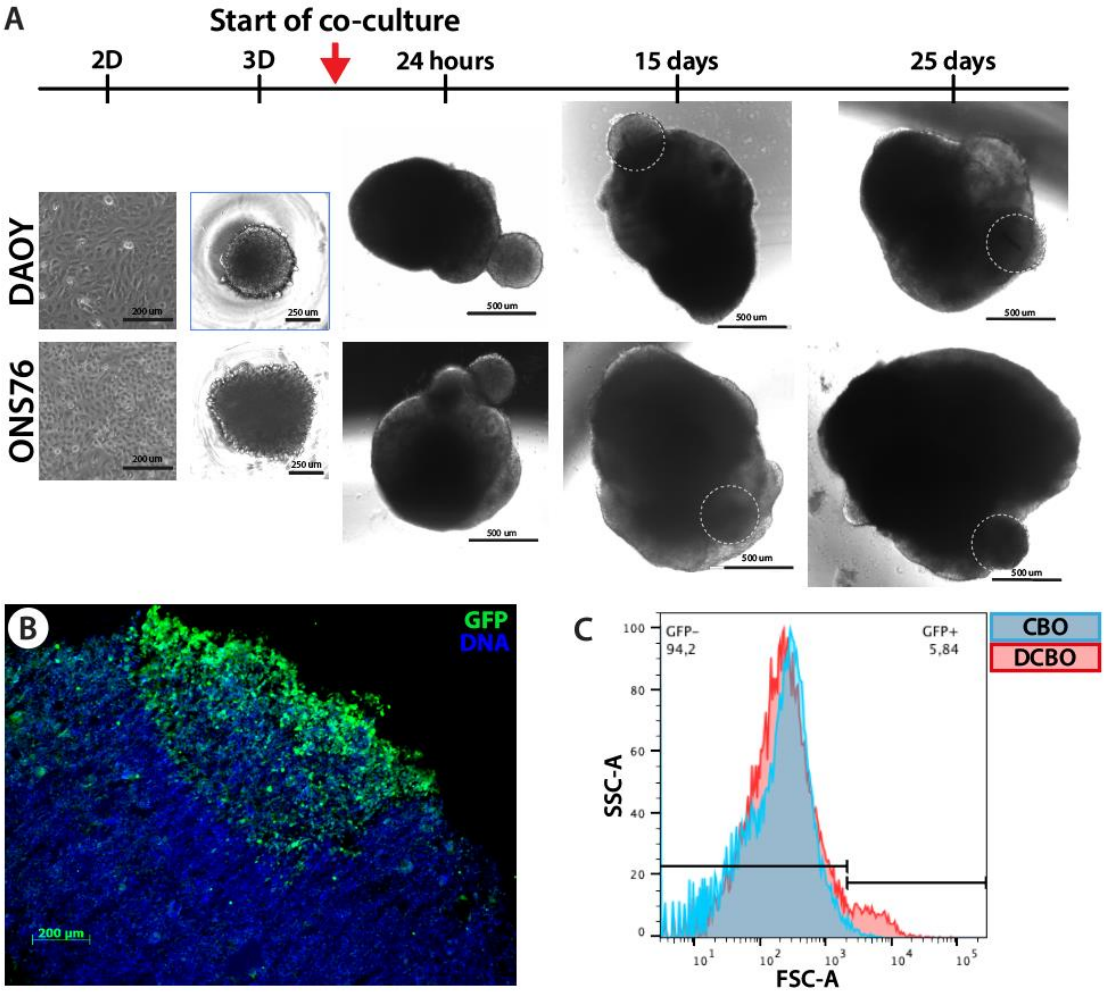


Figure 5.7: Establishment of an MB cell line – cerebellar organoid co-culture model. *A) Time course of cerebellar organoid co-culture with DAOY and ONS76 cells. Two-dimensional (2D) cultures are followed by three-dimensional (3D) cultures as spheroids. Spheroids were added to DIV 35 cerebellar organoids and fuse with the organoids during the subsequent 25 day of culture. Scale bars represent 500 µm. B) Immunofluorescent antibody labelling of GFP shows the integration of GFP-positive DAOY cells into the organoid. Few GFP-positive cells are detected outside of the spheroid. C) Flow cytometry was used to determine the proportion of GFP-positive DAOY cells as 5.84% of all co-cultured cells. CBO = Cerebellar organoid; DCBO = DAOY + Cerebellar organoid.*

5.2.5 Single cell RNA sequencing of organoid co-cultures

Having established that MB cell lines can be co-cultured with cerebellar organoids, I continued to assess whether this system would allow the study of the TME. To test the effects of different microenvironments, or rather TME, DAOY and ONS-76 cells

were cultured as classic monolayers (2D), spheroids (3D) and in co-culture with cerebellar organoids. The use of scRNAseq allows the identification of MB cells in the co-cultures and facilitates the investigation of different TME at the single cell level. Culture conditions were as described above, and single cells were isolated from each respective condition. Monolayer cultures were detached from cell culture plates using TrypLE™ while spheroids and cerebellar organoid conditions (CBO) were dissociated using a Papain based enzymatic digestion and gentle trituration. One six-well-plate well for each 2D condition, 30 pooled spheroids for each 3D condition, and five pooled organoids per CBO condition were used for subsequent analysis. Single-cell suspensions were submitted to the Oxford Genomics Centre's sequencing (OGC) service that uses the 10X Chromium platform. The 10X Chromium system uses a droplet-based technique to encapsulate individual cells together with gel beads in emulsion (GEM). Each GEM is labelled with oligonucleotides containing a ten-base pair unique molecular identifier (UMI) which are tagged onto the RNA molecules of the encapsulated cell. As a result, RNA from each cell gets a specific UMI (or barcode) which helps to resolve the origin of each transcript and the generation of single-cell transcriptomes. The OGC performed transcript quantification was using the CellRanger platform. Quantified transcripts were imported into *R* using *Seurat* (version 4.1.1). Relaxed quality thresholds were used for the initial analysis to maximise the detection of MB cells in the dataset. Mitochondrial gene content varies between cell types from 5% cells with low energy demands up to 30% in high energy consuming cells such as cardiomyocytes (AlJanahi, Danielsen and Dunbar, 2018). Cells with fewer than 200 reads and more than 18% mitochondrial gene content

were removed (Figure *2.1*) and the filtered dataset yielded a total of 12016 cells that were admitted to downstream analyses (see *Table **5-1*** for sample specific counts).

	DAOY 2D	***ONS76 2D***	***DAOY 3D***	***ONS-76 3D***	***CBO***	***DAOY + CBO***	***ONS-76 + CBO***
UMI resolved cells	199	654	761	1372	3987	3872	3602
Post-QC	193	568	690	1267	3242	3316	2739

Table 5-1: Cell counts before and after quality control*. Cell counts before filtering of low-quality cells and post quality control (QC). 2D = two-dimensional monolayer culture; 3D = three dimensional spheroid culture; CBO = cerebellar organoid.*

Transcriptomes of cells that passed quality control were normalised using SCTransform (Hafemeister and Satija, 2019) and processed using the *Seurat* package. Effects of mitochondrial gene content and cell cycle heterogeneity were regressed out. Uniform Manifold Approximation and Projection (UMAP) dimensionality reduction was visualised to assess transcriptomic differences between cells from the different samples (*Figure **5.8***). This showed a clear separation of 2D-cultured DAOY cells (D2D), 2D-ONS-76 cells (O2D), 3D-DAOY spheroids (D3D) and 3D-ONS-76 spheroids (O3D) (*Figure **5.8***). Cells originating from cerebellar organoids projected similarly between the cerebellar organoid mono- (CBO) and CBO-co-culture (DCBO for DAOY-CBO co-culture and OCBO for ONS-76-CBO) samples suggesting a consistent organoid composition. In addition, a small subset of cells of the DCBO and OCBO samples clustered with 3D spheroids generated from the respective MB cell line. These were identified as the DAOY and ONS-76 cells in the CBO co-cultures respectively and used as such for subsequent analyses. The high

degree of overlap in organoid samples demonstrates the consistency between pools of cerebellar organoid-derived cells. Furthermore, clear identification of co-cultured MB-cells enables the extraction of MB-cells to analyse microenvironment effects.

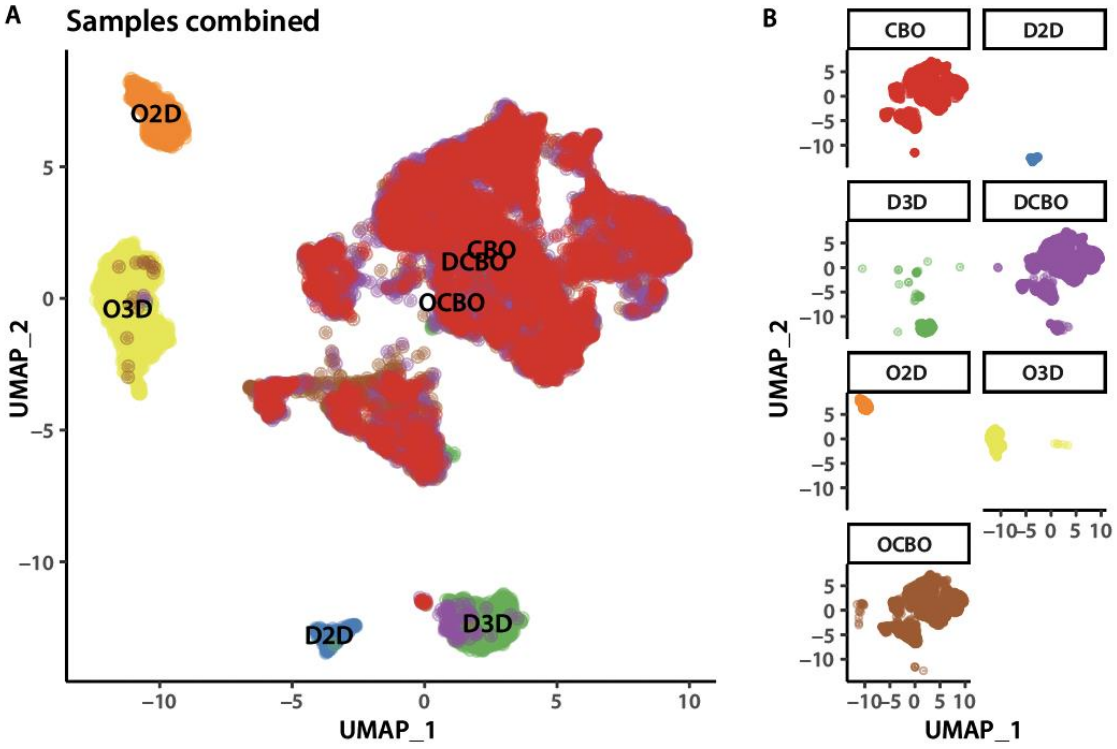


Figure 5.8: Cerebellar organoid and medulloblastoma cells have distinct transcriptomes and can easily be identified*. A) Uniform Manifold Approximation and Projection (UMAP) dimensionality reduction of merged single cell data sets of all seven samples. Clear clustering of cerebellar organoid (CBO) derived cells in the CBO monoculture, DAOY + CBO (DCBO), and ONS-76 + CBO (OCBO) co-cultures is seen, correlating to a high degree of similarity in organoid content. ONS-76 and DAOY monoculture conditions are separated from each other and CBO conditions. B) Separate UMAP-plotting of the different conditions demonstrates that DCBO and OCBO samples contribute a small proportion of cells to their respective spheroid counterparts. D2D = DAOY cultured in 2D; D3D = DAOY cultured in 3D; O2D = ONS-76 cultured in 2D; O3D = ONS-76 cultured in 3D.*

5.2.6 Extracellular matrix upregulation in 3D conditions

Cells identified as DAOY, or ONS-76, were extracted from each of the three culture conditions for proof-of-principle exploration of microenvironment-induced

transcriptomic changes. Cell clusters were determined using a graph-based clustering approach and clearly separated identified populations (*Figure **5.9***). DAOY cells were divided into five clusters (0 to 4) and maintained a clear separation between 2D- and 3D-cultured cells (either as spheroid or in CBO-co-culture). Cluster 2 contained all 2D-cultured cells and displayed high expression of genes associated with the cell cycle (*CCNB1, MKI67, TOP2A, UBE2C* and *CENPF*) (*Figure **5.9***). In contrast, cluster 1 expressed genes involved in collagen binding and ECM constituents (*COL1A2, COL3A1, LGALS3, VCAN*). Cells derived from the organoid co-culture allocated to this cluster. Clusters 0, 3 and 4 were less well defined, with cluster 0 expressing genes encoding secreted heparin-binding proteins (*PTN* and *MDK*) (Laaroubi *et al.*, 1995) and cluster 4 expressing cell cycle markers (*TOP2A, MKI67, UBE2C* and *CENPF*) (*Figure **5.9***) suggesting that this may be a proliferating cell population within DAOY spheroids. No clear phenotype was found in cells belonging to cluster 3. Similar to DAOY cells, 2D- and 3D-cultured ONS-76 cells separated into distinct clusters (*Figure **5.9***). Cluster 1 contained all 2D-ONS-76 cells and differentially expressed markers of proliferation and cell division (*CDC20, UBE2S, CENPF*) as well as *DKK1*, associated with WNT-signalling in MB (Northcott *et al.*, 2011), BMP antagonist follistatin (*FST*), induced by *GLI2* expression (Eichberger et al., 2006), and *KRT18*, which is upregulated in xenografted MB (Tsangaris *et al.*, 2017) (*Figure **5.9***). ONS-76 spheroids and ONS-76 cells co-cultured with organoids showed higher expression of different genes associated with ECM and collagen (cluster 0: *LGALS3, COL9A3, POSTN*; cluster 2: *VCAN, APOE, MGP*; cluster 3: *LINGO1, EMILIN1, PCOLCE*) similar to 3D-cultured DAOY cells. Taken together, these results

show clear differences between 2D- and 3D-cultured MB-cells, presenting increases in ECM genes and decreases in genes involved in cell proliferation.

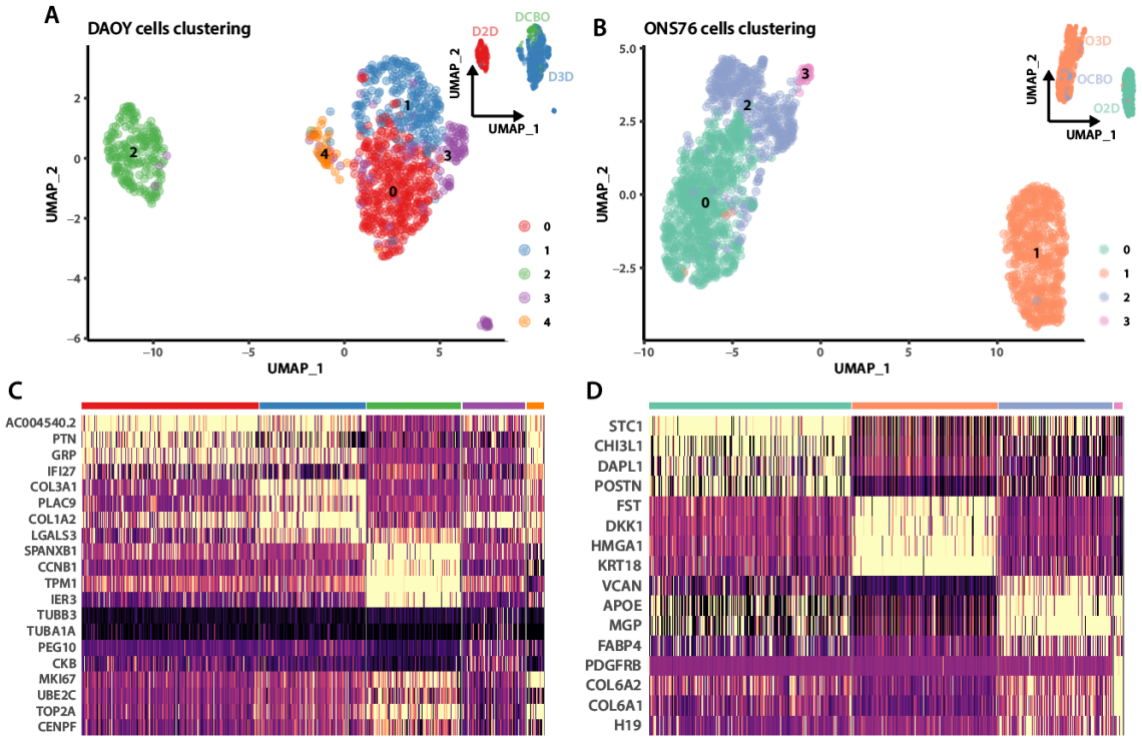


Figure 5.9: Three-dimensional culture DAOY- and ONS-76 cells induces expression of extracellular matrix genes *A) UMAP plot of DAOY cells extracted from each culture condition. Colours mark different cell clusters. The small UMAP plot in the upper right corner shows the distribution of cells from each culture condition in UMAP space. B) UMAP plot of ONS-76 cells with colours marking cell clusters and a small UMAP plot showing the distribution of ONS-76 cells from different conditions. C, D) Heatmap showing the top four differentially expressed genes (DEGs) of each cell cluster in the DAOY (C) and ONS=76 (D) conditions.*

In the context of the TME, it is most interesting to compare MB-cells cultured as spheroids to organoid co-cultures. As different cell states may obscure relevant TME related changes, differential gene expression analysis was performed only on cells from cluster 1 which contained the co-cultured DAOY cells (*Figure 5.10*). Few genes were differentially expressed in DCBO-DAOY cells, most of which related to binding to specific extracellular components such as carbohydrates, monosaccharides and L-

ascorbic acid (*P4HA1, P4HA2,* and *PAM*), glycolysis (*NDUFA4L2, PGK*), hypoxia (*CA9, FAM162A*), and oxidative stress (*TXNIP*) (*Figure 5.10*). DAOY spheroids cells differed primarily in the expression of specific mRNA binding genes (*HNRNP*-family genes) and genes encoding heparin binding growth factors pleiotropin (*PTN*) and midkine (*MDK*), and the SHH receptor Growth arrest-specific protein 1 (*GAS1*). Of note, Midkine (MDK) is elevated in MB (Kato et al., 1999), and relative downregulation in DCBO cells may indicate differentiation of these cells when exposed to the cerebellar microenvironment. GAS1 and BOC positively regulate GCP proliferation and act together as accessory SHH receptors for PTCH1 (Lee, May and Fan, 2001; Izzi *et al.*, 2011). While *PTCH1* and *GLI1* expression remained unchanged between spheroid and CBO co-culture conditions, these results suggest that SHH-signalling at the cell membrane might diverge in different microenvironments. Together, this analysis reveals changes induced by different microenvironments and supports the use of MB cell line – CBO co-culture for further investigations into TME interactions.

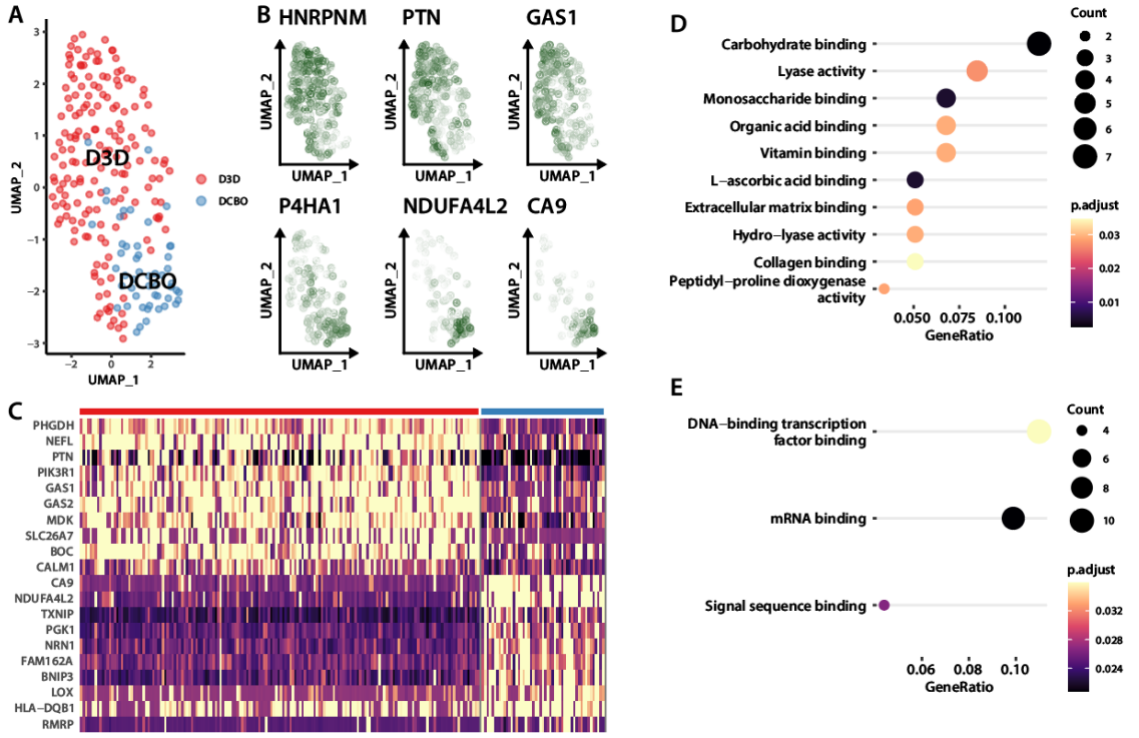


Figure 5.10: CBO co-cultured cells upregulate distinct cell binding pathways. *A) UMAP-plot showing the subset of DAOY cells cultured as spheroids (D3D) cells from cluster 1 and DAOY cells cultured with cerebellar organoids (DCBO) cells in different colours. B) Expression of differentially expressed genes in UMAP space. C) Heatmap showing the top 10 differentially expressed genes between the two culture conditions. D) Gene ontology analysis showing the top upregulated gene sets in DCBO cells compared to spheroid cultures. The X-axis represents the ratio of differentially expressed gene in each gene set, the size represents the number of differentially expressed genes, and the colour represents the Benjamini-Hochberg adjusted p-value. E) Gene ontology analysis showing the top upregulated gene sets in DAOY spheroid cells compared to organoid cultures.*

The abovementioned results demonstrate the potential of MB cell line – CBO co-culture to study the MB TME. However, these techniques also have potential shortcomings that are illustrated by the findings from ONS-76 cells co-cultured with cerebellar organoids. The low retrieval of ONS-76 cells in these samples (n=20), either due to technical reasons, lower engraftment of ONS-76 cells or reduced of ONS-76 cells in the organoid environment, impairs a differential gene expression analysis similar to that of the DAOY cells. When ONS-76 spheroids and OCBO cells

were analysed as described in the paragraph above, several genes associated with cell cycle and proliferation seemed to be upregulated in CBO co-cultured cells (*Figure* ***5.11***). However, examination of the relative proportions of cells in G1, S or G2/M phase of the cell cycle revealed unequal proportions of cells in each phase affecting the differential gene expression analysis. When cell numbers are low, cell cycle regression is not sufficient to correct for these different cell states. Furthermore, differences were less pronounced when looking at a larger set of neuron-specific cell cycle genes (O'Connor *et al.*, 2021). The interpretation of these results is hindered by the unequal sample sizes and reveal how limited control of which cells are isolated from CBO co-cultures impairs subsequent analyses.

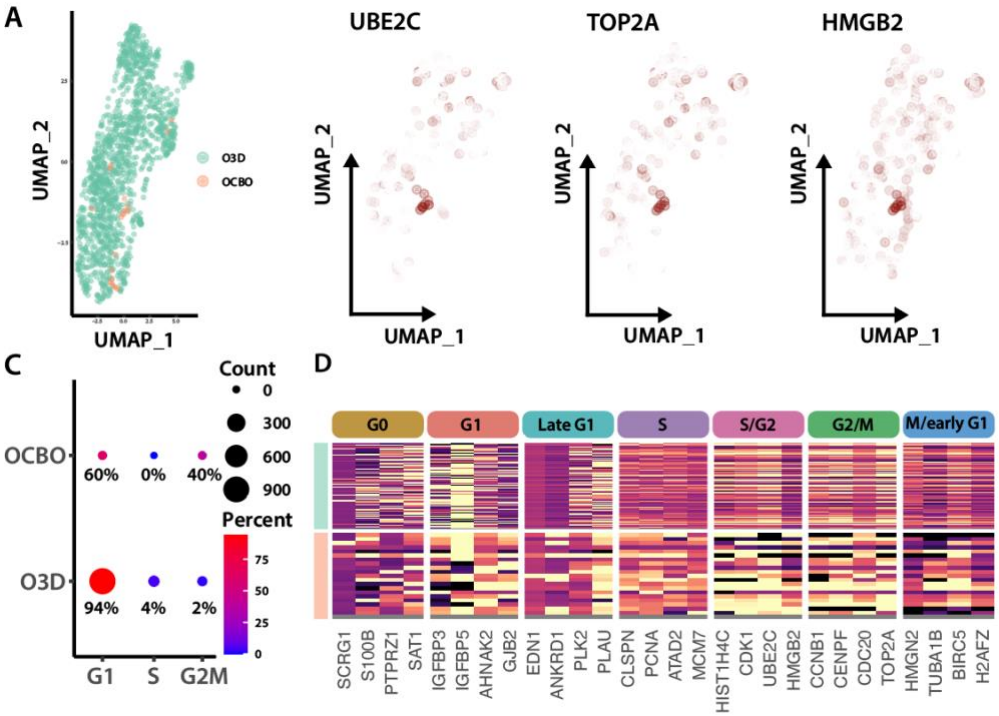


Figure 5.11: Low cell numbers prevent comparison of CBO co-cultured ONS-76 cells with 3D counterparts. *A) UMAP-plot showing O3D and OCBO cells in different colours. B) Expression of differentially expressed genes in UMAP space. C) Proportions of cells in different cell cycle phases within each sample type. D) Heatmap showing the expression of neural cell cycle genes in the two culture conditions.*

5.3 Discussion

This chapter describes alternative ways by which cerebellar organoids can be used to model different aspects of MB tumour biology. Induction of *MYCN* overexpression alone or in combination with TP53 loss-of-function and *GLI2* overexpression resulted in growths of highly proliferative cells that show tumorigenicity upon orthotopic injection in mice. Co-culture of cerebellar organoids with established MB cell lines showed specific ECM-related changes that can be further explored for therapy discovery. Combined, these results further demonstrate the potential that cerebellar organoids have for MB modelling.

The need for human-specific models is exemplified by stark differences in MB-specific genetic alterations in human and murine models. In the context of *MYCN*, studies have shown how GEMMs develop tumours that most closely resemble human group 3 MB (Swartling *et al.*, 2010). Importantly, *MYCN* overexpression in human MB is almost exclusively found in SHH and group 4 subtypes, exposing significant differences (Northcott *et al.*, 2017). Furthermore, lentiviral *MYCN* overexpression in human NES drives malignant transformation upon orthotopic injection in mice and produces tumours that mimic infant SHH-MB (Čančer et al., 2019; Huang et al., 2019), emphasising species-specific effects. Nevertheless, these models suffer from accessibility and safety issues due to the requirement of mice and oncogenic lentiviruses, preventing widespread use in the research community. This chapter demonstrates a novel way to overcome these issues, using PB transposons and

cerebellar organoids to model *MYCN* overexpressing MB while maintaining several benefits attributed to mouse models.

The great efficiency with which proliferative growth of targeted cells was induced in *MYCN* overexpressing conditions encourages the use of cerebellar organoids for comprehensive tumour biology studies and drug discovery. A high penetrance suggests a robust underlying biological mechanism and facilitates downstream applications such as therapy testing. *MYCN* overexpressing organoids showed signatures of increased mTOR signalling, a phenotype that was also seen in the NES models described in the previous paragraph (Čančer et al., 2019). NES-derived tumours displayed sensitivity to mTOR inhibition, a mechanism that could be used as a proof-of-principle for therapy testing in *MYCN* overexpressing cerebellar organoids. Additionally, the high reproducibility means a stable baseline to which the effect of different compound genetic events can be compared. The cerebellar organoids transfected with *MYCN* overexpression alone or combined with *TP53* LOF, and *GLI2* amplification will provide samples for future studies that aim to resolve the different phenotypes arising from a spectrum of increasing malignancy. Especially the effect of TP53 LOF will be of great interest as patients with *TP53* mutant tumours fall within the most high-risk classification and have very poor survival (Zhukova *et al.*, 2013). The generation and optimisation of the cerebellar organoid transfection platform will allow the future study of a wide variety of tumour-associated genetic alterations for their role in MB development, helping to find the targets that matter most.

Co-culture with malignant brain tumours has been used previously to model glioblastoma multiforme (GBM), to overcome limitations of *in vitro* culture of cancer cells that lack a TME (Linkous *et al.*, 2019; Azzarelli *et al.*, 2021). Compared to other model systems that do contain a TME, organoids are able to capture human-specific tumour biology studies. This is especially relevant as studies have shown that PDX models undergo mouse-specific tumour evolution that not accurately recapitulates the human disease (Ben-David *et al.*, 2017; Sachs *et al.*, 2018). MB are known to modulate the microenvironment resulting in distinct TME phenotypes from other paediatric tumours (Petralia *et al.*, 2020) that may be obscured in mouse models. This is evidenced by studies identifying human MB as 'cold' tumours, meaning low immune cell infiltration, likely due to tumour – TME interactions (Bockmayr et al., 2018). Furthermore, tumour-associated astrocytes have been shown to secrete SHH and chemokines that influence tumour stem cell maintenance (Liu *et al.*, 2017), induce necroptosis and promote metastasis (Liu et al., 2020). Specific to SHH-MB, treatment of SHH-MB bearing mice with chemokines such as CXCL3 can force migration and differentiation of (pre-)neoplastic GCPs (Ceccarelli, Micheli and Tirone, 2016) and demonstrate how modulation of the TME can serve as a potential therapeutic strategy. MB cell lines in co-culture with cerebellar organoids could be used to further investigate the role of the TME in human MB and offers a platform to test therapeutic targeting of the TME *in vitro*.

Several ECM-related factors were upregulated in 3D culture conditions of MB cells. The upregulation of collagen genes (*COL1A2, COL6A1* and *COL6A2*) found in MB

spheroids and MB-CBO co-cultures correlate with findings in MB tissues (Liang *et al.*, 2008). Furthermore, the modification of collagen conditions has been proposed as a cancer treatment (reviewed in Xu et al., 2019), and targeting of MB-specific collagens could be investigated in the CBO co-culture model. Another ECM constituent, Galectin–3 (*LGALS3*), was overexpressed in 3D cultures and has also been found upregulated in tumours formed after orthotopic injection of *PTCH1*-mutant iPSC-derived neuroepithelial stem cells (NES) (Susanto *et al.*, 2020). Moreover, micro-array studies have also found upregulation of *LGALS3* mRNA in human MB (Kool *et al.*, 2008; Weishaupt *et al.*, 2019). However, Galectin-3 was previously found to be absent MB tissues using immunostaining (Park *et al.*, 2008), suggesting *LGALS3* mRNA might not correlate with protein levels. Galectin-3 has been implicated in cancer progression and metastasis. The frequency of MB metastases therefore warrants further investigation in the role of Galectin-3 in MB biology. Cerebellar organoid co-culture could be used to study the role of these ECM factors in a relevant microenvironment and help resolve these RNA-to-protein discrepancies.

This chapter only describes the development of each model, illustrated by exemple analyses. John Jacob at the University of Oxford will perform a thorough examination of the MB cell line CBO co-culture model to study the role of the TME in MB. Future analyses of the scRNAseq dataset may include weighted gene network correlation analysis (WGCNA) (Langfelder and Horvath, 2008) that allows unbiased identification of gene sets differentially regulated in cerebellar organoid co-cultured MB cells. Furthermore, cell trajectory inference methods (also called pseudotime

analysis) may allow the investigation of differentiating MB cells (Saelens *et al.*, 2019). The group of Marcel Kool at the Princes Maxima Centrum in Utrecht will use the *MYCN* overexpression samples taken at different intervals and subject these to single-nuclei RNA sequencing (snRNAseq). These single nuclei datasets will be used to study tumour progression under the influence of MYCN. The use of snRNAseq allows comparison with recently published snRNAseq datasets of the developing cerebellum (Aldinger *et al.*, 2021; Sepp *et al.*, 2021) and can be used to reveal key differentially regulated processes that form the basis of malignant transformation. Each modelling technique allows the study of specific aspects of tumour biology and, coupled with single cell/nuclei RNA sequencing techniques, may provide unprecedented insights into MB.

5.4 Conclusion

This chapter demonstrates the successful exploration of two additional modelling strategies using cerebellar organoids. These techniques could be used alongside genetic predisposition modelling to unravel the key aspects of MB biology. Overexpression of MB driver gene *MYCN* reliably resulted in proliferative expansion of targeted cells that can be studied at various stages of progression, thereby providing an unprecedented look at MB tumour evolution. Co-culture of MB cell lines with cerebellar organoids allows the study of specific TME interactions for the first time in a human context. These results encourage the use of cerebellar organoids and present exciting approaches to preclinical MB modelling.

Chapter 6 Discussion and future directions

This thesis describes the development of novel SHH-MB models using cerebellar organoids. Using CRISPR/Cas9, heterozygous and homozygous mutations of *PTCH1* were successfully introduced in iPSC from a healthy donor. These iPSC clones were subjected to cerebellar organoid differentiation and demonstrated the effects of *PTCH1* LOF on neural and cerebellar development. Alternative strategies using the insertion of MB driver genes or established cell lines into cerebellar organoids illustrated how these techniques could be used to capture specific aspects of MB biology. Together, the work in this thesis demonstrates the exciting potential of cerebellar organoids for MB modelling.

6.1 CRISPR gene editing is an efficient tool to introduce germline mutations in human iPSC

Knockout models have been essential for the study of gene function. The advent of CRISPR gene editing has simplified the generation of these models. Especially for genetic diseases such as MB, this tool enables researchers to apply findings in genetic studies to make better models. In Chapter 3, human iPSC were genetically engineered to harbour heterozygous or homozygous *PTCH1* mutations. These mutant iPSC maintained the expression of pluripotency markers and morphology and were successfully used for subsequent differentiation experiments. A similar strategy could be used to create other SHH-MB-relevant models that harbour, for example, *SUFU* LOF or *SMO*-activating mutations. However, as seen with the

impaired cerebellar differentiation of homozygous *PTCH1* mutant iPSC, germline mutations can substantially impact the ability to differentiate into the cell type of interest. This problem could be overcome by using inducible versions of Cas9, either by an external stimulus such as doxycycline or by linking its expression to a lineage-specific gene. Other exciting new techniques, such as photoactivated versions of Cas9, may provide even more temporal control over Cas9 nuclease activity but are still early in their development (Nihongaki *et al.*, 2015). Nevertheless, these techniques cannot compete with the simplicity of introducing knockout mutations. Inducible systems require the insertion of a transgene into the genome. Transgenes can be inserted through HDR using a donor DNA template. This process is considerably less efficient than introducing a knockout mutation through NHEJ. Furthermore, recreating germline predisposition syndromes allows the study of the earliest effects of protein LOF in an unbiased manner, as evidenced by the findings in Chapter 4.

6.2 Cerebellar organoid differentiation models human development and aspects of early medulloblastoma tumorigenesis

Early homozygous LOF of PTCH1 prevented cerebellar differentiation of iPSC. The generated tissues exhibited an altered differentiation trajectory similar to the ventral forebrain under the influence of high levels of SHH-signalling. These results are consistent with findings in *Ptch1-/-* mice that fail to develop the dorsal neural tube. The role of SHH-signalling in this neural fate switch was further established by the rescue of cerebellar differentiation by SMO inhibition using Cyclopamine.

Importantly, the ease with which a rescue experiment could be performed is a testament to the potential of iPSC differentiation to study human development. Chapter 4 is the first description of the effects of *PTCH1* homozygous LOF on cerebellar development. Using these *PTCH1* mutant iPSC in differentiation protocols modelling other brain regions could shed further light on the broader effects of SHH signalling on neural development.

Organoids heterozygous for *PTCH1* LOF developed into cerebellar cells and contained an expanded glutamatergic lineage compared to wildtype organoids. Furthermore, the increased organoid growth, upregulation of cell cycle genes and increased expression of mitotic markers found in heterozygous organoids displays similarities with the preneoplastic stage in *Ptch1+/-* mice. Previous studies have found high levels of cell senescence evasion in murine preneoplastic *Ptch1* mutant MB lesions (Tamayo-Orrego *et al.* 2016). In this study, cell senescence evasion was driven by spontaneous *Tp53* mutations. However, *TP53* and *PTCH1* mutations rarely co-occur in human MB, questioning to what extend these findings can be translated to humans. *PTCH1* heterozygous organoids could be used in future studies to elucidate which factors prevent transformation during this preneoplastic stage for the first time in a human model.

The fact that cerebellar organoid differentiation of *PTCH1* heterozygous and homozygous organoids relates closely to previous findings in mouse models is exciting and encouraging. Furthermore, these findings were reproducible between different iPSC clones and differentiation experiments, supporting the robustness of

these results. Together, this data indicates that cerebellar organoid differentiation can accurately capture relevant human developmental phenotypes *in vivo*. Awareness of the differential effects of oncogenic mutations between mice and human pushes the field of oncology research towards human-specific models. Although two-dimensional cell cultures can be used to study certain aspects of cellular function, the importance of a microenvironment for accurate recapitulation of *in vivo* biology is increasingly clear. However, further refinement of differentiation protocols is required, as organoid development typically only covers the early stages of embryogenesis. Nevertheless, the results in this thesis already show the use of organoids for modelling human development and disease.

6.3 Cerebellar organoids provide a versatile platform for medulloblastoma modelling

The versatility of cerebellar organoids for MB modelling is further illustrated by the successful generation of two additional modelling strategies. Using the PiggyBac transposon system, *MYCN* overexpression was reliably induced in cerebellar organoids and caused the proliferative growth of targeted cells. Furthermore, orthotopic injection of these cells into the cerebella of immunocompromised mice resulted in the growth of aggressive tumours. The application of this technique can easily be extended to other MB drivers associated with the different MB subtypes. In recent years several new molecular drivers have been associated with MB, however, few of these have been tested in human models. Cerebellar organoids provide a platform that facilitates these tests and may help identify which genetic alterations are most important.

Few cancer therapies are able to translate efficacy in *in vitro* cell models to *in vivo* and clinical trials, partly due to the lack of a biologically relevant microenvironment. In recent years the influence of the TME on tumour biology has been recognised and gained attention for potential therapeutic targeting. The co-culture of MB cell lines with cerebellar organoids provides a way to create this TME *in vitro*. This technique is not only applicable to cancer cell lines but may also provide a way to keep primary MB cultures viable *in vitro* for prolonged periods. Primary MB cultures have been difficult to maintain in monolayer, limiting their use for molecular studies and therapy testing. Cerebellar organoids can be grown by hundreds to thousands at a time and thus provide a scalable platform for human-specific TME study and therapy testing in a more complete model.

6.4 Conclusion and future perspective

In this thesis, cerebellar organoids were successfully used to model important aspects of MB biology. These techniques can be used to discover new treatments that address current challenges in medulloblastoma treatment, such as metastases, secondary malignancies, and infertility. Future work could expand these techniques not only to other mutations within SHH-MB but also to other subtypes. In light of recent discoveries of the convergent RL origin of group 3 and group 4 MB, cerebellar organoids provide unprecedented access to the cells these tumours arise from. Efforts are already made to refine the cerebellar differentiation protocol and improve scalability, eventually making this model applicable to large-scale therapy testing. In conclusion, cerebellar organoids are an exciting new way to model MB and may support the next steps in MB treatment discovery.

Bibliography

Ackerman, S.L. *et al.* (1997) 'The mouse rostral cerebellar malformation gene encodes an UNC-5-like protein', *Nature*, 386(6627), pp. 838–842. Available at: https://doi.org/10.1038/386838a0.

Aguilar, A. *et al.* (2012) 'Analysis of human samples reveals impaired SHH-dependent cerebellar development in Joubert syndrome/Meckel syndrome', *Proceedings of the National Academy of Sciences of the United States of America*, 109(42), pp. 16951–16956. Available at: https://doi.org/10.1073/pnas.1201408109.

Ahn, S. and Joyner, A.L. (2005) 'In vivo analysis of quiescent adult neural stem cells responding to Sonic hedgehog', *Nature 2005 437:7060*, 437(7060), pp. 894–897. Available at: https://doi.org/10.1038/nature03994.

Albazron, F.M. *et al.* (2019) 'Pediatric postoperative cerebellar cognitive affective syndrome follows outflow pathway lesions', *Neurology*, 93(16), pp. E1561–E1571. Available at: https://doi.org/10.1212/WNL.0000000000008326.

Alder, J. *et al.* (1999) 'Generation of cerebellar granule neurons in vivo by transplantation of BMP-treated neural progenitor cells', *Nature Neuroscience*, 2(6), pp. 535–540. Available at: https://doi.org/10.1038/9189.

Aldinger, K.A. *et al.* (2021) 'Spatial and cell type transcriptional landscape of human cerebellar development', *Nature Neuroscience*, 24(8), pp. 1163–1175. Available at: https://doi.org/10.1038/s41593-021-00872-y.

Alfaro, A.C. *et al.* (2014) 'Ptch2 mediates the Shh response in Ptch1-/- cells', *Development (Cambridge)*, 141(17), pp. 3331–3339. Available at: https://doi.org/10.1242/DEV.110056/-/DC1.

AlJanahi, A.A., Danielsen, M. and Dunbar, C.E. (2018) 'An Introduction to the Analysis of Single-Cell RNA-Sequencing Data', *Molecular Therapy. Methods & Clinical Development*, 10, p. 189. Available at: https://doi.org/10.1016/J.OMTM.2018.07.003.

Allen, B.L. *et al.* (2011) 'Overlapping roles and collective requirement for the coreceptors GAS1, CDO, and BOC in SHH pathway function', *Developmental Cell*, 20(6), pp. 775–787. Available at: https://doi.org/10.1016/j.devcel.2011.04.018.

Apte, R.S., Chen, D.S. and Ferrara, N. (2019) 'VEGF in Signaling and Disease: Beyond Discovery and Development', *Cell*, pp. 1248–1264. Available at: https://doi.org/10.1016/j.cell.2019.01.021.

Arlt, M.F. *et al.* (2009) 'Replication Stress Induces Genome-wide Copy Number Changes in Human Cells that Resemble Polymorphic and Pathogenic Variants', *American Journal of Human Genetics*, 84(3), pp. 339–350. Available at: https://doi.org/10.1016/j.ajhg.2009.01.024.

Aruga, J. (2004) 'The role of Zic genes in neural development', *Molecular and Cellular Neuroscience*. Academic Press, pp. 205–221. Available at: https://doi.org/10.1016/j.mcn.2004.01.004.

Aszterbaum, M. *et al.* (1998) 'Identification of Mutations in the Human PATCHED Gene in Sporadic Basal Cell Carcinomas and in Patients with the Basal Cell Nevus Syndrome', *Journal of Investigative Dermatology*, 110(6), pp. 885–888. Available at: https://doi.org/10.1046/J.1523-1747.1998.00222.X.

Ayrault, O. *et al.* (2009) 'Two tumor suppressors, p27 Kip1 and Patched-1, collaborate to prevent medulloblastoma olivier ayrault', *Molecular Cancer Research*, 7(1), pp. 33–40. Available at: https://doi.org/10.1158/1541-7786.MCR-08-0369.

Aza-Blanc, P. *et al.* (2000) 'Expression of the vertebrate Gli proteins in Drosophila reveals a distribution of activator and repressor activities', *Development*, 127(19), pp. 4293–4301. Available at: https://doi.org/10.1242/dev.127.19.4293.

Azzarelli, R. *et al.* (2021) 'Three-dimensional model of glioblastoma by co-culturing tumor stem cells with human brain organoids', *Biology Open*, 10(2). Available at: https://doi.org/10.1242/bio.056416.

Baeriswyl, T. and Stoeckli, E.T. (2008) 'Axonin-1/TAG-1 is required for pathfinding of granule cell axons in the developing cerebellum', *Neural Development*, 3(1), pp. 1–19. Available at: https://doi.org/10.1186/1749-8104-3-7.

Bahn, S. *et al.* (1999) 'The intrinsic specification of γ-aminobutyric acid type A receptor α6 subunit gene expression in cerebellar granule cells', *European Journal of Neuroscience*, 11(6), pp. 2194–2198. Available at: https://doi.org/10.1046/J.1460-9568.1999.00662.X.

Bai, C.B. *et al.* (2002) 'Gli2, but not Gli1, is required for initial Shh signaling and ectopic activation of the Shh pathway', *Development*, 129(20), pp. 4753–4761. Available at: https://doi.org/10.1242/DEV.129.20.4753.

Bai, C.B., Stephen, D. and Joyner, A.L. (2004) 'All mouse ventral spinal cord patterning by Hedgehog is Gli dependent and involves an activator function of Gli3', *Developmental Cell*, 6(1), pp. 103–115. Available at: https://doi.org/10.1016/S1534-5807(03)00394-0.

Bailey, P. and Cushing, H. (1925) 'Medulloblastoma cerebelli: A common type of midcerebellar glioma of childhood', *Archives of Neurology & Psychiatry*, 14(2), pp.

192–224. Available at: https://doi.org/10.1001/archneurpsyc.1925.02200140055002.

Ballabio, C. *et al.* (2020) 'Modeling medulloblastoma in vivo and with human cerebellar organoids', *Nature Communications*, 11(1), pp. 1–18. Available at: https://doi.org/10.1038/s41467-019-13989-3.

Ballabio, C. *et al.* (2021) 'Notch1 switches progenitor competence in inducing medulloblastoma', *Science Advances*, 7(26), pp. 2781–2804. Available at: https://doi.org/10.1126/sciadv.abd2781.

Barnfield, P.C. *et al.* (2005) 'Negative regulation of Gli1 and Gli2 activator function by Suppressor of fused through multiple mechanisms', *Differentiation*, 73(8), pp. 397–405. Available at: https://doi.org/10.1111/j.1432-0436.2005.00042.x.

Bavetsias, V. and Linardopoulos, S. (2015) 'Aurora kinase inhibitors: Current status and outlook', *Frontiers in Oncology*. Frontiers Media SA. Available at: https://doi.org/10.3389/fonc.2015.00278.

Beauchamp, E.M. *et al.* (2011) 'Arsenic trioxide inhibits human cancer cell growth and tumor development in mice by blocking Hedgehog/GLI pathway', *Journal of Clinical Investigation*, 121(1), pp. 148–160. Available at: https://doi.org/10.1172/JCI42874.

Behesti, H. *et al.* (2021) 'Altered temporal sequence of transcriptional regulators in the generation of human cerebellar granule cells', *eLife*, 10. Available at: https://doi.org/10.7554/ELIFE.67074.

Ben-Arie, N. *et al.* (1997) 'Math1 is essential for genesis of cerebellar granule neurons', *Nature 1997 390:6656*, 390(6656), pp. 169–172. Available at: https://doi.org/10.1038/36579.

Ben-David, U. *et al.* (2017) 'Patient-derived xenografts undergo mouse-specific tumor evolution', *Nature Genetics*, 49(11), pp. 1567–1575. Available at: https://doi.org/10.1038/ng.3967.

Ben-David, U. *et al.* (2018) 'Genetic and transcriptional evolution alters cancer cell line drug response', *Nature*, 560(7718), pp. 325–330. Available at: https://doi.org/10.1038/s41586-018-0409-3.

Blassberg, R. and Jacob, J. (2017) 'Lipid metabolism fattens up hedgehog signaling', *BMC biology*, 15(1). Available at: https://doi.org/10.1186/S12915-017-0442-Y.

Bouaoun, L. *et al.* (2016) 'TP53 Variations in Human Cancers: New Lessons from the IARC TP53 Database and Genomics Data', *Human Mutation*, 37(9), pp. 865–876. Available at: https://doi.org/10.1002/humu.23035.

Brewster, R., Lee, J. and Altaba, A.R.I. (1998) 'Gli/Zic factors pattern the neural plate by defining domains of cell differentiation', *Nature*, 393(6685), pp. 579–583. Available at: https://doi.org/10.1038/31242.

Briggs, K.J. *et al.* (2008a) 'Cooperation between the Hic1 and Ptch1 tumor suppressors in medulloblastoma', *Genes & Development*, 22(6), pp. 770–785. Available at: https://doi.org/10.1101/GAD.1640908.

Briggs, K.J. *et al.* (2008b) 'Cooperation between the Hic1 and Ptch1 tumor suppressors in medulloblastoma', *Genes & Development*, 22(6), pp. 770–785. Available at: https://doi.org/10.1101/gad.1640908.

Briscoe, J. *et al.* (2000) 'A homeodomain protein code specifies progenitor cell identity and neuronal fate in the ventral neural tube', *Cell*, 101(4), pp. 435–445. Available at: https://doi.org/10.1016/S0092-8674(00)80853-3.

Briscoe, J. and Ericson, J. (1999) 'The specification of neuronal identity by graded sonic hedgehog signalling', *Seminars in Cell and Developmental Biology*, 10(3), pp. 353–362. Available at: https://doi.org/10.1006/scdb.1999.0295.

Brodowska, K. *et al.* (2014) 'The clinically used photosensitizer Verteporfin (VP) inhibits YAP-TEAD and human retinoblastoma cell growth invitro without light activation', *Experimental Eye Research*, 124, pp. 67–73. Available at: https://doi.org/10.1016/j.exer.2014.04.011.

Buglino, J.A. and Resh, M.D. (2008) 'Hhat is a palmitoylacyltransferase with specificity for N-palmitoylation of Sonic Hedgehog', *Journal of Biological Chemistry*, 283(32), pp. 22076–22088. Available at: https://doi.org/10.1074/jbc.M803901200.

Buonamici, S. *et al.* (2010) 'Interfering with resistance to smoothened antagonists by inhibition of the PI3K pathway in medulloblastoma', *Science Translational Medicine*, 2(51), pp. 51–70. Available at: https://doi.org/10.1126/scitranslmed.3001599.

Burke, R. *et al.* (1999) 'Dispatched, a novel sterol-sensing domain protein dedicated to the release of cholesterol-modified Hedgehog from signaling cells', *Cell*, 99(7), pp. 803–815. Available at: https://doi.org/10.1016/S0092-8674(00)81677-3.

Byrne, A.T. *et al.* (2017) 'Interrogating open issues in cancer precision medicine with patient-derived xenografts', *Nature Reviews Cancer*, pp. 254–268. Available at: https://doi.org/10.1038/nrc.2016.140.

Čančer, M. *et al.* (2019a) 'Humanized Stem Cell Models of Pediatric Medulloblastoma Reveal an Oct4/mTOR Axis that Promotes Malignancy', *Cell Stem Cell*, 25(6), pp. 855-870.e11. Available at: https://doi.org/10.1016/j.stem.2019.10.005.

Čančer, M. *et al.* (2019b) 'Humanized Stem Cell Models of Pediatric Medulloblastoma Reveal an Oct4/mTOR Axis that Promotes Malignancy', *Cell Stem Cell*, 25(6), pp. 855-870.e11. Available at: https://doi.org/10.1016/J.STEM.2019.10.005.

Cao, S.Y. *et al.* (2017) 'Enhanced derivation of human pluripotent stem cell-derived cortical glutamatergic neurons by a small molecule', *Scientific Reports*, 7(1), pp. 1–11. Available at: https://doi.org/10.1038/s41598-017-03519-w.

Cartegni, L., Chew, S.L. and Krainer, A.R. (2002) 'Listening to silence and understanding nonsense: Exonic mutations that affect splicing', *Nature Reviews Genetics*. Nature Publishing Group, pp. 285–298. Available at: https://doi.org/10.1038/nrg775.

Cavalli, F.M.G. *et al.* (2017) 'Intertumoral Heterogeneity within Medulloblastoma Subgroups', *Cancer Cell*, 31(6), pp. 737-754.e6. Available at: https://doi.org/10.1016/J.CCELL.2017.05.005.

Ceccarelli, M., Micheli, L. and Tirone, F. (2016) 'Suppression of medulloblastoma lesions by forced migration of preneoplastic precursor cells with intracerebellar administration of the chemokine Cxcl3', *Frontiers in Pharmacology*, 7(DEC), p. 484. Available at: https://doi.org/10.3389/fphar.2016.00484.

Cederquist, G.Y. *et al.* (2019) 'Specification of positional identity in forebrain organoids', *Nature Biotechnology*, 37(4), pp. 436–444. Available at: https://doi.org/10.1038/s41587-019-0085-3.

Chambers, S.M. *et al.* (2009) 'Highly efficient neural conversion of human ES and iPS cells by dual inhibition of SMAD signaling', *Nature Biotechnology*, 27(3), pp. 275–280. Available at: https://doi.org/10.1038/nbt.1529.

Chatterjee, I. *et al.* (2016) 'Induced pluripotent stem (iPS) cell culture methods and induction of differentiation into endothelial cells', in *Methods in Molecular Biology*. Methods Mol Biol, pp. 311–327. Available at: https://doi.org/10.1007/7651_2015_203.

Chen, J.K. *et al.* (2002) 'Inhibition of Hedgehog signaling by direct binding of cyclopamine to Smoothened', *Genes & Development*, 16(21). Available at: https://doi.org/10.1101/GAD.1025302.

Chen, J.K. (2016) 'I only have eye for ewe: The discovery of cyclopamine and development of Hedgehog pathway-targeting drugs', *Natural Product Reports*. The Royal Society of Chemistry, pp. 595–601. Available at: https://doi.org/10.1039/c5np00153f.

Chen, M.H. *et al.* (2009) 'Cilium-independent regulation of Gli protein function by Sufu in Hedgehog signaling is evolutionarily conserved', *Genes and Development*, 23(16), pp. 1910–1928. Available at: https://doi.org/10.1101/gad.1794109.

Cheng, F.Y. *et al.* (2012) 'Widespread Contribution of Gdf7 Lineage to Cerebellar Cell Types and Implications for Hedgehog-Driven Medulloblastoma Formation', *PLoS ONE*. Edited by P. Hitchcock, 7(4), p. e35541. Available at: https://doi.org/10.1371/journal.pone.0035541.

Cheng, Y. *et al.* (2020) 'Sustained hedgehog signaling in medulloblastoma tumoroids is attributed to stromal astrocytes and astrocyte-derived extracellular matrix', *Laboratory Investigation*, 100(9), pp. 1208–1222. Available at: https://doi.org/10.1038/s41374-020-0443-2.

Chizhikov, V. v *et al.* (2006) 'The roof plate regulates cerebellar cell-type specification and proliferation.', *Development (Cambridge, England)*, 133(15), pp. 2793–804. Available at: https://doi.org/10.1242/dev.02441.

Cong, L. *et al.* (2013) 'Multiplex genome engineering using CRISPR/Cas systems', *Science*, 339(6121), pp. 819–823. Available at: https://doi.org/10.1126/science.1231143.

Coni, S. *et al.* (2017) 'Selective targeting of HDAC1/2 elicits anticancer effects through Gli1 acetylation in preclinical models of SHH Medulloblastoma', *Scientific Reports*, 7(1), pp. 1–12. Available at: https://doi.org/10.1038/srep44079.

Cooper, M.K. *et al.* (1998) 'Teratogen-mediated inhibition of target tissue response to Shh signaling', *Science*, 280(5369), pp. 1603–1607. Available at: https://doi.org/10.1126/SCIENCE.280.5369.1603/ASSET/0ABA0332-8BD7-4C6C-9BC7-D51406B5A9A9/ASSETS/GRAPHIC/SE2386560004.JPEG.

Corbit, K.C. *et al.* (2005) 'Vertebrate Smoothened functions at the primary cilium', *Nature 2005 437:7061*, 437(7061), pp. 1018–1021. Available at: https://doi.org/10.1038/nature04117.

Corcoran, R.B. and Scott, M.P. (2006) 'Oxysterols stimulate Sonic hedgehog signal transduction and proliferation of medulloblastoma cells', *Proceedings of the National Academy of Sciences of the United States of America*, 103(22), pp. 8408–8413. Available at: https://doi.org/10.1073/pnas.0602852103.

Cotterman, R. and Knoepfler, P.S. (2009) 'N-Myc regulates expression of pluripotency genes in neuroblastoma including lif, klf2, klf4, and lin28b', *PLoS ONE*, 4(6), p. e5799. Available at: https://doi.org/10.1371/journal.pone.0005799.

Dagogo-Jack, I. and Shaw, A.T. (2018) 'Tumour heterogeneity and resistance to cancer therapies.', *Nature reviews. Clinical oncology*, 15(2), pp. 81–94. Available at: https://doi.org/10.1038/nrclinonc.2017.166.

Dahmane, N. and Ruiz I Altaba, A. (1999) 'Sonic hedgehog regulates the growth and patterning of the cerebellum', *Development*, 126(14), pp. 3089–3100. Available at: https://doi.org/10.1242/DEV.126.14.3089.

Dang, C. v. (2012) 'MYC on the path to cancer', *Cell*. Cell Press, pp. 22–35. Available at: https://doi.org/10.1016/j.cell.2012.03.003.

Dekkers, J.F. *et al.* (2019) 'High-resolution 3D imaging of fixed and cleared organoids', *Nature Protocols*, 14(6), pp. 1756–1771. Available at: https://doi.org/10.1038/s41596-019-0160-8.

Denef, N. *et al.* (2000) 'Hedgehog induces opposite changes in turnover and subcellular localization of patched and smoothened', *Cell*, 102(4), pp. 521–531. Available at: https://doi.org/10.1016/S0092-8674(00)00056-8.

Dey, J. *et al.* (2012) 'A Distinct Smoothened Mutation Causes Severe Cerebellar Developmental Defects and Medulloblastoma in a Novel Transgenic Mouse Model', *Molecular and Cellular Biology*, 32(20), pp. 4104–4115. Available at: https://doi.org/10.1128/mcb.00862-12.

Dhanyamraju, P.K. *et al.* (2015) 'Histone deacetylase 6 represents a novel drug target in the oncogenic Hedgehog signaling pathway', *Molecular Cancer Therapeutics*, 14(3), pp. 727–739. Available at: https://doi.org/10.1158/1535-7163.MCT-14-0481.

Ding, Q. *et al.* (1998) 'Diminished Sonic hedgehog signaling and lack of floor plate differentiation in Gli2 mutant mice', *Development*, 125(14), pp. 2533–2543. Available at: https://doi.org/10.1242/dev.125.14.2533.

Ding, S. *et al.* (2005) 'Efficient transposition of the piggyBac (PB) transposon in mammalian cells and mice', *Cell*, 122(3), pp. 473–483. Available at: https://doi.org/10.1016/j.cell.2005.07.013.

Dorsam, R.T. and Gutkind, J.S. (2007) 'G-protein-coupled receptors and cancer', *Nature Reviews Cancer*. Nature Publishing Group, pp. 79–94. Available at: https://doi.org/10.1038/nrc2069.

Duman-Scheel, M. *et al.* (2002) 'Hedgehog regulates cell growth and proliferation by inducing Cyclin D and Cyclin E', *Nature*, 417(6886), pp. 299–304. Available at: https://doi.org/10.1038/417299a.

Dwyer, J.R. *et al.* (2007) 'Oxysterols are novel activators of the hedgehog signaling pathway in pluripotent mesenchymal cells', *Journal of Biological Chemistry*, 282(12), pp. 8959–8968. Available at: https://doi.org/10.1074/jbc.M611741200.

Echelard, Y. *et al.* (1993) 'Sonic hedgehog, a member of a family of putative signaling molecules, is implicated in the regulation of CNS polarity', *Cell*, 75(7), pp. 1417–1430. Available at: https://doi.org/10.1016/0092-8674(93)90627-3.

Engelkamp, D. *et al.* (1999) 'Role of Pax6 in development of the cerebellar system', *Development*, 126(16), pp. 3585–3596. Available at: https://doi.org/10.1242/dev.126.16.3585.

Englund, C. *et al.* (2006) 'Unipolar brush cells of the cerebellum are produced in the rhombic lip and migrate through developing white matter.', *The Journal of neuroscience : the official journal of the Society for Neuroscience*, 26(36), pp. 9184–95. Available at: https://doi.org/10.1523/JNEUROSCI.1610-06.2006.

Ericson, J., Rashbass, P., Schedl, A., Brenner-Morton, S., Kawakami, A., van Heyningen, V., *et al.* (1997a) 'Pax6 Controls Progenitor Cell Identity and Neuronal Fate in Response to Graded Shh Signaling', *Cell*, 90(1), pp. 169–180. Available at: https://doi.org/10.1016/S0092-8674(00)80323-2.

Ericson, J., Rashbass, P., Schedl, A., Brenner-Morton, S., Kawakami, A., van Heyningen, V., *et al.* (1997b) 'Pax6 controls progenitor cell identity and neuronal fate in response to graded Shh signaling', *Cell*, 90(1), pp. 169–180. Available at: https://doi.org/10.1016/S0092-8674(00)80323-2.

Ericson, J., Rashbass, P., Schedl, A., Brenner-Morton, S., Kawakami, A., van Heyningen, V, *et al.* (1997) 'Pax6 controls progenitor cell identity and neuronal fate in response to graded Shh signaling.', *Cell*, 90(1), pp. 169–80. Available at: https://doi.org/10.1016/s0092-8674(00)80323-2.

van Essen, M., Riepsaame, J. and Jacob, J. (2021) 'CRISPR-Cas Gene Perturbation and Editing in Human Induced Pluripotent Stem Cells', *CRISPR Journal*. Mary Ann Liebert Inc., pp. 634–655. Available at: https://doi.org/10.1089/crispr.2021.0063.

van Essen, M.J. *et al.* (2022) 'Cerebellar Modelling Using Human Induced Pluripotent Stem Cells', in *Neuromethods*. Humana Press Inc., pp. 1–21. Available at: https://doi.org/10.1007/978-1-0716-2026-7_1.

Fink, A.J. *et al.* (2006) 'Development of the deep cerebellar nuclei: Transcription factors and cell migration from the rhombic lip', *Journal of Neuroscience*, 26(11), pp. 3066–3076. Available at: https://doi.org/10.1523/JNEUROSCI.5203-05.2006.

Forget, A. *et al.* (2014) 'Shh signaling protects Atoh1 from degradation mediated by the E3 ubiquitin ligase Huwe1 in neural precursors.', *Developmental cell*, 29(6), pp. 649–61. Available at: https://doi.org/10.1016/j.devcel.2014.05.014.

Gailani, M.R. *et al.* (1996) 'The role of the human homologue of Drosophila patched in sporadic basal cell carcinomas', *Nature Genetics*, 14(1), pp. 78–81. Available at: https://doi.org/10.1038/ng0996-78.

Gao, B. and Fritschy, J.M. (1995) 'Cerebellar granule cells in vitro recapitulate the in vivo pattern of GABAA-receptor subunit expression', *Developmental Brain Research*, 88(1), pp. 1–16. Available at: https://doi.org/10.1016/0165-3806(95)00062-I.

Garcia-Lopez, J. *et al.* (2021) 'Deconstructing Sonic Hedgehog Medulloblastoma: Molecular Subtypes, Drivers, and Beyond', *Trends in Genetics*, 37(3), pp. 235–250. Available at: https://doi.org/10.1016/J.TIG.2020.11.001.

Garwicz, S. *et al.* (2000) 'Second malignant neoplasms after cancer in childhood and adolescence: A population-based case-control study in the 5 nordic countries', *International Journal of Cancer*, 88(4), pp. 672–678. Available at: https://doi.org/10.1002/1097-0215(20001115)88:4<672::AID-IJC24>3.0.CO;2-N.

Gaspard, N. *et al.* (2009) 'Generation of cortical neurons from mouse embryonic stem cells', *Nature Protocols*, 4(10), pp. 1456–1463. Available at: https://doi.org/10.1038/nprot.2009.157.

Gazit, R., Krizhanovsky, V. and Ben-Arie, N. (2004) 'Math1 controls cerebellar granule cell differentiation by regulating multiple components of the Notch signaling pathway', *Development*, 131(4), pp. 903–913. Available at: https://doi.org/10.1242/dev.00982.

Ghezraoui, H. *et al.* (2014) 'Chromosomal Translocations in Human Cells Are Generated by Canonical Nonhomologous End-Joining', *Molecular Cell*, 55(6), pp. 829–842. Available at: https://doi.org/10.1016/j.molcel.2014.08.002.

Giandomenico, S.L. *et al.* (2019) 'Cerebral organoids at the air–liquid interface generate diverse nerve tracts with functional output', *Nature Neuroscience*, 22(4), pp. 669–679. Available at: https://doi.org/10.1038/s41593-019-0350-2.

Gilthorpe, J.D. *et al.* (2002) 'The migration of cerebellar rhombic lip derivatives', *Development*, 129(20), pp. 4719–4728. Available at: https://doi.org/10.1242/DEV.129.20.4719.

Gong, X. *et al.* (2018) 'Structural basis for the recognition of Sonic Hedgehog by human Patched1', *Science*, 361(6402). Available at: https://doi.org/10.1126/science.aas8935.

Goodrich, L. v *et al.* (1996) 'Conservation of the hedgehog/patched signaling pathway from flies to mice: Induction of a mouse patched gene by Hedgehog', *Genes and Development*, 10(3), pp. 301–312. Available at: https://doi.org/10.1101/gad.10.3.301.

Goodrich, L. v. *et al.* (1997) 'Altered neural cell fates and medulloblastoma in mouse patched mutants', *Science*, 277(5329), pp. 1109–1113. Available at: https://doi.org/10.1126/science.277.5329.1109.

Gorlin, R.J. (1995) 'Nevoid basal cell carcinoma syndrome', *Dermatologic Clinics*. Elsevier, pp. 113–125. Available at: https://doi.org/10.1016/s0733-8635(18)30114-1.

Gorlin, R.J. and Goltz, R.W. (1960) 'Multiple Nevoid Basal-Cell Epithelioma, Jaw Cysts and Bifid Rib', *New England Journal of Medicine*, 262(18), pp. 908–912. Available at: https://doi.org/10.1056/nejm196005052621803.

Guillemot, F. and Zimmer, C. (2011) 'From cradle to grave: The multiple roles of fibroblast growth factors in neural development', *Neuron*. Cell Press, pp. 574–588. Available at: https://doi.org/10.1016/j.neuron.2011.08.002.

Guizzetti, M. and Costa, L.G. (2008) 'Sonic hedgehog in smith-lemli-opitz syndrome and tumor development', *Journal of Pediatric Hematology/Oncology*, pp. 641–642. Available at: https://doi.org/10.1097/MPH.0b013e318180bbb9.

Hafemeister, C. and Satija, R. (2019) 'Normalization and variance stabilization of single-cell RNA-seq data using regularized negative binomial regression', *Genome Biology*, 20(1), pp. 1–15. Available at: https://doi.org/10.1186/s13059-019-1874-1.

Hahn, H. *et al.* (1996) 'Mutations of the human homolog of drosophila patched in the nevoid basal cell carcinoma syndrome', *Cell*, 85(6), pp. 841–851. Available at: https://doi.org/10.1016/S0092-8674(00)81268-4.

Haldipur, P. *et al.* (2012) 'Expression of sonic hedgehog during cell proliferation in the human cerebellum', *Stem Cells and Development*, 21(7), pp. 1059–1068. Available at: https://doi.org/10.1089/scd.2011.0206.

Haldipur, P. *et al.* (2019) 'Spatiotemporal expansion of primary progenitor zones in the developing human cerebellum', *Science*, 366(6464), pp. 454–460. Available at: https://doi.org/10.1126/science.aax7526.

Hallahan, A.R. *et al.* (2004) 'The SmoA1 mouse model reveals that notch signaling is critical for the growth and survival of Sonic Hedgehog-induced medulloblastomas', *Cancer Research*, 64(21), pp. 7794–7800. Available at: https://doi.org/10.1158/0008-5472.CAN-04-1813.

Hamanaka, N. *et al.* (2019) 'YES1 is a targetable oncogene in cancers harboring YES1 gene amplification', *Cancer Research*, 79(22), pp. 5734–5745. Available at: https://doi.org/10.1158/0008-5472.CAN-18-3376.

Hanaway, J. (1967) 'Formation and differentiation of the external granular layer of the chick cerebellum', *Journal of Comparative Neurology*, 131(1), pp. 1–13. Available at: https://doi.org/10.1002/CNE.901310102.

Handel, A.E. *et al.* (2016) 'Assessing similarity to primary tissue and cortical layer identity in induced pluripotent stem cell-derived cortical neurons through single-cell transcriptomics', *Human Molecular Genetics*, 25(5), pp. 989–1000. Available at: https://doi.org/10.1093/HMG/DDV637.

Hänzelmann, S., Castelo, R. and Guinney, J. (2013) 'GSVA: Gene set variation analysis for microarray and RNA-Seq data', *BMC Bioinformatics*, 14(1), pp. 1–15. Available at: https://doi.org/10.1186/1471-2105-14-7/FIGURES/7.

Haramoto, Y. *et al.* (2015) 'Insulin-like factor regulates neural induction through an IGF1 receptor-independent mechanism', *Scientific Reports*, 5. Available at: https://doi.org/10.1038/srep11603.

Hasegawa, D. *et al.* (2017) 'Gorlin syndrome-derived induced pluripotent stem cells are hypersensitive to hedgehog-mediated osteogenic induction', *PLoS ONE*, 12(10), p. e0186879. Available at: https://doi.org/10.1371/journal.pone.0186879.

Hastings, P.J. *et al.* (2009) 'Mechanisms of change in gene copy number', *Nature Reviews Genetics*. Nature Publishing Group, pp. 551–564. Available at: https://doi.org/10.1038/nrg2593.

Hatton, B.A. *et al.* (2008) 'The Smo/Smo model: Hedgehog-induced medulloblastoma with 90% incidence and leptomeningeal spread', *Cancer Research*, 68(6), pp. 1768–1776. Available at: https://doi.org/10.1158/0008-5472.CAN-07-5092.

He, X. *et al.* (2014) 'The G protein α subunit Gαs is a tumor suppressor in Sonic hedgehog-driven medulloblastoma', *Nature Medicine*, 20(9), pp. 1035–1042. Available at: https://doi.org/10.1038/nm.3666.

Hendel, A. *et al.* (2015) 'Chemically modified guide RNAs enhance CRISPR-Cas genome editing in human primary cells', *Nature Biotechnology*, 33(9), pp. 985–989. Available at: https://doi.org/10.1038/nbt.3290.

Hendrikse, L.D. *et al.* (2022) 'Failure of human rhombic lip differentiation underlies medulloblastoma formation', *Nature*, 609(7929), pp. 1021–1028. Available at: https://doi.org/10.1038/s41586-022-05215-w.

Herculano-Houzel, S. (2009) 'The human brain in numbers: a linearly scaled-up primate brain', *Frontiers in Human Neuroscience*, 3(NOV), p. 31. Available at: https://doi.org/10.3389/neuro.09.031.2009.

Heyer, W.D., Ehmsen, K.T. and Liu, J. (2010) 'Regulation of homologous recombination in eukaryotes', *Annual Review of Genetics*. NIH Public Access, pp. 113–139. Available at: https://doi.org/10.1146/annurev-genet-051710-150955.

le Hir, H., Nott, A. and Moore, M.J. (2003) 'How introns influence and enhance eukaryotic gene expression', *Trends in Biochemical Sciences*, 28(4), pp. 215–220. Available at: https://doi.org/10.1016/S0968-0004(03)00052-5.

Hollway, G.E. *et al.* (2006) 'Scube2 mediates Hedgehog signalling in the zebrafish embryo', *Developmental Biology*, 294(1), pp. 104–118. Available at: https://doi.org/10.1016/j.ydbio.2006.02.032.

Hornung, V. and Latz, E. (2010) 'Intracellular DNA recognition', *Nature Reviews Immunology*. Nature Publishing Group, pp. 123–130. Available at: https://doi.org/10.1038/nri2690.

Hoshino, M. *et al.* (2005) 'Ptf1a, a bHLH transcriptional gene, defines GABAergic neuronal fates in cerebellum.', *Neuron*, 47(2), pp. 201–13. Available at: https://doi.org/10.1016/j.neuron.2005.06.007.

Hsu, P.D. *et al.* (2013) 'DNA targeting specificity of RNA-guided Cas9 nucleases', *Nature Biotechnology 2013 31:9*, 31(9), pp. 827–832. Available at: https://doi.org/10.1038/nbt.2647.

Huang, M. *et al.* (2019) 'Engineering Genetic Predisposition in Human Neuroepithelial Stem Cells Recapitulates Medulloblastoma Tumorigenesis.', *Cell stem cell*, 25(3), pp. 433-446.e7. Available at: https://doi.org/10.1016/j.stem.2019.05.013.

Huang, X. *et al.* (2010) 'Transventricular delivery of sonic hedgehog is essential to cerebellar ventricular zone development', *Proceedings of the National Academy of Sciences of the United States of America*, 107(18), pp. 8422–8427. Available at: https://doi.org/10.1073/pnas.0911838107.

Hui, C.C. and Angers, S. (2011) 'Gli proteins in development and disease', *Annual Review of Cell and Developmental Biology*, 27(1), pp. 513–537. Available at: https://doi.org/10.1146/annurev-cellbio-092910-154048.

Hynes, N.E. and MacDonald, G. (2009) 'ErbB receptors and signaling pathways in cancer', *Current Opinion in Cell Biology*. Elsevier Current Trends, pp. 177–184. Available at: https://doi.org/10.1016/j.ceb.2008.12.010.

Ikehara, H. *et al.* (2019) 'Establishment of a Gorlin syndrome model from induced neural progenitor cells exhibiting constitutive GLI1 expression and high sensitivity to inhibition by smoothened (SMO)', *Laboratory Investigation*, 100(4), pp. 657–664. Available at: https://doi.org/10.1038/s41374-019-0346-2.

Ikemoto, Y. *et al.* (2017) 'Somatic mosaicism containing double mutations in PTCH1 revealed by generation of induced pluripotent stem cells from nevoid basal cell carcinoma syndrome', *Journal of Medical Genetics*, 54(8), pp. 579–584. Available at: https://doi.org/10.1136/jmedgenet-2016-104490.

Ikemoto, Y. *et al.* (2020) 'Gorlin syndrome-induced pluripotent stem cells form medulloblastoma with loss of heterozygosity in PTCH1', *Aging*, 12(10), pp. 9935–9947. Available at: https://doi.org/10.18632/aging.103258.

Iliakis, G. *et al.* (2004) 'Mechanisms of DNA double strand break repair and chromosome aberration formation', in *Cytogenetic and Genome Research*. Karger Publishers, pp. 14–20. Available at: https://doi.org/10.1159/000077461.

Incardona, J.P. *et al.* (1998) 'The teratogenic Veratrum alkaloid cyclopamine inhibits Sonic hedgehog signal transduction', *Development*, 125(18), pp. 3553–3562. Available at: https://doi.org/10.1242/dev.125.18.3553.

Ingham, P.W. and McMahon, A.P. (2001) 'Hedgehog signaling in animal development: Paradigms and principles', *Genes and Development*. Cold Spring Harbor Laboratory Press, pp. 3059–3087. Available at: https://doi.org/10.1101/gad.938601.

Ishida, Y. *et al.* (2016) 'Vulnerability of Purkinje Cells Generated from Spinocerebellar Ataxia Type 6 Patient-Derived iPSCs', *Cell Reports*, 17(6), pp. 1482–1490. Available at: https://doi.org/10.1016/j.celrep.2016.10.026.

Ivanov, D.P. *et al.* (2015) 'In vitro co-culture model of medulloblastoma and human neural stem cells for drug delivery assessment', *Journal of Biotechnology*, 205, pp. 3–13. Available at: https://doi.org/10.1016/J.JBIOTEC.2015.01.002.

Ivanov, D.P. *et al.* (2016) 'In vitro models of medulloblastoma: Choosing the right tool for the job', *Journal of Biotechnology*. Elsevier, pp. 10–25. Available at: https://doi.org/10.1016/j.jbiotec.2016.07.028.

Izzi, L. *et al.* (2011) 'Boc and gas1 each form distinct shh receptor complexes with ptch1 and are required for shh-mediated cell proliferation', *Developmental Cell*, 20(6), pp. 788–801. Available at: https://doi.org/10.1016/j.devcel.2011.04.017.

Jacks, T. *et al.* (1992) 'Effects of an Rb mutation in the mouse', *Nature*, 359(6393), pp. 295–300. Available at: https://doi.org/10.1038/359295a0.

Jacks, T. *et al.* (1994) 'Tumor spectrum analysis in p53-mutant mice', *Current Biology*, 4(1), pp. 1–7. Available at: https://doi.org/10.1016/S0960-9822(00)00002-6.

Jacobsen, P.F., Jenkyn, D.J. and Papadimitriou, J.M. (1985) 'Establishment of a human medulloblastoma cell line and its heterotransplantation into nude mice', *Journal of Neuropathology and Experimental Neurology*, 44(5), pp. 472–485. Available at: https://doi.org/10.1097/00005072-198509000-00003.

Jenkins, D. (2009) 'Hedgehog signalling: Emerging evidence for non-canonical pathways', *Cellular Signalling*. Pergamon, pp. 1023–1034. Available at: https://doi.org/10.1016/j.cellsig.2009.01.033.

Jin, M.Z. and Jin, W.L. (2020) 'The updated landscape of tumor microenvironment and drug repurposing', *Signal Transduction and Targeted Therapy*. Nature Publishing Group, pp. 1–16. Available at: https://doi.org/10.1038/s41392-020-00280-x.

Jinek, M. *et al.* (2012) 'A programmable dual-RNA-guided DNA endonuclease in adaptive bacterial immunity', *Science*, 337(6096), pp. 816–821. Available at: https://doi.org/10.1126/science.1225829.

Johnson, R.L. *et al.* (1996) 'Human homolog of patched, a candidate gene for the basal cell nevus syndrome', *Science*, 272(5268), pp. 1668–1671. Available at: https://doi.org/10.1126/science.272.5268.1668.

Junying, Y. *et al.* (2009) 'Human induced pluripotent stem cells free of vector and transgene sequences', *Science*, 324(5928), pp. 797–801. Available at: https://doi.org/10.1126/science.1172482.

Juraschka, K. and Taylor, M.D. (2019) 'Medulloblastoma in the age of molecular subgroups: A review: JNSPG 75th Anniversary invited review article', *Journal of Neurosurgery: Pediatrics*, 24(4), pp. 353–363. Available at: https://doi.org/10.3171/2019.5.PEDS18381.

Kang, H.J. *et al.* (2015) 'CCR5 disruption in induced pluripotent stem cells using CRISPR/Cas9 provides selective resistance of immune cells to CCR5-tropic HIV-1 virus', *Molecular Therapy - Nucleic Acids*, 4(12), p. e268. Available at: https://doi.org/10.1038/mtna.2015.42.

Kato, K. (1990) 'Novel GABAA receptor α subunit is expressed only in cerebellar granule cells', *Journal of Molecular Biology*, 214(3), pp. 619–624. Available at: https://doi.org/10.1016/0022-2836(90)90276-R.

Kato, S. *et al.* (1999) 'Monoclonal antibody to human midkine reveals increased midkine expression in human brain tumors', *Journal of Neuropathology and Experimental Neurology*, 58(5), pp. 430–441. Available at: https://doi.org/10.1097/00005072-199905000-00002.

Katoh, Y. and Katoh, M. (2008) 'Hedgehog signaling, epithelial-to-mesenchymal transition and miRNA (review)', *International Journal of Molecular Medicine*. Spandidos Publications, pp. 271–275. Available at: https://doi.org/10.3892/ijmm_00000019.

Kenney, A.M., Cole, M.D. and Rowitch, D.H. (2003) 'Nmyc upregulation by sonic hedgehog signaling promotes proliferation in developing cerebellar granule neuron precursors', *Development*, 130(1), pp. 15–28. Available at: https://doi.org/10.1242/DEV.00182.

Khaliullina, H. *et al.* (2009) 'Patched regulates Smoothened trafficking using lipoprotein-derived lipids', *Development*, 136(24), pp. 4111–4121. Available at: https://doi.org/10.1242/dev.041392.

Kieran, M.W. *et al.* (2017) 'Phase i study of oral sonidegib (LDE225) in pediatric brain and solid tumors and a phase II study in children and adults with relapsed medulloblastoma', *Neuro-Oncology*, 19(11), pp. 1542–1552. Available at: https://doi.org/10.1093/neuonc/nox109.

Kilander, M.B.C. *et al.* (2018) 'A rare human CEP290 variant disrupts the molecular integrity of the primary cilium and impairs Sonic Hedgehog machinery', *Scientific Reports*, 8(1), pp. 1–14. Available at: https://doi.org/10.1038/s41598-018-35614-x.

Kim, D. *et al.* (2009) 'Generation of Human Induced Pluripotent Stem Cells by Direct Delivery of Reprogramming Proteins', *Cell Stem Cell*. NIH Public Access, pp. 472–476. Available at: https://doi.org/10.1016/j.stem.2009.05.005.

Kim, K. *et al.* (2010) 'Epigenetic memory in induced pluripotent stem cells', *Nature 2010 467:7313*, 467(7313), pp. 285–290. Available at: https://doi.org/10.1038/nature09342.

Kim, K. *et al.* (2011) 'Donor cell type can influence the epigenome and differentiation potential of human induced pluripotent stem cells', *Nature Biotechnology 2011 29:12*, 29(12), pp. 1117–1119. Available at: https://doi.org/10.1038/nbt.2052.

Kim, S. *et al.* (2014) 'Highly efficient RNA-guided genome editing in human cells via delivery of purified Cas9 ribonucleoproteins', *Genome Research*, 24(6), pp. 1012–1019. Available at: https://doi.org/10.1101/gr.171322.113.

Kimberland, M.L. *et al.* (2018) 'Strategies for controlling CRISPR/Cas9 off-target effects and biological variations in mammalian genome editing experiments', *Journal of Biotechnology*. Elsevier, pp. 91–101. Available at: https://doi.org/10.1016/j.jbiotec.2018.08.007.

Kinzler, K.W. *et al.* (1987) 'Identification of an amplified, highly expressed gene in a human glioma', *Science*, 236(4797), pp. 70–73. Available at: https://doi.org/10.1126/science.3563490.

Kiprilov, E.N. *et al.* (2008) 'Human embryonic stem cells in culture possess primary cilia with hedgehog signaling machinery', *Journal of Cell Biology*, 180(5), pp. 897–904. Available at: https://doi.org/10.1083/jcb.200706028.

Kise, Y. *et al.* (2009) 'Sufu recruits GSK3β for efficient processing of Gli3', *Biochemical and Biophysical Research Communications*, 387(3), pp. 569–574. Available at: https://doi.org/10.1016/j.bbrc.2009.07.087.

Klein, R.S. *et al.* (2001) 'SDF-1α induces chemotaxis and enhances Sonic hedgehog-induced proliferation of cerebellar granule cells', *Development*, 128(11), pp. 1971–1981. Available at: https://doi.org/10.1242/DEV.128.11.1971.

Knoepfler, P.S., Cheng, P.F. and Eisenman, R.N. (2002) 'N-myc is essential during neurogenesis for the rapid expansion of progenitor cell populations and the inhibition of neuronal differentiation', *Genes & Development*, 16(20), p. 2699. Available at: https://doi.org/10.1101/GAD.1021202.

Kogerman, P. *et al.* (2002) 'Alternative first exons of PTCH1 are differentially regulated in vivo and may confer different functions to the PTCH1 protein', *Oncogene*, 21(39), pp. 6007–6016. Available at: https://doi.org/10.1038/sj.onc.1205865.

Kool, M. *et al.* (2008) 'Integrated genomics identifies five medulloblastoma subtypes with distinct genetic profiles, pathway signatures and clinicopathological features', *PLoS ONE*, 3(8). Available at: https://doi.org/10.1371/journal.pone.0003088.

Kool, M. *et al.* (2014) 'Genome sequencing of SHH medulloblastoma predicts genotype-related response to smoothened inhibition', *Cancer Cell*, 25(3), pp. 393–405. Available at: https://doi.org/10.1016/j.ccr.2014.02.004.

Koyabu, Y. *et al.* (2001) 'Physical and Functional Interactions between Zic and Gli Proteins', *Journal of Biological Chemistry*, 276(10), pp. 6889–6892. Available at: https://doi.org/10.1074/jbc.C000773200.

Krawczak, M., Reiss, J. and Cooper, D.N. (1992) 'The mutational spectrum of single base-pair substitutions in mRNA splice junctions of human genes: Causes and consequences', *Human Genetics*, 90(1–2), pp. 41–54. Available at: https://doi.org/10.1007/BF00210743.

Krook, M.A. *et al.* (2021) 'Fibroblast growth factor receptors in cancer: genetic alterations, diagnostics, therapeutic targets and mechanisms of resistance', *British Journal of Cancer*. Nature Publishing Group, pp. 880–892. Available at: https://doi.org/10.1038/s41416-020-01157-0.

Kurosaki, T., Popp, M.W. and Maquat, L.E. (2019) 'Quality and quantity control of gene expression by nonsense-mediated mRNA decay', *Nature Reviews Molecular Cell Biology 2019 20:7*, 20(7), pp. 406–420. Available at: https://doi.org/10.1038/s41580-019-0126-2.

Kutscher, L.M. *et al.* (2020) 'Functional loss of a noncanonical BCOR-PRC1.1 complex accelerates SHH-driven medulloblastoma formation.', *Genes & development*, 34(17–18), pp. 1161–1176. Available at: https://doi.org/10.1101/gad.337584.120.

Laaroubi, K. *et al.* (1995) 'Biochemical and mitogenic properties of the heparin-binding growth factor HARP', *Progress in Growth Factor Research*, 6(1), pp. 25–34. Available at: https://doi.org/10.1016/0955-2235(95)00002-X.

Lackner, D.H. *et al.* (2015) 'A generic strategy for CRISPR-Cas9-mediated gene tagging', *Nature Communications*, 6(1), pp. 1–7. Available at: https://doi.org/10.1038/ncomms10237.

Lacombe, D. *et al.* (1990) 'Medulloblastoma in the nevoid basal-cell carcinoma syndrome: Case reports and review of the literature', *Genetic Counseling*, 1(3–4), pp.

273–277. Available at: http://www.ncbi.nlm.nih.gov/pubmed/2098052 (Accessed: 1 October 2022).

Lancaster, M.A. *et al.* (2011) 'Defective Wnt-dependent cerebellar midline fusion in a mouse model of Joubert syndrome', *Nature Medicine*, 17(6), pp. 726–731. Available at: https://doi.org/10.1038/nm.2380.

Langfelder, P. and Horvath, S. (2008) 'WGCNA: An R package for weighted correlation network analysis', *BMC Bioinformatics*, 9(1), pp. 1–13. Available at: https://doi.org/10.1186/1471-2105-9-559.

Lasko, D., Cavenee, W. and Nordenskjöld, M. (1991) 'Loss of constitutional heterozygosity in human cancer', *Annual Review of Genetics*. Annual Reviews 4139 El Camino Way, P.O. Box 10139, Palo Alto, CA 94303-0139, USA, pp. 281–314. Available at: https://doi.org/10.1146/annurev.ge.25.120191.001433.

Lee, C.S., May, N.R. and Fan, C.M. (2001) 'Growth arrest specific gene 1 is a positive growth regulator for the cerebellum', *Developmental Biology*, 236(1), pp. 30–45. Available at: https://doi.org/10.1006/dbio.2000.0146.

Lee, J. *et al.* (1997) 'Gli1 is a target of Sonic hedgehog that induces ventral neural tube development', *Development*, 124(13), pp. 2537–2552. Available at: https://doi.org/10.1242/dev.124.13.2537.

Lee, K.J. and Jessell, T.M. (1999) 'The specification of dorsal cell fates in the vertebrate central nervous system.', *Annual review of neuroscience*, 22, pp. 261–94. Available at: https://doi.org/10.1146/annurev.neuro.22.1.261.

Lee, Y. *et al.* (2003) 'A molecular fingerprint for medulloblastoma', *Cancer Research*, 63(17), pp. 5428–5437. Available at: http://www.ncbi.nlm.nih.gov/pubmed/14500378 (Accessed: 3 October 2022).

Lee, Y. *et al.* (2006) 'Patched2 modulates tumorigenesis in Patched1 heterozygous mice', *Cancer Research*, 66(14), pp. 6964–71. Available at: https://doi.org/10.1158/0008-5472.CAN-06-0505.

Lee, Y. *et al.* (2007) 'Loss of suppressor-of-fused function promotes tumorigenesis', *Oncogene*, 26(44), pp. 6442–6447. Available at: https://doi.org/10.1038/sj.onc.1210467.

Lek, M. *et al.* (2010) 'A homeodomain feedback circuit underlies step-function interpretation of a Shh morphogen gradient during ventral neural patterning', *Development*, 137(23), pp. 4051–4060. Available at: https://doi.org/10.1242/dev.054288.

Leto, K. *et al.* (2009) 'Laminar Fate and Phenotype Specification of Cerebellar GABAergic Interneurons', *Journal of Neuroscience*, 29(21), pp. 7079–7091. Available at: https://doi.org/10.1523/JNEUROSCI.0957-09.2009.

Leto, K. *et al.* (2016) 'Consensus Paper: Cerebellar Development', *The Cerebellum*, 15(6), pp. 789–828. Available at: https://doi.org/10.1007/s12311-015-0724-2.

Li, J.Y.H. and Joyner, A.L. (2001) 'Otx2 and Gbx2 are required for refinement and not induction of mid-hindbrain gene expression', *Development*, 128(24), pp. 4979–4991. Available at: https://doi.org/10.1242/DEV.128.24.4979.

Li, P. *et al.* (2013) 'A population of Nestin-expressing progenitors in the cerebellum exhibits increased tumorigenicity', *Nature Neuroscience*, 16(12), pp. 1737–1744. Available at: https://doi.org/10.1038/nn.3553.

Li, P. *et al.* (2016) 'Nestin mediates hedgehog pathway tumorigenesis', *Cancer Research*, 76(18), pp. 5573–5583. Available at: https://doi.org/10.1158/0008-5472.CAN-16-1547/652530/AM/NESTIN-MEDIATES-HEDGEHOG-PATHWAY.

Liang, F. *et al.* (1998) 'Homology-directed repair is a major double-strand break repair pathway in mammalian cells', *Proceedings of the National Academy of Sciences of the United States of America*, 95(9), pp. 5172–5177. Available at: https://doi.org/10.1073/pnas.95.9.5172.

Liang, Y. *et al.* (2008) 'Type I collagen is overexpressed in medulloblastoma as a component of tumor microenvironment', *Journal of Neuro-Oncology*, 86(2), pp. 133–141. Available at: https://doi.org/10.1007/s11060-007-9457-5.

Lim, L.S. *et al.* (2007) 'Zic3 is required for maintenance of pluripotency in embryonic stem cells', *Molecular Biology of the Cell*, 18(4), pp. 1348–1358. Available at: https://doi.org/10.1091/mbc.E06-07-0624.

Limperopoulos, C. *et al.* (2005) 'Late Gestation Cerebellar Growth Is Rapid and Impeded by Premature Birth', *Pediatrics*, 115(3), pp. 688–695. Available at: https://doi.org/10.1542/PEDS.2004-1169.

Lin, Z. *et al.* (2016) 'Suppression of GLI sensitizes medulloblastoma cells to mitochondria-mediated apoptosis', *Journal of Cancer Research and Clinical Oncology*, 142(12), pp. 2469–2478. Available at: https://doi.org/10.1007/s00432-016-2241-1.

Linke, F. *et al.* (2021) '3D hydrogels reveal medulloblastoma subgroup differences and identify extracellular matrix subtypes that predict patient outcome', *Journal of Pathology*, 253(3), pp. 326–338. Available at: https://doi.org/10.1002/path.5591.

Linkous, A. *et al.* (2019) 'Modeling Patient-Derived Glioblastoma with Cerebral Organoids', *Cell Reports*, 26(12), pp. 3203-3211.e5. Available at: https://doi.org/10.1016/J.CELREP.2019.02.063.

Liu, A. and Joyner, A.L. (2001) 'Early anterior/posterior patterning of the midbrain and cerebellum', *Annual Review of Neuroscience*, 24, pp. 869–896. Available at: https://doi.org/10.1146/annurev.neuro.24.1.869.

Liu, A. and Niswander, L.A. (2005) 'Bone morphogenetic protein signalling and vertebrate nervous system development', *Nature Reviews Neuroscience*. Nature Publishing Group, pp. 945–954. Available at: https://doi.org/10.1038/nrn1805.

Liu, F. *et al.* (2019) 'CDK7 inhibition suppresses aberrant hedgehog pathway and overcomes resistance to smoothened antagonists', *Proceedings of the National Academy of Sciences of the United States of America*, 116(26), pp. 12986–12995. Available at: https://doi.org/10.1073/pnas.1815780116.

Liu, H. *et al.* (2020) 'Necroptotic astrocytes contribute to maintaining stemness of disseminated medulloblastoma through CCL2 secretion', *Neuro-Oncology*, 22(5), pp. 625–638. Available at: https://doi.org/10.1093/neuonc/noz214.

Liu, S. *et al.* (2006) 'Hedgehog signaling and Bmi-1 regulate self-renewal of normal and malignant human mammary stem cells', *Cancer Research*, 66(12), pp. 6063–6071. Available at: https://doi.org/10.1158/0008-5472.CAN-06-0054.

Liu, Y. *et al.* (2017) 'Astrocytes promote medulloblastoma progression through hedgehog secretion', *Cancer Research*, 77(23), pp. 6692–6703. Available at: https://doi.org/10.1158/0008-5472.CAN-17-1463/657801/AM/ASTROCYTES-PROMOTE-MEDULLOBLASTOMA-PROGRESSION.

Liu, Z. *et al.* (2016) 'Efficient CRISPR/Cas9-Mediated Versatile, Predictable, and Donor-Free Gene Knockout in Human Pluripotent Stem Cells', *Stem Cell Reports*, 7(3), pp. 496–507. Available at: https://doi.org/10.1016/j.stemcr.2016.07.021.

Lord, J. *et al.* (2019) 'Pathogenicity and selective constraint on variation near splice sites', *Genome Research*, 29(2), pp. 159–170. Available at: https://doi.org/10.1101/gr.238444.118.

Lou, E., Nelson, A.C. and Kool, M. (2019) 'Differential response of SHH-expressing adult medulloblastomas to the sonic hedgehog inhibitor vismodegib: whole-genome analysis', *Cancer Biology and Therapy*, 20(11), pp. 1398–1402. Available at: https://doi.org/10.1080/15384047.2019.1647057.

Love, M.I., Huber, W. and Anders, S. (2014) 'Moderated estimation of fold change and dispersion for RNA-seq data with DESeq2', *Genome Biology*, 15(12), pp. 1–21. Available at: https://doi.org/10.1186/s13059-014-0550-8.

Machold, R. *et al.* (2003) 'Sonic hedgehog is required for progenitor cell maintenance in telencephalic stem cell niches', *Neuron*, 39(6), pp. 937–950. Available at: https://doi.org/10.1016/S0896-6273(03)00561-0.

MacHold, R. and Fishell, G. (2005) 'Math1 is expressed in temporally discrete pools of cerebellar rhombic-lip neural progenitors.', *Neuron*, 48(1), pp. 17–24. Available at: https://doi.org/10.1016/j.neuron.2005.08.028.

Malhotra, A. *et al.* (2016) 'Sonic hedgehog signaling drives mitochondrial fragmentation by suppressing mitofusins in cerebellar granule neuron precursors and medulloblastoma', *Molecular Cancer Research*, 14(1), pp. 114–124. Available at: https://doi.org/10.1158/1541-7786.MCR-15-0278.

Mali, P. *et al.* (2013) 'RNA-guided human genome engineering via Cas9', *Science*, 339(6121), pp. 823–826. Available at: https://doi.org/10.1126/science.1232033.

Malkova, A. and Haber, J.E. (2012) 'Mutations arising during repair of chromosome breaks', *Annual Review of Genetics*. Annual Reviews, pp. 455–473. Available at: https://doi.org/10.1146/annurev-genet-110711-155547.

Mandal, P.K. *et al.* (2014) 'Efficient ablation of genes in human hematopoietic stem and effector cells using CRISPR/Cas9', *Cell Stem Cell*, 15(5), pp. 643–652. Available at: https://doi.org/10.1016/j.stem.2014.10.004.

Maricich, S.M. and Herrup, K. (1999) 'Pax-2 Expression Defines a Subset of GABAergic Interneurons and Their Precursors in the Developing Murine Cerebellum', *J Neurobiol*, 41, pp. 281–294. Available at: https://doi.org/10.1002/(SICI)1097-4695(19991105)41:2.

Marigo, V. *et al.* (1996) 'Biochemical evidence that patched is the hedgehog receptor', *Nature*, 384(6605), pp. 176–179. Available at: https://doi.org/10.1038/384176a0.

Martelli, C. *et al.* (2016) 'Top-down proteomic characterization of DAOY medulloblastoma tumor cell line', *EuPA Open Proteomics*, 12, pp. 13–21. Available at: https://doi.org/10.1016/j.euprot.2016.03.015.

Marti, E. *et al.* (1995) 'Requirement of 19K form of Sonic hedgehog for induction of distinct ventral cell types in CNS explants', *Nature*, 375(6529), pp. 322–325. Available at: https://doi.org/10.1038/375322a0.

Martí, E. and Bovolenta, P. (2002) 'Sonic hedgehog in CNS development: One signal, multiple outputs', *Trends in Neurosciences*. Elsevier Current Trends, pp. 89–96. Available at: https://doi.org/10.1016/S0166-2236(02)02062-3.

McMahon, A.P. and Bradley, A. (1990) 'The Wnt-1 (int-1) proto-oncogene is required for development of a large region of the mouse brain', *Cell*, 62(6), pp. 1073–1085. Available at: https://doi.org/10.1016/0092-8674(90)90385-R.

von Mering, C. and Basler, K. (1999) 'Distinct and regulated activities of human Gli proteins in Drosophila', *Current Biology*, 9(22), pp. 1319–1322. Available at: https://doi.org/10.1016/S0960-9822(00)80054-8.

di Micco, R. *et al.* (2006) 'Oncogene-induced senescence is a DNA damage response triggered by DNA hyper-replication', *Nature*, 444(7119), pp. 638–642. Available at: https://doi.org/10.1038/nature05327.

Mille, F. *et al.* (2014) 'The Shh receptor Boc promotes progression of early medulloblastoma to advanced tumors', *Developmental Cell*, 31(1), pp. 34–47. Available at: https://doi.org/10.1016/j.devcel.2014.08.010.

Miller, J.A. *et al.* (2014) 'Transcriptional landscape of the prenatal human brain', *Nature*, 508(7495), pp. 199–206. Available at: https://doi.org/10.1038/nature13185.

Millet, S. *et al.* (1996) 'The caudal limit of Otx2 gene expression as a marker of the midbrain/hindbrain boundary: a study using in situ hybridisation and chick/quail homotopic grafts.', *Development (Cambridge, England)*, 122(12), pp. 3785–97. Available at: https://doi.org/10.1242/dev.122.12.3785.

Miyata, T., Maeda, T. and Lee, J.E. (1999) 'NeuroD is required for differentiation of the granule cells in the cerebellum and hippocampus', *Genes and Development*, 13(13), pp. 1647–1652. Available at: https://doi.org/10.1101/gad.13.13.1647.

Mizugishi, K. *et al.* (2001) 'Molecular properties of Zic proteins as transcriptional regulators and their relationship to GLI proteins', *Journal of Biological Chemistry*, 276(3), pp. 2180–2188. Available at: https://doi.org/10.1074/jbc.M004430200.

Mizuhara, E. *et al.* (2010) 'Purkinje cells originate from cerebellar ventricular zone progenitors positive for Neph3 and E-cadherin', *Developmental Biology*, 338(2), pp. 202–214. Available at: https://doi.org/10.1016/J.YDBIO.2009.11.032.

Mizuseki, K. *et al.* (2003) 'Generation of neural crest-derived peripheral neurons and floor plate cells from mouse and primate embryonic stem cells', *Proceedings of the National Academy of Sciences of the United States of America*, 100(10), pp. 5828–5833. Available at: https://doi.org/10.1073/PNAS.1037282100.

Mugnaini, E., Sekerková, G. and Martina, M. (2011) 'The unipolar brush cell: A remarkable neuron finally receiving deserved attention', *Brain Research Reviews*. Elsevier, pp. 220–245. Available at: https://doi.org/10.1016/j.brainresrev.2010.10.001.

Muguruma, K. *et al.* (2015) 'Self-organization of polarized cerebellar tissue in 3D culture of human pluripotent stem cells', *Cell Reports*, 10(4), pp. 537–550. Available at: https://doi.org/10.1016/j.celrep.2014.12.051.

Muguruma, K. (2018) 'Self-Organized Cerebellar Tissue from Human Pluripotent Stem Cells and Disease Modeling with Patient-Derived iPSCs', *Cerebellum*. Springer New York LLC, pp. 37–41. Available at: https://doi.org/10.1007/s12311-017-0905-2.

Mukhopadhyay, M. *et al.* (2001) 'Dickkopf1 Is Required for Embryonic Head Induction and Limb Morphogenesis in the Mouse', *Developmental Cell*, 1(3), pp. 423–434. Available at: https://doi.org/10.1016/S1534-5807(01)00041-7.

Muñoz-López, M. and García-Pérez, J.L. (2010) 'DNA Transposons: Nature and Applications in Genomics', *Current Genomics*, 11(2), p. 115. Available at: https://doi.org/10.2174/138920210790886871.

Nachtergaele, S. *et al.* (2012) 'Oxysterols are allosteric activators of the oncoprotein Smoothened', *Nature Chemical Biology*, 8(2), pp. 211–220. Available at: https://doi.org/10.1038/nchembio.765.

Nagai, T. *et al.* (2002) 'A variant of yellow fluorescent protein with fast and efficient maturation for cell-biological applications', *Nature Biotechnology*, 20(1), pp. 87–90. Available at: https://doi.org/10.1038/nbt0102-87.

Nagao, K. *et al.* (2022) 'PTCH1-null induced pluripotent stem cells exclusively differentiate into immature ectodermal cells with large areas of medulloblastoma-like tissue', *Discover Oncology*, 13(1), pp. 1–12. Available at: https://doi.org/10.1007/s12672-022-00498-x.

Nathwani, B.B. *et al.* (2014) 'Morphological differences of primary cilia between human induced pluripotent stem cells and their parental somatic cells', *Stem Cells and Development*, 23(2), pp. 115–123. Available at: https://doi.org/10.1089/SCD.2013.0162.

Nayler, S. *et al.* (2021) 'High-resolution transcriptional landscape of xeno-free human induced pluripotent stem cell-derived cerebellar organoids', *Scientific Reports*, 11(1), pp. 1–17. Available at: https://doi.org/10.1038/s41598-021-91846-4.

Neglia, J.P. *et al.* (2001) 'Second malignant neoplasms in five-year survivors of childhood cancer: Childhood cancer survivor study', *Journal of the National Cancer Institute*, 93(8), pp. 618–629. Available at: https://doi.org/10.1093/jnci/93.8.618.

Neve, A. *et al.* (2017) 'Investigation of brain tissue infiltration by medulloblastoma cells in an ex vivo model', *Scientific Reports*, 7(1), pp. 1–12. Available at: https://doi.org/10.1038/s41598-017-05573-w.

Niesen, J. *et al.* (2020) 'Pik3ca mutations significantly enhance the growth of SHH medulloblastoma and lead to metastatic tumour growth in a novel mouse model',

Cancer Letters, 477, pp. 10–18. Available at: https://doi.org/10.1016/j.canlet.2020.02.028.

Niewiadomski, P. *et al.* (2014) 'Gli protein activity is controlled by multisite phosphorylation in vertebrate hedgehog signaling', *Cell Reports*, 6(1), pp. 168–181. Available at: https://doi.org/10.1016/j.celrep.2013.12.003.

Niewiadomski, P. *et al.* (2019) 'Gli proteins: Regulation in development and cancer', *Cells*. Multidisciplinary Digital Publishing Institute (MDPI). Available at: https://doi.org/10.3390/cells8020147.

Nihongaki, Y. *et al.* (2015) 'Photoactivatable CRISPR-Cas9 for optogenetic genome editing', *Nature Biotechnology 2015 33:7*, 33(7), pp. 755–760. Available at: https://doi.org/10.1038/nbt.3245.

Nishimura, K. *et al.* (2011) 'Development of defective and persistent Sendai virus vector: A unique gene delivery/expression system ideal for cell reprogramming', *Journal of Biological Chemistry*, 286(6), pp. 4760–4771. Available at: https://doi.org/10.1074/jbc.M110.183780.

Nishimura, K. *et al.* (2017) 'Simple and effective generation of transgene-free induced pluripotent stem cells using an auto-erasable Sendai virus vector responding to microRNA-302', *Stem Cell Research*, 23, pp. 13–19. Available at: https://doi.org/10.1016/j.scr.2017.06.011.

Nishino, K. *et al.* (2011) 'DNA Methylation Dynamics in Human Induced Pluripotent Stem Cells over Time', *PLOS Genetics*, 7(5), p. e1002085. Available at: https://doi.org/10.1371/JOURNAL.PGEN.1002085.

Northcott, P.A. *et al.* (2011) 'Medulloblastoma comprises four distinct molecular variants', *Journal of Clinical Oncology*, 29(11), pp. 1408–1414. Available at: https://doi.org/10.1200/JCO.2009.27.4324.

Northcott, P.A. *et al.* (2012) 'Subgroup-specific structural variation across 1,000 medulloblastoma genomes', *Nature 2012 488:7409*, 488(7409), pp. 49–56. Available at: https://doi.org/10.1038/nature11327.

Northcott, P.A. *et al.* (2017) 'The whole-genome landscape of medulloblastoma subtypes', *Nature*, 547(7663), pp. 311–317. Available at: https://doi.org/10.1038/nature22973.

Northcott, P.A. *et al.* (2019) 'Medulloblastoma', *Nature Reviews Disease Primers*, 5(1). Available at: https://doi.org/10.1038/s41572-019-0063-6.

Nozawa, Y.I., Lin, C. and Chuang, P.T. (2013) 'Hedgehog signaling from the primary cilium to the nucleus: An emerging picture of ciliary localization, trafficking and

transduction', *Current Opinion in Genetics and Development*. Elsevier Current Trends, pp. 429–437. Available at: https://doi.org/10.1016/j.gde.2013.04.008.

Nüsslein-Volhard, C. and Wieschaus, E. (1980) 'Mutations affecting segment number and polarity in Drosophila', *Nature*, 287(5785), pp. 795–801. Available at: https://doi.org/10.1038/287795a0.

O'Connor, S.A. *et al.* (2021) 'Neural G0: a quiescent-like state found in neuroepithelial-derived cells and glioma', *Molecular Systems Biology*, 17(6), p. 9522. Available at: https://doi.org/10.15252/msb.20209522.

Ogawa, J. *et al.* (2018) 'Glioblastoma Model Using Human Cerebral Organoids', *Cell Reports*, 23(4), pp. 1220–1229. Available at: https://doi.org/10.1016/j.celrep.2018.03.105.

Ogura, T. *et al.* (2018) 'Three-dimensional induction of dorsal, intermediate and ventral spinal cord tissues from human pluripotent stem cells', *Development (Cambridge)*, 145(16 Special Issue). Available at: https://doi.org/10.1242/dev.162214.

Okamoto, N. *et al.* (2014) 'A novel PTCH1 mutation in a patient with Gorlin syndrome', *Human Genome Variation*, 1(1), pp. 1–3. Available at: https://doi.org/10.1038/hgv.2014.22.

Okita, K. *et al.* (2008) 'Generation of mouse induced pluripotent stem cells without viral vectors', *Science*, 322(5903), pp. 949–953. Available at: https://doi.org/10.1126/science.1164270.

Okita, K. *et al.* (2011) 'A more efficient method to generate integration-free human iPS cells', *Nature Methods*, 8(5), pp. 409–412. Available at: https://doi.org/10.1038/nmeth.1591.

Oliver, T.G. *et al.* (2005) 'Loss of patched and disruption of granule cell development in a pre-neoplastic stage of medulloblastoma', *Development*, 132(10), pp. 2425–2439. Available at: https://doi.org/10.1242/dev.01793.

Ostrom, Q.T. *et al.* (2018) 'CBTRUS statistical report: Primary brain and other central nervous system tumors diagnosed in the United States in 2011-2015', *Neuro-Oncology*. Oxford Academic, pp. iv1–iv86. Available at: https://doi.org/10.1093/neuonc/noy131.

Owa, T. *et al.* (2018) 'Meis1 coordinates cerebellar granule cell development by regulating pax6 transcription, BMP signaling and atoh1 degradation', *Journal of Neuroscience*, 38(5), pp. 1277–1294. Available at: https://doi.org/10.1523/JNEUROSCI.1545-17.2017.

Pan, N. *et al.* (2009) 'Defects in the cerebella of conditional Neurod1 null mice correlate with effective Tg(Atoh1-cre) recombination and granule cell requirements for Neurod1 for differentiation', *Cell and Tissue Research*, 337(3), pp. 407–428. Available at: https://doi.org/10.1007/S00441-009-0826-6/FIGURES/14.

Pan, S. *et al.* (2010) 'Discovery of NVP-LDE225, a potent and selective smoothened antagonist', *ACS Medicinal Chemistry Letters*, 1(3), pp. 130–134. Available at: https://doi.org/10.1021/ml1000307.

Pan, Y., Wang, C. and Wang, B. (2009) 'Phosphorylation of Gli2 by protein kinase A is required for Gli2 processing and degradation and the Sonic Hedgehog-regulated mouse development', *Developmental Biology*, 326(1), pp. 177–189. Available at: https://doi.org/10.1016/j.ydbio.2008.11.009.

Park, H.L. *et al.* (2000) 'Mouse Gli1 mutants are viable but have defects in SHH signaling in combination with a Gli2 mutation', *Development*, 127(8), pp. 1593–1605. Available at: https://doi.org/10.1242/dev.127.8.1593.

Park, S.H. *et al.* (2008) 'Galectin-3: A useful biomarker for differential diagnosis of brain tumors', *Neuropathology*, 28(5), pp. 497–506. Available at: https://doi.org/10.1111/j.1440-1789.2008.00909.x.

Pascual, M. *et al.* (2007) 'Cerebellar GABAergic progenitors adopt an external granule cell-like phenotype in the absence of Ptf1a transcription factor expression', *Proceedings of the National Academy of Sciences*, 104(12), pp. 5193–5198. Available at: https://doi.org/10.1073/pnas.0605699104.

Pattanayak, V. *et al.* (2013) 'High-throughput profiling of off-target DNA cleavage reveals RNA-programmed Cas9 nuclease specificity', *Nature Biotechnology*, 31(9), pp. 839–843. Available at: https://doi.org/10.1038/nbt.2673.

Patten, I. and Placzek, M. (2000) 'The role of sonic hedgehog in neural tube patterning', *Cellular and Molecular Life Sciences*. Springer, pp. 1695–1708. Available at: https://doi.org/10.1007/PL00000652.

Pepinsky, R.B. *et al.* (1998) 'Identification of a palmitic acid-modified form of human Sonic hedgehog', *Journal of Biological Chemistry*, 273(22), pp. 14037–14045. Available at: https://doi.org/10.1074/jbc.273.22.14037.

Pera, E.M. *et al.* (2001) 'Neural and Head Induction by Insulin-like Growth Factor Signals', *Developmental Cell*, 1(5), pp. 655–665. Available at: https://doi.org/10.1016/S1534-5807(01)00069-7.

Perla, A. *et al.* (2020) 'Histone Deacetylase Inhibitors in Pediatric Brain Cancers: Biological Activities and Therapeutic Potential', *Frontiers in Cell and Developmental Biology*. Frontiers Media S.A., p. 546. Available at: https://doi.org/10.3389/fcell.2020.00546.

Persson, M. *et al.* (2002) 'Dorsal-ventral patterning of the spinal cord requires Gli3 transcriptional repressor activity', *Genes and Development*, 16(22), pp. 2865–2878. Available at: https://doi.org/10.1101/gad.243402.

Petralia, F. *et al.* (2020) 'Integrated Proteogenomic Characterization across Major Histological Types of Pediatric Brain Cancer', *Cell*, 183(7), pp. 1962-1985.e31. Available at: https://doi.org/10.1016/j.cell.2020.10.044.

Phoenix, T.N. *et al.* (2016) 'Medulloblastoma genotype dictates blood brain barrier phenotype', *Cancer cell*, 29(4), p. 508. Available at: https://doi.org/10.1016/J.CCELL.2016.03.002.

Pola, R. *et al.* (2001) 'The morphogen Sonic hedgehog is an indirect angiogenic agent upregulating two families of angiogenic growth factors', *Nature Medicine 2001 7:6*, 7(6), pp. 706–711. Available at: https://doi.org/10.1038/89083.

Polizio, A.H. *et al.* (2011) 'Heterotrimeric Gi proteins link hedgehog signaling to activation of Rho small GTPases to promote fibroblast migration', *Journal of Biological Chemistry*, 286(22), pp. 19589–19596. Available at: https://doi.org/10.1074/jbc.M110.197111.

Porter, J.A., Young, K.E. and Beachy, P.A. (1996) 'Cholesterol modification of hedgehog signaling proteins in animal development', *Science*, 274(5285), pp. 255–259. Available at: https://doi.org/10.1126/science.274.5285.255.

Purzner, T. *et al.* (2018) 'Developmental phosphoproteomics identifies the kinase CK2 as a driver of Hedgehog signaling and a therapeutic target in medulloblastoma', *Science Signaling*, 11(547), p. 5147. Available at: https://doi.org/10.1126/scisignal.aau5147.

Qi, C. *et al.* (2019) 'Structural basis of sterol recognition by human hedgehog receptor PTCH1', *Science Advances*, 5(9). Available at: https://doi.org/10.1126/SCIADV.AAW6490/SUPPL_FILE/AAW6490_SM.PDF.

Qi, X. *et al.* (2018) 'Structures of human Patched and its complex with native palmitoylated sonic hedgehog', *Nature*, 560(7716), pp. 128–132. Available at: https://doi.org/10.1038/s41586-018-0308-7.

Qi, X. and Li, X. (2020) 'Mechanistic insights into the generation and transduction of Hedgehog Signaling', *Trends in biochemical sciences*, 45(5), p. 397. Available at: https://doi.org/10.1016/J.TIBS.2020.01.006.

Quail, D.F. and Joyce, J.A. (2017) 'The Microenvironmental Landscape of Brain Tumors', *Cancer Cell*, 31(3), pp. 326–341. Available at: https://doi.org/10.1016/J.CCELL.2017.02.009.

Rahimi-Balaei, M. *et al.* (2018) 'Neuronal migration during development of the cerebellum', *Frontiers in Cellular Neuroscience*. Frontiers Media S.A., p. 484. Available at: https://doi.org/10.3389/fncel.2018.00484.

Ramaswamy, V. *et al.* (2016) 'Risk stratification of childhood medulloblastoma in the molecular era: the current consensus', *Acta Neuropathologica*, 131(6), pp. 821–831. Available at: https://doi.org/10.1007/s00401-016-1569-6.

Rausch, T. *et al.* (2012) 'Genome Sequencing of Pediatric Medulloblastoma Links Catastrophic DNA Rearrangements with TP53 Mutations', *Cell*, 148(1–2), pp. 59–71. Available at: https://doi.org/10.1016/J.CELL.2011.12.013.

Reifenberger, J. *et al.* (1998) 'Missense mutations in SMOH in sporadic basal cell carcinomas of the skin and primitive neuroectodermal tumors of the central nervous system.', *Cancer research*, 58(9), pp. 1798–803. Available at: http://www.ncbi.nlm.nih.gov/pubmed/9581815 (Accessed: 1 October 2022).

Reinders, M.G. *et al.* (2018) 'New mutations and an updated database for the patched-1 (PTCH1) gene', *Molecular Genetics & Genomic Medicine*, 6(3), pp. 409–415. Available at: https://doi.org/10.1002/MGG3.380.

Renaud, J. *et al.* (2008) 'Plexin-A2 and its ligand, Sema6A, control nucleus-centrosome coupling in migrating granule cells', *Nature Neuroscience 2008 11:4*, 11(4), pp. 440–449. Available at: https://doi.org/10.1038/nn2064.

Ribes, V. and Briscoe, J. (2009) 'Establishing and interpreting graded Sonic Hedgehog signaling during vertebrate neural tube patterning: the role of negative feedback.', *Cold Spring Harbor perspectives in biology*. Cold Spring Harbor Laboratory Press. Available at: https://doi.org/10.1101/cshperspect.a002014.

Richard-Parpaillon, L. *et al.* (2002) 'The IGF pathway regulates head formation by inhibiting Wnt signaling in Xenopus', *Developmental Biology*, 244(2), pp. 407–417. Available at: https://doi.org/10.1006/dbio.2002.0605.

Robarge, K.D. *et al.* (2009) 'GDC-0449-A potent inhibitor of the hedgehog pathway', *Bioorganic and Medicinal Chemistry Letters*, 19(19), pp. 5576–5581. Available at: https://doi.org/10.1016/j.bmcl.2009.08.049.

Robertson, J.A. (2001) 'Human embryonic stem cell research: Ethical and legal issues', *Nature Reviews Genetics*. Nature Publishing Group, pp. 74–78. Available at: https://doi.org/10.1038/35047594.

Roelink, H. *et al.* (1994) 'Floor plate and motor neuron induction by vhh-1, a vertebrate homolog of hedgehog expressed by the notochord', *Cell*, 76(4), pp. 761–775. Available at: https://doi.org/10.1016/0092-8674(94)90514-2.

Roper, S.J. *et al.* (2021) '3D spheroid models of paediatric SHH medulloblastoma mimic tumour biology, drug response and metastatic dissemination', *Scientific Reports 2021 11:1*, 11(1), pp. 1–17. Available at: https://doi.org/10.1038/s41598-021-83809-6.

Roussel, M.F. and Stripay, J.L. (2020) 'Modeling pediatric medulloblastoma', *Brain Pathology*, 30(3), pp. 703–712. Available at: https://doi.org/10.1111/bpa.12803.

Rubin, J.B., Choi, Y. and Segal, R.A. (2002) 'Cerebellar proteoglycans regulate sonic hedgehog responses during development', *Development*, 129(9), pp. 2223–2232. Available at: https://doi.org/10.1242/DEV.129.9.2223.

Rubin, L.L. and de Sauvage, F.J. (2006) 'Targeting the Hedgehog pathway in cancer', *Nature Reviews Drug Discovery*. Nature Publishing Group, pp. 1026–1033. Available at: https://doi.org/10.1038/nrd2086.

Ruggiero, A. *et al.* (2010) 'Phase i study of temozolomide combined with oral etoposide in children with recurrent or progressive medulloblastoma', *European Journal of Cancer*, 46(16), pp. 2943–2949. Available at: https://doi.org/10.1016/j.ejca.2010.05.016.

Ruiz i Altaba, A., Palma, V. and Dahmane, N. (2002) 'Hedgehog–GLI signaling and the growth of the brain', *Nature Reviews Neuroscience*, 3(1), pp. 24–33. Available at: https://doi.org/10.1038/nrn704.

Ruiz i Altaba, A., Sánchez, P. and Dahmane, N. (2002) 'Gli and hedgehog in cancer: Tumours, embryos and stem cells', *Nature Reviews Cancer*. Nature Publishing Group, pp. 361–372. Available at: https://doi.org/10.1038/nrc796.

Ruppert, J.M. *et al.* (1988) 'The GLI-Kruppel family of human genes', *Molecular and Cellular Biology*, 8(8), pp. 3104–3113. Available at: https://doi.org/10.1128/mcb.8.8.3104-3113.1988.

Ryder, E.F. and Cepko, C.L. (1994) 'Migration patterns of clonally related granule cells and their progenitors in the developing chick cerebellum', *Neuron*, 12(5), pp. 1011–1029. Available at: https://doi.org/10.1016/0896-6273(94)90310-7.

Sachs, N. *et al.* (2018) 'A Living Biobank of Breast Cancer Organoids Captures Disease Heterogeneity', *Cell*, 172(1–2), pp. 373-386.e10. Available at: https://doi.org/10.1016/j.cell.2017.11.010.

Saelens, W. *et al.* (2019) 'A comparison of single-cell trajectory inference methods', *Nature Biotechnology 2019 37:5*, 37(5), pp. 547–554. Available at: https://doi.org/10.1038/s41587-019-0071-9.

Salero, E. and Hatten, M.E. (2007) 'Differentiation of ES cells into cerebellar neurons', *Proceedings of the National Academy of Sciences of the United States of America*, 104(8), pp. 2997–3002. Available at: https://doi.org/10.1073/pnas.0610879104.

Salloum, R. *et al.* (2019) 'Late morbidity and mortality among medulloblastoma survivors diagnosed across three decades: A report from the Childhood Cancer Survivor Study', *Journal of Clinical Oncology*, 37(9), pp. 731–740. Available at: https://doi.org/10.1200/JCO.18.00969.

Sander, M. *et al.* (2000) 'Ventral neural patterning by Nkx homeobox genes: Nkx6.1 controls somatic motor neuron and ventral interneuron fates', *Genes and Development*, 14(17), pp. 2134–2139. Available at: https://doi.org/10.1101/gad.820400.

Santhana Kumar, K. *et al.* (2018) 'TGF-β Determines the Pro-migratory Potential of bFGF Signaling in Medulloblastoma', *Cell Reports*, 23(13), pp. 3798-3812.e8. Available at: https://doi.org/10.1016/j.celrep.2018.05.083.

Sasai, K. *et al.* (2006) 'Shh Pathway Activity Is Down-Regulated in Cultured Medulloblastoma Cells: Implications for Preclinical Studies', *Cancer Research*, 66(8), pp. 4215–4222. Available at: https://doi.org/10.1158/0008-5472.CAN-05-4505.

Sathyanesan, A. *et al.* (2019) 'Emerging connections between cerebellar development, behaviour and complex brain disorders', *Nature Reviews Neuroscience*, 20(5), pp. 298–313. Available at: https://doi.org/10.1038/s41583-019-0152-2.

Schmidt, S. *et al.* (2022) 'Primary cilia and SHH signaling impairments in human and mouse models of Parkinson's disease', *Nature Communications 2022 13:1*, 13(1), pp. 1–25. Available at: https://doi.org/10.1038/s41467-022-32229-9.

Schönholzer, M.T. *et al.* (2020) 'Real-time sensing of MAPK signaling in medulloblastoma cells reveals cellular evasion mechanism counteracting dasatinib blockade of ERK activation during invasion', *Neoplasia (United States)*, 22(10), pp. 470–483. Available at: https://doi.org/10.1016/j.neo.2020.07.006.

Schreiber, J.E. *et al.* (2017) 'Posterior fossa syndrome and long-term neuropsychological outcomes among children treated for medulloblastoma on a multi-institutional, prospective study', *Neuro-Oncology*, 19(12), pp. 1673–1682. Available at: https://doi.org/10.1093/neuonc/nox135.

Schüller, U. *et al.* (2008) 'Acquisition of Granule Neuron Precursor Identity Is a Critical Determinant of Progenitor Cell Competence to Form Shh-Induced Medulloblastoma', *Cancer Cell*, 14(2), pp. 123–134. Available at: https://doi.org/10.1016/j.ccr.2008.07.005.

Schwalbe, E.C. *et al.* (2017) 'Novel molecular subgroups for clinical classification and outcome prediction in childhood medulloblastoma: a cohort study', *The Lancet.*

Oncology, 18(7), p. 958. Available at: https://doi.org/10.1016/S1470-2045(17)30243-7.

Sepp, M. *et al.* (2021) 'Cellular development and evolution of the mammalian cerebellum', *bioRxiv*, p. 2021.12.20.473443. Available at: https://doi.org/10.1101/2021.12.20.473443.

Seto, Y. *et al.* (2014) 'Temporal identity transition from Purkinje cell progenitors to GABAergic interneuron progenitors in the cerebellum', *Nature Communications 2014 5:1*, 5(1), pp. 1–13. Available at: https://doi.org/10.1038/ncomms4337.

Shaul, O. (2017) 'How introns enhance gene expression', *The International Journal of Biochemistry & Cell Biology*, 91, pp. 145–155. Available at: https://doi.org/10.1016/J.BIOCEL.2017.06.016.

Shi, Y. *et al.* (2017) 'Induced pluripotent stem cell technology: A decade of progress', *Nature Reviews Drug Discovery*. Nature Publishing Group, pp. 115–130. Available at: https://doi.org/10.1038/nrd.2016.245.

Shimokawa, T. *et al.* (2007) 'Distinct roles of first exon variants of the tumor-suppressor Patched1 in Hedgehog signaling', *Oncogene 2007 26:34*, 26(34), pp. 4889–4896. Available at: https://doi.org/10.1038/sj.onc.1210301.

Shimokawa, T., Rahnama, F. and Zaphiropoulos, P.G. (2004) 'A novel first exon of the Patched1 gene is upregulated by Hedgehog signaling resulting in a protein with pathway inhibitory functions', *FEBS Letters*, 578(1–2), pp. 157–162. Available at: https://doi.org/10.1016/J.FEBSLET.2004.11.006.

Sillitoe, R. v and Joyner, A.L. (2007) 'Morphology, molecular codes, and circuitry produce the three-dimensional complexity of the cerebellum.', *Annual review of cell and developmental biology*, 23, pp. 549–77. Available at: https://doi.org/10.1146/annurev.cellbio.23.090506.123237.

Singh, H.P. *et al.* (2022) 'An immature, dedifferentiated, and lineage-deconstrained cone precursor origin of N-Myc-initiated retinoblastoma', *Proceedings of the National Academy of Sciences of the United States of America*, 119(28), p. e2200721119. Available at: https://doi.org/10.1073/PNAS.2200721119/SUPPL_FILE/PNAS.2200721119.SAPP.PDF.

Skowron, P. *et al.* (2021) 'The transcriptional landscape of Shh medulloblastoma', *Nature Communications*, 12(1). Available at: https://doi.org/10.1038/s41467-021-21883-0.

Smeyne, R.J. *et al.* (1995) 'Local Control of Granule Cell Generation by Cerebellar Purkinje Cells', *Molecular and Cellular Neuroscience*, 6(3), pp. 230–251. Available at: https://doi.org/10.1006/mcne.1995.1019.

Smith, K.S. *et al.* (2022) 'Unified rhombic lip origins of group 3 and group 4 medulloblastoma', *Nature*, 609(7929), pp. 1012–1020. Available at: https://doi.org/10.1038/s41586-022-05208-9.

Smoll, N.R. and Drummond, K.J. (2012) 'The incidence of medulloblastomas and primitive neurectodermal tumours in adults and children', *Journal of Clinical Neuroscience*, 19(11), pp. 1541–1544. Available at: https://doi.org/10.1016/j.jocn.2012.04.009.

Solecki, D.J. *et al.* (2001) 'Activated Notch2 signaling inhibits differentiation of cerebellar granule neuron precursors by maintaining proliferation', *Neuron*, 31(4), pp. 557–568. Available at: https://doi.org/10.1016/S0896-6273(01)00395-6.

Sommer, C.A. *et al.* (2009) 'Induced Pluripotent Stem Cell Generation Using a Single Lentiviral Stem Cell Cassette', *Stem Cells*, 27(3), pp. 543–549. Available at: https://doi.org/10.1634/stemcells.2008-1075.

Srivastava, V.K. and Nalbantoglu, J. (2008) 'Flow cytometric characterization of the DAOY medulloblastoma cell line for the cancer stem-like phenotype', *Cytometry Part A*, 73(10), pp. 940–948. Available at: https://doi.org/10.1002/cyto.a.20633.

Stadtfeld, M. *et al.* (2008) 'Induced pluripotent stem cells generated without viral integration', *Science*, 322(5903), pp. 945–949. Available at: https://doi.org/10.1126/science.1162494.

Stemmer, M. *et al.* (2015) 'CCTop: An intuitive, flexible and reliable CRISPR/Cas9 target prediction tool', *PLoS ONE*, 10(4), p. e0124633. Available at: https://doi.org/10.1371/journal.pone.0124633.

St-Jacques, B., Hammerschmidt, M. and McMahon, A.P. (1999) 'Indian hedgehog signaling regulates proliferation and differentiation of chondrocytes and is essential for bone formation', *Genes and Development*, 13(16), pp. 2072–2086. Available at: https://doi.org/10.1101/gad.13.16.2072.

Stoykova, A. and Gruss, P. (1994) 'Roles of Pax-genes in developing and adult brain as suggested by expression patterns', *Journal of Neuroscience*, 14(3 II), pp. 1395–1412. Available at: https://doi.org/10.1523/jneurosci.14-03-01395.1994.

Su, H.-L. *et al.* (2006) 'Generation of cerebellar neuron precursors from embryonic stem cells.', *Developmental biology*, 290(2), pp. 287–96. Available at: https://doi.org/10.1016/j.ydbio.2005.11.010.

Su, S. *et al.* (2022) 'PLK1 inhibition-based combination therapies for cancer management', *Translational Oncology*. Elsevier, p. 101332. Available at: https://doi.org/10.1016/j.tranon.2021.101332.

Sundberg, M. *et al.* (2018) 'Purkinje cells derived from TSC patients display hypoexcitability and synaptic deficits associated with reduced FMRP levels and reversed by rapamycin', *Molecular Psychiatry*, 23(11), pp. 2167–2183. Available at: https://doi.org/10.1038/s41380-018-0018-4.

Sunmonu, N.A. *et al.* (2011) '*Gbx2* and *Fgf8* are sequentially required for formation of the midbrain-hindbrain compartment boundary', *Development*, 138(4), pp. 725–734. Available at: https://doi.org/10.1242/dev.055665.

Susanto, E. *et al.* (2020) 'Modeling SHH-driven medulloblastoma with patient iPS cell-derived neural stem cells', *Proceedings of the National Academy of Sciences of the United States of America*, 117(33), pp. 20127–20138. Available at: https://doi.org/10.1073/PNAS.1920521117.

Swanson, D.J., Tong, Y. and Goldowitz, D. (2005) 'Disruption of cerebellar granule cell development in the Pax6 mutant, Sey mouse', *Developmental Brain Research*, 160(2), pp. 176–193. Available at: https://doi.org/10.1016/j.devbrainres.2005.09.005.

Swartling, F.J. *et al.* (2010) 'Pleiotropic role for MYCN in medulloblastoma', *Genes and Development*, 24(10), pp. 1059–1072. Available at: https://doi.org/10.1101/gad.1907510.

Taapken, S.M. *et al.* (2011) 'Karyotypic abnormalities in human induced pluripotent stem cells and embryonic stem cells', *Nature Biotechnology 2011 29:4*, 29(4), pp. 313–314. Available at: https://doi.org/10.1038/nbt.1835.

Taipale, J. *et al.* (2002) 'Patched acts catalytically to suppress the activity of smoothened', *Nature*, 418(6900), pp. 892–897. Available at: https://doi.org/10.1038/nature00989.

Takahashi, K. *et al.* (2007) 'Induction of Pluripotent Stem Cells from Adult Human Fibroblasts by Defined Factors', *Cell*, 131(5), pp. 861–872. Available at: https://doi.org/10.1016/j.cell.2007.11.019.

Takahashi, K. and Yamanaka, S. (2006) 'Induction of Pluripotent Stem Cells from Mouse Embryonic and Adult Fibroblast Cultures by Defined Factors', *Cell*, 126(4), pp. 663–676. Available at: https://doi.org/10.1016/J.CELL.2006.07.024/ATTACHMENT/A7BA2E0F-99EF-4A86-88AA-418202149347/MMC1.PDF.

Talpale, J. *et al.* (2000) 'Effects of oncogenic mutations in Smoothened and Patched can be reversed by cyclopamine', *Nature 2000 406:6799*, 406(6799), pp. 1005–1009. Available at: https://doi.org/10.1038/35023008.

Tamayo-Orrego, L. *et al.* (2016a) 'Evasion of Cell Senescence Leads to Medulloblastoma Progression', *Cell Reports*, 14. Available at: https://doi.org/10.1016/j.celrep.2016.02.061.

Tamayo-Orrego, L. *et al.* (2016b) 'Evasion of Cell Senescence Leads to Medulloblastoma Progression', 14, pp. 2925–2937. Available at: https://doi.org/10.1016/j.celrep.2016.02.061.

Tamayo-Orrego, L. *et al.* (2020) 'Sonic hedgehog accelerates DNA replication to cause replication stress promoting cancer initiation in medulloblastoma', *Nature Cancer*, 1(8), pp. 840–854. Available at: https://doi.org/10.1038/s43018-020-0094-7.

Tang, Y. *et al.* (2014) 'Epigenetic targeting of Hedgehog pathway transcriptional output through BET bromodomain inhibition', *Nature Medicine*, 20(7), pp. 732–740. Available at: https://doi.org/10.1038/nm.3613.

Taylor, M.D. *et al.* (2002) 'Mutations in SUFU predispose to medulloblastoma', *Nature Genetics*, 31(3), pp. 306–310. Available at: https://doi.org/10.1038/ng916.

Tenzen, T. *et al.* (2006) 'The Cell Surface Membrane Proteins Cdo and Boc Are Components and Targets of the Hedgehog Signaling Pathway and Feedback Network in Mice', *Developmental Cell*, 10(5), pp. 647–656. Available at: https://doi.org/10.1016/j.devcel.2006.04.004.

Toftgård, R. (2000) 'Hedgehog signalling in cancer', *Cellular and Molecular Life Sciences*, pp. 1720–1731. Available at: https://doi.org/10.1007/PL00000654.

Tomasetti, C., Li, L. and Vogelstein, B. (2017) 'Stem cell divisions, somatic mutations, cancer etiology, and cancer prevention', *Science*, 355(6331), pp. 1330–1334. Available at: https://doi.org/10.1126/science.aaf9011.

Tsangaris, G.T. *et al.* (2017) 'Molecular proteomic characterization of a pediatric medulloblastoma xenograft', *Cancer Genomics and Proteomics*, 14(4), pp. 267–275. Available at: https://doi.org/10.21873/cgp.20037.

Tuladhar, R. *et al.* (2019) 'CRISPR-Cas9-based mutagenesis frequently provokes on-target mRNA misregulation', *Nature Communications*, 10(1), pp. 1–10. Available at: https://doi.org/10.1038/s41467-019-12028-5.

Tuson, M., He, M. and Anderson, K. v. (2011) 'Protein kinase A acts at the basal body of the primary cilium to prevent Gli2 activation and ventralization of the mouse neural tube', *Development*, 138(22), pp. 4921–4930. Available at: https://doi.org/10.1242/dev.070805.

Tutt, A. *et al.* (2001) 'Mutation in Brca2 stimulates error-prone homology-directed repair of DNA double-strand breaks occurring between repeated sequences', *EMBO Journal*, 20(17), pp. 4704–4716. Available at: https://doi.org/10.1093/emboj/20.17.4704.

Ulloa, F. and Martí, E. (2010) 'Wnt won the war: Antagonistic role of Wnt over Shh controls dorso-ventral patterning of the vertebrate neural tube', *Developmental Dynamics*. John Wiley & Sons, Ltd, pp. 69–76. Available at: https://doi.org/10.1002/dvdy.22058.

Uziel, T. *et al.* (2005) 'The tumor suppressors Ink4c and p53 collaborate independently with Patched to suppress medulloblastoma formation', *Genes & Development*, 19(22), pp. 2656–2667. Available at: https://doi.org/10.1101/GAD.1368605.

Vakulskas, C.A. *et al.* (2018) 'A high-fidelity Cas9 mutant delivered as a ribonucleoprotein complex enables efficient gene editing in human hematopoietic stem and progenitor cells', *Nature Medicine*, 24(8), pp. 1216–1224. Available at: https://doi.org/10.1038/s41591-018-0137-0.

Vaughan-Jackson, A. *et al.* (2021) 'Differentiation of human induced pluripotent stem cells to authentic macrophages using a defined, serum-free, open-source medium', *Stem Cell Reports*, 16(7), pp. 1735–1748. Available at: https://doi.org/10.1016/J.STEMCR.2021.05.018/ATTACHMENT/AAD22208-56B0-4057-BC81-2EC058A12013/MMC1.PDF.

Volpato, V. and Webber, C. (2020) 'Addressing variability in iPSC-derived models of human disease: Guidelines to promote reproducibility', *DMM Disease Models and Mechanisms*, 13(1). Available at: https://doi.org/10.1242/DMM.042317/223104.

Volpe, J.J. (2009) 'Cerebellum of the Premature Infant: Rapidly Developing, Vulnerable, Clinically Important', *http://dx.doi.org/10.1177/0883073809338067*, 24(9), pp. 1085–1104. Available at: https://doi.org/10.1177/0883073809338067.

Wallace, V.A. (1999) 'Purkinje-cell-derived Sonic hedgehog regulates granule neuron precursor cell proliferation in the developing mouse cerebellum', *Current Biology*, 9(8), pp. 445–448. Available at: https://doi.org/10.1016/S0960-9822(99)80195-X.

Wang, V.Y., Rose, M.F. and Zoghbi, H.Y. (2005) 'Math1 Expression Redefines the Rhombic Lip Derivatives and Reveals Novel Lineages within the Brainstem and Cerebellum', *Neuron*, 48(1), pp. 31–43. Available at: https://doi.org/10.1016/J.NEURON.2005.08.024.

Warren, L. *et al.* (2010) 'Highly efficient reprogramming to pluripotency and directed differentiation of human cells with synthetic modified mRNA', *Cell Stem Cell*, 7(5), pp. 618–630. Available at: https://doi.org/10.1016/j.stem.2010.08.012.

Waszak, S.M. *et al.* (2018) 'Spectrum and prevalence of genetic predisposition in medulloblastoma: a retrospective genetic study and prospective validation in a clinical trial cohort', *The Lancet Oncology*, 19(6), pp. 785–798. Available at: https://doi.org/10.1016/S1470-2045(18)30242-0.

Waszak, S.M. *et al.* (2020) 'Germline Elongator mutations in Sonic Hedgehog medulloblastoma', *Nature*, 580(7803), pp. 396–401. Available at: https://doi.org/10.1038/s41586-020-2164-5.

Watanabe, K. *et al.* (2005) 'Directed differentiation of telencephalic precursors from embryonic stem cells', *Nature Neuroscience*, 8(3), pp. 288–296. Available at: https://doi.org/10.1038/nn1402.

Watanabe, K. *et al.* (2007) 'A ROCK inhibitor permits survival of dissociated human embryonic stem cells', *Nature Biotechnology*, 25(6), pp. 681–686. Available at: https://doi.org/10.1038/nbt1310.

Wataya, T. *et al.* (2008) 'Minimization of exogenous signals in ES cell culture induces rostral hypothalamic differentiation', *Proceedings of the National Academy of Sciences of the United States of America*, 105(33), pp. 11796–11801. Available at: https://doi.org/10.1073/pnas.0803078105.

Watson, L.M. *et al.* (2018) 'A Simplified Method for Generating Purkinje Cells from Human-Induced Pluripotent Stem Cells', *Cerebellum*, 17(4), pp. 419–427. Available at: https://doi.org/10.1007/s12311-017-0913-2.

Wechsler-Reya, R.J. and Scott, M.P. (1999) 'Control of Neuronal Precursor Proliferation in the Cerebellum by Sonic Hedgehog', *Neuron*, 22(1), pp. 103–114. Available at: https://doi.org/10.1016/S0896-6273(00)80682-0.

Weishaupt, H. *et al.* (2019) 'Batch-normalization of cerebellar and medulloblastoma gene expression datasets utilizing empirically defined negative control genes', *Bioinformatics*, 35(18), pp. 3357–3364. Available at: https://doi.org/10.1093/bioinformatics/btz066.

Weisheit, G. *et al.* (2006) 'Postnatal development of the murine cerebellar cortex: formation and early dispersal of basket, stellate and Golgi neurons', *European Journal of Neuroscience*, 24(2), pp. 466–478. Available at: https://doi.org/10.1111/J.1460-9568.2006.04915.X.

Wells, J.N. and Feschotte, C. (2020) 'A Field Guide to Eukaryotic Transposable Elements', *Annual Review of Genetics*. NIH Public Access, pp. 539–561. Available at: https://doi.org/10.1146/annurev-genet-040620-022145.

de Wert, G. and Mummery, C. (2003) 'Human embryonic stem cells: Research, ethics and policy', *Human Reproduction*. Oxford Academic, pp. 672–682. Available at: https://doi.org/10.1093/humrep/deg143.

Wetmore, C. (2003) 'Sonic hedgehog in normal and neoplastic proliferation: Insight gained from human tumors and animal models', *Current Opinion in Genetics and Development*. Elsevier Current Trends, pp. 34–42. Available at: https://doi.org/10.1016/S0959-437X(03)00002-9.

Wetmore, C., Eberhart, D.E. and Curran, T. (2001) *Loss of p53 but not ARF Accelerates Medulloblastoma in Mice Heterozygous for patched 1*, *CANCER RESEARCH*. Available at: https://cancerres.aacrjournals.org/content/canres/61/2/513.full.pdf (Accessed: 17 June 2020).

Wilson, C.W., Chen, M.H. and Chuang, P.T. (2009) 'Smoothened adopts multiple active and inactive conformations capable of trafficking to the primary cilium', *PLoS ONE*, 4(4). Available at: https://doi.org/10.1371/journal.pone.0005182.

Wingate, R.J. and Hatten, M.E. (1999) 'The role of the rhombic lip in avian cerebellum development', *Development*, 126(20), pp. 4395–4404. Available at: https://doi.org/10.1242/dev.126.20.4395.

Wingate, R.J.R.J.T. and Hatten, M.E.M.E. (1999) 'The role of the rhombic lip in avian cerebellum development', *Development*, 126(20), pp. 4395–4404. Available at: https://doi.org/10.1242/dev.126.20.4395.

Wingate, R.J.T. (2001) 'The rhombic lip and early cerebellar development', *Current Opinion in Neurobiology*, 11(1), pp. 82–88. Available at: https://doi.org/10.1016/S0959-4388(00)00177-X.

Winkler, J. *et al.* (2020) 'Concepts of extracellular matrix remodelling in tumour progression and metastasis', *Nature Communications*. Nature Publishing Group, pp. 1–19. Available at: https://doi.org/10.1038/s41467-020-18794-x.

Woltjen, K. *et al.* (2009) 'PiggyBac transposition reprograms fibroblasts to induced pluripotent stem cells', *Nature*, 458(7239), pp. 766–770. Available at: https://doi.org/10.1038/nature07863.

Wong, M.M.K., Watson, L.M. and Becker, E.B.E. (2017) 'Recent advances in modelling of cerebellar ataxia using induced pluripotent stem cells.', *Journal of Neurology & Neuromedicine*, 2(7), pp. 11–15. Available at: https://doi.org/10.29245/2572.942x/2017/7.1134.

Wu, S.M. *et al.* (2010) 'Role of Sonic hedgehog signaling and the expression of its components in human embryonic stem cells', *Stem Cell Research*, 4(1), pp. 38–49. Available at: https://doi.org/10.1016/J.SCR.2009.09.002.

Wyman, C. and Kanaar, R. (2006) 'DNA double-strand break repair: All's well that ends well', *Annual Review of Genetics*. Annu Rev Genet, pp. 363–383. Available at: https://doi.org/10.1146/annurev.genet.40.110405.090451.

Xie, J. *et al.* (1998) 'Activating Smoothened mutations in sporadic basal-cell carcinoma', *Nature*, 391(6662), pp. 90–92. Available at: https://doi.org/10.1038/34201.

Xu, S. *et al.* (2019) 'The role of collagen in cancer: From bench to bedside', *Journal of Translational Medicine*. BioMed Central, pp. 1–22. Available at: https://doi.org/10.1186/s12967-019-2058-1.

Yam, P.T. *et al.* (2009) 'Sonic Hedgehog Guides Axons through a Noncanonical, Src-Family-Kinase-Dependent Signaling Pathway', *Neuron*, 62(3), pp. 349–362. Available at: https://doi.org/10.1016/j.neuron.2009.03.022.

Yamada, M. *et al.* (1989) 'Establishment and biological characterization of human medulloblastoma cell lines', *Brain and Nerve*, 41(7), pp. 695–702. Available at: https://europepmc.org/article/med/2818910 (Accessed: 16 September 2022).

Yamada, M. *et al.* (2014) 'Specification of spatial identities of cerebellar neuron progenitors by ptf1a and atoh1 for proper production of GABAergic and glutamatergic neurons', *Journal of Neuroscience*, 34(14), pp. 4786–4800. Available at: https://doi.org/10.1523/JNEUROSCI.2722-13.2014.

Yang, L. *et al.* (2013) 'Optimization of scarless human stem cell genome editing', *Nucleic Acids Research*, 41(19), pp. 9049–9061. Available at: https://doi.org/10.1093/NAR/GKT555.

Yang, Z.-J.J. *et al.* (2008) 'Medulloblastoma Can Be Initiated by Deletion of Patched in Lineage-Restricted Progenitors or Stem Cells', *Cancer Cell*, 14(2), pp. 135–145. Available at: https://doi.org/10.1016/j.ccr.2008.07.003.

Yant, S.R. *et al.* (2005) 'High-Resolution Genome-Wide Mapping of Transposon Integration in Mammals', *Molecular and Cellular Biology*, 25(6), pp. 2085–2094. Available at: https://doi.org/10.1128/mcb.25.6.2085-2094.2005.

Yao, H.H.C., Whoriskey, W. and Capel, B. (2002) 'Desert Hedgehog/Patched 1 signaling specifies fetal Leydig cell fate in testis organogenesis', *Genes and Development*, 16(11), pp. 1433–1440. Available at: https://doi.org/10.1101/gad.981202.

Yasar, B. *et al.* (2015) 'Common variants modify the age of onset for basal cell carcinomas in Gorlin syndrome', *European Journal of Human Genetics*, 23(5), pp. 708–710. Available at: https://doi.org/10.1038/ejhg.2014.167.

Yeung, J. *et al.* (2014) 'Wls Provides a New Compartmental View of the Rhombic Lip in Mouse Cerebellar Development', *Journal of Neuroscience*, 34(37), pp. 12527–12537. Available at: https://doi.org/10.1523/JNEUROSCI.1330-14.2014.

Zecevic, N. and Rakic, P. (1976) 'Differentiation of Purkinje cells and their relationship to other components of developing cerebellar cortex in man', *Journal of Comparative Neurology*, 167(1), pp. 27–47. Available at: https://doi.org/10.1002/cne.901670103.

Zhao, H. *et al.* (2008) 'Post-transcriptional down-regulation of Atoh1/Math1 by bone morphogenic proteins suppresses medulloblastoma development', *Genes and Development*, 22(6), pp. 722–727. Available at: https://doi.org/10.1101/gad.1636408.

Zhao, Q. *et al.* (2002) 'Identification of genes expressed with temporal-spatial restriction to developing cerebellar neuron precursors by a functional genomic approach', *Proceedings of the National Academy of Sciences of the United States of America*, 99(8), p. 5704. Available at: https://doi.org/10.1073/PNAS.082092399.

Zhao, X. *et al.* (2012) 'Global gene expression profiling confirms the molecular fidelity of primary tumor-based orthotopic xenograft mouse models of medulloblastoma', *Neuro-Oncology*, 14(5), pp. 574–583. Available at: https://doi.org/10.1093/neuonc/nos061.

Zhao, Y., Tong, C. and Jiang, J. (2007) 'Hedgehog regulates smoothened activity by inducing a conformational switch', *Nature 2007 450:7167*, 450(7167), pp. 252–258. Available at: https://doi.org/10.1038/nature06225.

Zheng, D.Q. *et al.* (2016) 'Global analysis of genomic instability caused by DNA replication stress in Saccharomyces cerevisiae', *Proceedings of the National Academy of Sciences of the United States of America*, 113(50), pp. E8114–E8121. Available at: https://doi.org/10.1073/pnas.1618129113.

Zheng, Q. *et al.* (2014) 'Precise gene deletion and replacement using the CRISPR/Cas9 system in human cells', *BioTechniques*, 57(3), pp. 115–124. Available at: https://doi.org/10.2144/000114196.

Zheng, Y. *et al.* (2019) 'Dorsal-ventral patterned neural cyst from human pluripotent stem cells in a neurogenic niche', *Science Advances*, 5(12), pp. 5933–5944. Available at: https://doi.org/10.1126/sciadv.aax5933.

Zhou, J. *et al.* (2014) 'Dual sgRNAs facilitate CRISPR/Cas9-mediated mouse genome targeting', *FEBS Journal*. John Wiley & Sons, Ltd, pp. 1717–1725. Available at: https://doi.org/10.1111/febs.12735.

Zhou, S. *et al.* (2016) 'The positional identity of iPSC-derived neural progenitor cells along the anterior-posterior axis is controlled in a dosage-dependent manner by bFGF and EGF', *Differentiation*, 92(4), pp. 183–194. Available at: https://doi.org/10.1016/j.diff.2016.06.002.

Zhu, A., Ibrahim, J.G. and Love, M.I. (2019) 'Heavy-tailed prior distributions for sequence count data: removing the noise and preserving large differences', *Bioinformatics*, 35(12), pp. 2084–2092. Available at: https://doi.org/10.1093/BIOINFORMATICS/BTY895.

Zhukova, N. *et al.* (2013) 'Subgroup-specific prognostic implications of TP53 mutation in medulloblastoma', *Journal of Clinical Oncology*, 31(23), pp. 2927–2935. Available at: https://doi.org/10.1200/JCO.2012.48.5052.

Zu, B. *et al.* (2021) 'Generation of a homozygous CRISPR/Cas9-mediated knockout human iPSC line for PTCH1 gene', *Stem Cell Research*, 56, p. 102517. Available at: https://doi.org/10.1016/j.scr.2021.102517.

Appendix

Appendix Table 1: Oligonucleotides used in this thesis.

Gene	Fw/Rv	Sequence	cDNA/ gDNA	An. temp.	Usage
ACTB	Fw	GCCGGGACCTGACTGACTAC	cDNA	60	Reference
ACTB	Rv	TTCTCCTTAATGTCACGCACGAT	cDNA	60	Reference
ATOH1	Fw	TGTTATCCCGTCGTTCAACAAC	cDNA	60	Rel. gene expr.
ATOH1	Rv	TGGGCGTTTGTAGCAGCTC	cDNA	60	Rel. gene expr.
BARHL1	Fw	TTCTGATCAGGGACATCCTTGCC	cDNA	60	Rel. gene expr.
BARHL1	Rv	TGCCACTTTTGTCCAGCTTGTC	cDNA	60	Rel. gene expr.
CNTN2	Fw	CCCAGCAGAGACCTATGCAC	cDNA	60	Rel. gene expr.
CNTN2	Rv	ACTTTGCGCCACTTGATCC	cDNA	60	Rel. gene expr.
EN1	Fw	CGTGGTCAAAACTGACTCGC	cDNA	60	Rel. gene expr.
EN1	Rv	CGCTTGTCCTCCTTCTCGTT	cDNA	60	Rel. gene expr.
GAPDH	Fw	GGAAGGTGAAGGTCGGAGTC	cDNA	60	Reference
GAPDH	Rv	GTTGAGGTCAATGAAGGGGTC	cDNA	60	Reference
GBX2	Fw	AAAGAGGGCTCGCTGCTC	cDNA	60	Rel. gene expr.
GBX2	Rv	GGTCGTCTTCCACCTTTGAC	cDNA	60	Rel. gene expr.
GLI1	Fw	CCCAGTACATGCTGGTGGTT	cDNA	60	Rel. gene expr.
GLI1	Rv	GCTTTACTGCAGCCCTCGT	cDNA	60	Rel. gene expr.
KIRREL2	Fw	CCTGAAGAAGAGGAGACAGGC	cDNA	60	Rel. gene expr.
KIRREL2	Rv	TCCTCCAGAACCAGATCACTG	cDNA	60	Rel. gene expr.
MYCN	Fw	GACCACAAGGCCCTCAGTACC	cDNA	60	Rel. gene expr.
MYCN	Rv	TGACCACGTCGATTTCTTCCT	cDNA	60	Rel. gene expr.
NANOG	Fw	GCAGAAGGCCTCAGCACCTA	cDNA	60	Rel. gene expr.
NANOG	Rv	AGGTTCCCAGTCGGGTTCA	cDNA	60	Rel. gene expr.
NEUROD1	Fw	GGTGCCTTGCTATTCTAAGACGC	cDNA	60	Rel. gene expr.
NEUROD1	Rv	GCAAAGCGTCTGAACGAAGGAG	cDNA	60	Rel. gene expr.
NKX2.1	Fw	CAAAGGCCAAACTGCTGGAC	cDNA	60	Rel. gene expr.
NKX2.1	Rv	TGAGATTGGATGCGCTTGGT	cDNA	60	Rel. gene expr.
NKX2.2	Fw	AGCTTCGCTTCTTTGCCTCT	cDNA	60	Rel. gene expr.
NKX2.2	Rv	GGGGTCGGTCTTTTTCTCGT	cDNA	60	Rel. gene expr.
OCT4	Fw	GCTCGAGAAGGATGTGGTCC	cDNA	60	Rel. gene expr.
OCT4	Rv	CGTTGTGCATAGTCGCTGCT	cDNA	60	Rel. gene expr.
OTX2	Fw	CACTTCGGGTATGGACTTGC	cDNA	60	Rel. gene expr.
OTX2	Rv	GTGAACGTCGTCCTCTCCC	cDNA	60	Rel. gene expr.
PAX6	Fw	AGCTAGCTCACAGCGGGG	cDNA	60	Rel. gene expr.
PAX6	Rv	TCTGATGGAGCCAGTCTCGT	cDNA	60	Rel. gene expr.
PDE1C	Fw	GAGTCGCCAACCAAGGAGAT	cDNA	60	Rel. gene expr.
PDE1C	Rv	GACCGTAATCTCTGGGACGTT	cDNA	60	Rel. gene expr.
PTCH1	Fw	TACTGCTCACACATCAGCCAG	gDNA	56	Genotyping

PTCH1	Rv	AGTTCAGCAAGGGCAATTCAA	gDNA	56	Genotyping
PTCH1	Fw	GGCAGCGGTAGTAGTGGTGTTC	cDNA	60	Rel. gene expr.
PTCH1	Rv	TGTAGCGGGTATTGTCGTGTGTG	cDNA	60	Rel. gene expr.
PTCH1	Fw	ACATGTACAACAGGCAGTGGA	cDNA	60	Exon 3 expr.
PTCH1	Rv	ATTTCGCCCCTTCCCAGAAG	cDNA	60	Exon 3 expr.
PTCH1	Fw	TTTGCGGTGGACAAACTTCG	cDNA	60	Total PTCH1 expr
PTCH1	Rv	TTCAGCATTTCCTCCCAGCT	cDNA	60	Total PTCH1 expr
PTCH2	Fw	GATGGGGCCATCTCCACATT	cDNA	60	Rel. gene expr.
PTCH2	Rv	CGCCGCAAAGAAGTACCTTACA	cDNA	60	Rel. gene expr.
SHH	Fw	CTCGCTGCTGGTATGCTCG	cDNA	60	Rel. gene expr.
SHH	Rv	ATCGCTCGGAGTTTCTGGAGA	cDNA	60	Rel. gene expr.
ZIC1	Fw	GCCCTTCAAAGCCAAATACA	cDNA	60	Rel. gene expr.
ZIC1	Rv	AGCCCTCAAACTCGCACTT	cDNA	60	Rel. gene expr.
ZIC3	Fw	ATCTGCAAAGTGTGCGACAA	cDNA	60	Rel. gene expr.
ZIC3	Rv	ATAGCCTGAACTGGCAGCAG	cDNA	60	Rel. gene expr.

Appendix Table 2: Primary antibodies used in this thesis.

Target	Catalogue number	Manufacturer	Host species	Dilution ICC
ATOH1	AB5692	Chemicon	Rabbit	1:200
EN1	ab190080-200ul	Abcam	Rabbit	1:250
GBX2	H00002637-M01	Novus bio	Mouse	1:200
KIRREL2	AF2930	RnD systems	Goat	1:500
MKI67	Ab16667	Abcam	Rabbit	1:1000
PAX6	GTX113241	Genetex	Rabbit	1:1000
CCNB1	05-373	Milipore	Mouse	1:1000
TUBB3	GT1338	Genetex	Mouse	1:1000
NKX2-2	ab191077	Abcam	Rabbit	1:1000
CALB1	300	Swant	Rabbit	1:1000

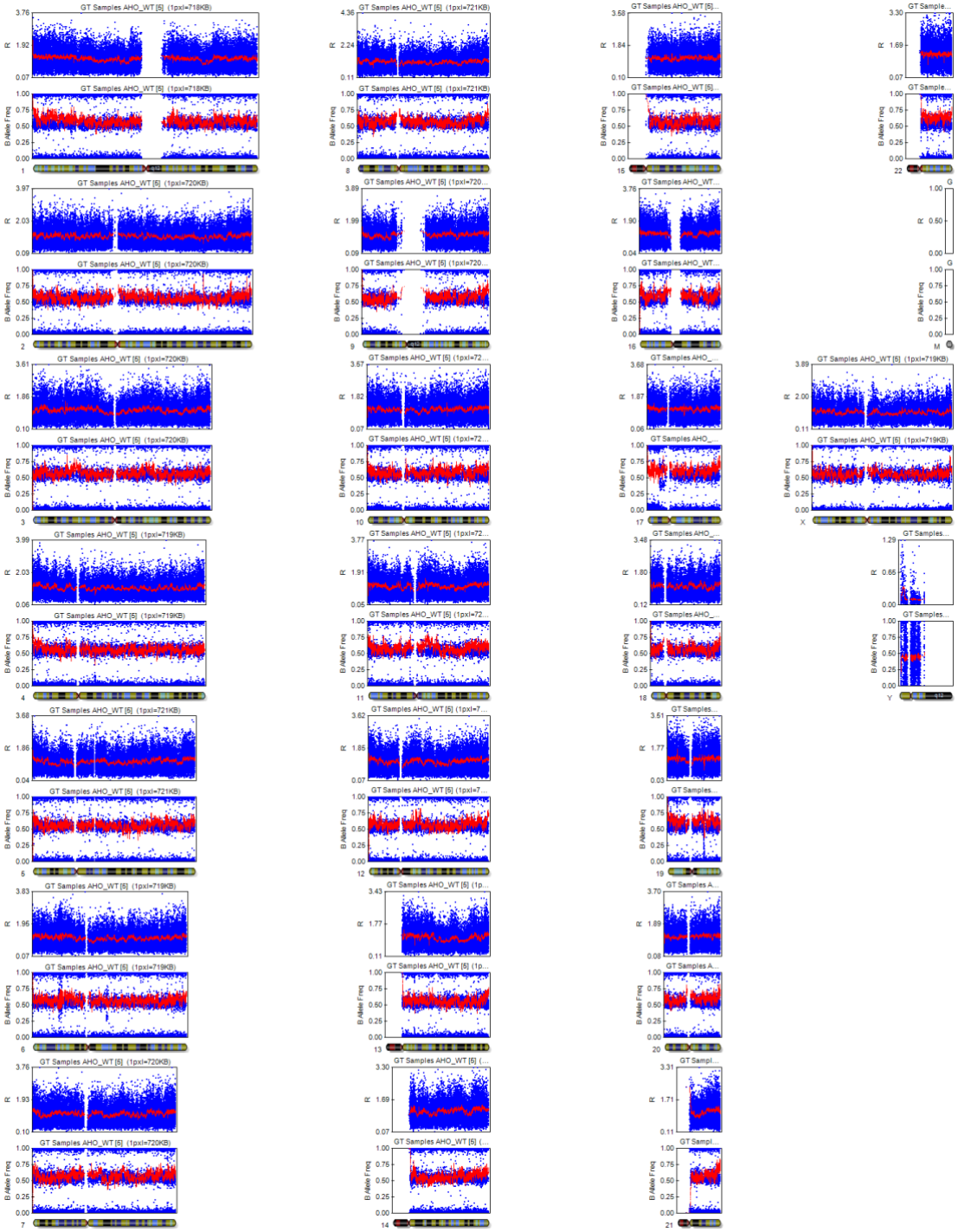
Appendix Table 3: Secondary antibodies used in this thesis.

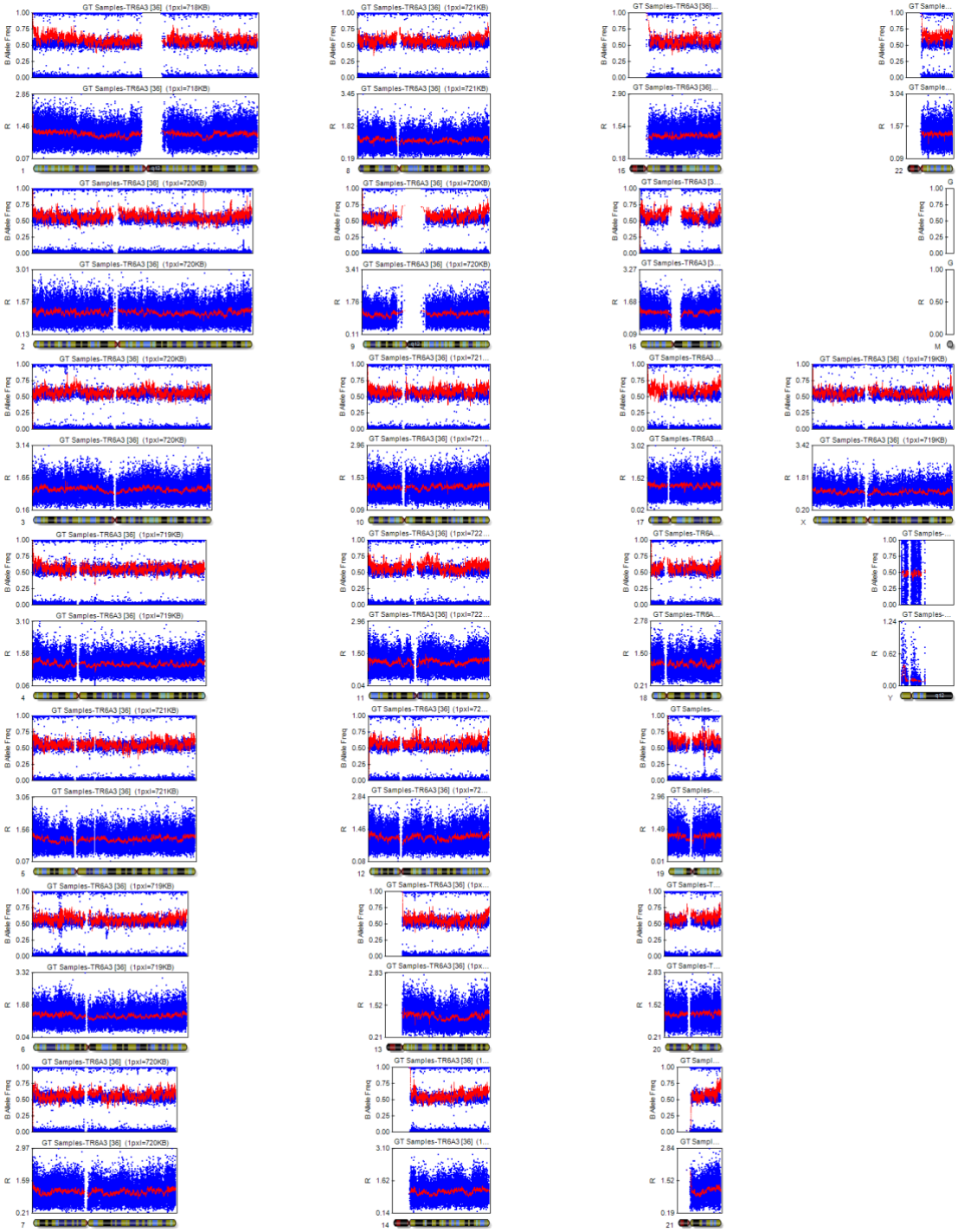
Target species	Host species	Conjugate	Catalogue number	Manufacturer	Dilution ICC
Rabbit	Goat	Alexa Fluor 594	A11037	Invitrogen	1:1000
Mouse	Goat	Alexa Fluor 488	A11029	Invitrogen	1:1000
Goat	Donkey	Alexa Fluor 594	A11058	Invitrogen	1:1000
Rabbit	Donkey	Alexa Fluor 488	A21206	Invitrogen	1:1000

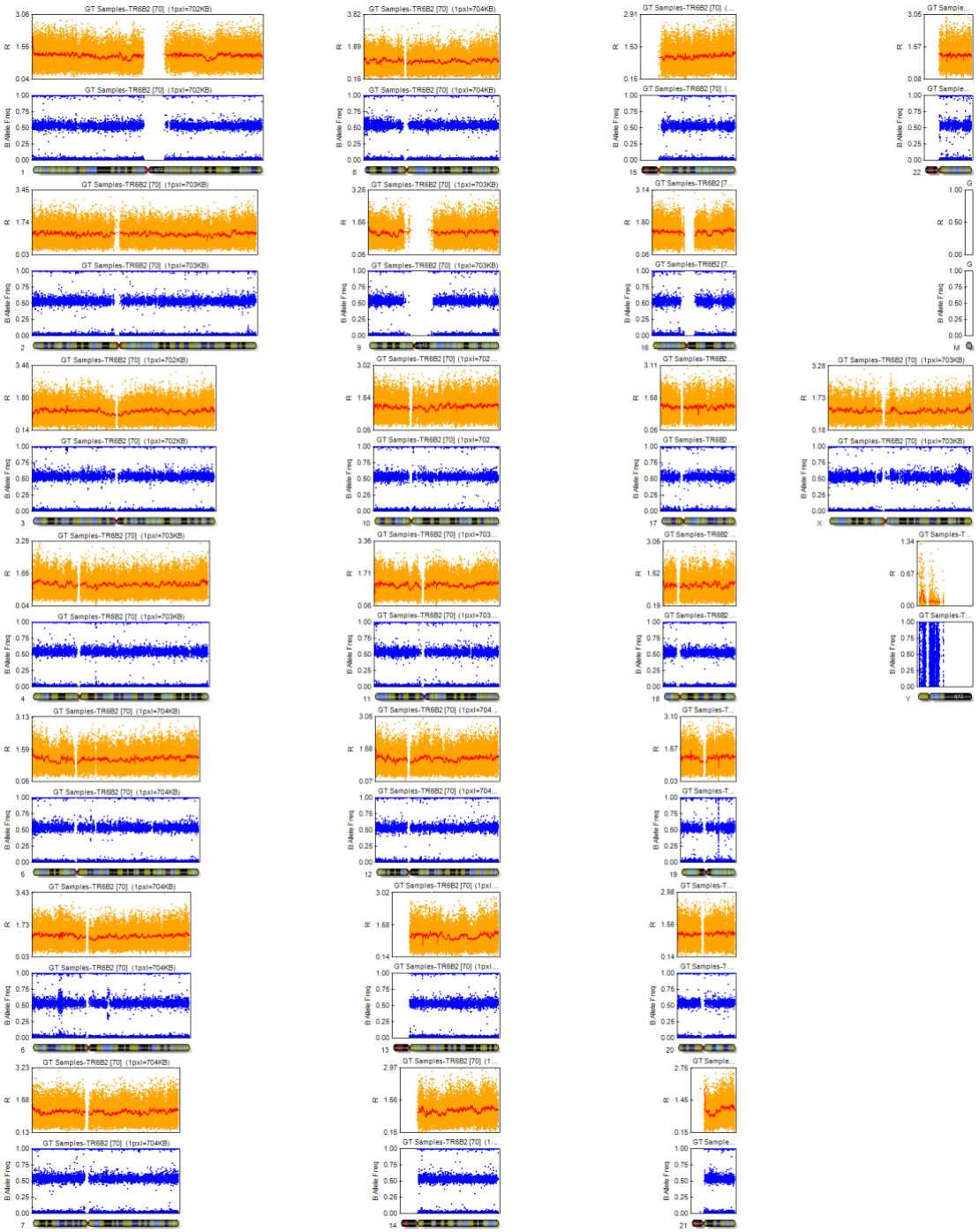
Appendix Table 4: Off-target sites as predicted by CRISPOR.org.

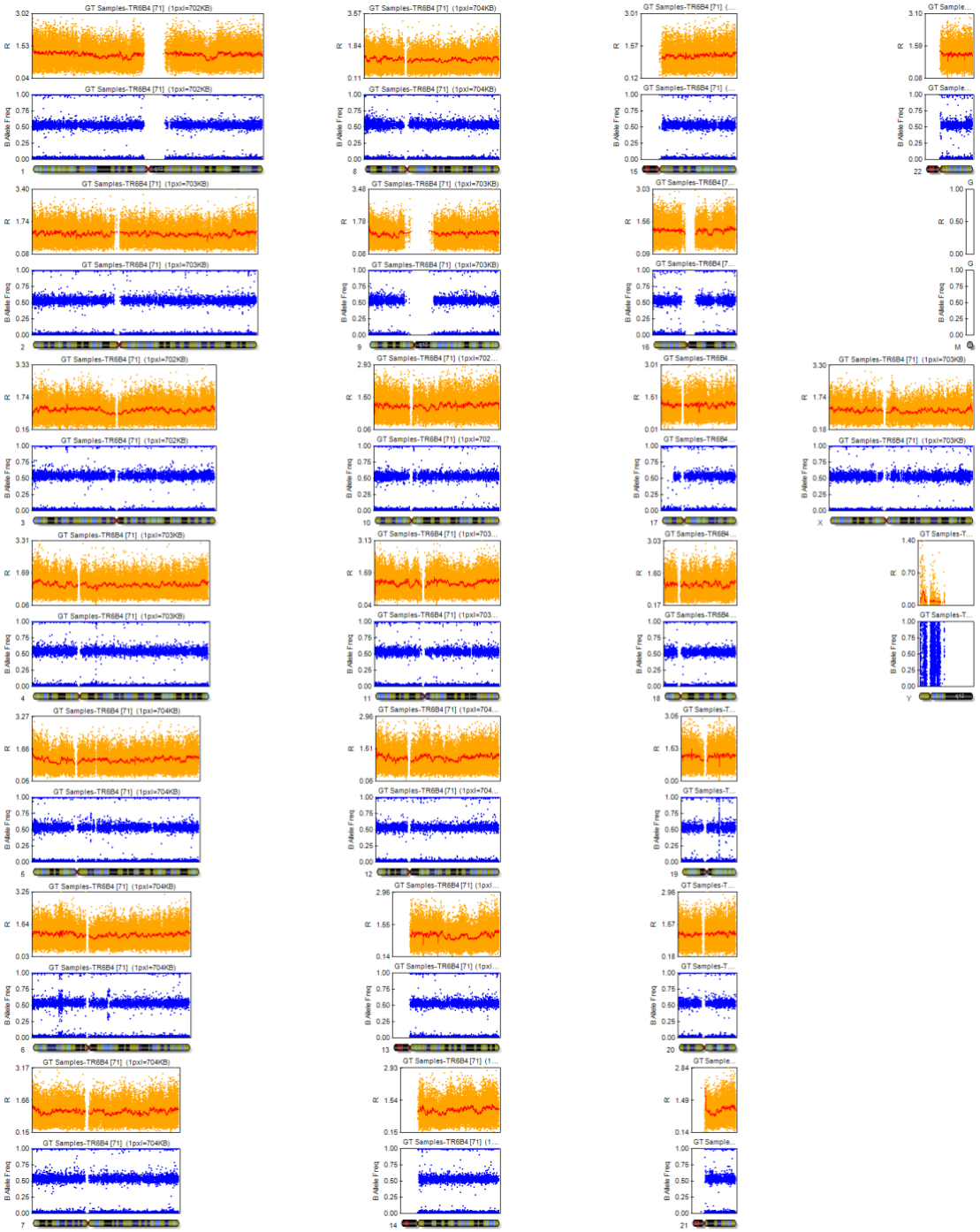
		Coordinates	Strand	MM	Target sequence	Type	(Closest) gene	Fw	Rv
gRNA Exonic	Intended target	chr9:95485735-95485757	+	0	GTGTTGTAGGAGCGCTTCTG	Exonic	PTCH1	TACTGCTCACACATCAGCCAG	AGTTCAGCAAGGGCAATTCAA
	Off target 1	chr7:107199458-107199480	+	4	CACTTGTAGGAGAGCTTCTG	Intronic	HBP1	GAACTCGTGGCCTCAAGTGA	CAGTCTCACCTAGGCACACA
	Off target 2	chr8:140090333-140090355	-	3	GTGCGGTAGGAGGGCTTCTG	Intronic	PEG13	AGGGCAGGCAATGTCTATGC	TGGTAATACGCCAGTGGAGC
	Off target 3	chr4:1786477-1786499	+	4	GAGTGGCAGGAGGGCTTCTG	-	FGFR3	CTGCACAGGGATGAGGTGTC	AACAGAAGCCACCTCTTGCC
	Off target 4	chr5:1999371-1999393	-	4	TTGTTCTTGGAGAGCTTCTG	-	RP11-259O2.3	AGGGAACTATGGCCAGGTCT	CCTGAAGGATGGGTGGTGAG
	Off target 5	chr16:3972786-3972808	+	4	GTGGGGTTGGAGGGCTTCTG	Intronic	ADCY9	CCTCAGCCTCCCAAAGTGTT	TTCACCAGAGAACACACCCA
gRNA intronic	Intended target	chr9:95485503-95485525	-	0	GATTTATCGTTTCTCGAGTT	Intronic	PTCH1	TACTGCTCACACATCAGCCAG	AGTTCAGCAAGGGCAATTCAA
	Off target 1	chr1:988701-988723	+	4	GGTTGATTGTTTCTGGAGTT	-	PERM1	GCTGACCATCCATCCATGGG	AATCCTGAACTCCACAGTCAAC
	Off target 2	chr1:988931-988953	+	4	GGTTGATTGTTTCTGGAGTT	-	PERM1	GCTGACCATCCATCCATGGG	AATCCTGAACTCCACAGTCAAC
	Off target 3	chr1:989044-989066	+	4	GGTTGACTGTTTCTGGAGTT	-	RP11-54O7.17	GCTGACCATCCATCCATGGG	AATCCTGAACTCCACAGTCAAC
	Off target 4	chr1:989000-989022	+	4	GGTTGATTGTTTCTGGAGTT	-	PERM1	GCTGACCATCCATCCATGGG	AATCCTGAACTCCACAGTCAAC
	Off target 5	chr4:136129513-136129535	+	4	GTTTTCTCATTTCTTGAGTT	Intronic	RP11-775H9.1	TGCTCATCTGTGTTGCTGGT	GCACCATTGCCTGTAACTGAC

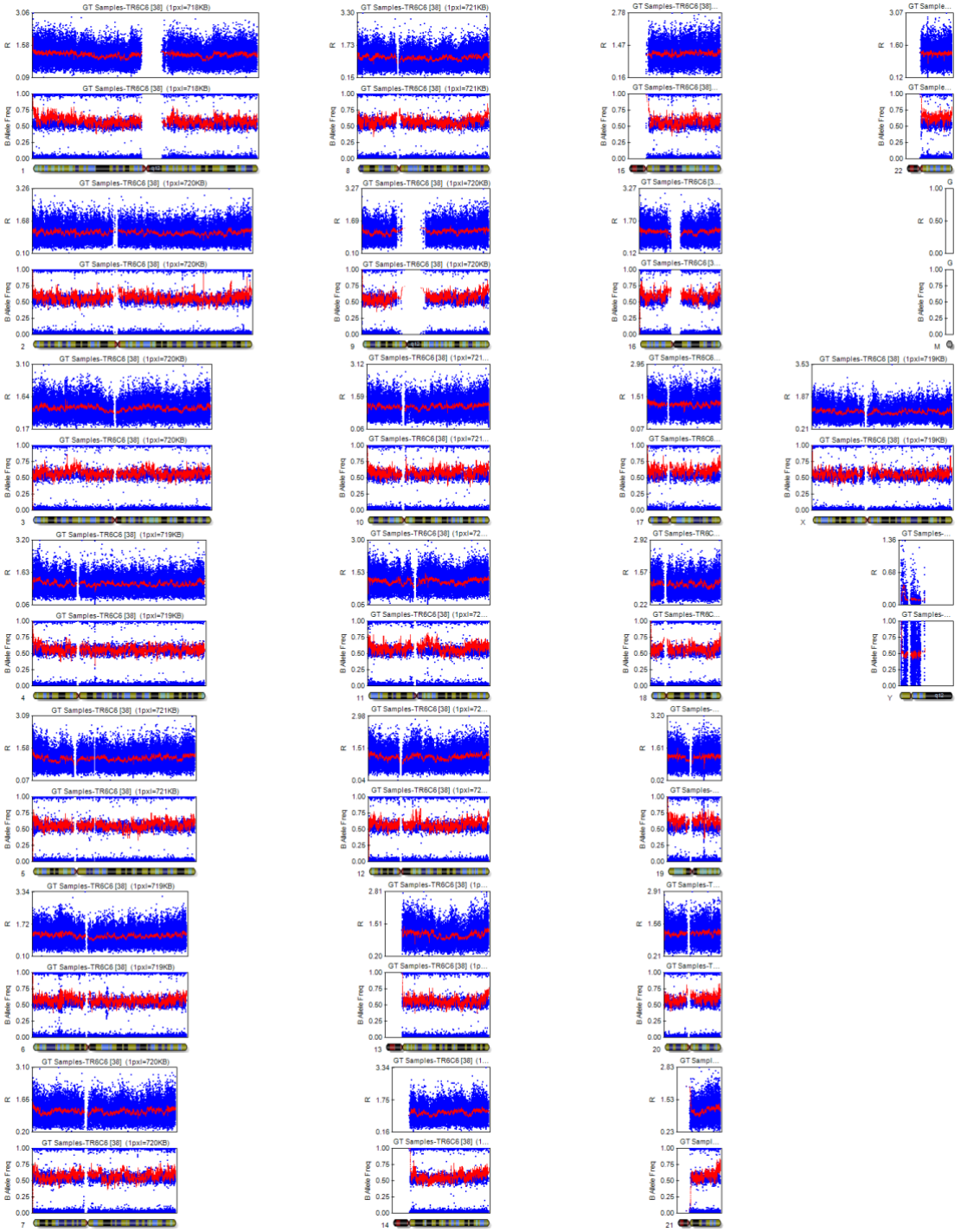
Appendix figure 1: SNP array to test for chromosomal aberrations in gene edited iPSC clones. *For each chromosome the R value (first dot plot, indicated with R on the left side) is given, representing the probe intensity of individual SNVs. The second dot plot displays the B-allele frequency and indicates whether the SNV is heterozygous (data points fall at around 0.5) or homozygous (data point at around 0.0 of 1.0). Chromosomal gains are identified by doubling of the R value while halving the R value indicates loss.*

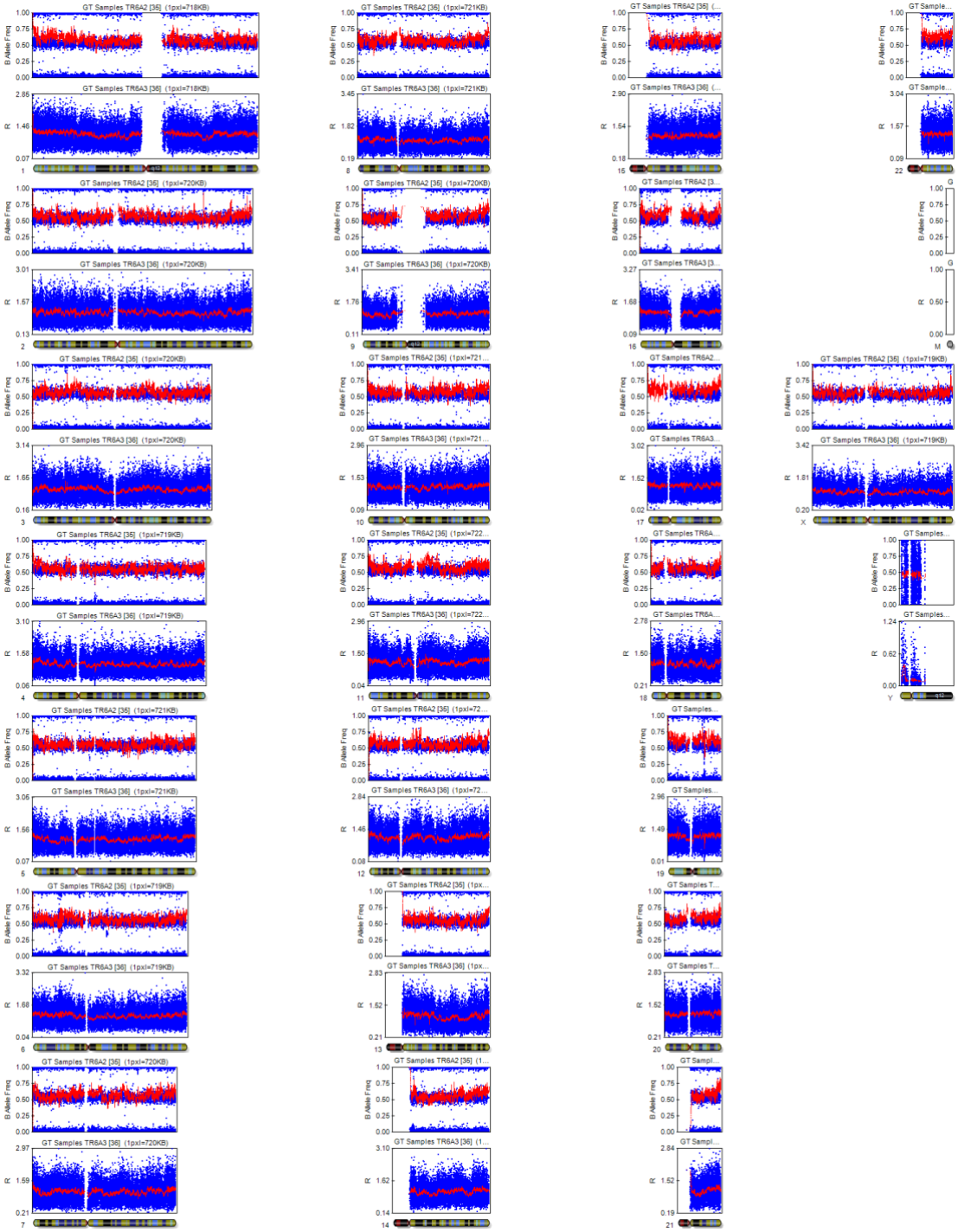

GT Samples AHO_WT [5] (1pxl=718KB)
GT Samples AHO_WT [5] (1pxl=721KB)
GT Samples AHO_WT [5] (1pxl=720KB)
GT Samples AHO_WT [5] (1pxl=719KB)
R
B Allele Freq

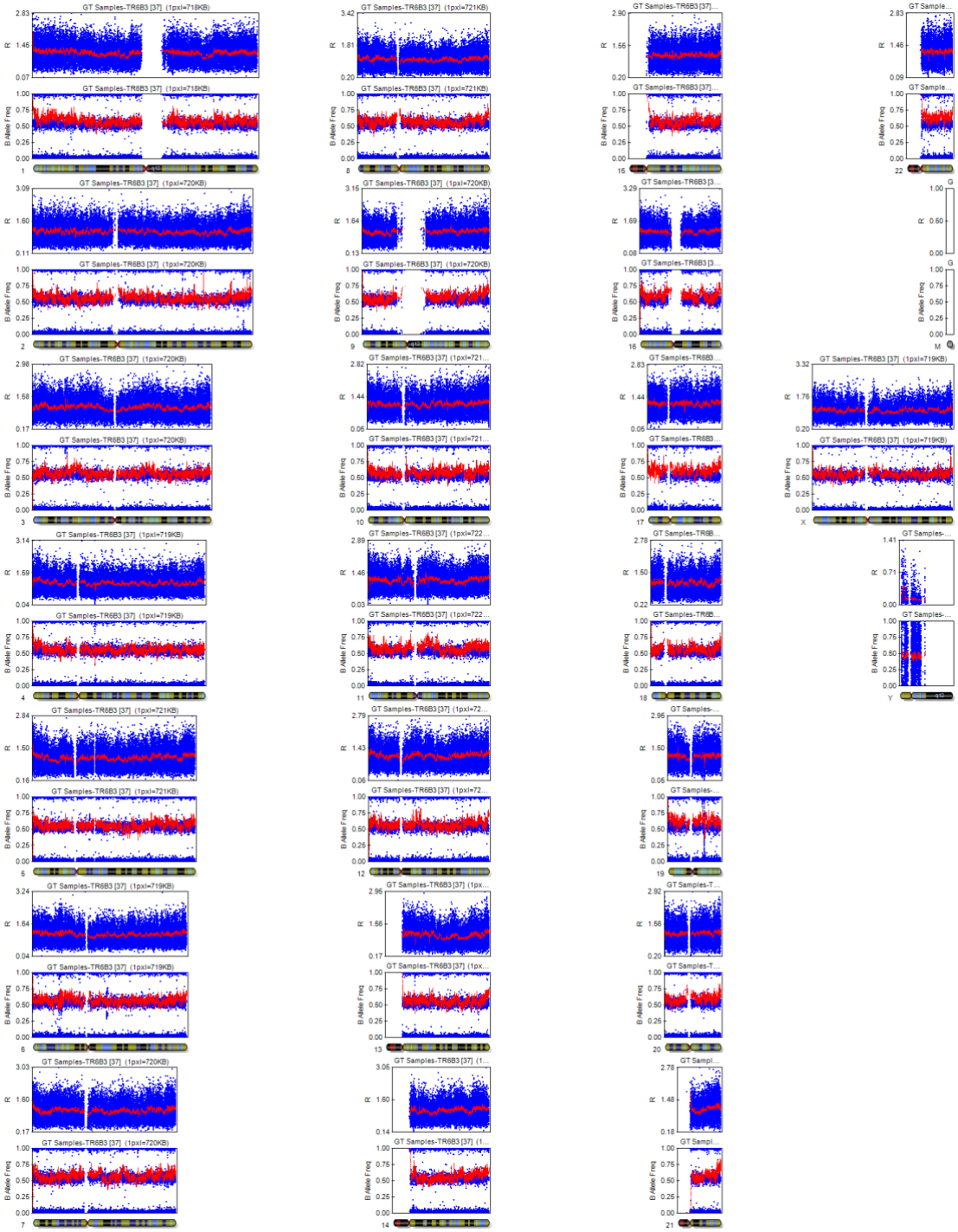

GT Samples-TR6A3 [36] (1pxl=718KB)
GT Samples-TR6A3 [36] (1pxl=721KB)
GT Samples-TR6A3 [36] (1pxl=720KB)
GT Samples-TR6A3 [36] (1pxl=719KB)
B Allele Freq
R

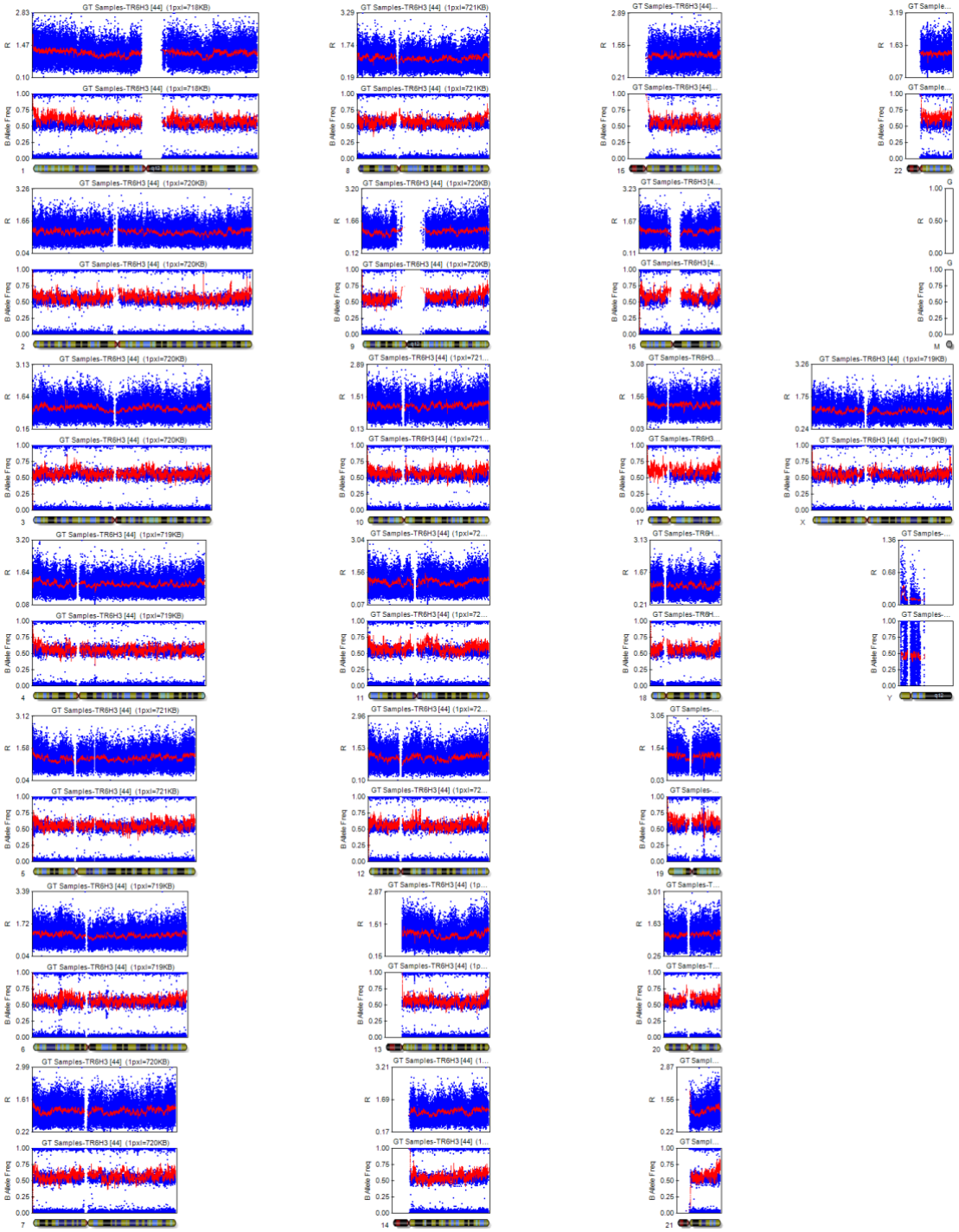

GT Samples-TR6B2 [70] (1pxl=702KB)
GT Samples-TR6B2 [70] (1pxl=703KB)
GT Samples-TR6B2 [70] (1pxl=704KB)
R
B Allele Freq


GT Samples-TR6B4 [71] (1pxl=702KB)
GT Samples-TR6B4 [71] (1pxl=704KB)
GT Samples-TR6B4 [71] (1pxl=703KB)
R
B Allele Freq


GT Samples-TR6C6 [38] (1pxl=718KB)
GT Samples-TR6C6 [38] (1pxl=721KB)
GT Samples-TR6C6 [38] (1pxl=720KB)
GT Samples-TR6C6 [38] (1pxl=719KB)
R
B Allele Freq


GT Samples TR6A2 [36] (1pxl=718KB)
GT Samples TR6A3 [36] (1pxl=718KB)
GT Samples TR6A2 [36] (1pxl=721KB)
GT Samples TR6A3 [36] (1pxl=721KB)
GT Samples TR6A2 [35] (...
GT Samples TR6A3 [36] (...
GT Sample...
GT Sample...
GT Samples TR6A2 [36] (1pxl=720KB)
GT Samples TR6A3 [36] (1pxl=720KB)
GT Samples TR6A2 [3...
GT Samples TR6A3 [3...
GT Samples TR6A2 [36] (1pxl=721...
GT Samples TR6A3 [36] (1pxl=721...
GT Samples TR6A2...
GT Samples TR6A3...
GT Samples TR6A2 [36] (1pxl=719KB)
GT Samples TR6A3 [36] (1pxl=719KB)
GT Samples TR6A2 [36] (1pxl=722...
GT Samples TR6A3 [36] (1pxl=722...
GT Samples TR6A...
GT Samples TR6A...
GT Samples...
GT Samples...
GT Samples TR6A2 [36] (1pxl=721KB)
GT Samples TR6A3 [36] (1pxl=721KB)
GT Samples TR6A2 [36] (1pxl=72...
GT Samples TR6A3 [36] (1pxl=72...
GT Samples...
GT Samples...
GT Samples TR6A2 [36] (1pxl=719KB)
GT Samples TR6A3 [36] (1pxl=719KB)
GT Samples TR6A2 [36] (1px...
GT Samples TR6A3 [36] (1px...
GT Samples T...
GT Samples T...
GT Samples TR6A2 [36] (1pxl=720KB)
GT Samples TR6A3 [36] (1pxl=720KB)
GT Samples TR6A2 [36] (1...
GT Samples TR6A3 [36] (1...
GT Sampl...
GT Sampl...
B Allele Freq
R


GT Samples-TR6B3 [37] (1pxl=718KB)
GT Samples-TR6B3 [37] (1pxl=721KB)
GT Samples-TR6B3 [37] (1pxl=720KB)
GT Samples-TR6B3 [37] (1pxl=719KB)
GT Samples-TR6B3 [37] (1pxl=721KB)
R
B Allele Freq


GT Samples-TR6H3 [44] (1pxl=718KB)
GT Samples-TR6H3 [44] (1pxl=721KB)
GT Samples-TR6H3 [44] (1pxl=720KB)
GT Samples-TR6H3 [44] (1pxl=719KB)
R
B Allele Freq